Determination of p53 role in cancer biology and therapy through interactome development and analysis

Michelle Hussain

School of Environment and Life Sciences, College of Science & Technology,

University of Salford, Salford, UK

Submitted in Fulfilment of the Requirements of the Degree of Doctor of Philosophy, 2016

Volume I

Word Count: 69665

Table of Contents

List of Tables

List of Figures

List of Images

1 Acknowledgements

I dedicate this entire thesis to my beloved grandmother, Enid-Myrna, who passed away in 2015 from hepatocellular carcinoma. She gave me so much strength and love throughout my life, and tried so hard to fight her disease to see the completion of my PhD. I miss her dearly.

I especially wish to thank my supervisor, Prof.Marija Krstic-Demonacos for both her academic and personal support, and her encouragement. Especially for her patience and understanding with my ever demanding diabetes. A very special supervisor. A special thank you to Dr Costas Demonacos, for his continual academic help and use of his facilities

Gratitude to academic peers. Dr Jean Marc Schwartz and Dr Kun Tian for their expertise and support with computational techniques, and my forever email traffic to them and, Prof. Luciano Mutti for his help and support with my research, in particular mesothelioma.

I would also like to thank Prof Geoff Hide and Dr Stephen Heath for being special people throughout my life at the university of Salford. Who continually encouraged and believed in me throughout my studies. To my dear friends Helen Bradshaw and May Rajab, thank you for everything.

To my family, Mum, Aleem, Jarrad, Astharr, for their patience throughout my PhD, continual love and support and, putting up with me, and lastly to my faithful dogs (my writing partners).

2 Abbreviations

AP1	Activator protein 1
ARF	Alternate reading frame
ATM	Ataxia telangiectasia mutated
ATR	Ataxia telangiectasia RAD 3 related
AURKA	Aurora Kinase A
BAX	BCL2 associated protein
BCL2	B cell / lymphoma 2
BER	Base excision repair
BN	Boolean network
BRAC1	Breast cancer 1
CNA	CellNetAnalyzer
CBP	CREBB binding protein
CDK4	Cyclin dependent kinase 2
CDKI	Cyclin dependant kinase inhibitors
CDKNA1	p21
cDNA	Complementary DNA
CHEK	Checkpoint kinase
CRD	C-terminal regulatory domain
DBD	DNA binding domain
DMSO	Dimethyl Sulfoxide
DNA	Deoxyribonucleic acid
DNA-PK	DNA protein kinase
dsDNA	Double stranded DNA
DUB	De ubiquitination enzymes
DYRK	Dual specificity tyrosine-phosphorylation-regulated kinase
E2F	E2F transcription factor
EGF	Epithelial growth factor
ERRB2	V-erb-b2 erythoblastic leukaemia viral oncogene homolog 2
FAS	Fas (TNF receptor superfamily, member 8)
FGF2	Fibroblast growth factor 2
G1	Gap 1
G2	Gap 2
GADD45	Growth arrest and DNA damage inducible, alpha
HAUSP	Herpes virus associated USP
HDM2	Human Double Minute 2
HIFI	Hypoxia inducible transcription factor
IGF1	Insulin like growth factor
IL-8	Interleukin 8
JNK	c-Jun N-terminal kinases
KD	Knockdown
KO	Knockout
Lys	Lysine
M phase	Mitosis

MAP	Microtubule associated protein
MAPK	Mitogen activated kinase
MDM2	Murine Double Minute 2
MDMX	Murine Double Minute X (4)
MMR	Mismatch repair
mRNA	Messenger RNA
MYC	V-myc- myleocytomatosis viral oncogene homolog
NCBI	National center for biotechnology information
NF/KB	Nuclear factor kappa light
NHEJ	Non homologous end joining
ODE	Ordinary differential equations
Otub1	Otubaine 1
P300	Protein 300
p53	Tumor protein p53
PCNA	Proliferating Cell Nuclear Antigen
PIKKs	phosphatidylinositol 3-kinase related kinases
Pirh2	Periperin2
PKT206	p53 interactome Kun Tian 206 Nodes
PMH260	p53 interactome Michelle Hussain 260 Nodes
PRD	Proline rich domain
PNPs	Potential novel predictions
PTGS2	Prostaglandin endoperoxide synthase
PTM	Post translational modifications
PTTG1	Pituitary tumor transforming 1
q RT PCR	Quantitative real time PCR
RB	Retinoblastoma protein
ROS	Reactive oxygen species
S phase	DNA synthesis
SaOS2	Human osteosarcoma cell line p53 null
SDS page	SDS - poly acrylamide gel electrophoresis
Ser	Serine
ssDNA	Single stranded DNA
STRING	Search Tool for the Retrieval of Interacting Proteins
TAD	Transactivation domain
TD	Tetramerisation domain
TF	Transcription factor
TGFB1	Transforming growth factor beta 1
Thr	Threonine
TopB1	Topoisomerase binding protein
TP53	Human p53 gene
TSG	Tumor supressor gene
U20S	Human osteosarcoma cell line p53 wildtype
USP	Ubiquitin specific proteins
UV	Ultraviolet radiation
WT	Wildtype

3 Abstract

Cancer is a heterogeneous pathology of cell and tissue type, involving multi-dysregulation of pathways that govern fundamental cellular processes. Chemotherapy efficacy is highly affected by these molecular deviations and the majority of patients are non-responsive. The stress responsive transcription factor, p53 is a powerful tumour suppressor implicated in over 50 % of all human cancers, and the chemo-therapeutic applications of p53 have been well described. However, the vast literature base of p53 and complexity of its interactions makes it a challenging system for integration of this diverse information.

Computational methodologies are novel tools for integration of diverse molecular information into a coherent framework. The *in silico* Boolean PKT206 p53–DNA damage model has previously demonstrated good predictive capability for p53 wildtype and null tumours. Here, we have expanded PKT206 to generate a more clinically robust representation of p53-cancer dynamics. The Boolean PMH260 and PMH302 p53 models were constructed to consider 260 nodes and 980 interactions (PMH260) and 302 nodes with 1398 interactions (PMH302). Processes of angiogenesis, DNA repair and cell cycle arrest were amalgamated into both models with an additional input of hypoxia included into PMH302. For greater representation we further constructed a logical model that was more relevant to a specific cancer and integrated 61 deregulated genes considered as important to mesothelioma (Meso-PMH61 model), and superimposed microarray data generated in our laboratory of mesothelioma cells treated with etoposide and 1 % O_2 oxygen.

We analysed all models, *in silico*, using CellNetAnalyzer. *In silico* knockout analysis of various nodes mimicking *in vivo* mutations revealed 98 and 514 potential novel predictions (PNPs) for PMH260 and PMH302 respectively, some were validated by laboratory and literature verification. Validation of 4 PNPs were investigated in our laboratory using transient gene and protein knockdown, q-PCR and western blot analysis. Of these, 2 PNPs were in agreement with the models prediction.
For further validation we superimposed various human cancer transcriptome *in vitro* profiles and compared omics results to *in silico* LSSA data. Greater correct predictions

were achieved than the earlier p53 logical models (PKT206 and PMH260) when using the expanded p53 interactomes (PMH302 and Meso-PMH61) resulting in 68.5 - 83 % dependant on model and simulation. We further tested the models capability to predict gene expression changes on a clinical and individual patient basis, and superimposed patient derived *in vivo* transcriptome tumour profiles with a p53 mutant and wild type status. Correct predictions were again in the majority ranging between 57 - 61.5 % for NSCLC and between 56-63 % for biphasic and epithelioid mesothelioma tumours.

Gene expression analysis of individual tumour profiles identified several significantly over-represented pathways and deregulated genes common and unique contributing to these tumours, correctly predicted by the model. In particular, we highlight pathways, MAPK, Erbb and Ca^{+} as contributing to non-small cell lung cancer dependant on patient. For malignant pleural mesothelioma, we highlight cell cycle and MAPK pathways and the cell cycle genes; CCNB1, CCNB2 along with KIF14, PDGFRB and SULF1. These offer potential for further investigation that could be exploited for greater therapeutic efficacy in sarcomatoid, and CYP24A1, HIPK4 and PEG3 in biphasic p53 (+/+) malignant mesothelioma tumours. Drug profile analysis of deregulated genes identified by the model highlight the need for individualised therapeutic approaches, and we offer putative combined targeted therapeutic suggestions dependant on tumour profile.

In summary, we have generated the largest p53 signalling model to date, and have successfully identified overall system attributes when compared to *in vitro* and *in vivo* patient derived data. We show the importance of individualised therapies and highlight the enlarged p53 interactome as a promising predictive tool for further investigation into personalised anti-cancer therapies with clinical relevance.

4 Introduction

4.1 Systems biology

The advent of the 'omics' era (genomics, proteomics, transcriptomics etc.) and high throughput methodologies has highlighted the complexity of many diseases such as cancer, and allowed for the identification of numerous deregulated genes and perturbed pathways. Despite this, the molecular heterogeneity displayed in diseases such as cancer, along with the vast literature base makes it a challenging system for integration of this diverse information into a coherent framework. This is particularly true for p53, where over 80,500 publications are linked with the keyword p53 (PubMed, May, 2016).

Systems biology may be defined as the study of complex interactions within biological systems and the emergent properties that arise from those interactions. The developing field of systems biology in parallel with the generation of high-throughput data, computationally has heralded a new era of network analysis and medicine. Indeed, network medicine is a new term coined by many cancer researchers (Pawson *et al.*2008). Systems biology teamed with traditional reductionist approaches are novel, yet, promising tools to model such complexity. Indeed, this intricacy cannot be effectively described by traditional reductionist approaches alone (Wang, 2010). Thus, transforming the traditional reductionism based methods by combining with a systems approach provides a greater unbiased opportunity to understand complex network diseases for development of effective therapeutic strategies, in particular for cancer.

4.1.1 Systems biology and cancer

Cancer involves multivariate deregulation of numerous pathways which govern fundamental cellular processes including proliferation, differentiation, migration and death (Pawson et al. 2008). As stated, these molecular deviations have been demonstrated with the advent of high-throughput studies, highlighting a plethora of genes and pathways that contribute to the malignant phenotype (Ngo *et al.*2006). Nevertheless, the complexity of cancer networks is a challenging system, in particular for chemo-resistance and the development of effective anti-cancer strategies. For

example, identification of a specific deregulated gene maybe insufficient for a targeted treatment due to the complex signalling pathways of posttranslational and transcriptional mechanisms (Luo *et al.*2009). This is further hampered by the redundancy and cross talk within multiple signalling pathways arising from synchronous interactions of a single molecule. Moreover, pathways rarely operate in isolation. For example, one may lead into another directly by protein – protein interactions or, indirectly via transcriptional programmes to modify others. In addition, the heterogeneity frequently observed in molecular signatures within different tumours of the same tissue can result in varying clinical responses in different patients using the same anti-cancer treatment. This underscores the need for targeted treatment which can address the genetic deregulations associated with a particular individual for greater therapeutic efficacy.

A systems approach provides this opportunity, to assimilate large - scale information into a coherent framework to address some of these questions. It can provide an unbiased approach to understand the initiation, progression and biological behaviour of cancer, addressing the different levels by integrative analysis.

Three key aspects of cancer research are thought to benefit from system biology approaches; discovery of drug responsive tumour biomarkers, the understanding of network focused molecular mechanisms of different stages of cancer progression, and lastly personalised targeted treatment (Wang, 2010). Indeed, many studies have started to address these using different mathematical complexities. For example, Chand *et* a*l*. (2012) investigated the association between wildtype genes involved in breast carcinoma by analysing their expression patterns using microarray data and as a result designed a gene interaction map of both gene types where function and interactions were analysed by gene ontology of biological categories such as molecular function. These were statistically analysed and functional characterisation of novel genes were identified via BINGO an independent Cytoscape platform (discussed in 4.1.2.3 and section 6) which delivers P value for significant genes. Interactions of genes (CREBB, CHIK and INSR) were found to be involved in breast carcinoma p53 signalling pathways along with STS5A which had no previous predicted function in breast

carcinoma development (Chand *et al.*2012). Whilst, Faratian et al. (2009) using a kinetic model identified PTEN as a contributing factor to anti-HER2 therapy resistance. Klinger et al. (2014) constructed a kinetic model, and compared *in silico* to *in vitro* data to explore combinational therapy and found that P13K or mTOR inhibition can inhibit both AKT and ERK activity. Lastly, Tian *et al*. (2013) designed a predictive logical based p53 network model of DNA damage inducible pathways and identified 58 novel changes during *in silico* analysis of various knock out tests; this model has shown potential for targeted therapies. This particular study is discussed in section 4.1.2.7.

4.1.2 Computational techniques

4.1.2.1 Text mining approaches for protein – protein interaction analysis

For construction of cancer networks, systematic integration of biological information from literature is fundamental to establish a robust model. This is particularly true for p53 where the literature base is extensive. A text mining approach is less exhaustive. It allows the user to extract large data via automated information retrieval and thus less time consuming. To date, various text mining approaches and tools exist for information retrieval. Text mining may be applied to system biology networks by searching for genes / proteins and the parameters that define their interactions. Parsing (dividing words for identification of each component, i.e. verb, adjective, or noun) techniques are a prerequisite for describing more than one biological interaction, and refer to retrieval of syntactic (arrangements of words in a sentence) relations from a complete sentence between verbs and object (Ananiadou *et al.* 2006; 2010). For example, ATM activates p53, where ATM is the object and p53 is the sentence subject. Commonly used text mining tools that consider natural language processing based upon syntactic and semantic analysis are available through several biochemical databases. For example; MEDIE and InfoPubMed (Ohta *et al.*2010). MEDIE retrieves biochemical information and relations from the complete Medline database which contains a large number of citations and publication abstracts. It allows the user to perform a semantic query for retrieval of the particular information, where semantic refers to the meaning of a word such as a protein or gene, for instance p53 in the above example. InfoPubMed also uses full parsing to recognise various interaction

types of such as inhibition, activation or enhance between proteins and genes based upon ontology. Others include, PESCADOR (Platform for Exploration of Significant Concepts Associated to Co- occurrence Relationships) which extracts interactions from PUBMED abstracts and can be used to build pathways upon existing knowledge. KEGG is another commonly used database which uses PUBMED and MEDLINE. KEGG provides over-represented pathway maps that investigate particular networks or interactions, and similar to PESCADOR is useful for building upon existing knowledge. Whilst informative, these databases are limited in information, and confidence scores are not assigned to interactions which may allow the user to extract significant data. Furthermore, the information is not as regularly updated or as extensive as that of STRING database, described hereafter.

4.1.2.2 STRING database

A prerequisite for a systems level understanding of signalling pathways is to dissect and annotate functional interactions within the system. The extensive and continual research of protein function and interactions make it less amenable to collect the diverse information using literature search only. Text mining approaches offer the potential to extract this information based upon previous literature in an automated manner.

The Search Tool for the Retrieval of Interacting Genes (STRING) is a protein to protein interaction database which integrates this extensive information and aims to provide 'a one stop shop' for all information on protein links and interactions. STRING extracts protein information from four main sources; high throughput experiments, genomic content, conserved co expression and previous literature knowledge by natural language processing. This information links to the PUBMED database where text mining retrieval is offered via STRING itself. Using this application, STRING provides around 50 scientific publications in response to the users' interaction query.
Key features of STRING is a probabilistic confidence score schema that is calculated from the four main sources. Scores represent an estimate of functional interaction between protein pairs in a pathway, which may guide users. For example, STRING schema states that a confidence score of over 0.7 is considered as high. Interactive

protein interaction maps are user friendly and include interactions of activating or inhibiting. Whilst, the nature of the interaction is also considered such as: post-translational modifications, binding, or expression. It also considers partner sites such as Cytoscape software where STRING data may be imported. Importantly, STRING is updated on a regular basis, every 6-12 months, thus allowing retrieval of novel information outdating those previous (Jenson *et al*.2009; Szklarcyzk *et al.*2011).

4.1.2.3 Cytoscape software

Cytoscape is an open source software platform. It allows for integrative analysis and visualisation of molecular interaction networks and biological pathways by amalgamation of large information that can be represented into a coherent framework (Shannon *et al*.2003). Cytoscape software allows the user to link to several databases of functional annotations, for example STRING and KEGG. Cytoscape functional analysis is provided by various plugins for version 2.9 and lower, nomenclature however has changed to 'apps' for versions of 3.0 or higher. These are publicly available allowing the user to perform network analyses and visualisation of pathways. Moreover, any user may develop these 'apps' and as such the Cytoscape app community is continually increasing allowing for greater analysis power and network choice. Similar to STRING, Cytoscape is capable of the construction of molecular networks through these apps, for example via the Agilentsearchliterature app. However, networks retrieved are limited in size and literature evidence is not available or updated on a regular basis. Thus, Cytoscape is more apt for input of new networks from independent manual construction for functional analysis.

Unlike CellNetAnalyzer, Cytoscape is an independent platform and as such is capable of handling large datasets including high throughput expression profiles. With the availability of transcriptome data, Cytoscape is becoming a promising tool and may provide better analyses for large networks. Indeed, a recent study termed the novel signal transduction flow algorithm (STFSA) has been successfully used and is publicly available as a Cytoscape app. STSFA utilizes large scale 'omics' data to assign dynamic gene scores throughout the network from source node to final cellular processes for pathway analysis. It has demonstrated good correlation with experimental

transcriptome data of ChiPSeq and microarray profiles to accurately predict multiple *in silico* gene knockouts (Isik *et al*.2012). Indeed, Cytoscape is considered most powerful when used in conjunction with large datasets (Shannon *et al.*2003).

4.1.2.4 System biology approaches

The metabolic nature of cellular pathways may be approached in either a bottom up or top down directionality as depicted in a simplified diagram (figure 4). The latter approach constitutes data processing from 'omics' levels to pathways and individual gene levels, whilst bottom up encompasses automated tools and mathematical modelling (Shahzad and Loor, 2012). Both directionalities encompass different steps for experimental hypotheses and required outcome. Different levels of complexity are later addressed by mathematical modelling dependant on analysis required which may be quantitative or qualitative, simple or complex (figure 4.1).

4.1.2.4.1 Top down approach

The top down approach originates from experimental data, to identify and describe the 'bottom' biological interactions by network construction, via the flow of information occurring from the 'omics' level. This directionality can help to dissect interactions using the 'omics' data extracted from top down methodologies of high throughput experiments (Bruggeman, 2006). Top down aims to identify new molecular mechanisms of interactions recursively from initial experimental data of several hypotheses. Subsequent data analysis and integration for determination of correlations may consequently be applied with the endpoint of a hypothesis of the co - interaction and regulation of these molecule groups. Subsequent hypotheses may be utilised for prediction of novel correlations for further analysis by laboratory based methodologies (Bruggeman 2006). This approach is useful for network structure determination and identification of novel cellular molecular mechanisms and interactions

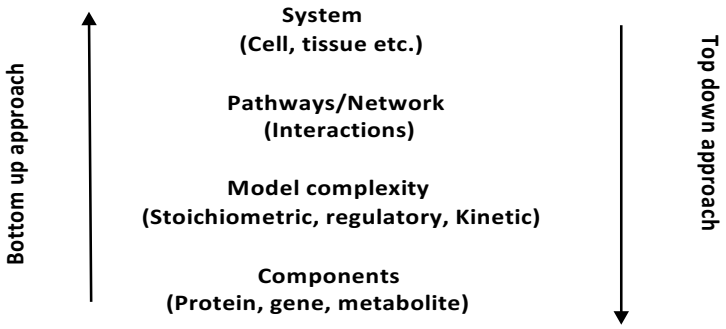

Figure 4 Bottom-up and top- down methodologies
Bottom up approaches begin with detailed knowledge about individual components and assemble these into larger elements, such as pathways and networks for behaviour. Top-down approaches start from typically large data sets which represents 'omics' of a biological system aiming to identify those components that are most responsible for the systems behaviour such as phenotype.

4.1.2.4.2 Bottom up approach

The bottom up approach is aimed at constructing detailed models which may be replicated under various physiological conditions. It combines all molecular specific information into a genome scale model providing an integrative *in silico* view of biological interactions within living systems and based upon constraint based modelling. In contrast to a top down approach the bottom-up directionality builds upon pre-existing data for analysis of their systemic consequences for the cell (Westerhoff and Palsson, 2004) and utilises experimental data of steady state and transient metabolite and flux data. Experiments are on the basis of detailed networks for subsequent validation and improvement of the model to investigate the hypothesis generated by i*n silico* model analysis. After full characterisation of the network, top down approaches may also be combined with bottom down systems biology at later experimental stages. The two combined may provide a strong framework for dissecting cellular molecular interactions (Bruggeman, 2006).

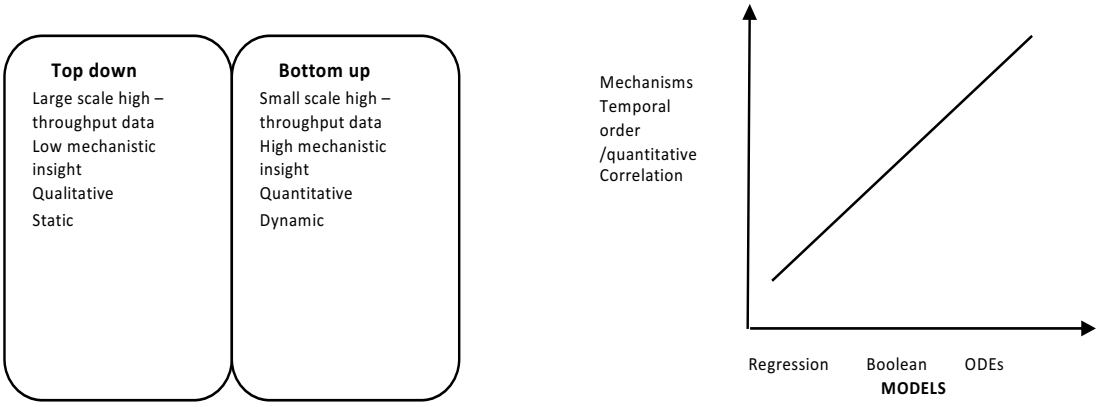

Figure 4.1 Different levels of complexity in System biology approaches
The two system approaches of top down and bottom up. **b)** Complexity of mathematical methods of regression analysis being the simplest approach for correlation identification. ODE models may be utilised to describe kinetic mechanisms, whilst Boolean models are more simplistic. Redrawn from (Bachmann *et al.*2011)

4.1.2.5 Mathematical modelling

The most commonly applied mathematical equations for signalling pathways are ordinary differential equations (ODEs), and Boolean mathematical modelling. Applications of continuous and discrete models are dependent upon the desired output. Kinetic modelling is more suitable for quantitative modelling, i.e. investigating the treatment efficacy of cancer models. For instance, Mamat *et al*. (2013) used ODE modelling with *in silico* simulations to investigate the effects of IL-2 (Interleukin -2) and INF-α (Interferon- α) on tumour cell dynamics under the influence of chemotherapy, immunotherapy and bio- chemotherapy in ten patients. The study concluded that these treatments played pivotal roles in remission and death of tumour cells. In contrast, Boolean models are more sufficient for measuring qualitative aspects of biological phenomena for example, steady state protein / gene activity and knock down or knock in effects (Bachmann *et al*.2011)

4.1.2.5.1 Ordinary differential equations

Ordinary differential equations (ODEs) have been extensively used to model molecular signalling pathways and considered the most natural equation for translation of detailed reaction networks into a model. Constructions of ODEs are dependent upon a single variable, such as time. Their networks represent reaction rates of a particular

species such as degradation, production and association in terms of mass action kinetics where the rates are proportional to the reactant concentrations (Bachmann, 2011). ODE networks however have limitations. For example, a large number of parameters are required. Further drawbacks are network sizes, ODE models may only describe a few nodes, whilst Boolean models may constitute hundreds (Mai and Liu, 2009).

4.1.2.5.2 Boolean modelling

Boolean modelling is another commonly used approach for construction of signalling pathways. Boolean models were first described by Kaufmann, (1969) as models of genetic regulatory networks. These logical networks are simplistic, yet effective in capturing the dynamics of gene / protein signal flow networks. For example, described by binary states of ON or OFF, they can effectively recapitulate signalling events, referring to a gene transcribed (ON) or non-transcribed (OFF), a protein activated (ON) or inhibited (OFF).

Boolean logic has been applied successfully to model various complex biological phenomena (Shmulevich and Kauffmann,2004). Boolean models are represented by directed graphs where nodes represent genes or proteins and edges or hyper-edges represent the interactions between them. Boolean logic states that a node is capable of only discrete expression values contrasting the continuous value ranges in kinetic models such as ODEs. A logical rule linking the inputs is assigned to each node and as such no real parameter values are needed to be adjusted apart from the applicable logical Boolean rules that describe the system. Each node according to Boolean logic is parameterized by binary interactions, 1 or 0 operators referring to activation or no activation. Nodes are assigned two separate states of ON or OFF; where at each time point the state of a particular node is determined by the state of another node typically upstream by transfer of Boolean logical function.

Klamt *et al.* (2006) proposed two different graph theories for Boolean network formation. The choice of graph is dependent on the required outcome of model, data type and input. Biological processes and cellular signalling pathways exhibit multi-

lateral relationships and thus graph choice must represent such reactions. Directed logical hypergraphs consider and facilitate these multiple reactions. Furthermore, biological cancer networks frequently undergo feedback loops of both positive and negative nature. Whilst interaction graphs may represent such processes they cannot incorporate Boolean logic of OR, NOT, AND operators (Klamt, 2006). For these synchronous connections, Boolean logic must be considered to represent a truer state of signalling pathways and as such depict a greater representation of cellular networks whilst also providing confident *in silico* prediction. The AND, OR, NOT relationships are thus best represented by hyper-graphs where directed hyper-arcs connect more than one node (Klamt, 2006; 2011). In contrast, multi-lateral signalling is not possible using interaction graphs where only the two states exist and separate arcs of positive pathways influencing target node fail to truly represent the relationship between three species. Figure 4.1.1 summarises differences between both graph theories.

In addition to the logical model constructed by Tian et al. (2013) discussed above, Boolean modelling has been utilised in several cancer studies. For example, a Boolean system was constructed of 96 nodes of known cancer causing genes with 249 edges and five input nodes of cellular stresses. (Fumia and Martins, 2013). The study identified 62 attractors with distinct cellular cancer phenotypes in response to upstream inputs. *In silico* mutations were introduced into the network and, ten proteins were identified as having the capability to transform into malignant phenotypes. Lastly this study considered targeted pathways of treatment of individual nodes to block cancer pathways. Inhibition of PDK1, AKT E2F, Cyclins D and E, and MDM2 or activation of p53, RB, CDK11, p21, p27, and SMAD4 enhanced senescent phenotypes, impairing proliferative ones. However, treatment was dependent on cancer stage and type (Fumia and Martins, 2013). Kirouiac et al. (2013) successfully developed a Boolean predictive model of drug resistance in Erbb2 amplified breast cancer and tested the *in silico* interactome prediction using *in vitro and* in *vivo* mouse model systems.

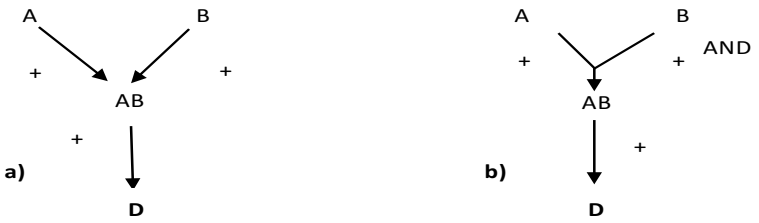

Figure 4.1.1 Simplified illustration of graph theories: Interaction and logical interaction hyper-graph. a) Interaction graph the reaction comprises two separate arcs of A and B both having an effect on AB of positive paths leading to D-E. The two positive paths of, both A and B (AB) are required for activation of D, however removal of one species for example, A is sufficient to disrupt activation of D. Thus, a signalling path in an interaction graph will not ensure a signal may flow via this path. In contrast**, b) Interaction Hyper-graph** depicts the example as a logical interaction hypergraph in which a hyperarc connects A and B by capturing the AND-connection between both species. (Redrawn from Klamt, 2009).

4.1.2.6 CellNetAnalyzer

CellNetAnalyzer (CNA) is an independent graphical user interface for Matrix laboratory (MATLAB) (discussed in section 6), that provides structural and functional analysis of various cellular networks (Klamt, 2006). CNA has been designed with MATLAB nomenclature enabling the user to incorporate MATLAB algorithms. In particular, for analysis of *in silico* signalling networks, using distance and dependency matrix formalisms such as dependency relationships, and node state changes in the network arising from input perturbations using logical steady state analysis.

CNA provides a comprehensive independent platform for complex structural, functional and qualitative analysis of biochemical, metabolic, signalling and regulatory networks (Klamt, 2006). Network projects constructed by CNA may be represented and analysed with either mass flow (stochichometric/metabolic) or signal flow (signal/regulatory). Nomenclature used for network descriptive in both network examples requires declaration of both species and reactions.

For example, using mass flow networks reactions correspond to stoichiometric reaction equation where:

A + B -> C

This equation states that two reactants (A and B) are converted into C, with A and B totally consumed in the process. In contrast signal flow networks are represented by logical Boolean operators of true or false expressed by the equation:

A -> B = C

Where the product (end node) is activated by the reactant (start node), for example C is activated if A and B are active. However, A and B is not consumed during the process. For example, C may be activated, if A and B are in an active state.

In both networks, declaration of species and reactions are required with their corresponding attributes. Declaration of nomenclature in both is equal however both have different interpretations. For example, and as described above, in mass flow networks reactions are defined by stoichiometric conversions, referring to products consumed in a single reaction. In contrast, signal flow considers Boolean logic of AND, OR and NOT operators and defines interactions by the end node (product) being activated by start node (reactants). These signal flow networks can be represented by either interaction graphs or hyper- graphs as previously discussed (figure 4.1.1).

For any biological process, feedback loops and crosstalk are frequent and important events in cellular signalling pathways. CNA considers such reactions which are represented within an interaction matrix of species and reactions for analysis and also may be visualised graphically. Dependency relationships between species may be analysed with the construction of a dependency matrix defined as *M* which displays all pair-wise node dependencies. These relationships are calculated by the shortest or positive or negative pathway distance between node pairs and represented by six different colours or values of 1 – 6 indicating the different species relationships of: weak/strong activator, inhibitor, or ambivalent factor or non-influencing node.

Furthermore, positive or negative feedback loops are considered within the matrix.. These are described in section 6, material and methods.

Logical steady state analysis is a good method for predictive behaviour of the input – output dynamics of signalling networks (Klamt *et al.*2007). The steady state between node pairs can be analysed in CNA via logical steady state analysis, where the state of each node is consistent with its Boolean function and as such once a node has progressed into a logical steady state it will remain. In this logical steady state and in accordance with Klamt et al. (2006), each node can have three different states of; 0, inactivated, 1, activated and NaN, undetermined. Exclusion of node (s) and its interaction (s) from a network allow for analysis of the interactome in response to their absence. These *in silico* knock outs can represent biological phenomena of in vivo mutations in diseased states such as cancer.

CNA has been utilized in several studies using Boolean logic. For example, a dynamic model was constructed to analyse p53 and NF-kB pathways in response to DNA damage. This study undertook *in silico* knock out tests for prediction of novel gene function. Dependency matrices were also constructed to identify potential cancer therapy targets (Plotz and Naumann, 2012). Whilst another more recent study constructed a p53 predictive interactome defined as PKT206 and analysed its response to DNA damage inducible pathways via i*n silico* knock out tests (Tian *et al.*2013). As PKT206 is a continuum of this study, a brief introduction is necessitated, discussed in the next section.

4.1.2.7 The PKT206 Model

The Boolean p53- DNA damage inducible model designated as PKT206, generated by Tian *et al.* (2013) was analysed in CNA and constructed via data extraction utilising the STRING database, and additionally manually curated for model accuracy. PKT206 comprises five layers; the input signal of DNA damage, upstream nodes of p53, the core p53 and MDM2, downstream nodes of p53 and the output signals of apoptosis and cellular senescence. The p53 core comprises 738 interactions between 206 genes /

nodes connected with p53 as the network hub. Nodes represent genes or proteins with edges representing the inhibiting or activating interactions between them.

Analysis of the network by CNA identified thirty feedback loops, of which fourteen involved p53, the majority significant to p53 regulation such as MDM2 and MDM4. Logical dependency relationships between nodes were calculated where 23,191 nodes were found to have no effect, 16,425 ambivalent factors, 1100, weak inhibitors, 1240, weak activators, 20, strong inhibitors and 49 being strong activators. Various *in silico* p53 knock outs were constructed to investigate and predict the role of p53 and the response of the network upon node deletion. Of these 11, 753 nodes changed after p53 node deletion from the original 41,616 p53 interactome. The majority of changed nodes were ambivalent factors arising from feedback loops within the system also highlighting p53 regulatory role within the *in silico* network coinciding with known *in vivo* p53 effects. 11 of 30 i*n silico* node deletions demonstrated major dependency changes to wildtype matrix proceeding removal of a specific node. 58 possible predictions of change were obtained from the 11 initial *in silico* knock out tests and, of which 4 were validated via literature searches and 2 via laboratory validation.

Microarray analysis of human osteosarcoma and colon cancer cell lines of p53 null and wild type treated with etoposide induced DNA damage has highlighted the models predictive capability. Up to 75 % of predictions were considered as true when compared to LSS *in silico* results. This highlights the prospective of employing PKT206 in a clinical setting as one future direction in cancer. However, limitations to this is network size, in particular for p53 where a plethora of responsive genes have been described (Riley et al. 2008). 'Omics' data is high throughput and as such model size is of importance for superimposition of expression profiles for greater biological representation. Furthermore, inclusion of additional stresses or processes involved in cellular fate should be considered.

4.1.3 Cancer

Cancer is the result of abnormal cell growth due to gene expression changes resulting in dysregulated cell proliferation. Tumours are the outcome of a process of clonal selection whereby multiple alterations for example, oncogene activation or the loss of tumour suppressors, provide a selective advantage to the cells that carry them. This can ultimately progress into a more invasive cell population which may metastasise into adjacent and distant sites (Ruddon, 2007).

Cancer has been described as one of the main causes of deaths worldwide. The most recent statistics of all cancer incidences in the UK was more than 324,500 in 2011, with a mortality rate of 7.6 million cancer combined deaths globally (Cancer Research UK). Various chemotherapies are employed for treatment with efficacy reported as 25 % by Glaxo Smith Kline. In addition, chemo-resistance is frequent problem, and different molecular signatures exist dependant on the individual. Thus more effective anti-cancer strategies are necessitated, in particular focusing upon the molecular deviations that govern a particular tumour.

The biological features of cancer progression to tumour formation has been coined by Hanahan *et al.* (2000) of six tumour phenotypes required for full malignancy; self-sufficiency of growth signals in oncogenes, insensitivity to anti-growth signals, evasion of apoptosis, sustained angiogenesis, limitless replicative potential and lastly tissue evasion and metastasis. Two further emerging phenotypes have recently been described; deregulated cellular epigenetics of reprogrammed cellular energy metabolism and immunological evasion (Hanahan and Weinberg, 2011).

Genetic changes of human cancers are typically due to two distinct types; gain of function proto oncogene mutations resulting in oncogenic transformation and activation, thereby promoting cell growth, and loss of function mutations in tumour suppressor genes resulting in failure of functions such as activation of anti-proliferative programs and maintenance of DNA replication and integrity resulting in genomic instability. The tumour suppressor p53 protein for example has a crucial role as it is

mutated in over half of all human cancers. More than 26,000 mutations of p53 are recorded within the International agency for cancer research (Suzuki and Matsubara, 2011). In this form, loss of function results in failure of p53 tumour suppressive activities. Indeed, p53 is considered pivotal to tumour development and as such has been the focus of extensive research for its role in both cancer development and therapeutic strategies, in particular for reactivation of its regulatory pathways (Lane, 2010).

4.1.3.1 p53 overview

The p53 protein was first described in (1979) by Levine *et al.* as an oncogene which accrued within cancerous cells nuclei. Later studies on wildtype p53 however confirmed its definitive function as a tumour suppressor, and transcription factor with a crucial role in cancer, maintaining genomic integrity and as such is termed as 'the guardian of the genome' (Levine, 1997). Since then the complexity of p53 within its intricate network has unravelled with over 85,000 publications to date (May, 2016), linked with the keyword p53 pathways and more than several hundred p53 responsive genes described (Riley *et al.*2008). The significance of p53 as a tumour suppressor is highlighted by the fact that over 50 % of human cancers comprise p53 gene mutations or defects within p53 regulatory pathway.

p53 protein is a stress responsive transcription factor, stabilised and activated in response to cellular stresses of a genotoxic and non-genotoxic nature including; DNA damage, hypoxia, nutrient deprivation and oncogenic activation (Levine, 2009). Once activated, p53 initiates a transcriptional program via a complex network of multiple signalling layers to promote cellular homeostasis and genomic integrity. This may result in several biological outcomes dependant on stress type, severity and cellular / tissue context that include cellular senescence, apoptosis, cell cycle arrest, and angiogenesis (Anderson and Appella, 2009).

The vast amount of literature on p53 and interacting proteins has made it less amenable to a greater understanding of p53 pathways involved in tumorigenesis. Thus, dissecting these pathways that govern p53 is fundamental.

4.1.3.2 The tumour suppressor p53 – role in cancer

p53 is a powerful tumour suppressor protein, with various anti-proliferative roles in response to aberrant cellular stresses (Anderson and Appella, 2001). p53 displays all the characteristics of a tumour suppressor gene (TSG):

i. TSGs are recessive and undergo biallellic inactivation in tumours (loss of both alleles) (although p53 is considered a recessive TSG, several studies have shown a profound effect from loss of one allele or inactivation via a single mutation
ii. Inheritance of a single mutant allele accelerates tumour susceptibility formation
iii. The same gene is frequently inactivated in sporadic cancers
iv. It has a powerful anti-proliferative role

Under homeostatic conditions, a latent form of p53 exists at low concentrations. However, in response to stresses such as DNA damage, increased p53 levels result in its stabilisation from attenuation of its negative regulator E3 ligase Murine double minute 2 (MDM2) or HDM2 in human. Consequently, p53 initiates an anti-proliferative program transcriptionally activating or repressing target genes. Abrogation of this pathway or its components, specifically p53 has been shown to contribute to tumour formation and cancer (Vousden and Lane, 2007).

The fundamental role of p53 and its network is highlighted by the rare familial Li-Fraumeni syndrome, a dominant inherited disease arising from germline mutations where individuals are predisposed with premature onset to leukaemia, breast cancer and osteosarcomas arising from abrogation of apoptotic and senescence programs by DNA damage checkpoint defects (Malkin *et al.* 1990). p53 mutations or inactivation are present in over half of all human cancers, with the non-mutated allele typically lost. Indeed, p53 gene null mice are tumour prone and susceptible to neoplastic disease (Reinhart *et al.*2012).

Mutations are variable between tumour types, with p53 mutation hot spots typically located in its central DNA binding domain (figure 4.1.2), and include cancers of skin,

bladder, lung, liver, breast, colon and more. Mutations are largely missense (80%), with aberrant modifications imposing several diverse effects on gene activity dependant on locality. For example, mutations within the promoter region may result in cellular p53 decrease or absence, whilst those within the protein coding region may impact gene expression or protein activity. Furthermore, a mutation type may dictate different elements of p53 signalling pathways. For example, some p53 mediated responses may be lost, whilst other p53 mutations may confer gain of wild type function directly enhancing cancer progression, and include interactions with related p63/p73 (Goh et al. 2012). Lastly, mutated components of the pathway may directly affect p53 activity such as mutated ATM, which causes ataxia telangiectasia (Malkin et al. 1990). This highlights not only the importance of p53 in cancer, but that a fully functional and regulated level of p53 is fundamental to maintain a tightly co-ordinated network and response for genomic integrity.

Recent studies have highlighted the importance of p53 in other pathologies including longevity, diabetes mellitus and myocardial infarction (Reinhardt et al.2012). Taken together, these studies demonstrate the comprehensive role of p53 in numerous processes including cancer and inflammation.

4.1.3.3 TP53 gene and structure

p53 is a nuclear protein encoded by a 20kb gene, comprising 11 exons and 10 introns located on the short arm of chromosome 17. p.13. Wild type p53 contains 393 amino acids composed of several structural and five functional domains crucial for mediating interactions (figure 4.1.2). The N- terminal domain (1-43) constitutes two adjacent transactivation domains; TAD1 and TAD2 where the majority of phosphorylation occurs. This is typically in response to DNA damage. TAD2 overlaps the proline rich region (63-97) with important roles in apoptosis, transcriptional activation and repression (Lin et al. 1994) and p53 activation as shown proceeding gamma irradiation (Campbell *et al*. 2013). Redundancy is observed at the N- terminus, where a single site may be phosphorylated by several kinases, conversely a single kinase may phosphorylate multiple sites. The DNA binding domain (DBD) (102-292) constitutes the core site specific DNA binding site of p53, ensuring p53 function as a transcription

factor, regulating expression of target genes. The majority of human mutations (90%) occur within the DBD corresponding to highly conserved II – V regions. These result in loss of wildtype function and thus the inability to bind to the consensus sequences within promoters of p53 responsive genes (Sigal and Rotter, 2000). The C- terminal region (323-393) constitutes the tetramerisation domain (TD) and C-terminal regulatory region (CRD). Here sequences are involved in nuclear localisation, regulation and tetramerisation. The formation of p53 tetramer is pivotal to p53 dependant trans-activation and suppression (Kruse, 2009). This regulatory region comprises a non-specific DNA binding domain that binds to damaged DNA and, undergoes several post translational modifications crucial to p53 activity and control (Loughery and Meek, 2013).

4.1.3.4 Regulation and control of the stress responsive transcription factor p53

The tumour suppressor p53 is a stress responsive transcription factor, mediating the expression of a plethora of target genes via interactions with numerous co-factors. As such, p53 activity must be tightly regulated and maintained at steady state levels. Adverse effects of decreased or increased p53 activity have been demonstrated in various mouse models of altered p53 levels using gene manipulation studies (Tyner et al. 2002: Dumble *et al.* 2007). p53 null mice were largely tumour prone, in contrast p53 $^{+}/^{+}$ mice were less tumour susceptible, yet displayed other pathologies that were age related.

In its latent state the half-life of p53 is limited to minutes and its function repressed by MDM2 (Kruse and Gu, 2009). In response to stress, the attenuated p53 – MDM2 complex stabilises p53 with its half-life prolonged to hours. Accumulated p53 is subject to extensive post translational modifications in response to genotoxic stress. PTMs are crucial to p53 modification and as such its activation, regulation and control (Toledo and Wahl, 2006). These include ubiquitination, phosphorylation and acetylation amongst others.

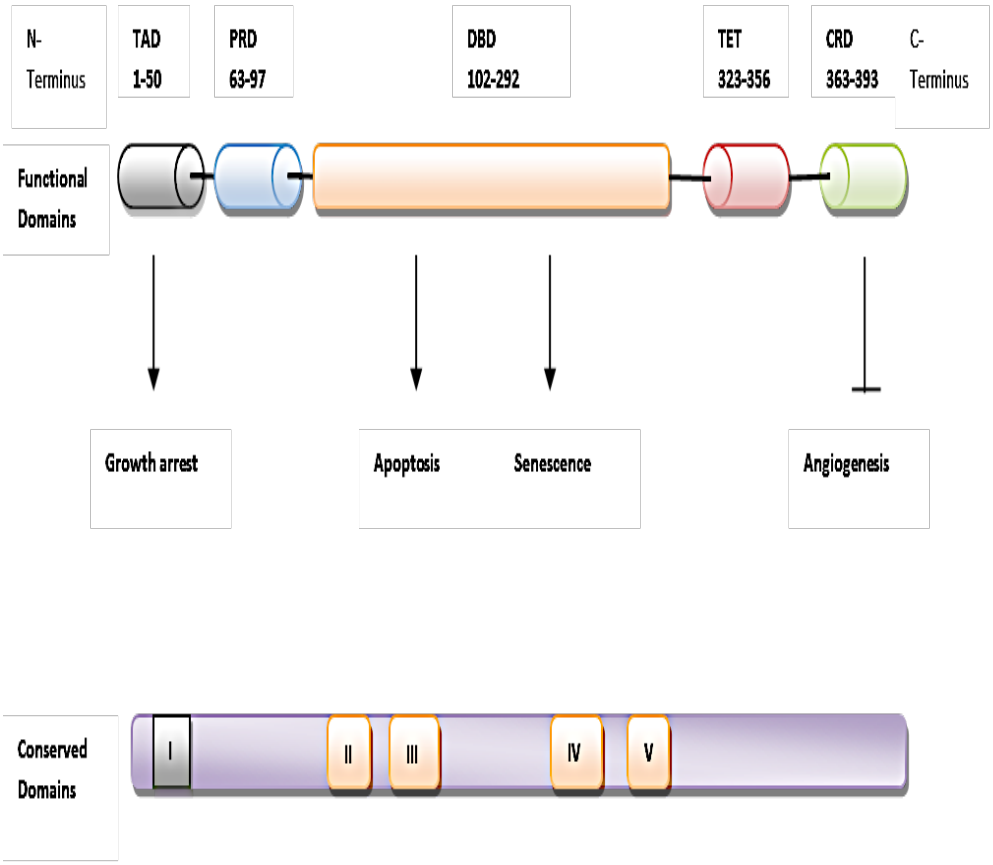

Figure 4.1.2 Functional and structural domains of p53 relating to the various anti-proliferative roles. Functional domains: comprising transactivation and proline rich domain within the N-terminus, the core DNA binding domain and the C –terminus of tetrmerisation and regulatory regions. These correspond to **highly conserved domains** of I, II – V respectively and highlighted by the same colour. Once activated p53 exerts its anti proliferative function by growth arrest, apoptosis, cellular senescene and angiogenisis inhibition with the functional p53 domains responsible indictated by arrows. TAD, transactivation domain, PRD, proline rich domain, DBD, DNA binding domain, TET, tetramesaristion domain and CRD, C terminal regulatory domain.

4.1.3.5 Post translational modifications of p53

4.1.3.5.1 Phosphorylation

Phosphorylation simply defined refers to the addition of a phosphate group to the one side of an amino acid chain of a protein. Due to the negative charge of phosphates, their addition results in modification of protein characteristics, typically

conformational. The organisation of kinases in response to a particular signal induces phosphorylation cascades. This reaction is reversible via de-phosphorylation catalysed by phosphatases allowing the protein to conform back to its original structure upon phosphate removal. Conformational modifications can induce subtle activity changes to the protein with phosphorylation typically activating. Phosphorylation events are catalysed by kinases where hydroxyl groups (-OH) of serine, threonine, tyrosine amino acid side chains the most important. TP53 has 23 different phosphorylation and de-phosphorylation sites typically within N and C-terminal regions. Following DNA damage p53 is phosphorylated by a plethora of kinases resulting in its stabilisation. Numerous kinases involved in phosphorylation have been described, some highlighted in figure 4.1.3.

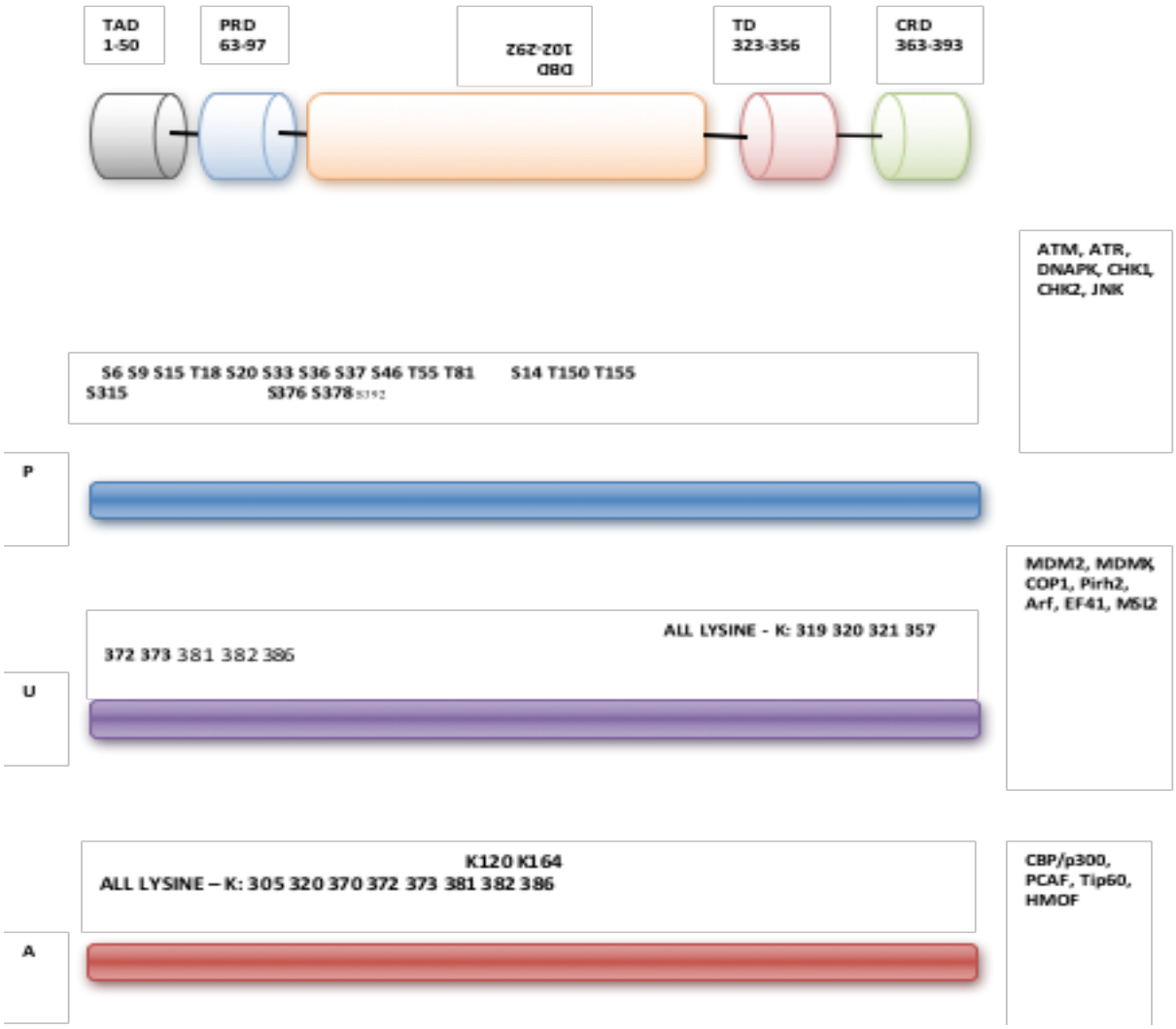

Figure 4.1.3 p53 post translational modifications: phosphorylation, ubiquitination and acetylation.

Specific PTMs are shown corresponding to p53 domains of TAD, transactivation domain, PRD, proline rich domain, DNA binding domain, TD, transactivation domain and CRD, C terminus regulatory domain. Modifying PTM enzymes are shown on the right, but not limited too. Compare this figure with figure 4.1.2 for anti-proliferative programs corresponding to functional domains. For example, Ser^{46} in DB is crucial for apoptosis induction. P – phosphorylation, U – ubiquitination and A representing acetylation.

Typically induced by DNA damage, phosphorylation of p53 is crucial for protein – protein interactions and potentially regulates target gene selectivity. For example, phosphorylation by Chk1 and Chk2 at Ser^{20}, ATR and ATM on Ser^{15}, and Thr^{32} by JNK (c-Jun N-terminal) kinases in response to DNA damage is crucial for disrupting and reducing the affinity of p53-MDM2 interaction, enabling a tighter association with co factors and nuclear accumulation (Buschmann *et al.* 2001: Anderson and Appella, 2001). Other phosphorylation events resulting in attenuation of p53 – MDM2 interaction are highlighted in figure 4.1. 4. For example, p16/ARF induced oncogenic stress inhibits MDM2. Indeed, the importance of phosphorylation on these sites for apoptosis has been demonstrated. Transgenic mice expressing mutated Ser^{15} and Ser^{20} residues displayed decreased p53 stability and an abrogated apoptotic response (Chao *et al.* 2006). Whilst Ser^{46} phosphorylation by DYRK2 (Dual specificity tyrosine-phosphorylation-regulated kinase) is pivotal for the induction of pro-apoptotic gene p53AIP1 and p53 dependent apoptosis evidenced by p53 knock in mouse (Tiara et al. 2007).

4.1.3.5.2 Acetylation

Acetylation refers to the addition of an acetyl group (CH_3CO). Similar to phosphorylation, acetylation is a reversible process via the action of HDACs (histone deacetylases). HATs are a well characterised acetyltransferase group (Histone acetyltransferases) due to their histone targets. HATs transfer an acetyl group from acetyl CoA to the terminal amino side chain of lysines (Legube and Trouche, 2003). Similar to phosphates, the addition and conversion of the +ve charged lysine to acetyl – lysine results in modification of protein conformation and trans-activities. For instance, histone acetylation typically results in the recruitment of co-factors, regulates transcription factors. This results in increased transcriptional activity, thus has a major

role in cellular fate. HATs in addition to histone chromatin opening also target transcription factors such as p53 to modulate their transcriptional activity. Acetylation is thus an important protein modification which correlates with increased p53 transcriptional activity (Kouzarides, 2000). The importance of p53 acetylation is three-fold: 1) promoting p53 stabilisation by eliminating ubiquitination on the same site, 2) it attenuates MDM2/MDMX complex on target gene promoters and lastly, 3) recruits co-factors for activation of p53 transcriptional activity.

Various studies have reported how DNA damage pathways activate p53 acetylation via acetyltransferases, or induce them via p53 phosphorylation. The C – terminus comprises six lysines that are targeted for acetylation by HATs and p53 transcriptional co factors. For example, p300 and CBP which include lysine sites: K305, K370, K372, K381, K382 and K386 (Meek and Anderson, 2009). MDM2 also targets the same C – terminal sites for ubiquitination. Therefore, a key function of acetylation is inhibition of ubiquitination and p53 downregulation (Li et al.2002). Acetylation also opposes MDMX and MDM2 recruitment, attenuating MDM2/MDMX – p53 complexes, resulting in transcriptional activation (Li *et al.* 2002). Acetylation of K320 in the TET domain by PCAF promotes activation of p53 responsive cell cycle arrest genes (figure 4.1.3) thus favouring cell survival over apoptosis (Knights et al.2006). In parallel, another study using mice expressing p53 (317 residue) lysine – arginine substitution (K320 in human) exhibited enhanced p53 dependant apoptosis following DNA damage (Chao et al. 2006). Furthermore, human cell lines expressing lysine – arginine substitution failed to induce apoptosis and cell cycle arrest by non-expression of pro apoptotic genes, yet retained the ability to mediate MDM2 expression (Tang et al.2008). This study concludes that non- acetylated p53 is able to sustain a negative feedback loop, however acetylation is a prerequisite for p53 function. Collectively, these studies indicate that acetylation is important PTM for p53 activities.

4.1.3.5.3 Ubiquitination

Ubiquitination refers to the process of covalent conjugation of one or more ubiquitin molecules to a specific protein substrate. Typically resulting in protein degradation.

This requires interactions of three enzymes: E1 ubiquitin activating, E2 ubiquitin conjugating and E3 ubiquitin ligating enzyme. TP53 comprises 20 lysine sites clustered around three locations: one within TAD, five at the N- terminus within the DBD, the remainder located within C - terminus. Ubiquitination is pivotal to p53 stabilization, activation and localization. One of the most important ubiquitination events of protein – protein interactions is the p53-MDM2 affiliation which lies at the core of the p53 network.

4.1.3.6 The p53-MDM2-MDMX relationship

As previously described, p53 expression must be tightly regulated and maintained at steady state levels for genomic integrity. Perturbation of this system may result in aberrant proliferation and malignant cellular phenotypes. This regulation is maintained through p53's primary negative regulator, oncoprotein RING finger type E3 ligase MDM2, and to a lesser extent, MDMX (MDM4).

p53 is maintained at low cellular concentrations through MDM2 26S mediated proteasome degradation and ubiquitination (Ringshausen et al.2006). This occurs on several lysine residues within p53 C-terminus as demonstrated *in vivo;* K101, K120, K132, K139, K370, K372, K373, K381, K382, and K386 (Feng *et al.* 2005) (figure 4.1.3). Mono and poly ubiquitination adds complexity to p53 regulation involving other key players. High levels of MDM2 induce p53 poly - ubiquitination, leading to degradation, with co factors E4 ligases CBP/p300 mediating this process. Lower levels induce mono-ubiquitination leading to p53 nuclear exportation and cytoplasmic translocation (Li et al. 2003). Mono-ubiquitination typically occurs on several lysine residues in the C-terminus as above. However, a recent study using spectrometry analysis has identified the central p53 domain as the dominant acceptor sites for MDM2 and E3 ligase PirH2 (Shloush et al.2012).

MDM2 expression is transcriptionally regulated by p53 within an auto regulatory feedback loop. MDM2 binds directly to p53 N - terminal transactivation domain, termed BOX-1 via negative feedback mechanisms inhibiting phosphorylation, p53 stabilisation and trans-activation function. The relevance of this feedback mechanism

has been demonstrated in early studies of MDM2 null mice which displayed embryonic lethality arising from over expressed p53, rescued only by simultaneous deletion of p53 (Montes et al.1995). Furthermore, dysfunction of this loop results in tumour prone cells. For example, mice over expressing MDM2 inhibit p53 function promoting tumorigenesis (Montes et al. 1995). Taken together these studies indicate MDM2 as p53's primary negative regulator.

Another important negative regulator, non E3 ligase MDMX, a MDM2 homolog, also binds to p53 trans-activation domain inhibiting p53 stabilisation and transcriptional activity, however with less efficiency than MDM2. MDMX contains a RING domain structurally similar to MDM2, however does not possess E3 activity (Jackson et al.2000; Stad et al.2001). Even so, MDMX has been shown to be as fundamentally important for p53 regulation. Similar to MDM2, loss of MDMX in mice models results in embryonic lethality and rescued only by p53 gene deletion (Zhang et al.2014). This feedback loop is therefore a key signalling pathway within the p53 network. The above summarises a modest version of p53-MDM2 relationship. Indeed, this core loop is embedded within an intricate network of p53 responsive genes which converge onto the p53 / MDM2/MDMX axis providing additional layers of complexity and regulation to the p53-MDM2 pathway and network.

4.1.3.7 The p53 network

p53 along with its upstream regulators and downstream effectors comprise a complex network of multiple signalling layers. As previously stated, dysfunction of this pathway arising from deregulation of its components, specifically p53 may result in tumour formation. Indeed, majority of human cancers acquire mutations which abrogate p53 network. This complex network may be divided into several layers as highlighted in figure 4.1.4 of a simple model comprising upstream and downstream events and the network core- p53 and MDM2.

4.1.3.7.1 Upstream events

p53 activation typically manifests in three distinct steps; stabilisation, sequence specific DNA binding and transcriptional activation or repression of target genes in response to genotoxic and non-genotoxic stresses that include; ultraviolet, ionising radiation or oncogenic stress and hypoxia respectively. Activation and induction of p53 are important steps for initiating the anti-proliferative program, however many questions remain unanswered regarding pathways and upstream signals that initiate p53 activity, highlighting the complexity of the network (Loughery and Meek, 2013). Whilst both genotoxic and non-genotoxic stresses are important processes for tumorigenesis, this report focuses upon upstream genotoxic stresses of DNA damage only.

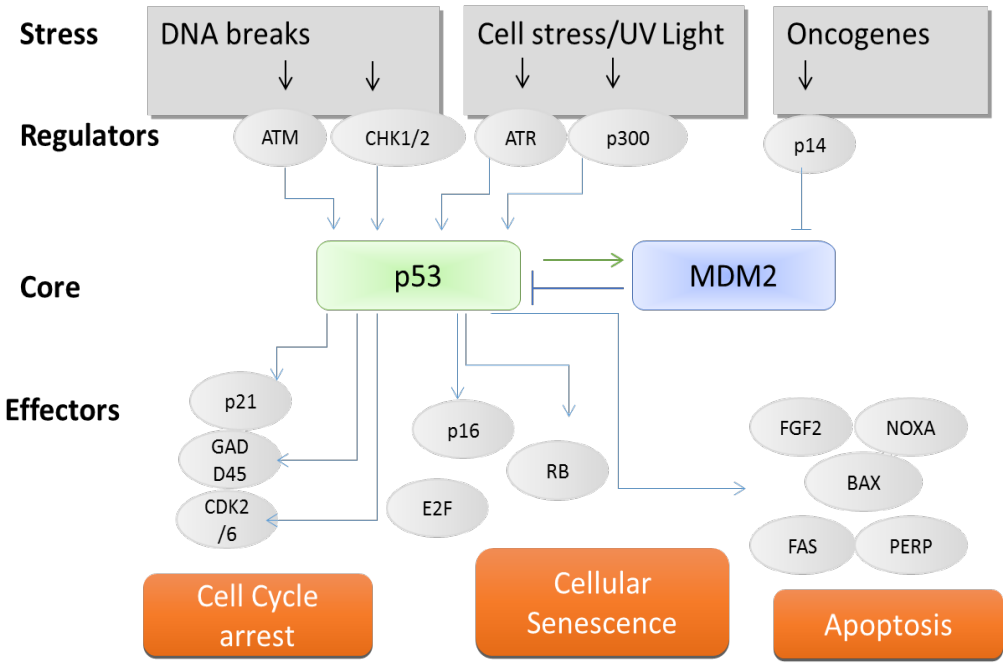

Figure 4.1.4 A simplified model of the p53 network
The p53 pathway is complex. At least 50 different proteins can modify p53s stability, cellular location or activity. The above image depicts a minority of these. Five layers of regulation are observed; Cellular stresses including DNA damage, and oncogenic activation. Upstream regulators that activate p53, the p53-MDM2 core for p53 stabilisation, lastly p53 responsive downstream effectors which elicit the different responses dependant on stress severity and type. A single effector may regulate different processes. For example, E2F1 and p21 can exert effect on both cell cycle arrest and senescence.

4.1.3.7.2 DNA damage

The integrity and fidelity of DNA is crucial for accurate hereditary genetic replication. DNA is continually exposed to endogenous and exogenous stresses including reactive oxygen species arising from metabolic processes, ionising radiation, ultraviolet lights, and chemicals respectively. A tightly controlled and competent DNA damage response arising from DNA lesions and chromosomal damage is pivotal, allowing for DNA repair, genomic integrity and thus inhibition of tumorigenesis

Dependant on DNA damage type and severity, p53 regulatory pathways may initiate cell cycle arrest or apoptosis for repair or cell death respectively. For example, moderate DNA damage induces a slight increase in p53 levels resulting in transient cell cycle arrest, whilst severe and irreparable damage results in highly increased p53 levels and apoptosis (Vousden and Liu, 2003). Severe DNA damage such as in transcription-coupled repair defects appears to display constitutive DNA damage signalling, however a loss of DNA damage downstream effectors appears to display a tumour susceptible phenotype. Indeed, p53 gene null mice are tumour prone and susceptible to neoplastic disease (Jacks *et al.*1994). The severity of DNA damage also impacts p53 dynamics of a bimodal switch function in U20S and A549 etoposide treated cell lines in a dose dependant manner which shifted cell profile fate. Mild DNA damage induced at lower etoposide concentrations resulted in periodic oscillations of p53 activity and cell cycle arrest, whereas, at higher levels of etoposide (100 μmol/l) strong monotonic increases of p53 where observed with a cell profile shift to apoptosis. Moreover, this DNA damage dose dependant bimodal switch was induced by differential MDM2 upregulation with higher levels allowing continuous accumulation of p53, conversely, lower levels dictated cellular fate (Chen *et al.*2013). Indeed, this coincides with p53 activity, for example prolonged p53 stabilisation leads to expression of pro apoptotic genes (Jackson and Bartek, 2009).

4.1.3.7.3 Hypoxia

Hypoxia results from an insufficient oxygen supply that compromises biologic processes. Along with cancer, tissue hypoxia is implicated in various pathologies

including those of pulmonary, cardiovascular and inflammatory origin (Airley *et al.*2000).

Hypoxia is a characteristic state in solid tumours (Vaupel and Mayer, 2007) arising from the oxygen deprivation in the tumour microenvironment, and, along with ischemia initiates the various processes associated with tumour angiogenesis (Ching et al.2010). Tumour hypoxia can be defined dependant on severity typically being a reduction of oxygen consisting of less than 10 – 15 mm Hg partial pressure of internal oxygen (pO2) or, severe hypoxia pO2 <0.33%, 2.5 mmHg (Khan *et al.* 2012).

Hypoxia is associated with tumour aggressiveness, progression and a poor patient survival rate (Chang *et al.*2011). Low oxygen levels in tumour cells reduce the efficacy of anti-cancer treatments resulting in a resistant tumour. This is largely due to the fact that specific anti-cancer drugs or ionising radiation require oxygen free radicals to effectively destroy cells. Additional drug resistance arises from the low oxygen levels that reduce cell proliferation and enhance growth arrest. This is problematic as anti-cancer drugs typically target high proliferating cells. Moreover, the reduced oxygen level results in ineffective drug delivery to the intended hypoxic region. Thus, elucidating the molecular mechanisms of hypoxic regulation is of central importance to effective cancer strategies.

The biological and molecular signatures of hypoxic tumours to normal tissues are distinct. The insufficient vasculature in a solid tumour mass results in a heterogeneous, dynamic micro - environment of perturbed molecular signatures, promoting genomic instability via point mutations, gene amplification or inhibition, and chromosomal rearrangements and low pH and glucose concentrations.

The transcription factor HIF-1a is well postulated as the main hypoxia inducible gene. Under normoxic conditions the tumour suppressor, VHL ubiquitinates and degrades HIF – 1a conversely, under low oxygen levels this interaction is inhibited (Ziello *et al.*2007). It is well established that hypoxia promotes angiogenesis, a situation created from the metabolic demands of the proliferative tumour. HIF-1a dependant induction of VEGFA is central to this process inducing endothelial cell migration and tumour survival and is highlighted by the fact that HIF- 1a levels correlate with tumour grade (ZagZag *et*

*al.*2000). Upon activation, HIF-1a regulates a plethora of target genes involved in proliferation, vascularisation and glucose metabolism.

Even though in the majority of tumours, p53 pathways are inactive and hypoxia tolerance can result from the loss of p53, hypoxia at 0.02 % O2 can activate p53 and its apoptotic pathways independent of HIF – 1a (Soussi and Beroud, 2001; Hammond and Giaccia, 2005). However, the activity of p53 and its resultant induction of typical target genes differ to those induced by DNA damage. It has been postulated that this is due to the failure of CBP and p300 co factor recruitment to p53 promoters (Hammond *et al.*2006). Additionally, under these hypoxic conditions, p53 activity is typically trans-repressive rather than trans - activating. For example, p53 acetylation by PCAF at K320 is decreased under low oxygen conditions. The acetylation of this residue has been determined as crucial for the induction of p53 target genes (Xenaki *et al.*2008). Moreover, hypoxia induced p53 has also been shown to interact with the transcriptional corepressor mSin3A in place of its traditional co activator p300 (Koumenis *et al.*2001). Only a few hypoxia regulated p53 dependant inhibited genes have been described such as BIRC3 and p21 (Long *et al.*1997; Liu *et al.*2007). With this in mind, uncovering the hypoxic pathways that govern p53 is of importance.

4.1.3.8 Downstream events

In response to stresses, activated p53 protein functions as a transcription factor inducing a transcriptional program reflecting the stress signal and corresponding proteins and their modifications. Upon activation, p53 represses or activates its downstream target genes binding mainly to a specific 21 nucleotide DNA sequence termed the responsive element (El-Deiry *et al.* 1992). These effector genes which work in concert may initiate various independent anti- proliferative outcomes, discussed below.

4.1.3.8.1 Cell cycle arrest

The cell cycle constitutes several important phases; S phase (DNA synthesis), M phase (mitosis) and the gap phases G_O and $G_1/_2$. In response to various stresses such as DNA damage, cells may undergo growth arrest at the various checkpoints for prevention of

DNA mutations prior to replication. Checkpoints are important stages which ensure fidelity and accuracy of cell division during each phase prior to proceeding to replication. The various checkpoints are regulated by various cyclins (cell cycle proteins), CDKs (Cyclin dependant kinases) and their inhibitors, CDKIs (Cyclin dependant kinase inhibitors). Negative modulators of the cell cycle, CDKIs constitute two families; KIP/CIP (p^{21}, $p^{57KIPII}$ and $p^{27KIPII}$) and INK4 (p^{19Ink}, p^{18Ink} and p^{16ink}). These are highlighted in figure 4.1.5.

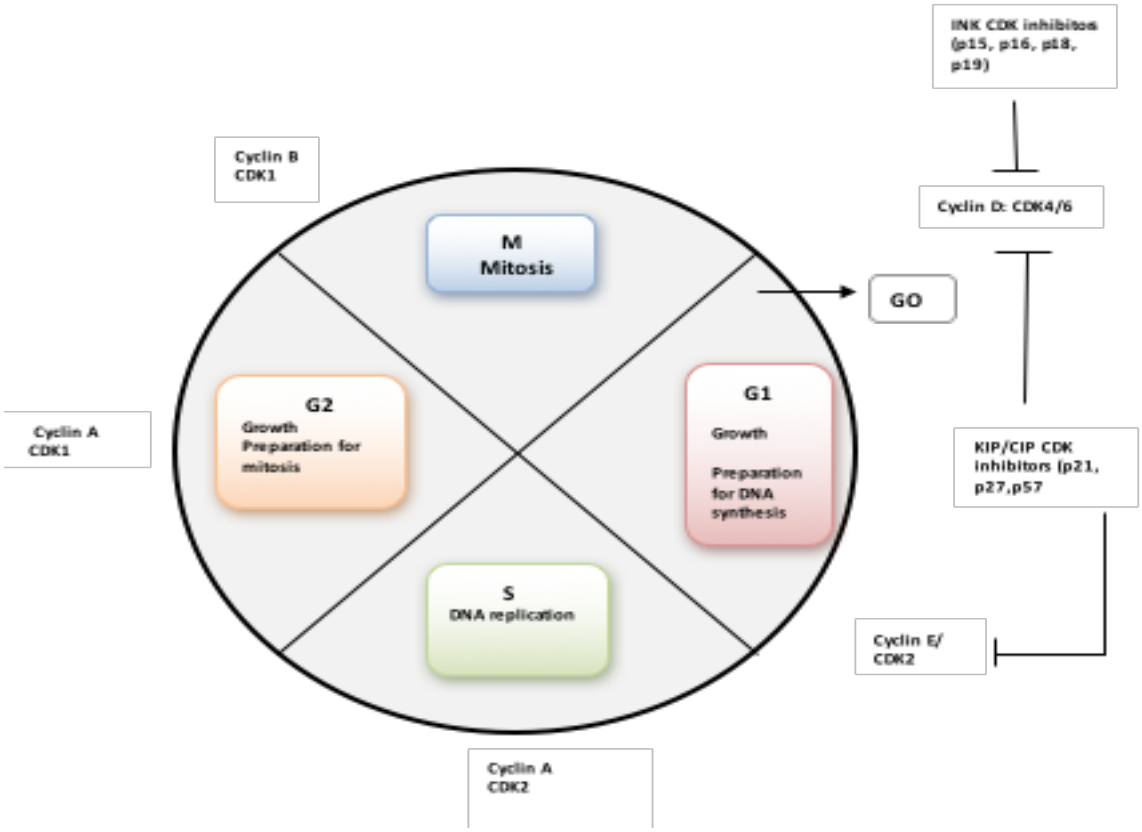

Figure 4.1.5 Cell cycle phases and the corresponding CDKs and CDKIs

The four different phases are shown. Cell-cycle checkpoints G1/S and G2/M control cell-cycle transitions, ensuring the critical events (DNA replication and chromosome segregation) are completed correctly pre progression. The major cell-cycle restriction point (R) is located the end of the G1 phase. After this point, they will complete cell cycle. Progression through M is via CDKs and their activating cyclin subunits. CDK activity is suppressed by CDKIs: INK4 family which selectively inhibits CDK4/6, and the CIP/KIP family which displays a wider CDK inhibitory activity range.

In response to DNA damage, p53 trans-activates these downstream effectors to promote cell cycle arrest. Many key upstream regulators and downstream p53 effectors have been extensively described, some highlighted in figure 4.1.6 of DNA damage utilising the p53/p21/pRB/E2F pathway. Feedback loops exist, specifically RB, E2F1 and CDK2 (retinoblastoma protein, E2F transcription factor 1, cyclin dependant kinase 2) (Yi *et al.*2013). The upstream ATM/ATR pathway has shown to be pivotal for p53 activation and subsequent expression of downstream targets for G_1 arrest as shown in murine embryo fibroblasts in response to DNA damage. Disruption of the p21 gene has demonstrated abrogation of the $G_1/_S$ checkpoint in MEFs which extended their lifespan displaying a proliferative phenotype; as such G_1 arrest through this pathway is primarily induced via p53 - p21 (Deng *et al*. 2005). The trans-activation of p21 by p53 can inhibit CDK2/cyclin E as such retinoblastoma (RB) cannot be phosphorylated. Activated RB leads to E2F1 inhibition and as a result, cells undergo proliferation arrest for DNA damage repair with failure of cell cycle completion (Dulic *et al*.1994). Moreover, p53 downstream target p21 has shown to be a key player with various effector functions in cell cycle regulation. For example, p21 induces inhibition of CDK4 and PCNA (Proliferating Cell Nuclear Antigen) preventing DNA synthesis in response to DNA damage (Rousseau *et al,* 1999). Other important checkpoint arrests induced by p53 in response to DNA damage include for example: $G_2/_M$ arrest from repression of mitosis promoting phosphatase cdc25c and also 14-3-3a (St Clair and Manfredi, 2006).

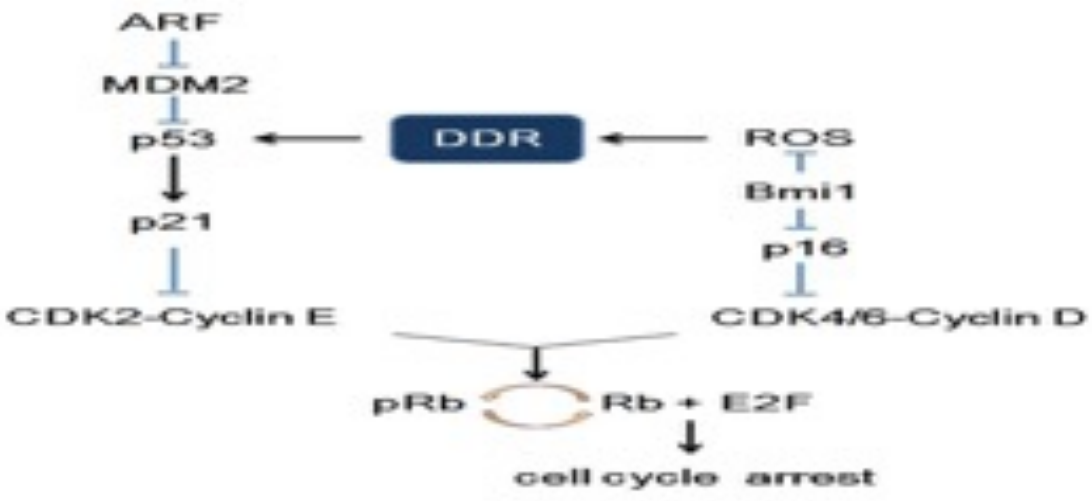

Figure 4.1.6 DNA damage response utilising the p53/p21/pRB/E2F pathway.
The *INK4a/ARF* locus encodes both ARF / p16 protein. ARF stimulates and activates p53 through inhibition and degradation of MDM2, in turn trans -activating p21. p21, which inhibits CDK2/cyclin E with the consequent inhibition of CDK2-dependent phosphorylation of Rb. Un phosphorylated RB suppresses the function of the G1/S phase-promoting factor, E2F, resulting in proliferation arrest and DNA damage repair. Similarly, p16 may inhibit CDK4-6/cyclin D complex thereby reducing Rb phosphorylation and subsequent downstream signal transduction pathways, resulting in G1 arrest. Bmi1 has a inhibitory role on ROS (reactive oxygen species).

4.1.3.8.2 Cellular senescence

Senescence is a permanent form of cell cycle arrest, first described in human fibroblast cells (Hayflick, 1965). Senescent cells are relatively stable, lack proliferation yet retain metabolic activity, contrasting cancerous cells which are invasive with uncontrolled proliferation and resistant to apoptotic signals. The importance of senescence in repression of tumorigenesis has been highlighted with senescence gene mutations frequently associated with tumour progression. Indeed, senescent cells have been identified in various pre malignant human tumours (Chen *et al*.2005). The RAF / MEK pathway downstream of oncogene Ras seems to be the most important in activating the senescence program (Loughery and Meek, 2013).

Senescence cellular phenotypes are distinct; morphologically larger and flatter comprising intracellular particles. In normal cell growth, replicative senescence is induced upon maximum telomere length and thus cell proliferation halted (Herbig *et al.* 2004). DNA damaged induced premature senescence however is via oncogene

induced replicative stress, or oxidative stress (Bartek *et al.*2008), utilising different pathways. For example, premature senescence is signalled by either downstream p53/p21/pRb/E2F or p16/p21/pRb/E2F pathways, along with anti -proliferative mir-34. In contrast regulators of replicative senescence are induced by p53/p21/pRb/E2F solely (Campisi *et al*.2005). As such senescence markers include β-galactosidase, p53INK4b and p53INK4a cyclin kinase inhibitors (Campisi *et al.*2007). A link between both p53 and RB have recently been described for the E421 transcription factor functioning as a direct p53 target for senescence, inducing repression of several E2F target genes promoting cell cycle arrest and tumorigenesis development (Aksoy *et al*.2013). This highlights the importance of p53 as core regulator, p21 as a key player and retinoblastoma protein for the tumour suppressor pathway consistent with senescence being a permanent form of cell cycle arrest.

4.1.3.8.3 Apoptosis

The role of p53 and apoptosis was first described in p53 wildtype leukemic cells which displayed apoptotic characteristics such as chromatin condensation and fragmented nuclei (Yonish-Rouach *et al.* 1991). Later studies shortly thereafter revealed that p53 dependant apoptosis contributed to chemotherapeutic induced cell death against DNA damaging stresses (Lowe and Ruley, 1993). Indeed, p53 inactivation in lymphoma mouse model demonstrated accelerated tumour development with increased invasiveness (Eiscen *et al.*1999: Schmitt *et al.* 2003). The apoptotic program is complex and regulated at multiple levels. It operates by two main pathways of intrinsic and extrinsic referring to cell death receptor pathway and intrinsic mitochondrial activity respectively. p53 is a master regulator of both, however p53 – dependent apoptosis typically follows the mitochondrial pathway.

I. Extrinsic Pathways

p53 – dependant apoptosis involves both transcription dependant and independent p53 mechanisms in concert. The extrinsic pathway as stated is also p53 regulated, however less is understood regarding the overall program

leading to apoptosis than intrinsic. FAS / CD95, DR5 death receptor and TNFSF6 the gene encoding FAS loci are all direct p53 targets inducing expression of FADD and TRADD (Fas –TNFRSF6-associated via death domain and TNFRSF1A-associated death domain respectively). These in turn initiate a caspase cascade via caspase-8 orchestrating the apoptotic program. Conversely, p53 may induce apoptosis via repression of anti-apoptotic genes, further promoting caspase expression (Hoffman *et al.*2002). Considerable cross talk exists within the caspase cascade between both signalling pathways including p53s ability to trans-activate BID, further facilitating the crosstalk between intrinsic and extrinsic pathways, (Sax *et al*. 2002). Similarly, apoptotic inhibitors such as the candidate therapeutic target - IAP protein (Vucic and Fairbrother, 2007) was also observed in both pathways functioning to prevent apoptosis, maintaining tumour survival. Either way, p53 can sensitise cells to death receptor ligands enhancing the apoptotic program.

II. **Intrinsic pathway**

At the mitochondria p53 tran-sactivates various pro-apoptotic genes of intrinsic pathway in response to various cell death signals such as DNA damage including; PIG3, perp, Killer/DR5 and members of the Bcl-2 family, such as BAX, Puma and NOXA (Riley *et al.*2008). Gene targeting studies in mice models and in various cell lines have demonstrated the importance of p53 inducing these downstream effectors during apoptosis for repression of Bcl-2 members. For example, Bax null mice embryo fibroblasts are desensitised to p53 oncogene induced apoptosis resulting in enhanced tumorigenesis *in vivo* and *in vitro* (Yin *et al.* 1997). Bcl2 members down regulate pro-apoptotic genes BAK and BAX, which in turn release cytochrome c enhancing apoptosis via the caspase cascade. Whilst puma knockout mice display decreased apoptosis with NOXA contributing to this outcome (Jeffers *et al.*2003). Even so, the complexity of p53 pathways is highlighted in this study that Puma null mice were not overly tumour susceptible, thus signifying the requirement of various p53 effector targets for inducing tumorigenesis. This complexity is further evidenced by

cross talk within the p53 network of a particular effector comprising more than one function. For example, p21 functions in cell cycle arrest, however has the capability to attenuate apoptosis (Seonane *et al.*2002), similarly for the described miR34 mRNA family (He *et al*.2007).

The existence of feedback loops, pathway cross talk and synchronous effector functions with various gene deletion studies creating phenotypes of a particular effector loss, yet p53 and other effector functions remain intact; highlight the complexity of the p53 signalling network holistically as a tumour suppressive program. Therefore, dissecting the p53 network and its components are crucial to gain a better understanding of its role in cancer and development of effective therapies.

4.1.3.8.4 Angiogenesis

Angiogenesis may be defined as the formation of new blood vessels and vasculature. This is a complex process requiring the synchronised activity of various cell and vascular components; endothelial cells division and later migration, with vascular basement membrane and surrounding extracellular matrix degradation (Folkman, 2002). In adults, angiogenesis is involved in many normal physiological processes including wound repair, ischemia and embryogenesis (Ching *et al.* 2010). Its role in cancer pathogenesis has been well defined. Both tumour growth and metastasis are dependent on angiogenesis and lymphangiogenesis. Indeed, angiogenesis is characterised as one of the hallmarks of cancer (Hanahan and Weinberg, 2011) where quiescent endothelial cells display a proliferative phenotype in response to pro angiogenic signals.

Hypoxia is a characteristic state in solid tumours (Voupel and Mayer, 2007). This arises from oxygen deprivation in the tumour microenvironment that initiates various processes associated with tumour angiogenesis (Ching *et al*.2010). Other stimulus includes mechanical stress and hypoglycaemia (Ferrara, 2004). The' angiogenic switch' whereby tumours progress exponentially to propagate past their primary location from unbalanced equilibrium of pro and anti angiogenic factors has been observed in both human tumour and experimental models (Folkman, 2002). These various studies have led to the characterisation of a plethora of angiogenic factors involved in tumour angiogenesis. In particular, VEGFA, a potent pro angiogenic factor (Ferrara 2009).

Under normal physiological processes, the angiogenic network is tightly controlled. Conversely, in tumour angiogenesis perturbation of this controlled network is typical due to an upregulated state arising from the shift 'switch' between pro and anti angiogenic factors (Folkman, 2002). Hypoxia is the most well studied stimuli for tumour angiogenesis. This hypoxic micro-environment stimulates the angiogenic network resulting in sprouting angiogenesis (sprouting of blood vessels) from adjacent tissues into the tumour (Folkman, 2002). Growth of the tumour at this stage around 2 mm in diameter is typical. Angiogenesis pathology may be defined by a change in endothelial cell phenotype to that of invasive and proliferative with atypical tumour vasculature morphology arising from structural abnormalities of venules, capillaries and arterioles. The typically tight vasculature becomes leaky due to the loose EC monolayer.

The angiogenic signalling network involved in tumour pathogenesis is both complex and dynamic. It comprises a plethora of pro and angiogenic signals including angiopoietins, endothelial and oxygen sensors, growth factors and integrins, in addition to various others described in detail in (Ferrara, 2004). Numerous studies *in vivo* and *in vitro* have uncovered numerous key pro angiogenic factors involved in this process; VEGF, TGFβ, IL-8, angiogenin and growth factors: endothelial, placental, hepatocyte and epidermal, probably the most significant (Nishida *et al.*2006). In particular, the VEGF family (A-D), (Ribatti, 2008). Each has varying angiogenic roles differing in their receptor binding specificity dependant on function and tissue. VEGF C and D are typically involved in lymphanogenesis, whilst the role of VEGFB is less defined (Nishida

et al.2006). VEGFA however is a well characterised pro angiogenic stimulator inducing various independent angiogenic cascades. This heparin binding glycoprotein constitutes six isoforms as a consequence of alternative mRNA splicing (Stalmans *et al.*2002). Figure 4.1.7 depicts a simplified view of hypoxia induced VEGFA angiogenic pathways.

VEGFA expression is highly regulated by the HIF family members, particularly HIF-1a (Ribatti *et al*.1999). However, hypoxia induced VEGF expression may also be via HIF independent mechanisms (Mizukami *et al*.2007). EGF, TGFβ cytokines along with p53 are also pivotal in inducing VEGF expression by several different mechanisms (Dvorak *et al*.1999). VEGFA is the most studied member and its increased expression is correlated with poor patient prognosis. VEGFA intra-tumoral expression has been observed in various tumours including breast, lung, ovarian and bladder (Ferrara, 2004). VEGFA mechanism of action is exerted via interaction with tyrosine kinase receptors; VEGFR-1/2, resulting in perturbed effects to vascular ECs and an aggressive tumour phenotype. This is characterised by extracellular matrix degradation, increased vascular permeability and enhancement of EC survival via opposing apoptosis (Ferrara, 2004), thereby allowing tumour formation and progression. These various different, yet overlapping independent angiogenic pathways are challenging. Indeed, numerous anti angiogenic therapies targeting VEGF have low efficacy with limited clinical success. Some has even shown to promote cancer progression by increased invasion and metastasis (Ribatti, 2010). This inefficacy is probably as a result of such complexity and resistance. Even systematic approaches have been used to dissect angiogenic network dynamics for effective single and multi-combined angiogenic therapies (Montanez *et al.*2011).

Given this, elucidating the role of pro and anti angiogenic factors, identifying effective markers and targeting these pro-proliferative processes is pivotal to implementation of successful anti-cancer therapy.

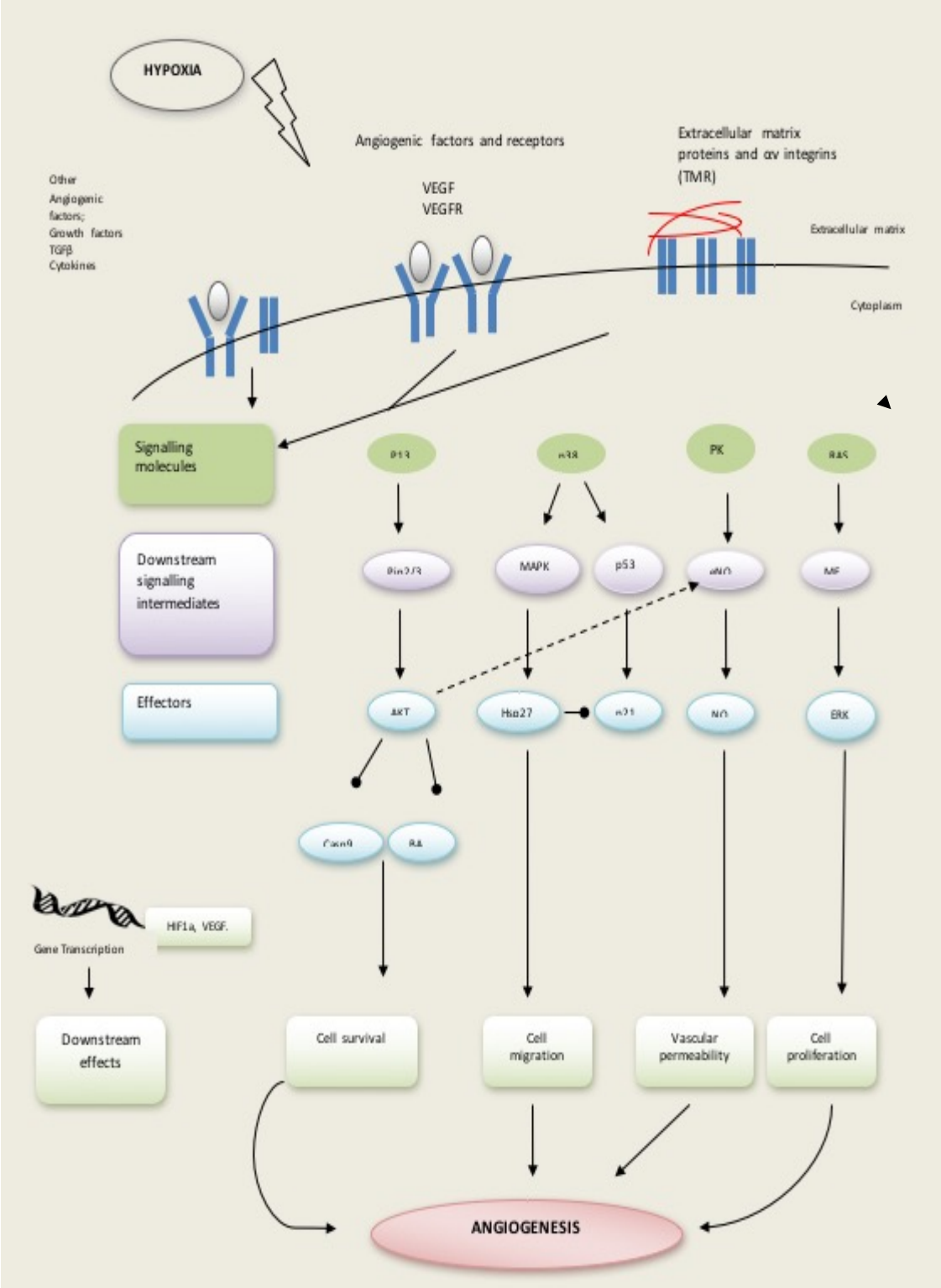

Figure 4.1.7 A simplified view of the hypoxia induced angiogenic pathway via VEGF
VEGFA activation via VEGFR induces several pathways to induce angiogenesis via cell proliferation, survival migration and vascular permeability. Signalling via RAS/MEK.ERK induces expression and proliferation. Signalling via PLC activates PKC which results in increased intracellular Ca+ inducing vascular permeability by Nitric oxide (NO) production and also prostaglandin (Not shown). FAK (focal adhesion kinase) signalling results in cell migration. VEGFA induction of p38 results in MAP2/3 and hsp27 activation and subsequent cell migration.

p38 further induces p53 with p21 activation, however hsp27 inhibits p21 affecting cell cycle arrest. The p13K pathway ensures cell survival via PI3K activated conversion of PIP2 to PIP3. This results in cellular membrane translocation and activation of AKT which also induces endothelial NO synthase further affecting vascular permeability, however in parallel inhibits caspase 9 and BAD (Pro apoptotic genes) thus maintaining cell survival. Other angiogenic inducers; αv integrins, (transmembrane receptors which bind EM proteins promote sprouting), cytokines such as IL6, and growth factors including FGF2 and PDGFRB.

4.1.3.8.5 DNA repair

Genotoxic and non-genotoxic insults arising from endogenous and exogenous sources continually challenge genome integrity. Over 10,000 estimated DNA damaging insults are thought to impose on each human cell per year (Lindahl and Barnes, 2000). These can impinge upon all normal cellular functional aspects with severe consequence to cell homeostasis. Transcription and replication may affect cell viability, whilst DNA lesions arising from DNA damage may induce mutations contributing to aging or diseases such as cancer (Lindhall and Barnes, 2000). DNA repair mechanisms are pivotal for reversal and elimination of intrinsic and extrinsic damage. The DNA damage response (DDR) is a controlled cascade of signal transduction events that has evolved to maintain genomic integrity and cell survival during replication by DNA damage sensing and inducement of various repair factors (Harper and Elledge, 2007). This response can exert its effect via several different mechanisms, dependant on damage severity and type. For example; transcriptional activation, inducing cell cycle arrest, senescence for DNA repair prior to replication, or apoptosis arising from irreparable or severe damage (Zhou and Elledge, 2000). The importance of this and a fully functional DDR are underscored by several diseases, in particular cancer or neurological pathologies such as ataxia telangiectasia from mutated ATM, and Fanconi anemia as a result from mutations in 5 genes which regulate removal of inter-strand DNA cross links mainly through homologous repair and non-end joining pathways. Briefly, at the core of this response are ATM and ATR DDR kinases, activated by DNA damage of dsDNA and ssDNA breaks by interaction with regulators MRN and ATRIP complexes respectively. Activation of these kinases induces a signalling cascade by phosphorylation of a plethora of downstream responsive genes including the well characterised CHK1 and CHK2 and later BRCA1 / 2. Matsukoa *et al.* (2007) has described over 900 phosphorylation sites of over 700 ATM/ATR responsive

proteins phosphorylated from the DDR on consensus sites by high throughput proteomic analysis. Other well defined DDR regulators include CDK and DNA-PK. Five major types of DNA repair mechanisms exist and are discussed briefly These events are simplified and illustrated in Figures 4.1.8. - 4.1.9.

Base excision repair

BER is responsible for repair of damaged DNA base modifications, which are the most common form of endogenous damage (Kim and Wilson, 2012). Typical insults include excising of incorrect, damaged bases from deamination (cytosine and 5-methylcytosine) which results in uracil and thymine mispaired with guanine, respectively, and C-G --> T-A mutation, or oxidation (8-oxoG). 8-oxoG tends to pair with adenine, resulting in G-C --> T-A mutation. Two pathways constitute this mechanism: short and long patch being repair of a single or more than two nucleotide bases respectively (Robertson *et al.*2009).

Mismatch repair

This repair mechanism (MMR), in addition to mismatched bases also involves post replication repair of incorrect intercalated bases from error prone activities of DNA polymerases such as slippage during repair or incorrect base recognition. Elevated and mutation prone phenotypes are observed in MMR deficient cells, from MMR inactivation, whilst germline MMR mutations are cancer prone, in particular for non-polyposis cancer (Zhang *et al*.2005). Furthermore, MMR is pivotal to many anti-tumour processes such as DNA damaged induced apoptosis (Wu, 1999). The MMR pathway comprises three major steps; 1) recognition of mis-paired bases, 2) excision of the error-containing strand resulting in a gap, and 3) repair synthesis, by gap filling processes.

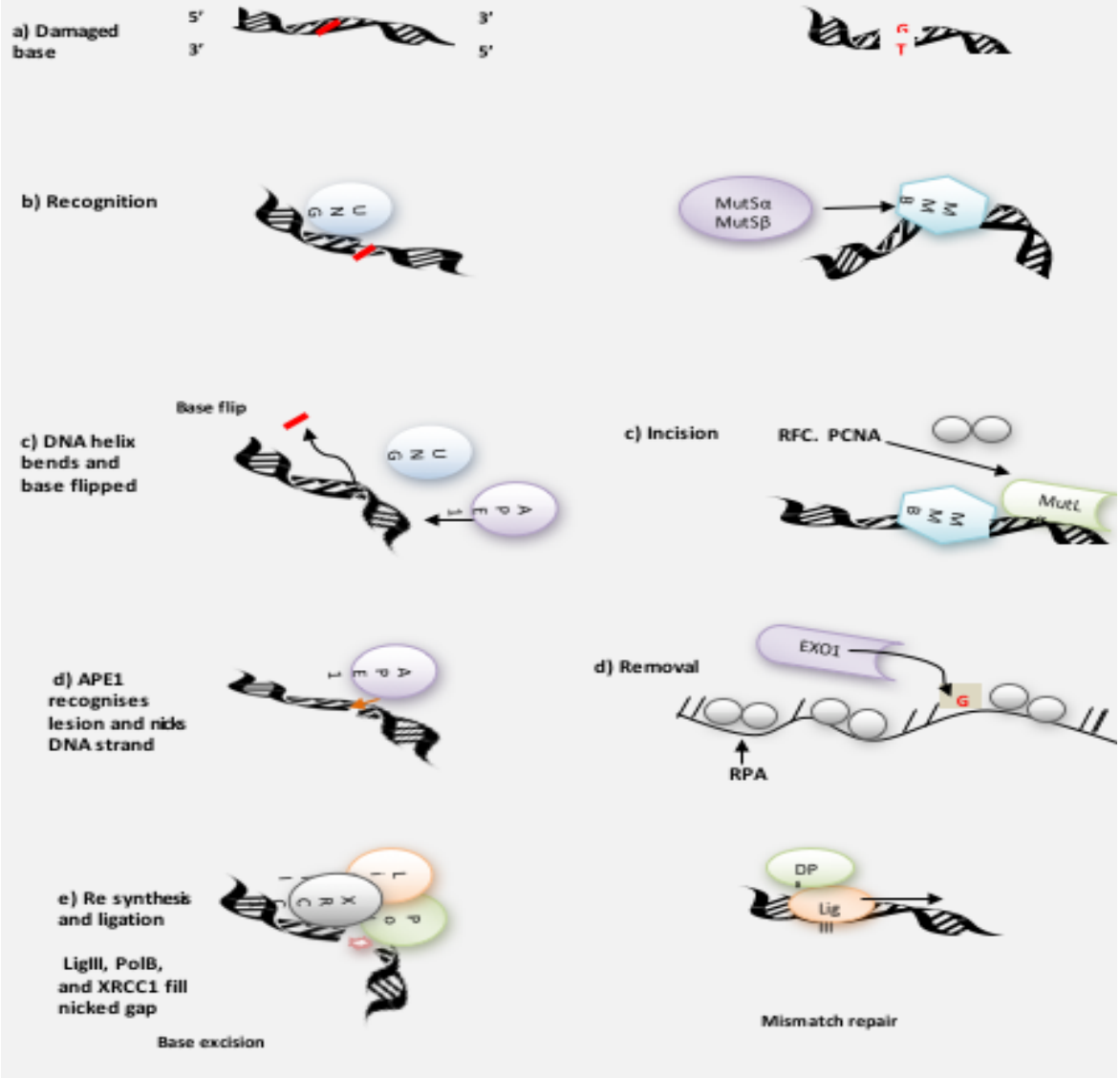

Figure 4.1.8. Base excision repair – Short patch and mismatch repair pathways
A) Base mutation (red) arising from DNA damage (U>G mismatch for eg with UNG) and mismatch base recognised by b) Mutsa and DNA glycosylase (UNG) induces BER pathway, by recognition of and binding to the base lesion. After base binding (uracil for UNG), the base is flipped out of the helix by bending of the DNA and into catalytic pocket of UNG where it is targeted for a subsequent nucleophilic attack to the N glycosidic bond. In c) an AP site is produced as a result of base release by UNG and for MMR; MutLα nicks the 3' or 5' of the mismatched base on the discontinuous strand. This incision by MutLα requires MutSα, RFC, PCNA, and also ATP (Not shown) **d**) For BER, this site is further processed by AP-endonuclease, APE-1, which cleaves the phosphate backbone 5’ to the AP site, producing a 3’OH and a 5’deoxyribose-phosphate moiety (5’dRP) and for MMR, the resulting DNA is excised by EXO1 a 5'->3' exonuclease in cooperation with RPA ssDNA-binding protein.The 5’dRP is hydrolysed by PolB who fills in the single nucleotide gap in the 5>3 direction ligated and sealed by DNA ligase III, and supported by XRCC1 a scaffold protein to restore the original base sequence. The position of the helix moves from 90 C angle to around 35 C from a – d. Whilst the resultant error free DNA strand is re synthesised by DNA polymerase δ and ligated by DNA ligase (DP) shown in e of MMR.

Nucleotide excision repair

NER is considered to be the most versatile of all DNA repair mechanisms. This pathway responds to and repairs a plethora of unrelated DNA lesions. It removes lesions which may distort the DNA helix, base pairing interference and also blocks DNA transcription and replication. The most commonly responded to lesions by NER are: cyclobutane pyrimidine dimers (CPDs) and 6-4 photoproducts (6-4 PPs). These are formed between adjacent pyrimidines, constituting the two major types of UV induced lesions. The other most typical is bulky distorted helix lesions induced by chemical agents (Leiber *et al.*2010). such as cigarette smoke arising from aromatic hydrocarbons, and inter-strand cross linkage induced by chemo therapeutic agents such as etoposide and cisplatin (de Boer and Hoijemaker, 2000).

The NER program comprises two pathways which differ in the recognition stage and whether DNA is transcribed or not. The global genome repair (GGR) repairs transcriptional inactive genomic lesions (Reidel *et al.*2003), whilst transcription coupled repair (TCR) focuses upon actively transcribed DNA lesions (Hanawalt and Spivak, 2008). (Sagasawa *et al*.2008). The importance of the NER repair system is highlighted by several clinical pathologies linked to recessive defects in NER proteins or pathways. At least eleven mutations out of the total 28 NER genes have been linked with rare genetic diseases comprising at least 8 overlapping phenotypes. Examples include: Cockayene syndrome, xeroderma pigmentosum and trichothiodystrophy. These are linked to photo sensitivity as a result of NER errors which typically respond to sun damage. As such, these individuals are pre disposed to skin cancer (Kraemer *et al.*2007).

Double stranded DNA breaks

Double stranded DNA breaks (dsDNA) are considered the most damaging lesions to genomic integrity. This may impinge upon critical cellular process such as replication and transcription. Conversely, highly controlled dsDNA breaks are thought to be beneficial in some instances. For example, immune system development and during

meiosis (Maizels *et al.*2005; Loidl et al. 2016). Different repair mechanisms are employed dependant on type of damage and DNA termini break. dsDNA breaks are induced in response to DNA damage insults such as ionising radiation (IR), which are responded to by ATM triggering a cascade of downstream events. Other sources are aberrant enzymatic or endonuclease activity such as topoisomerase activity, or those endogenous such as reactive oxygen species (ROS). These may promote carcinogenesis by genomic rearrangements (Hoijemakers, 2001). Two different repair mechanisms respond to this type of insult; homologous recombination (HR) and non-homologous DNA end joining (NHEJ). Both mechanisms can respond to dsDNA breaks however, one end termini break frequently observed during replication are repaired by HR typically in S phase of cell division. Two stranded breaks are responded to by the continually cell cycle active NHEJ repair pathway. Both pathways are shown in figure 4.1.9.

HR is induced if the damage is not repaired pre- replication by homologous pairing. HR similar to single strand annealing simply defined is whereby homologous information within a secondary intact DNA duplex of a homologous chromosome serves as template to maintain repair fidelity. The HR pathway is highly conserved. HR only functions during S phase and if sequence homology is apt. For example, at least 100 homologous bp are required for this repair mechanism to operate (Leiber *et al*.2010). Conversely, NHEJ does not require this specific sequence homology and can function at any given time being active in all cell cycle stages. NHEJ thus, may re-join damaged DNA incorrectly. Indeed, NHEJ error is typically always mutagenic (Van De Bosch, 2002). Translocation is a common example of this process, arising from the incorrect joining of independent chromosomes. This occurs due to two different breaks which may occur on separate chromosomes thus giving rise to two DNA termini at each break (Lieber et al.1998). The importance of this is seen in lymphomas and leukaemia where translocations induce oncogene activation arising from aberrant NHEJ events (Gelb and Mederios, 2009). This highlights the importance of error free joining in maintain genomic stability.

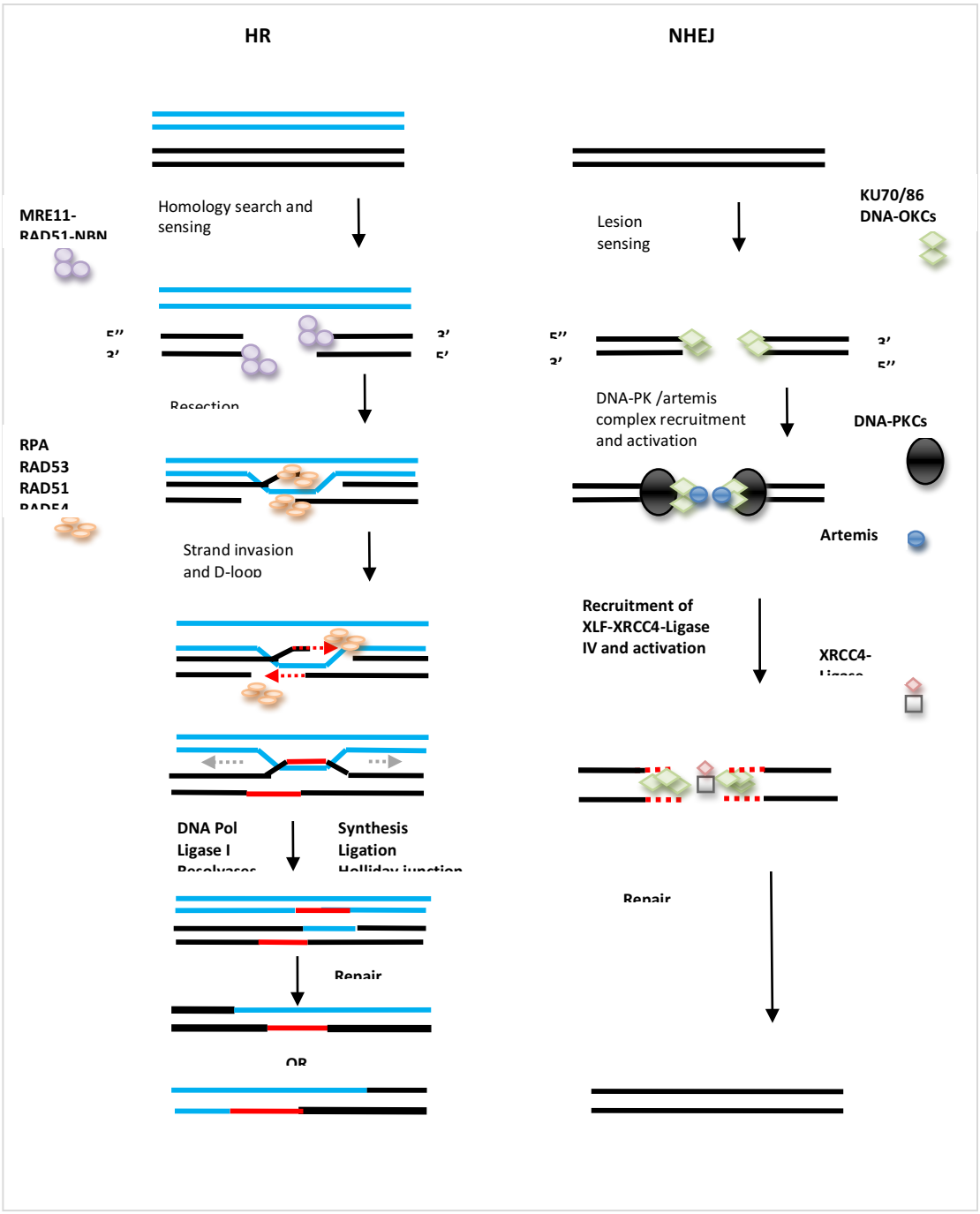

Figure 4.1.9 dsDNA break repair by homologous recombination and non-homologous end joining. **HR:** Black and red lines represent dsDNA homologous sequence. DNA lesions are recognised by the MRN complex recruited to the lesion (black), nucleoytically processed forming the 3' ssDNA, bound by RPA-RAD51/52 which subsequently invades homologous intact sequences (blue). DNA strand exchange results in a joint molecule of damaged and non - damaged DNA. Missing sequence information at the lesion is restored via DNA re-synthesis (red). Interconnected molecules are processed (grey arrows) by DNA ligation**. NHEJ:** Following dsDNA breaks, lesions are sensed by Ku70/80 complex to recruit the DNA-PK. This enhances XRCC4-Ligase-Artemis-XLF recruitment and activity facilitating re-joining, and direct ligation. Sequence homology is not required. dsDNA breaks may be joined accurately, however typically translocations of indels are generated.

5 Aims and hypothesis

This study is a continuum of previous research conducted by (Tian, K, PhD Thesis, University of Manchester, 2013). The overall aim of this study is to generate a model which is more representative of p53 cancer dynamics. By this, our main aim to expand upon the Tian, K. (2013) study, to enlarge the initial PKT206 - p53 - DNA damage model, increasing network size using data mining and extensive literature curation approaches. By inclusion of more in and outputs into the expanded models, we hypothesise that the expanded p53 models will be have increased predictive potential, provide a greater representation of p53 signalling pathways and its role in cancer. We further hypotheses that the expanded model will have promising clinical relevance for use in a personalised therapeutic approach. For this, we will undertake several approaches.

i) We aim to undertake a systems biology approach using Boolean logic to establish if larger Boolean models can be successfully simulated, and identify overall system attributes of p53 - cancer dynamics. After expansion of the model, we aimed to undertake several computational logical based approaches using *in silico* knockout comparative scenarios to mimic *in vivo* processes, identify network perturbations and derive potential predictions in response to these *in silico* conditions.

ii) We aimed to validate these *in silico* predictions by various approaches including extensive literature curation, laboratory methodologies and superimposition of high - throughput transcriptome *in vitro* data. We further aimed to explore the models predictive capability to predict gene changes on a clinical basis. By this, we aim to superimpose *in vivo* patient derived tumour profiles of various cancers and compare it to *in silico* generated results.

iii) We further aimed to construct a Boolean model which is more relevant to specific cancer by addition of cancer specific genes and test the models potential to predict gene changes in a particular cancer by comparison to in vitro and in vivo generated data of the same cancer.

iv) Lastly, we will use the clinically derived *in vivo* data to highlight the predictive potential of the p53 logical model to correctly identify genetic perturbations on an individual basis, and suggest personalised targeted treatment dependant on tumour.

6 Material and Methods

6.1 Systems biology and computational methodologies

Matrix Laboratory (MATLAB) software was the base platform used for computational methodologies here and as such is briefly described. All analyses including statistical analysis were undertaken using Minitab, Graphpad software and excel functions.

6.1.1 MATLAB

MATLAB Is a high performance language software for scientific computing. MATLAB integrates numerical computation, visualisation and programming where formalisms are expressed in mathematical notations using MATLAB commands. Toolboxes are comprehensive collections of MATLAB functions (M-Files) which use logical Boolean operators of AND, OR, NOT. Analysis is in the form of numerical matrices referred to as scalars (a single number represented by a 1 x 1 matrix) and vectors (a one dimensional array of numbers represented by *n* x 1 column vector, or a 1 x *n* vector of *n* elements). Matlab (v.8.30) was downloaded from Mathworks Inc. available at: (https://www.mathworks.co.uk/downloads/web_downloads) and used for all software extension platforms; CellNetAnalyzer and Cytoscape both described in below and in section 4, literature review.

6.1.2 Generation of all p53 models

6.1.2.1 Retrieval of protein - protein interaction evidence using STRING database

Tian et al. (2013), previously conducted extensive screening of over 30 protein – protein interaction databases, identifying the The Search Tool for the Retrieval of Interacting Genes (STRING) database as the most suitable for model generation (Tian K, PhD Thesis, University of Manchester, 2013). The STRING database is a protein to protein interaction database that integrates extensive information of protein links and interactions from four main sources described in detail in section 4 of this report. An example screenshot of STRING interaction evidence is shown in image 6, between p53 and MDM2.

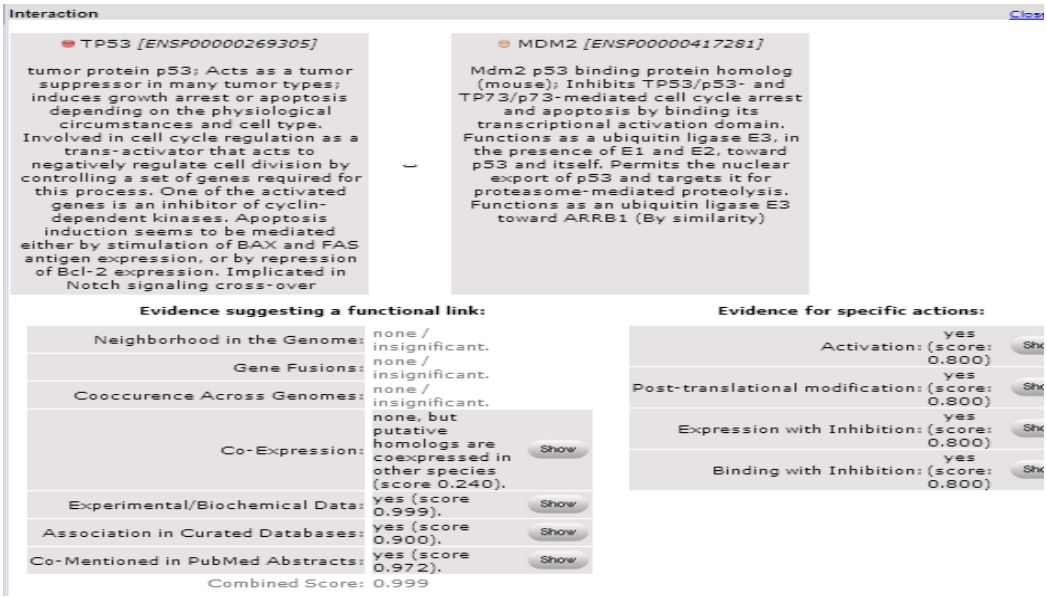

Image 6 STRING interaction evidence for p53 – MDM2 derived from the four main sources
Screenshot example of interaction evidence derived from STRING, assigned by the confidence schema shown as combined score above (0.999).

A total of 81,000 interactions were extracted from STRING using ULTRAEDIT, a text editor programme capable of handling large datasets, available at: (http://www.ultraedit.com/products). Interactions with a confidence scores over 0.7 a high confidence schema assigned by STRING were only considered. Key identifiers assigned by STRING were used for extraction of target data. For example, in STRING the identifier of p53 is '*ENSP00000269305'.* This identifier was input into ULTRAEDIT and filtered to direct interactions with p53 only. These interactions were considered as direct to p53. To close and complete all models, evidence was extracted from STRING to include interactions between other nodes. For example, considering two interactions included in the p53 model linking directly to p53: p53 activates CDKN1A and p53 activates PRKG1. These are direct and referred to as the first layer of the model. However for interactions between other nodes (as an example here PRKG1 activates CDKN1A) were referred to as the second layer of the model. This was performed for all nodes in the p53 models using the same confidence score of over 0.7. The nature of all interactions (post translational modification, activation, inhibition or binding) were also extracted. Activation and inhibition were the key interactions considered which refer to the state of gene transcription if a gene is transcribed or not

transcribed respectfully, or if protein was activated or inactivated by other means such as protein degradation, subcellular localisation or post - translational modifications.

Due to several issues of STRING reporting incorrect interactions (discussed in section 8, final discussion), all interactions extracted were additionally manually curated by literature evidence for model accuracy. This was undertaken initially utilising the STRING text mining tool which links to PUBMED. For example, image 6.1 depicts the STRING text mining evidence between p53 and MDM2 linking to the PUBMED database. In addition to the STRING text mining tool, manual curation of interactions was also performed using other literature sources; Google, Google Scholar and additional PUBMED searches. Further validation for all interactions in all p53 models were also confirmed by supervisor to ensure accuracy of model. At least one documented scientific publication was used for a confirmed interaction, some described by more.

Image 6.1 Predicted evidence from STRING text mining application for p53-MDM2
In the above example, text mining evidence shows that p53 induces (activates) MDM2 with corresponding link to the PUBMED source.

6.1.2.2 Construction of all p53 models

All p53 models were generated by expansion of the PKT206 model generated by Tian et al. (2013). The Boolean PKT206 model was also constructed using the STRING database. Briefly PKT206 comprises 783 interactions of inhibition, activation or

ambivalent factor amongst 203 internal nodes. An input of DNA damage and two outputs of cellular senescence and apoptosis were also considered in PKT206. For consistency we used the same methodology as applied by Tian et al. (2013) and extracted all protein information from the STRING database as described above. All confirmed interactions from manual curation and validation were incorporated into the relevant models (PMH260, PMH302 and Meso-PMH61). The Meso-PMH61 model was constructed by integration of nodes representing genes considered as important to malignant mesothelioma, obtained from Melaiu et al. (2015). For consistency we followed the same principle (6.1.2.1) and input the total 119 genes into the STRING (v9.1) database to extract information for mesothelioma genes that interact with genes in the PMH302 model.

6.1.2.3 Addition of biological outputs and input to the p53 models

Three additional biological outputs were initially integrated into PMH260; angiogenesis, cell cycle arrest and DNA repair, an additional input of hypoxia was further included into the PMH302 model. Dependant on their biological processes that they regulate, all nodes within the relevant models were linked to these three additional outputs and one input by their edge function of inhibition, activation or ambivalent factor. This was primarily undertaken using the Gene Ontology (GO) database available at (http://geneontology.org/). The GO database provides a list of defined gene terms considering, biological processes, molecular function and cellular components. Additional literature search was also undertaken for model accuracy to confirm these interactions using; PUBMED, Google and Google Scholar. As PKT206 did not consider these additional 3 outputs (DNA repair, angiogenesis and cell cycle arrest) PKT206 internal nodes (n = 203) were also linked to their relevant outputs. All additional nodes included to generate the larger three models were also linked to the PKT206 outputs of apoptosis and cellular senescence and to the input of DNA damage.

6.1.3 Cytoscape

Cytoscape available at (http://www.cytoscape.org)is an open source platform used with MATLAB for viewing and constructing interaction networks and biological

pathways. Cytoscape allows for integration of these networks with annotations, gene expression and other state data analyses. Cytoscape (v.3.1) was utilised for the p53 interactome models serving two main purposes; visualisation of all p53 models and functional analysis of PKT206 by application of STSFA described in 6.4.

6.1.3.1 Visualisation of networks

For visualisation of p53 models, tab. delimited files were constructed in accordance with Kline et al. (2007). A new network was declared and relevant files imported into Cytoscape. Source interaction, interaction type and target interaction were subsequently declared generating the visual networks for all models. For example, source interaction may be defined as p53, target interaction as MDM2 and interaction type given as activation. The network / model style may be modified accordingly with the user's requirement using the Vizmapper tool.

6.2 *In silico* analyses of the p53 models

6.2.1 Functional network analysis using CellNetAnalyzer

CellNetAnalyzer (CNA) is discussed in section 4 of this report.

All p53 models (PMH260, PMH300 and Meso – PMH61) were constructed via retrieval of protein – protein interaction information derived from STRING and imported into CNA (v.2013.1). All Confirmed interaction records were input into tab delimited text. file and processed to a node and reaction transcript readable by CNA as described by Klamt *et al.* (2007). A new signal flow network project was declared and data files of species/nodes and their edges/interactions were uploaded. Two approaches facilitated by CNA were used for various *in silico* knock out tests and comparative *in silico* simulations; dependency matrix calculations and logical steady state analysis (LSSA) described below (6.2.1.2).

6.2.1.1 Application of dependency matrices to the p53 models

CNA facilitates construction and calculation of dependency matrices within a given network. The dependency matrix represents the effects between node pairs by calculation of positive and negative pathways between them and considers the

presence of feedback loops within the system. Two nodes may be represented, *i* and *j* with six dependency effects observed in a matrix: Strong activator, weak activator, strong inhibitor, weak inhibitor, ambivalent factor and no effect defined by:

1. If no negative or positive path exists between node *i* and node *j*, then *I* will have no effect on node *j*
2. If both a positive and negative path exists between node *i* to node *j*, then *i* is an ambivalent factor of node *j*
3. If only negative paths exist between node *i to* node *j*, with only negative feedback loops present in these paths, then node *i i*s a weak inhibitor of node *j*
4. If only positive paths exist between node *i* to node *j* with negative feedback loops present in these positive paths, then node *i* is a weak activator of node *j*
5. If only negative paths exist between node *i* to node *j* with negative feedback loops absent in these paths, then node *i* is a strong inhibitor of node *j*
6. If only positive paths exist between node *i* to node *j* with negative feedback loops absent in positive paths, then node *i* is a strong activator of node *j*.

The connectivity of all nodes was determined using Cytoscape (v. 3.1) and the most highly connected nodes of the network deleted to generate an *in silico* knockout simulation. The particular nodes deleted were dependant on model being analysed. For all models, ASCII files were generated and imported into CNA in accordance with the format described in (Klamt *et al*.2007). For the deleted node, default values of 'NaN' given as' #' in species files were altered to '0' in the network composer. Shortest paths and species dependencies were calculated using approximate algorithm for each knockout (KO) scenario by declaration of exclusion of any given species/node defined as '0'. Dependency matrices were subsequently calculated where the 6 possible relationships may be derived as defined above. Result files of data corresponding to the values of 1 – 6 defining the above relationships were exported as raw data in tab

delimited format and subsequently converted into a readable format accepted by excel for analysis by comparison to the default model.

6.2.1.2 Application of logical steady state analysis to the p53 models

LSSA is a method for predictive input and output relationships in signalling networks. Interaction hypergraphs supported in CNA are used to represent signalling events that allow for a synchronous interaction targeting the same node(s) to be combined, referring to the relationship operators of AND, OR, NOT (Klamt et al. 2007). The logical behaviour of node states within a Boolean network can be analysed by LSSA in response to various in silico perturbations of different input and knock out tests.

In LSSA, each scenario is defined by declaration of the value of input signals. For example, declaring the values below where:

'0' represents inactivated
'1' represents activated
'NaN' represents undetermined

The state of some nodes may remain undetermined if several logical steady states are possible (NaN). Proceeding declaration of each scenario from the given values, CNA calculates the steady state of each node and its interactions within a network by logical operation (above). Resultant node and interaction states for each scenario are returned by CNA which can be compared to default model for investigation of network perturbations.

ASCII files of interactions were generated for all models in accordance with (Klamt *et al.*2007). Four different scenarios were constructed for application of LSSA which can represent or mimic *in vivo* processes such as loss of p53 function arising from mutation (p53 deletion from the network) in the presence or absence of DNA damage or hypoxia. DNA damage and p53 simulations are summarised in table 6 for PMH260,

PMH300 and Meso- PMH61 models and table 6.1 for hypoxia and p53 simulations (PMH302 and Meso – PMH61 models).

Table 6 Four *in silico* scenarios generated for LSSA of DNA damage ON/OFF in the presence / absence of p53

Scenario No.	Input signal	Model background
1	DNA damage ON	p53 knockout
2	DNA damage OFF	p53 knockout
3	DNA damage ON	p53 wildtype
4	DNA damage OFF	p53 wildtype

Table 6.1 Four *in silico* scenarios generated for LSSA of hypoxia ON/OFF in the presence / absence of p53

Scenario No.	Input signal	Model background
1	Hypoxia ON	p53 knockout
2	Hypoxia OFF	p53 knockout
3	Hypoxia ON	p53 wildtype
4	Hypoxia OFF	p53 wildtype

To mimic loss of p53, deletion of p53 from the network was via total node/ species deletion from the network composer and all associated edges were removed to generate a p53 knockout scenario. For construction of a p53 wild type background, the p53 node was switched to 1 in CNA network composer. The DNA damage or hypoxia input was switched to '0' referring to hypoxia or DNA damage OFF or '1' referring to hypoxia or DNA damage ON for the various scenarios as described above in table 6 and table 6.1.

Each scenario was subsequently imported and computed separately by CNA and compared against the default model for investigation of the network response to p53, DNA damage or hypoxia presence or absence. Results obtained from CNA in tab delimited format were subsequently converted and imported into excel files for analysis.

Four comparative scenarios of different DNA damage, hypoxia and p53 statuses were additionally constructed to investigate network perturbations in response to the different *in silico* stresses. In particular node state changes of angiogenic and apoptotic nodes were explored. The various *in silico* scenarios simulated are summarised in tables 6.2 and 6.3 for DNA damage and hypoxia respectively.

Table 6.2 List of four different scenario comparisons for *in silico* simulations using LSSA for DNA damage

	***In silico* simulation**
Scenario No.	
1	p53 wildtype DNA damage ON vs. p53 knockout DNA damage OFF
2	p53 wildtype DNA damage OFF vs. p53 knockout DNA damage OFF
3	p53 wildtype DNA damage OFF vs. p53 wildtype DNA damage ON
4	p53 knockout DNA damage OFF vs. p53 knockout DNA damage ON

Table 6.3 List of four different scenario comparisons for *in silico* simulations using LSSA for hypoxia

	***In silico* simulation**
Scenario No.	
1	p53 wildtype hypoxia ON vs. p53 knockout hypoxia OFF
2	p53 wildtype hypoxia OFF vs. p53 knockout hypoxia OFF
3	p53 wildtype hypoxia OFF vs. p53 wildtype hypoxia ON
4	p53 knockout hypoxia OFF vs. p53 knockout hypoxia ON

6.3 Genome wide validation of the p53 interactome models

To evaluate the predictive strength of all models on a genome wide level*, in silico* predictions of LSSA generated as described in 6.2.1.2 were compared to various experimental gene expression profiles as described below. LSSA provides a steady state in each scenario where differential gene expression states can be compared between model predictions and experimental data in accordance with Christensen et al. (2009).

6.3.1 Model validation using transcriptome profiles

To evaluate the predictive strength of all models generated; PMH260, PMH302 and Meso-PMH61, *in silico* results derived from the four *in silico* LSSA scenarios of different p53 backgrounds, DNA damage and hypoxia input signals (tables 6 – 6.3) were compared to several gene expression *in vitro* and *in vivo* profiles of various human cancers; osteosarcoma U2OS p53 $^{+}/^{+}$ and SaOS2 p53 $^{-}/^{-}$ cell lines with and without 10 µM etoposide treatment for 24 hr (Tian *et al*.2013), untreated HTC116 p53 null and wildtype colon cancer cell lines available from the gene expression omnibus ID: GSE10795 and (Wilhelm *et al.*2008), non-small cell lung cancer profiles (Peifer et al. 2012) and microarray profiles generated in our laboratory of malignant mesothelioma Mero-14 cell lines untreated and treated with 10 µM etoposide for 24 h. For comparison of *in silico* hypoxia to experimental hypoxic conditions, Mero – 14 cells were exposed to hypoxic conditions of 1 % O_2 for 24 hr compared to untreated maintained at 37 ^{o} C with 5% CO_2 for 24 h. All transcriptome profiles described above were superimposed to the p53 models for investigation of model predictive capability. Comparison of *in vitro* and *in vivo* data to *in silico* data was undertaken in accordance with the formula described by (Christensen *et al*.2009) and (Tian et al. 2013) using the dynamic threshold. This is defined by the predicted state of a variable E_{mod} where a node given as *(i)* is defined as $S(i)_{wt}$ and $S(i)_{mu}$ for p53 wildtype and p53 knockout respectively. For any given state, both could take any three values defined as;

0 representing downregulated
1 representing upregulated
NaN representing unchanged

The variable E_{mod} represents the predicted change of gene state from p53 wild type to knockout where:

$E_{mod} = 0$, if $S(i)_{wt} = 1$ and $S(i)_{mu} = 1$
$E_{mod} = 0$, if $S(i)_{wt} = 0$ and $S(i)_{mu} = 0$
$E_{mod} = 0$, if $S(i)_{wt} = NaN$ and $S(i)_{mu} = NaN$
$E_{mod} = 1$, if $S(i)_{wt} = 0$ and $S(i)_{mu} = 1$

E_{mod} = 1, if $S(i)_{wt}$ = 0 and $S(i)_{mu}$ = NaN

E_{mod} = 1, if $S(i)_{wt}$ = NaN and $S(i)_{mu}$ = 1

E_{mod} = -1, if $S(i)_{wt}$ = 1 and $S(i)_{mu}$ = 0

E_{mod} = -1, if $S(i)_{wt}$ = 1 and $S(i)_{mu}$ = NaN

E_{mod} = -1, if $S(i)_{wt}$ = NaN and $S(i)_{mu}$ = 0

The differential expression level of a gene *(i)* derived from experimental validation was defined by the parameter E_{exp} where:

If the expression level of a gene was upregulated, E_{exp} = 1

If the expression level of a gene was downregulated, E_{exp} = -1

If the expression level of a gene was unchanged, E_{exp} = 0

The $\log_{10}$ fold change (FC) between experimental and simulated data was subsequently calculated for each gene / node also in accordance with (Christensen *et al*.2009), defined by the equation:

$$\mathrm{FC}(i) = \frac{M1(i)}{M2\ (i)}$$

Where M1*(i)* is the median of expression values in the target condition and, M2*(i)* the median of expression values in the source condition Threshold values defined as (ϑ), the mean as $(\bar{x})$ and standard deviation as (σ) were applied to normalise expression profile distributions of (θ_{max} and θ_{min}), defined as:

$$\theta_{max} = \bar{x} + \sigma$$

$$\theta_{min} = \bar{x} - \sigma.$$

Gene activity was further determined for both datasets, where:

$$\text{If } \mathrm{Log}_{10} = \mathrm{FC} > \bar{x} + \sigma = \text{gene } (i) \text{ upregulated}$$

If Log_{10} FC < $\bar{x}$ - σ =gene *(i)* downregulated

If- σ <= log_{10} FC <= + σ = gene *(i)* was unchanged

The differences between experimental and predicted simulations were defined as (E_{mod} – E_{exp}), which could take one of three values given below where:

'0' represents a correct prediction where both outcomes of experimental and *in silico* results were the same

'1' represents a small error prediction between experimental and *in silico* results where one outcome was 'no change' and the other 'up or downregulated'.

'2' represents a large error prediction between experimental and *in silico* results where one outcome was 'upregulated 'and the other 'downregulated'.

6.4 Functional analysis of the PKT206 network

Original construction and analysis of the PKT206 p53 interactome is described in detail elsewhere (Tian *et al.*2013).

STSFA utilizes transcriptome data for node score generation, and is provided as a Cytoscape app/plugin for versions above 2.7. Node and edge attributes were assigned to the network in accordance with Isik et al. (2012), and imported into Cytoscape (v.3.1.). Gene expression profiles of HTC116 p53 null and wildtype colon cancer cell lines were analyzed available from GSE10795 and (Tian *et al.*2013). Experimental results were compared to *in silico* data generated from LSSA.

To overcome high background noise typically associated with microarray data, the median score of each gene in the network was taken as its expression value. Expression scores generated from microarray data were imported in a 3 tab-delimited .txt file in accordance with Isik et al. (2012) and imported into Cytoscape. However, as PKT206 comprises an extremely high number of nodes downstream to p53 (*n*=154), scores traversed to these were low and often negative. This would suggest that p53 has little influence on its downstream target nodes, when in reality it is the hub of the network.

To overcome this, log_2 microarray scores were scaled up by a factor of 100. For HTC116 transcriptome data, expression scores were extremely low, and raw microarray scores were additionally scaled up by the same factor. This allowed for an increased score in p53 for downstream signals, whilst leaving network ratios of edge and nodes unaffected.

6.5 Laboratory based methodologies and materials

6.5.1 Mammalian cell culture

6.5.1.1 Cell line maintenance

Three main cell lines were used; human adherent mesothelioma cell line, Mero – 25 and human osteosarcoma adherent cell lines U2OS p53 ($^{+}/^{+}$) and SaOS2 p53 ($^{-}/^{-}$). All cell lines were maintained at 37 ^{o} C with 5% CO_2 (Wolf Laboratories, Galaxy S). Cell culture procedures were performed in Laminar flow Class II culture cabinets (Esco Class II Biological Safety Cabinet) under strict aseptic conditions. Mero – 25 and U2OS cell lines were cultured in T^{75} cm² culture flasks with Dulbecco's Modified Eagles Medium (DMEM) (Sigma, UK) supplemented with 10 % (v/v) Foetal Bovine Serum (FBS), 0.05U/ml penicillin and 0.05U/ml of streptomycin. SaOS2 cell lines were cultured in T^{75} cm^2 flasks, maintained with Dulbecco's Modified Eagles Medium 4 (DMEM4) (Sigma, UK), supplemented with above described antimicrobial agents and 15 % (v/v) FBS.

6.5.1.2 Passage of cell lines

All cell lines were passaged every 2-3 days to avoid over confluence. Sub culture of cell lines was performed when cells reached 80 % confluence, typically in a 1:4 or 1:2 ratios for human osteosarcoma cell lines U20S and SaOS2 respectively and 1:3 ratios for malignant mesothelioma mero – 14 cells. Specific media, 1x phosphate buffered saline (PBS) and Trypsin-Ethylenediaminetetraacetic acid (trypsin) (Sigma, UK) were pre warmed at 37^{o}C for 5 mins, existing media was aspirated and cells washed in 7 ml of 1 X PBS for removal of any dead cells. 1 x PBS was subsequently aspirated, prior to addition of 1ml of trypsin for detachment of adherent cells and incubated for 3 min at

37^{o}C. Trypsinised cells were removed from incubator and 7.5 ml of fresh media was added. 2.5 ml of suspension was aliquoted to the new flasks making a total volume of 10 ml media and incubated at 37 °C (1:4 ratio).

6.5.1.3 Freezing of cell lines

Once fully confluent or to a specific cell count, typically 1 x 10^6, cells were pelleted by centrifugation at 1,200 rpm for 3 min (Meadowrose Scientific Ltd HERMLE Z 400), and resuspended in 1 ml FBS / 20 % Dimethyl Sulfoxide (DMSO) solution for prevention of intracellular ice crystal formation. FBS/DMSO solution was added slowly in a drop wise fashion to ensure avoidance of osmotic cell shock. Resultant cell suspension was transferred into cryovials and transferred to - 80^{o}C for 24h, prior to storage in liquid nitrogen -196^{o}C. This slow freezing process avoids shock to cells.

6.5.1.4 Thawing of cell lines

Cells were rapidly thawed at 37^{o}C and transferred quickly for recovery to 7 ml of pre warmed medium in T^{25} cm² flasks. Rapid thawing ensures the reduction and/or prevention of ice crystals within the cells during rehydration which are damaging to the cells. Cells were later pelleted by centrifugation to remove DMSO at 1,200 for 3 mins prior to re-suspension in specific growth medium. Cells were transferred to T^{75} cm² flasks once 70% confluence was reached in 10 ml of specific media.

6.5.2 Immuno - detection of proteins

6.5.2.1 Preparation of whole cell extract

U2OS and SaOS2 cells were seeded at 10^6 in 100mm culture plates and incubated overnight at 37 ^{o}C. 10µM of etoposide was added 24 hr pre extraction. Etoposide is a chemotherapeutic agent which induces DNA double strand breaks (dsDNA) via inhibition of topoisomerase II and therefore is a good choice when studying DNA damage (Zhou *et al,* 1999). Media was subsequently removed from plates and cells washed twice with cold 1 x PBS, prior to cell scraping on ice with addition of 125 µl (six

well plates) 250 μM (100 mm plate) of high salt lysis buffer (HSLB) (45mM Hepes, 400mM NaCl, 1mM EDTA, 10 % glycerol, 0.5 % IgePal, phosphatase inhibitors; 2mM sodium orthovanadate, 5mM NaPPi, and 20mM β glycerol phosphate) and 1 μg /ml protease inhibitor cocktail comprising aprotinin, leupeptin, pepstain A, 1mM DTT, and 1mM PMSF was added fresh. Resultant extracts were collected in a fresh 1.5 ml eppendorf tube and rotated at 4 ^{o}C for 20 mins on a miniroller (Mini Labroller^{TM}, Labnet Inc), followed by centrifugation (GenFuge 24D, Progen Scientific) at 4^{o}C for 20 mins at 13,000rpm. Pellets were discarded and supernatant transferred to fresh 1.5 ml eppendorf tubes kept on ice.

6.5.2.2 Protein concentration determination

Protein concentration of whole cell extract was determined using the Bio-Rad protein assay reagent, which relies upon colour changes of Coomassie Brilliant Blue dye from the binding to arginyl and lysyl protein residues (Bradford, 1976).

Bio – Rad stock solution was diluted 1:5 with distilled water prepared in a 1.6 ml, 1 cm path visible cuvette. 2 μl of bio-rad mixture was used to calibrate the spectrophotometer (Jenway, G305). 2 μl of extract was transferred to the bio-rad working solution, incubated at room temperature (RT) for 5 mins prior to absorbance measurement at 595 nm. Protein concentration was performed in duplicates and the average taken as value. This was determined using a relative method defined by the equation below:

$$Lowest\ absorbance = 40\mu l$$

$$Extract\ volume\ = \frac{Lowest\ absorbance \times 40}{\times\ 2nd\ lowest\ absorbance}$$

The resultant extracts were transferred to fresh eppendorf tubes mixed with 3X Sodium dodecyl sulphate sample buffer (187 mM Tris, 30% Glycerol, 6% SDS, 2-Mercaptoethanol, 0.01% bromophenol blue) and stored at -20^{o}C if not used on day.

6.5.2.3 SDS gel electrophoresis

SDS- poly acrylamide (SDS – page) gel electrophoresis is the primary stage of immunoblotting and relies upon the principle of electrophoresis where macromolecules are separated according to their molecular weight. A polyacrylamide gel serves as the supporting medium, whilst the SDS acts to denature the proteins. Two gels were used; resolving of a basic pH 8.8 with a higher acrylamide concentration comprising smaller pores allowing for easier migration of smaller proteins. The stacking gel is slightly acidic (pH 6.8) with a lower acrylamide content constituting a porous gel aiding protein alignment. During electrophoresis the denatured proteins possess a negative charge and therefore migrate towards the positive electrode upon voltage.

SDS - PAGE was performed using either a 7.5 % or 12.5 % polyacrylamide gel dependant on protein size. The resolving gel was prepared as described in Table. 6.4 and poured into the casting apparatus (Mini-Protean 3 – Bio-Rad, UK) Ammonium persulfate (APS) and N, N, N, N- Tetramethylethylenediamine (TEMED) was added last to the gel solution to ensure gel solidification did not occur rapidly. 500 µl isopropanol was later added to ensure absence of air bubbles. After gel solidification, isopropanol was removed and the stacking gel added (table 6) prior to insertion of 1.5 mm well combs. Proceeding solidification, the stacking gel was removed from the casting apparatus and placed into an electrophoresis mini buffer tank (Bio-Rad) filled with 1X SDS PAGE running buffer (0.25M Tris, 1.9M glycine, and 30mM SDS) and combs subsequently removed.

Protein samples were incubated at 95^{o}C for 3 mins on a heating block (Techne Dri-Block, DB-2P) then centrifuged for 1 min at 13,000rpm (GenFuge 24D, Progen Scientific). Sample volumes were loaded accordingly to direct equation above and 5µl of PageRuler protein ladder (26616, Fermentas, UK) into respective wells using a fine microsyringe. Samples were subsequently run at 80 volts for 20 mins so samples may enter resolving gel, then 120 volts for 1.5 h.

6.5.2.4 Western transfer

The resolved protein gel sample was removed from the buffer tank for transfer using western transfer apparatus (Bio-Rad, UK). Polyvinyllidene fluoride (PVDF) membranes (Millipore, UK) were used for protein transfer. PVDF membranes provide greater mechanical support than nitrocellulose and allows for membrane re use (Mahmood and Yang, 2012). Components of the apparatus were set up accordingly and transferred to a universal buffer tank (Bio-Rad, UK) filled with western transfer buffer (150mM Glycine, 25mM Tris- HCl, ph 8.3, and 20% methanol). A magnetic stirrer and ice pack was placed within the buffer tank and the transfer run at 0.4 amp for 2 h, with ice pack renewal every hour.

After transfer, the membrane was blocked in 5 % dried milk in 1X PBS for 1 hr at RT prior to incubation with specific primary antibody (Santa Cruz, Biotechnology) in 2.5 % milk / PBS/0.1% Tween solution on a roller overnight at 4 ^{o}C. Primary antibody volume added were as per supplier instructions for optimum concentration. After incubation, membranes were washed three times for 10 min intervals with 10 ml PBS/0.1% Tween and incubated with corresponding secondary anti – mouse or anti – rabbit IgG horseradish antibody (Amersham, GE Healthcare) in 2.5 % / PBS/ 0.1% Tween for 1 hr at RT on a rocking platform (Stuart Platform Rocker, STR6).

Table 6.4 Different % composition of SDS polyacrylamide gel

	7.5% gel		10 % gel	
Solutions	**Resolving**	**Stacking**	**Resolving**	**Stacking**
Distilled water	13.3 ml	6.73 ml	10.94 ml	6.73 ml
Acrylamide	7 ml	1.67 ml	9.33 ml	1.67 ml
1.5M Tris pH 8.95	7 ml	-	7 ml	-
1M Tris pH 6.95	-	1.25 ml	-	1.25 ml
0.2M EDTA	280 µl	100 µl	280 µl	100 µl
10% SDS	280 µl	100 µl	280 µl	100 µl
10% APS	157 µl	157 µl	157 µl	157 µl
TEMED	17 µl	17 µl	17 µl	17 µl

Membranes were further washed three times at 10 min intervals with PBS/0.1% Tween at RT on a rocking platform prior to immuno-detection. Membranes were removed

from washing solution and dependant on protein size or detection method used either 1 ml of SuperSignal West Pico chemiluminescent substrate (ThermoScientific, UK) was added for 3 min at RT or 750 µl of femto chemiluminescent substrate (ThermoScientific, UK) added for 1 min at RT prior to viewing.
For the X ray method, the membrane was placed into a X-ray cassette wrapped with cling film, exposed to medical X ray film (Fujifilm, UK) and developed using X-ray film processor (AFP, X-ray film processor, mini medical series) or viewed directly using the Syngene G:BOX XT4: Chemiluminescence and Fluorescence Imaging System.

6.5.2.5 Membrane stripping

The membrane was stripped prior to secondary detection if molecular weights of protein were similar. Membranes were incubated in stripping buffer (100mM 2-Mercaptoethanol, 2% SDS, 62.5 mM Tris-HCl pH6.7) for 30 min at 55^{o}C and washed three times in 10 ml of PBS/0.1% Tween at 10 min intervals. The membrane was subsequently blocked in 5% milk/PBS for 1 hr at RT, prior to incubation with the specific primary antibody.

6.6 Quantitative Real Time PCR

Quantitative RT – PCR (q PCR) is a powerful and sensitive method for gene expression analysis where cDNA levels correspond to mRNA content of target gene. It allows for continuous data logging in real time for each DNA amplification cycle. Different fluorescence dyes may be utilised where the fluorescence signal is directly proportional to the number of amplified copies (Arya, 2005).

6.6.1 Total RNA isolation

For investigation of target mRNA expression in response to DNA damage and the absence and presence of p53, human osteosarcoma cells U2OS (p53 +/+) and SaOS2 p53 null were used. 1 x 10^{6} U2OS and SaOS2 cells were seeded and incubated in 6 well plates. The chemo therapeutic agent Etoposide (10 µM) was introduced 24 h pre RNA isolation to induce DNA damage.

Total RNA was extracted from both cell lines using RNeasy plus mini kit (Qiagen, UK). This was performed in sterile conditions. The method was performed in accordance with manufacturer's instructions utilising the direct isolation method. Briefly, cells were washed twice with 1X PBS and RLT buffer. Cell lysates were added to Qiashredder spin columns and centrifuged for 2 mins at 13,000rpm. Subsequent homogenised lysates were transferred to gDNA eliminator columns for removal of genomic DNA and centrifuged for 30 sec at 13,000rpm. Cell lysates were further transferred to a fresh RNase free eppendorf tube and one volume of 70% ethanol added to flow through columns. Total RNA bound on spin columns were washed with RW1 and RPE buffer, prior to elution with 30µl of RNase free H_2O. RNA concentration and purity was determined post isolation using a NanoDrop (NanoDrop 2000, ThermoScientific) at 260/280 nm and 260/230 nm with the ratio of 1.8 is generally accepted as 'pure' for DNA and a ratio of 2.0 'pure' for RNA. Lower ratios are indicative of protein, phenol or other contaminants which absorb strongly at 280 nm. 260/230 values are typically higher for nucleic acids as a measure of purity. Generally, 2.0-2.2 is acceptable. Each reading was performed three times and the mean taken as exact concentration and normalised for subsequent cDNA synthesis. Isolated RNA was stored at - 80^{o}C.

6.6.2 Reverse transcription for cDNA synthesis

cDNA was transcribed from total isolated mRNA by reverse transcription. Eukaryotic mRNA comprises poly-A tail located at 3' end of mRNA sequence, and as such a poly-T oligonucleotide is utilised as primer in the reaction annealing to 3'end of mRNA, allowing for primer extension by reverse transcriptase enzyme using target mRNA strand as template.

Reverse transcription was performed using Tetro cDNA synthesis kit (Qiagen, UK) followed in accordance with instructions. Synthesised cDNA concentration was determined using NanoDrop and normalised as required using the mean value of three readings. Synthesised cDNA was subsequently used for gene expression analysis in qRT PCR with specific oligonucleotide primers designed for amplification of target genes. cDNA concentration was ascertained using a nanodrop at 260/280 nm. cDNA not used on day was stored at -20^{o}C.

6.6.3 Oligonucleotide primer design

Target gene sequences were obtained from National Center for Biotechnology (NCBI) database and primers ordered from Eurofins or PrimerDesign (PrimerDesign LTD, UK). The full mRNA coding sequences were converted to fasta formats and input into Basic alignment tool (BLAST) for alignment and similarity against other sequences. GC clamp presence, absence of hairpin loop, similar Tm and GC % content, and less than four polynucleotide runs where ensured. Sequences were input into Primer3 for specificity of target gene, available at (http://www.ncbi.nlm.nih.gov/tools/primer-blast) Primer sequences and NCBI data (table 6.5).

Table 6.5 Primer sequences and results for target genes

Primers		Sequence (5'-> 3')	Tm	GC %	Self 3'
FGF2	Forward	GCTGAAGACAATGGTGAGCCG	60.12	57.14	2.00
	Reverse	GGATTTGCCTCTAGAAGGGCG	60.99	57.14	2.00
CDK4	Forward	GCGTTCCGCGGATTGCATTAC	60.50	57.14	4.00
	Reverse	CTTCGACAGAAGGTCAGTGGC	60.19	57.14	3.00
E2F1	Forward	AAATGCCCATTCTCCACTTC	54.00	45.00	1.8
	Reverse	GAGGCTGACCTTTCTTCGAG	54.20	50.00	1.8
RPL19	Forward	GTTAGACCCAATGAGACCAATG	57.8	47.8	3.0
	Reverse	GTCACAGGCTTGCGGATGA	58.1	57.9	3.5

6.6.4 Quantitative Real Time PCR to determine mRNA expression levels of target genes

Synthesised cDNA was used for qRT PCR as a 2- step protocol for target gene expression analysis (MJ Research Opticon 2 monitor, BIORAD). SYBR Green SensiFAST SYBR Lo-ROX kit (Bioline, UK) and PrecisionPlus SYBR green master mix (PrimerDesign LTD, UK) were used in accordance with manufactures instructions. SYBR Green dye intercalates specifically to dsDNA, with an emission maxima and excitation of 494 nm and 521 nm respectively (Amaya, 2005). For SYBR Green SensiFAST SYBR Lo-ROX kit (Bioline, UK), a total volume reaction of 20 µl was used comprising; 4µl (25 ng) target cDNA, 10µl sensiFAST SYBR Lo-ROX kit (1X), 4.4µl Rnase/Dnase free H_2O, 0.8µl (400nM) FGF2 and CDK4 primer sequences.

For the protocol using PrimerDesign SYBR master mix, a 20 µl total volume reaction was used comprising; 10 µl of PrecisionPlus master mix, 1.2 µl (6 pmols) of target primer and 5 µl (10 ng) of target cDNA made up to the total volume with 3.8 µl Rnase/Dnase free H_2O. Samples were run in triplicate wells twice or duplicate wells three times for determination of relative gene expression compared against endogenous gene RPL19. Primer sequences are provided in table 6.5.

Cycling parameters are described in table 6.6 for gene expression analysis using SYBR Green SensiFAST SYBR Lo-ROX kit (Bioline, UK). Cycling parameters using PrecisionPlus SYBR green master mix (PrimerDesign LTD, UK) are summarised in table 6.7. mRNA expression analysis was performed using the Opticon system Monitor 3.1, BIORAD.

Table 6.6 Cycling conditions for q RT PCR using SYBR Green SensiFAST SYBR Lo-ROX kit (Bioline, UK) A 2- step protocol was undertaken using cDNA of target genes.

.

Parameters	Time	Temperature (°C)	Cycles
Enzyme activation	10 min	95	1
2 – step cycling			
Denaturation	15 sec	95	40
Annealing	30 sec	60	
Extension	5 min	72	
Melt curve analysis	15secs	60 – 90	1

Table 6.7 Cycling conditions for q RT PCR using PrecisionPlus master mix (PrimerDesign) A 2- step protocol was undertaken using cDNA of target genes. No final extension phase was used for this particular protocol as per manufacturer's guidance

Parameters	Time	Temperature (°C)	Cycles
Enzyme activation	2 min	95	1
2 – step cycling			
Denaturation	15 sec	95	50
Annealing	60 sec	60	
Melt curve analysis	30 secs	72 – 90	1

6.7 Small interfering RNA (siRNA) method

The term RNAi (RNA interference) was coined by Fire and Coll (1998) describing the phenomenon of introduction of dsRNA into a cell typically due to dsRNA activated protein kinase R from anti-viral response (Williams, 1999). This process triggers non-specific silencing of transcription and translation (Moselin and Preovenzano, 2004). Small interfering RNAs (siRNAs) thus occur naturally at the cellular level as a component of the post-transcriptional gene silencing mechanism. dsRNA nucleotides termed siRNAs can suppress mammalian gene expression in a specific manner resulting in gene silencing and gene knock down as opposed to gene knock out. siRNA

mechanism of action is a multi-step process shown as a schematic in figure 6 and briefly described: Long dsRNAs are initially processed by the functional RNAse III enzyme Dicer constituting helicase, dsRNA binding, and PAZ (piwi, argonaute, and zwille proteins) domains. The former two domains are important for dsRNA unwinding and mediation of protein-RNA interactions. Dicer produces 21–23 nucleotide dsRNA fragments with two nucleotides 3' end overhangs, i.e. siRNAs. RNAi is mediated by the RNA-induced silencing complex (RISC) guided by the siRNA, it recognises homologous mRNA to the siRNA sequence. RISC subsequently cleaves the mRNA in the middle of the homologous region. Thus, gene expression is specifically inactivated at a post-transcriptional (mRNA) level. Commercially available siRNA systems are available which use the above principle also resolving the issue of anti-viral response discussed in detail in (Williams, 1999). This is achieved by generation of synthetic siRNA from segmenting long dsRNAs or dicing small hairpin RNA with two base overhangs which are mRNA specific. These can be subsequently introduced into the cell via transfection for target gene silencing/knock down.

6.7.1 siRNA transfection for knockdown of target genes

For transient protein or mRNA knockdown of target genes; E2F1 and FGF2, 2 x 10^5 U2OS p53 ($^+/^+$) cells were seeded into 6 well plates in 2 ml antibiotic free DMEM media supplemented with 10 % FBS, and incubated at 37 ° C for 24 h. siRNA transfection for target gene silencing was performed using the commercially available siRNA transfection system from (SantaCruz Biotechnology Inc). The protocol was followed in accordance with manufacturer's instructions.

For optimum transient knockdown of target genes at the mRNA level a series of concentrations in increments of 20 pmols was performed as follows to make following solutions; Solution A; for 20 pmols; 2 µl (20 pmols) of target siRNA duplex was added to 100 µl of siRNA transfection medium (SantaCruz, sc: 36868). For 40 pmols; 4 µl (40 pmols) of target siRNA duplex was added to 100 µl of siRNA transfection medium. For 60 pmols; 6 µl (60 pmols) of target siRNA duplex was added to 100 µl of siRNA transfection medium.

For each transfection and to prepare Solution B; 2 µl (20 pmols) of transfection reagent (SantaCruz, sc – 29528) was added to 100 µl of siRNA transfection medium (SantaCruz, sc -36868). For 40 pmols; 4 µl (40 pmols) of transfection reagent was added to 100 µl of siRNA transfection medium. For 60 pmols; 6 µl (60 pmols) of transfection reagent was added to 100 µl of siRNA transfection medium. Solution A was directly added to the siRNA transfection Solution B prior to incubation at RT for 45 min. For each transfection, a non-coding scramble control was included (SantaCruz sc: 37007) to ascertain successful transfection and for comparison against target mRNA level. Scramble concentrations were prepared in exactly the same manner as Solution A and B above substituting scramble for siRNA duplex using; 2 µl (20 pmols), 4 µl (40 pmols) and 6 µl (60 pmols) of scramble instead of target siRNA duplex. The non-coding control contains a scrambled sequence which will not lead to specific degradation of any cellular mRNA.

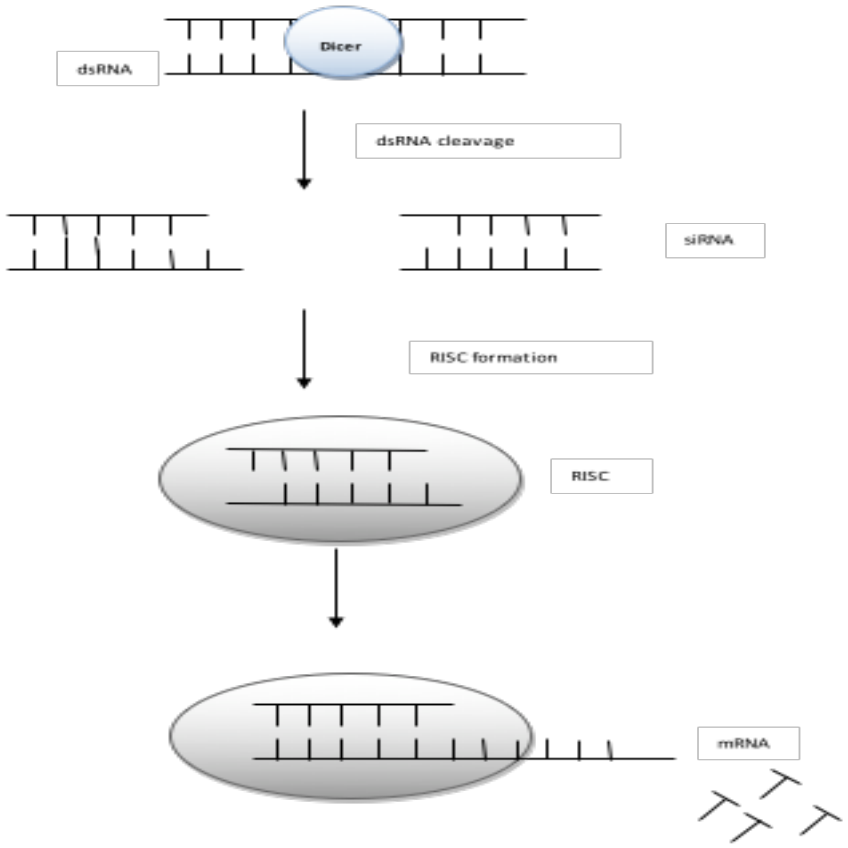

Figure 6 RNAi mechanism of action
dsRNA introduced into a cell for subsequent cleavage by DICER which binds and cleaves into short nucleotide pairs around 20 bp resulting in siRNA. In turn this RISC silencing complex utilises one siRNA strand to bind to homologous sequence of mRNA. RISC in turn degrades the mRNA thus silencing the expression of the target gene. This principle may be used in experimental settings to knock down target genes.

Proceeding 45 min incubation of both siRNA duplex and scramble solutions all cells were washed with 1 ml of transfection medium and aspirated. 0.8 ml of siRNA transfection media was added to both siRNA duplex and scramble solutions and mixed gently with a pipette prior to overlaying onto the washed cells. Cells were further incubated for 7 hr at 37 ° C. After incubation, 1 ml of DMEM media supplemented with 2 x FBS (20 %) and 2 x Penicillin streptomycin (2 %) was added to each well without removal of transfection mixture prior to incubation at 37 ° C for 24h for mRNA and 72h for protein.

Proceeding incubation (24 or 72 h), the media was aspirated from all wells and replaced with 1 x normal DMEM media containing 10 % FBS and 1 % P/S and incubated for a further 24 hr 37 ° C prior to RNA isolation. RNA isolation was performed as in 6.6.1 using the exact RNA isolation kit (QIAGEN, UK). qRT PCR was subsequently performed to ensure successful transfection via quantification of mRNA levels of target knockdown by comparison to controls of scrambled sequence. qRT PCR was performed as described in 6.6 using the exact same cycling parameters and conditions as set out in table 6.7 and analysed using the Opticon monitor 3.1, BIORAD. For protein isolation, methods were performed exactly as in 6.5.2.1. Protein concentration was determined by the relative method described in 6.5.2.2. Western blot analysis was subsequently performed to ensure successful transfection via analysis of protein levels and by comparison to controls of scrambled sequence as described in 6.5.2.

6.7.2 Fluorescein isothiocyanate based measurement for transfection efficiency

Fluorescein isothiocyanate (FITC) was performed to investigate transfection efficiency. Fluorescein is a light reactive dye for visual fluorescent microscopy which can be used to assess transfection efficiency. Fluorescein has an absorption maximum of 490 nm and emission maximum of 514 nm. Control siRNA Fluorescein Conjugate A (SantaCruz, sc – 36869) a non-coding scrambled sequence was used to measure transfection efficiency for the above mentioned transfections described in 6.7.1.
U2OS cells were seeded at 2 x 10^5 and incubated for 24 hr as in 6.7.1. The FITC protocol was performed as per manufacturer's guidelines (SantaCruz Biotechnology INC.). To measure optimum transfection efficiency, a series of FITC control concentrations in increments of 20 pmoles was used as follows; 20 pmols of siRNA Fluorescein Conjugate A was added to 100 µl of siRNA transfection medium (SantaCruz, sc: 36868), 40 pmols of siRNA Fluorescein Conjugate A was added to 100 µl of siRNA transfection medium and 60 pmols of siRNA Fluorescein Conjugate A added to 100 µl of siRNA transfection medium.

Solution A and solution B containing FITC was prepared exactly as described above in 6.7.1 Analysis of transfection efficiency was performed using adobe and with the kind help of Dr Geoff Parr of Salford Analytical Services.

6.8 MTT assay

A standard 5 day MTT [3-(4,5-dimethylthiazol-2-yl)-2,5-diphenyltetrazolium bromide] assay was used to determine the inhibitory concentration, 50 % (IC:50) of etoposide, gemcitabine and doxycycline on malignant mesothelioma Mero-14 cell lines. The IC:50 may be defined as is the concentration of drug that is required for 50 % inhibition *in vitro*.

Mero-14 cells were detached as described in 6.5.2.1 and 4.5 ml of fresh media was added to isolated cells in a 10 ml conical test tube. 10 μl of cell suspension was transferred to a hemocytometer for cell count to establish 2000 cells / well and a total of 100 μl cell suspension was seeded into MTT 96 flat well – plates

Serial dilutions of decreasing drug concentrations were undertaken in 10 ml conical test tubes supplemented with DMEM media and the relevant drug concentration added to each 96 well in triplicate. 100 μM cisplatin was used as control also serially diluted and added to relevant well in triplicate. Proceeding the plate set-up, cells were incubated for five days maintained at 37 ^{o} C with 5% CO_2. Following incubation, 50 μl of MTT [3-(4,5-dimethylthiazol-2-yl)-2,5-diphenyltetrazolium bromide) reagent was added to each well using a multi-channel pipette and incubated for 3 h maintained at 37 ^{o} C with 5% CO_2. Following this, MTT solution was aspirated from each well and 200 μl DMSO was added to each well using a multi-channel pipette. Results were read on a MTT plate reader using ascent software which measures the difference between 540 and 690 absorbance. 690 is a background reading providing a default to compare with 540 which shows cell viability. The IC:50 of each drug was determined using ascent software.

6.9 Microarray

Microarray technique is a high-throughput technology allowing for parallel gene expression analysis on a genome wide level. Microarrays allow for the identification of

many differentially expressed genes that have an established or redundant function in the specific area of interest.

Microarray methodology works on the principle of hybridization probing using fluorescently labelled nucleic molecules to detect complementary sequences (immobilized target DNA and mobile probe DNA, mRNA or cDNA). Proceeding mRNA isolation, cDNA probes are fluorescently labelled, if complementary hybridizing of the sample to the immobile target occurs. Image acquisition and data analysis is undertaken using specialist software that detects fluorescent labels of cDNA (probe) bound to each target spot on the hybridization plate. This is typically of a green to red ratio intensity, where green represents genes upregulated compared to control, red represents those downregulated compared to control. Yellow typically represents genes of equal abundance between experimental and control samples.

6.9.1 The Affymetrix Human Genome U133 plus 2.0 Array

The Affymetrix Human Genome U133 plus 2.0 Array (Eurofins, UK) was chosen as it provides complete coverage of the human genome U133 set plus an additional 6.500 genes for analysis of over 47.000 transcripts with accuracy and reproducibility.

6.9.2 Preparation of microarray samples

Human malignant mesothelioma adherent Mero-14 cell lines were seeded at 10^6 cells and treated with 10 μM etoposide, 1 μM gemcitabine (SIGMA, UK) and 50 μM doxycycline (SIGMA, UK) for 24 h with a control of untreated. To expose cells to low oxygen conditions to mimic hypoxia, Mero-14 cells were placed in a hypoxic chamber with 1 % oxygen for 24h with a control of untreated cells that were maintained at 37 ^{o} C with 5% CO_2 for 24 h. This was performed in duplicate as biological replicates.

Proceeding 24 h treatment and in accordance with Eurofins genomics UK, cells were washed twice with 1X PBS and collected using RLT buffer on ice, and centrifuged at 1500 RPM for 4 mins. Cell pellets were collected in a fresh Eppendorf tube containing RLT buffer and shipped on dry ice to Eurofins genomics (AROS, Denmark). RNA extraction and microarray procedure were performed by Eurofins, AROS, Denmark.

6.9.2.1 Microarray analysis

In order for gene expression levels to be comparable across microarrays, normalization procedures have to be undertaken (Smyth and Speed, 2003). Normalization tries to take into account variations arising from background noise, sample preparation and technology variation

On an array, an individual gene is represented by different oligonucleotide probes. Each probe pair consists of a perfect match (PM) oligonucleotide and a mismatch (MM) oligonucleotide. The PM probe contains an exact sequence complimentary to the target gene, thus measuring gene expression. The MM probe differs from the PM probe arising from a single base substitution which disrupts the binding of the target gene transcript. This helps to determine the background and nonspecific hybridization that contributes to the signal measured for the perfect match oligonucleotide. Two algorithms are typically used for normalization of microarray data, Mas5 and RMA. The Mas5 algorithm considers mismatch probes (MM) and calculates an average of the logged perfect match – mismatch probes (PM-MM) as such increased variation is noted at low signal strength arising, in part from the extra noise by subtraction of MM values from PM values. This can result in false positives. Robust multi-array (RMA) in contrast is a quantile normalization, ignoring MM values and as such do not suffer from this variation (Izarry et al. 2003). Thus, the RMA was used for background correction, quantile normalization of gene expression data and subsequent analysis.

All gene expression analysis using RMA CEL. files were undertaken using the Affymetrix expression console software, and in Bioconductor available in R. Tests were performed as one-way ANOVA comparisons. and statistically differentially expressed genes were determined by log fold changes > 1.5 and < - 1.5, Anova, $P < 0.05$ and adjusted Q value.

7 Results

7.1 Application of the signal transduction score flow algorithm to PKT206

The Boolean p53 model (PKT206) (discussed in section 4 and 6) and in detail in (Tian *et al.*2013) has been shown as a promising predictive interactome for investigating network perturbations of p53 – DNA damage pathways, highlighting its potential in anti-cancer strategies. Correct predictions of 52- 71 % were obtained using Boolean PKT206 from various *in silico* KO tests and comparison to various human microarray datasets revealing several potential novel predictions. Even so, greater predictive ratios are required to represent biological phenomena for future clinical relevance.

Boolean models whilst informative are often limited in their ability to truly depict the system providing an approximate representation. As discussed in section 4, discrete modelling approaches which consider only binary states are advantageous; they allow for the construction of large scale networks due to their simplification, therefore are computationally more efficient. This is in contrast to continuous models such as ordinary differential equations (Albert *et al.*2008). However, these simplifications have drawbacks, they cannot fully describe system dynamics frequently observed in diseased states or biological phenomena. Characteristically, genes may be assigned as either 'ON'/transcribed or 'OFF'/not transcribed and as such Boolean models are competent for such representation. However, consideration must be given to the complexity of the cellular interactome and its accompanying dynamics. Indeed, differential gene expression exhibits considerable inherent stochasticity and ambiguity which cannot always be described sufficiently by only two states. Therefore, a quantitative approach was undertaken to refine PKT206 for a more robust *in silico* model to clinical data and investigate the potential and use of a quantitative method.

The novel Signal Transduction Score Flow Algorithm (STSFA), described in detail in (Isik et al.2012) depicted as a schematic in figure 7, has demonstrated good correlation with transcriptome profiles. STSFA quantitatively evaluates biological activities of a cyclic

cellular network, and stimulates cell signalling flow on cyclic pathway topology, as opposed to the Boolean binary states of on or off in Boolean. Moreover, STSFA is capable of handling large data sets typically infeasible in extensive models. Using large scale 'omics' driven data, STSFA assigns dynamic gene scores throughout the network from source node to final cellular processes for pathway analysis, incorporating crucial topological signalling information such as feedback cycles and node stoichiometry, often lacking in logical models. Thus application of STSFA to PKT206 may provide a better representation of the complex p53 system.

7.1.1 Application of STSFA to the PKT206 model

The logical PKT206 model was constructed and described in detail by Tian *et al.* (2013) through text mining approaches and manual curation using the STRING database. Although PKT206 is a simplified view of the p53 system, it has established overall system attributes with good predictive ratios. Whilst extensive, the Boolean model remains qualitative. Both greater predictive ratios with a quantitative view are required for a more robust p53 network and truer representation of the biological system for clinical significance. The STSFA has demonstrated as a promising method for a quantitative view of large scale transcriptional networks. As such the STSFA was applied to the p53 interactome for investigation of p53 interactome performance to accurately stimulate experimental conditions using microarray data of human osteosarcoma SaOS2 ($p53^{-}/^{-}$), U2OS ($p53^{+}/^{+}$) untreated and treated with DNA damage inducing etoposide and, untreated human colon HCT116 p53 null and wildtype cells. These results were further compared to the LSSA analysed model for evaluation of p53 model performance.

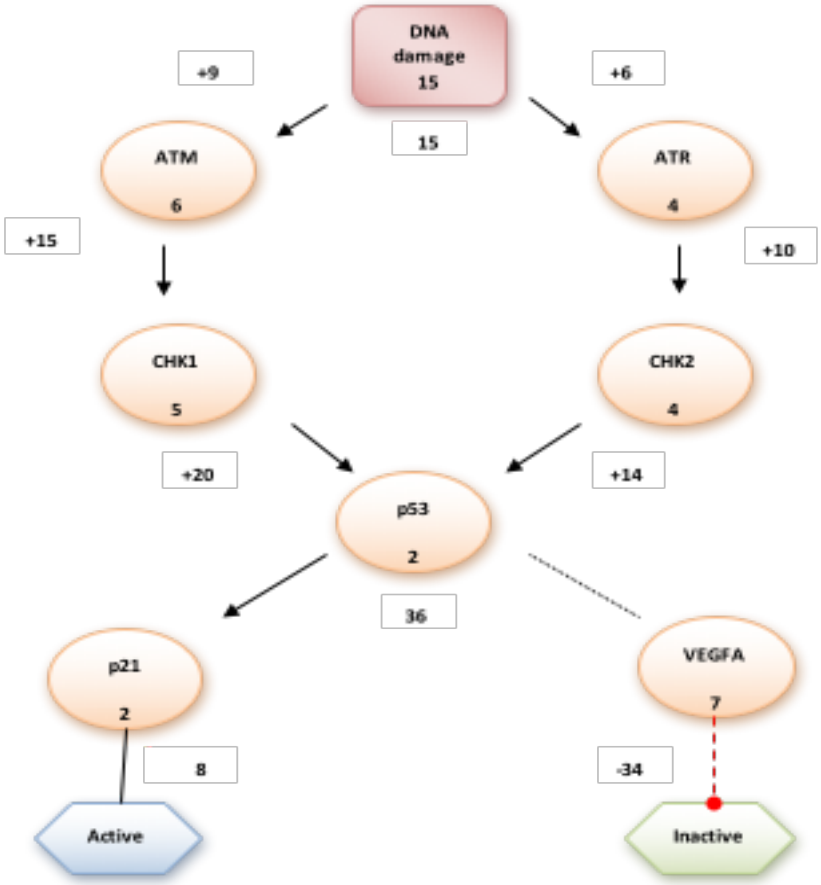

Figure 7 The signal transduction score flow algorithm principle. The initial score is shown in the square node of DNA damage. The score is subsequently transmitted downstream. For example, ATM and ATR, the sum of these is 10 therefore, 6/15 of protein ATM raw score is transmitted downstream to CHK1, and 4/10 is transferred to ATR. These scores subsequently transmit to p53 which receives the total score of 36 (2+20+14). This transmits to both VEGFA and p21. However, p53 to VEGFA edge is inhibitory, thus the score outcome is -34 and therefore considered inactive. Conversely, p21 is active with a score of 8.

7.1.2 Validation of the STSFA p53 interactome using genome wide analysis

To compare experimental to *in silico* model data, the $\log_{10}$ fold change (FC) (section 6) in gene expression scores, between experimental, and *in silico* conditions for each simulation were calculated, summarised in table 7, defined by the thresholds given in section 6 for each comparison. Figure 7.1 shows the frequency distribution of the $\log_{10}$ FC in STSFA gene activity scores between experimental and simulated conditions.

The STSFA model accurately predicted gene activity changes between both conditions of DNA damage and p53 knockdown for the majority of genes, with correct predictions

derived 73.5 - 82%, considered highly statistically significant (P=<1x10^{-16}) (table 7.1). Considering this accuracy, comparison of the STFSA model against the Boolean model performance and predictions was further evaluated.

7.1.3 Comparison of STSFA and LSSA for model performance and prediction to experimental data

Distributions of correct, small error and large error predictions were compared across all conditions (figure 7.1.1). The STSFA consistently demonstrated a higher proportion of correct predictions than LSSA, with average percentage of all U20S p53 $^{+}/^{+}$ and SaOS2 p53 $^{-}/^{-}$ simulations between LSSA (61%) and STSFA (75%) considered very highly significant, (P < 0.005). Similar results were also observed for untreated HTC116 p53 wildtype and null simulations of STSFA correct predictions (79%) and LSSA (52%), with over a two-fold increase of small errors, and a two - fold increase in large error predictions observed for LSSA than the STSFA model respectively. For every condition, the proportion of correct predictions were considered significantly significant (P, < 1x10^{-16}).

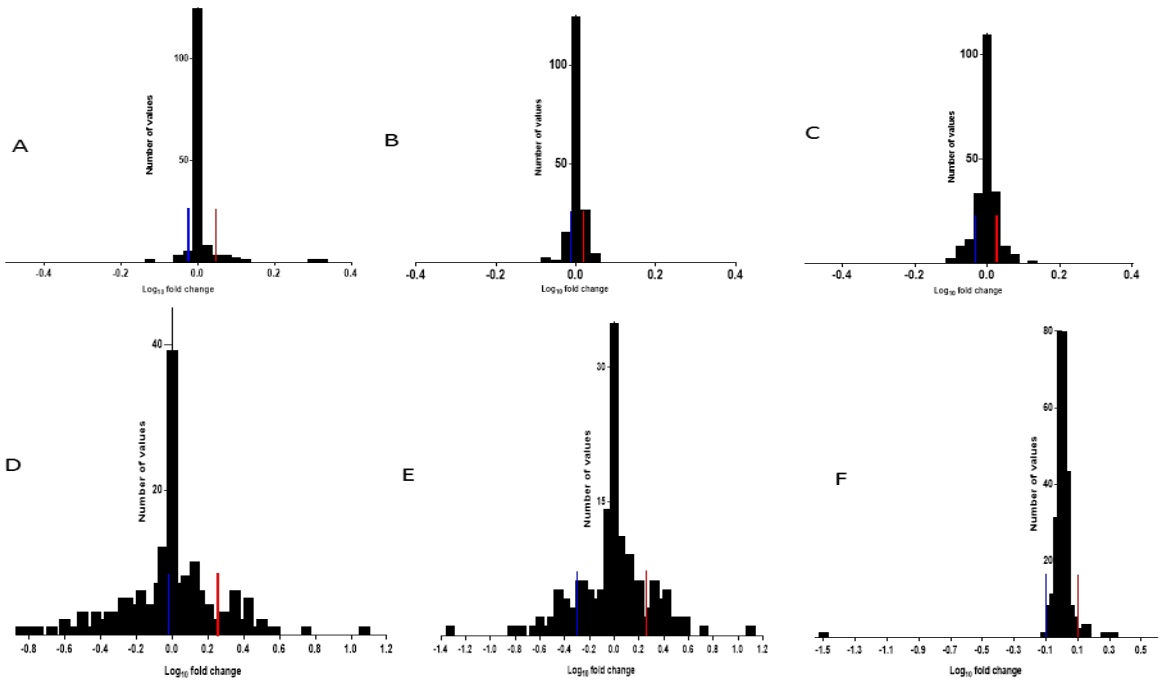

Figure 7.1 Frequency distribution of the log$_{10}$ FC in STSFA gene activity scores of experimental and simulated conditions. Two thresholds are shown for each condition, $\bar{x}$ - σ (blue bars) and $\bar{x}$ ± σ (red bars). Genes whose log$_{10}$ FC of gene activity score fell between these values were classified as 'no change', those above and below threshold values were 'upregulated' or

'downregulated', respectively. A) p53 wt DNA damage on vs p53 wt DNA damage off B) p53 null DNA damage on vs p53 null DNA damage off C) p53 wt DNA damage on vs p53 null DNA damage on D) p53 wt DNA damage off vs p53 null DNA damage off E) p53 wt DNA damage off vs p53 null DNA damage on F) p53 wt DNA damage on vs p53 null DNA damage off.

Taken together, these results demonstrate the STSFA accurately predicts gene activity changes between transcriptome data and *in silico* simulations. Moreover, the STSFA model is consistently more accurate than the logical p53 model providing a semi - quantitative representation of the PKT206 model.

Table 7 STSFA model performance by distribution of PKT206 and HTC116 predictions for each condition. Model predictive performance was evaluated with various gene expression profiles. Gene activity changes between experimental and simulated conditions were analysed using the approach given in section 6. Results were considered significant ($P<1x10^{-16}$) for all conditions. wt = wild type.

Condition	Prediction		
	True	Small error	Large error
p53 wt DNA damage off vs. p53 wt DNA damage on	159 (77%)	44 (21%)	4 (2%)
p53 wt DNA damage on vs. p53 null DNA damage on	158 (77%)	47 (22%)	2 (1%)
p53 wt DNA damage off vs. p53 null DNA damage off	158 (77%)	43 (20%)	6 (3%)
p53 wt DNA damage off vs. p53 null DNA damage on	152 (73.5%)	52 (25%)	3 (1.5%)
p53 null DNA damage on vs. p53 null DNA damage off	156 (75%)	49 (24%)	2 (1%)
p53 wt DNA damage on vs. p53 null DNA damage off	170 (82%)	35 (17%)	2 (1%)
HTC116 p53 wt DNA damage off vs. p53 null DNA damage off	137 (79%)	32 (19%)	3 (1.7%)

A)

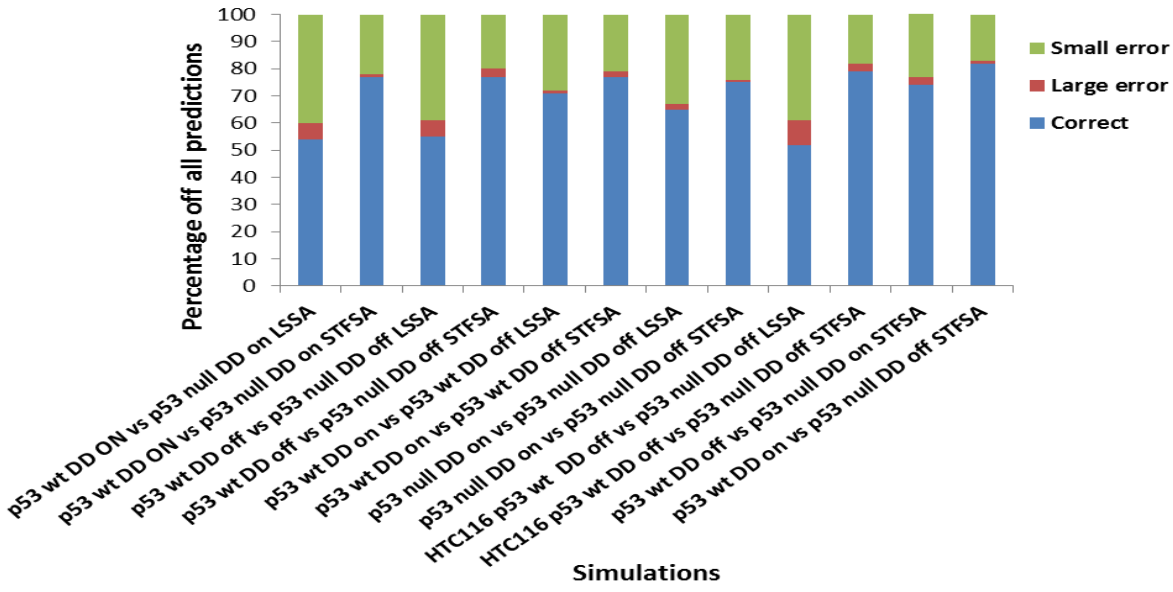

B)

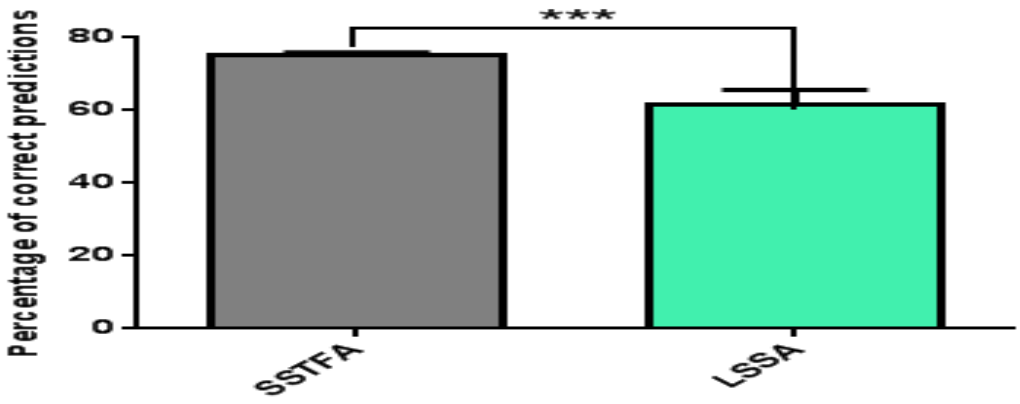

Figure 7.1.1 The STSFA p53 interactome is able to correctly predict the response to DNA damage and p53 knockout, and is more accurate than LSSA. **A)** The distribution of predictions made in each comparison (table 7), defined by the $\bar{x} \pm \sigma$ threshold. **B)** Comparison of mean percentage of correct predictions for each PKT206 SaOS2 p53 $^{-}/^{-}$ and U20S p53 $^{+}/^{+}$ simulations from Table.3 (Unpaired T Test, P = <0.005), ($\bar{x}$ ± SEM).

7.1.4 *In silico* knock out analysis of anti-apoptotic genes

Given the high level of accuracy demonstrated by the STSFA p53 model, *in silico* knock out analysis of potent anti-apoptotic genes were simulated. Apoptosis is well studied

and the most clinically relevant anti-proliferative program, thus identification of novel drug candidates targeting apoptosis is pivotal to effective therapies.

Genes chosen were those who had direct apoptotic effects, with fewest off target effects on the rest of the network. CKS2, IER3, C12orf5, WWP1, PSEN1, EPHB4 and PRSS50 were investigated as a result (figure 7.1.2 and 7.1.3). Knock out analysis demonstrated increased apoptotic $\log_{10}$ FC scores in target gene deletion backgrounds than that of wildtype (figure 7.1.2) with little effect on the rest of the network, indicative of the prospective of these as novel drug targets.

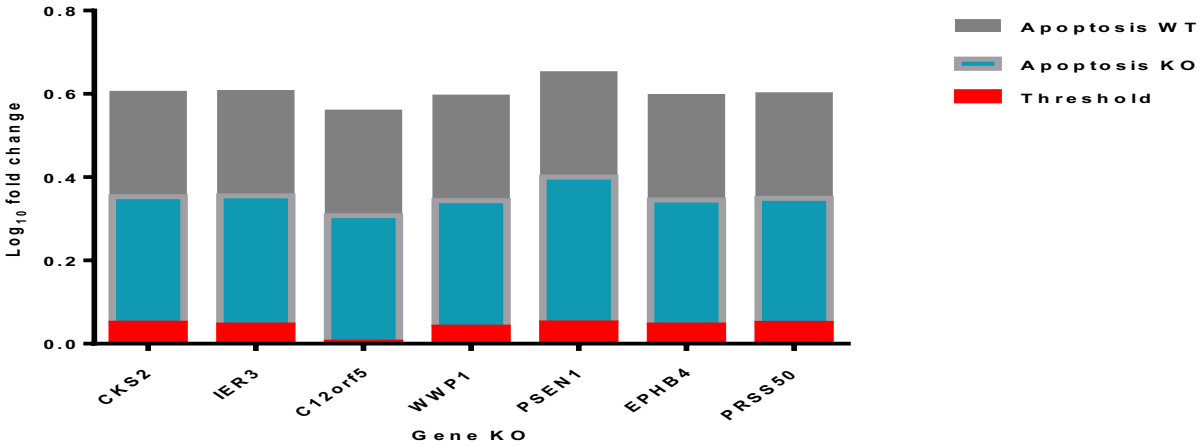

Figure 7.1.2 The Log_{10} fold change of STSFA activity scores for apoptosis and the x + σ threshold for each *in silico* gene knockout. Increased apoptotic scores were observed in target gene deletion backgrounds than in wildtype.

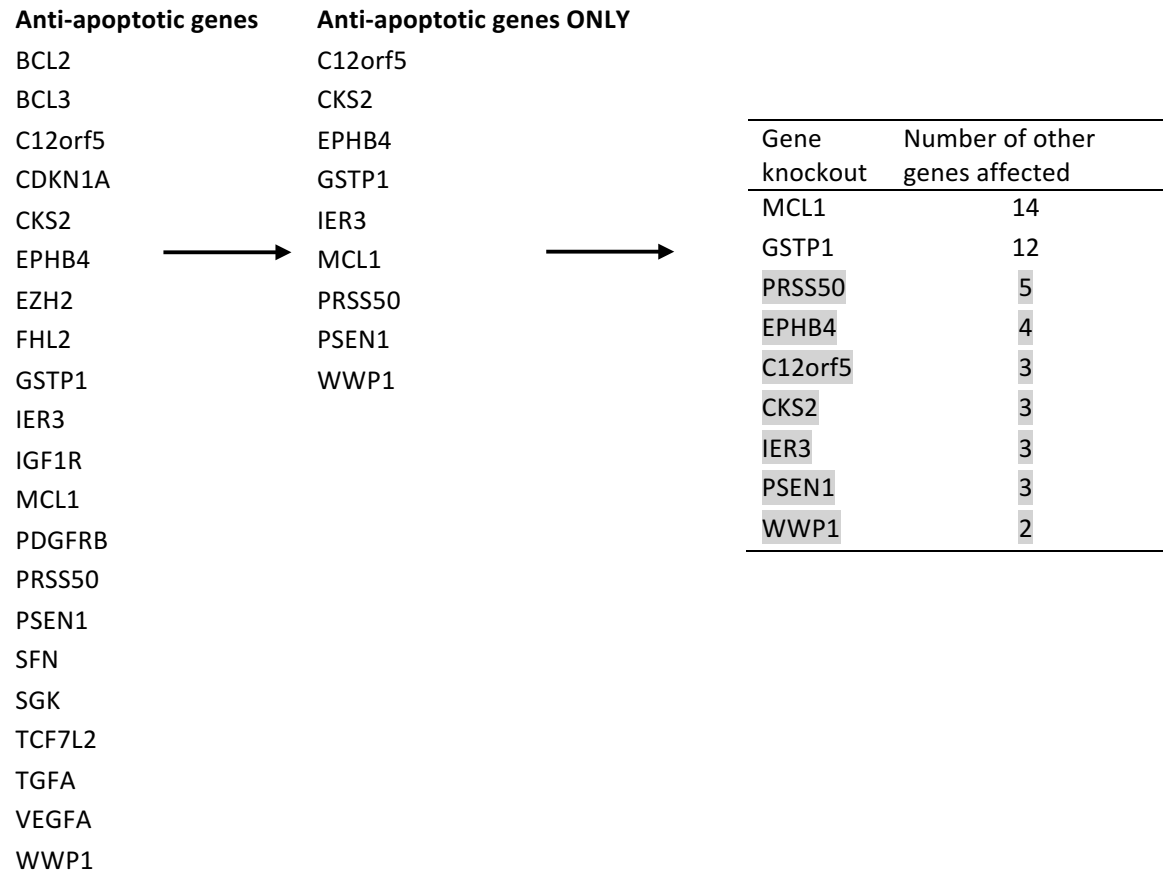

Figure 7.1.3 CKS2, IER3, C12orf5, WWP1, PSEN1, EPHB4 and PRSS50 are potential targets for inhibitory anti-cancer therapeutics. A flow diagram highlighting the selection of the identification of anti-apoptotic genes (highlighted in grey) from the PKT206 network, genes with the least effect on the network node population were chosen.

7.1.5 Conclusion

Here we have applied a novel algorithm recently described (Isik *et al.*2012) to the PKT206 p53 interactome utilising raw expression data of U2OS p53 $^{+}/^{+}$ and SaOS2 p53 $^{-}/^{-}$, and untreated HTC116 colon cancer p53 null and wildtype cell lines (Tian *et al*.2013) to investigate overall STSFA model enactment and, finally compare *in silico* prediction of experimental data to the PKT206 logical model.

Dynamic biological phenomena such as cancer and p53 networks display system complexity, involving multivariate dysregulation of signalling pathways governing fundamental cellular processes (Hornberg *et al.*2006). Thus, *in silico* representations must encode mathematical models of a quantitative nature for true representation (Wilkinson *et al.*2000: Bachmann *et al.*2011). The STSFA p53 interactome described

here has accurately predicted overall system attributes in response to p53 – DNA damage inducible pathways when compared to transcriptome *in vitro* experimental data. These results provided a semi quantitative representation of the p53 system as opposed to the qualitative Boolean approach. Furthermore, to investigate potent anti-apoptotic candidates, we mimicked *in vivo* mutations of anti-apoptotic nodes using in various *in silico* knock out backgrounds. Here we describe, WWP1, CKS2 and EPHB4 as putative cancer drug targets.

Slightly greater predictive ratios were obtained utilising STSFA than LSSA (73.5 - 82 %) (table 7), achieved by incorporation of stoichiometric processes during signal flow pathway analysis not considered in LSSA. Deterministic qualitative models such as Boolean often fail to capture the heterogeneity and stochasticity associated with large 'omics' driven biochemical networks. Boolean logic assigns static gene states only, of ("ON/1") and ("OFF/0") referring to genes expressed or non-expressed respectively, thus are limited for true system representation. Discrete models provide good approximation of the qualitative behaviour of the system (Kauffman *et al.*1969: Albert *et al.*2008). These networks may be represented by directed graphs or hypergraphs where transfer states of edges are derived using logical operators of; AND, OR and NOT (Klamt *et al.*2009). In naïve Boolean models no reaction rates are incorporated in transfer functions, thus no kinetic parameters are required. This simplicity allows for large scale modelling, which has been applied successfully to cancer networks (Schlater *et al.*2009; Sridhoron *et al.*2012; Rodrigeuz *et al.*2012). However, Boolean models have limitations. Differential gene expression exhibits considerable inherent stochasticity and ambiguity, which cannot be described sufficiently by only two states. Therefore, poor predictive accuracy may be a consequence of the inference of deterministic functions. Indeed, many of these simplistic approaches appear robust when analysed *in silico,* however display considerably reduced enactment once applied to experimental 'omics' datasets and can only be used for approximates and statistical based system analysis rather than experimental representation (Soranzo *et al.*2007; Zhongxing *et al.*2008). The score flow algorithm however, captures such gene dynamics applying an empirical approach utilising 'omics' data driven gene enrichment of a particular pathway. It incorporates stoichiometric processes as score partitions, stimulating

cellular signal flow on cyclic pathway topology rather than static binary node states. Thus is more apt for genome wide data analysis and *in silico* representation.

The STSFA p53 interactome has revealed several anti- apoptotic genes which may offer therapeutic potential. These had little effect on the rest of the network, and as such were considered good candidates (figure 7.1.3). Moreover, downstream nodes which were affected by the target gene KO were also of interest. For example, deletion of EPHB4 resulted in downregulation of the potent pro angiogenic factor VEGFA. Those considered as putative drug candidates are briefly described.

CKS2 (essential for cyclin dependent kinase function) expression is upregulated in several tumour types and associated with poor prognosis. CSK2 knockdown resulted in increased apoptosis and tumorigenic loss in prostate cancer cells (Lan *et al.*2008), whilst its overexpression results in a loss of S phase checkpoint and continuation of cell cycle progression (Liberal *et al.*2012). The E3 ubiquitin ligase, WWP1 role in cancer is less defined. However, its upregulation is associated with cell proliferation in breast cancer cells promoting growth. Conversely, this study also revealed that decreased WWP1 expression had a worse prognosis than in WWP1 wt tumours in another breast cancer tumour type. Thus, WWP1 may be tissue specific (Zhi and Chen, 2012), and may be promising for novel, targeted cancer therapeutics.

The receptor tyrosine kinase EPHB4 is also a pro angiogenic factor, overexpressed in several cancers (Chen *et a*l.2013; Hasina *et al.*2013; Li and Zhao, 2013). A recent study blocking EPHB4 function resulted in decreased tumour growth (Krasnoperov *et al.* 2010). Therefore, this protein seems to be a promising target for novel, broad range cancer therapeutics.

Even though the STSFA p53 model identified overall system attributes, limitations were observed of several incorrectly predicted genes. Those identified were in the majority connected only to, and downstream of p53. Considering the plethora of upstream genes influencing p53 activity (71 nodes), this is not surprising, with any small error within these nodes traversing to p53. This could be challenging as the network

increases. One factor to consider is that p53 has nine isoforms differing at the N and C termini arising from the presence of a second promoter in intron one, alternative mRNA splicing and an alternative translation initiation site at AUG40 (Courtois *et al.*2002; Bourdon et al.2005; Khoury *et al*.2010). As such the p53 node in PKT206 represents all gene isoforms. Different isoforms have distinct roles and binding partners, thus amalgamation into one node may compromise its ability to simulate the response of signalling pathways to changes in experimental conditions. Therefore, consideration of integration of these isoforms into the network, may resolve such network limitations. Another factor to consider is that PKT206 is a global cancer model. Downstream responses by p53 are both cell type dependant and also governed by the differentiation state of the cell (Marcel and Hainaut, 2005). Thus, constructing cell / tissue specific models may overcome this issue. Lastly, a sole input of DNA damage and output of apoptosis are only described by PKT206, where in fact p53 initiates several anti-proliferative downstream programs and is also induced by various other stresses in addition to DNA damage, for example, hypoxia. Indeed, even DNA damage has different forms of ssDNA and dsDNA break which influence downstream nodes. Possible addition of this diversity in the model should be explored.

Nevertheless, and in conclusion, the STSFA PKT206 model described here has provided a semi quantitative representation of the p53 interactome producing a promising platform for a fully quantitative, predictive transcriptional p53 model.

7.2 Generation of the PMH260 model

Both quantitative (Hussain et al. 2014) (section 7.1) and the qualitative p53 DNA – damage model (Tian et al. 2013) have shown good predictive potential for dissecting p53 network dynamics, both deriving over 70 % average correct predictions when compared to various human *in vitro* generated microarray profiles. This has provided a promising platform for further studies using predictive logical models for personalised anti-cancer strategies.

Nevertheless, the network complexity of p53 and its regulatory pathways with the vast literature base makes it a challenging system. Although over 85, 000 PubMed publications are linked with the keyword p53 (PubMed, May, 2016), we are still far from fully elucidating the role of p53 and its associated pathways governing tumorigenesis. In order to gain an increased understanding of p53 regulatory networks, information at the molecular level must be integrated into a coherent framework, and computational methodologies are novel tools to depict the heterogeneity of disease networks such as cancer.

Cancer systems biology is a relatively novel, yet promising field that can utilize high-throughput data to analyse intracellular network perturbations (Wang, 2010). These integrative approaches can offer potential to systematize and predict molecular deviations of the cancer phenotype. Predictive models can be of both clinical and pharmaceutical relevance for the development of novel effective therapies. Indeed, several computational studies of different mathematical complexities have already been developed in an effort to address this, including the modelling of p53 (Kreeger and Lafenberger, 2010).

Even though the quantitative model (Hussain et al.2014) has successfully simulated overall system attributes, Boolean networks are a promising predictive framework for cancer modelling. The most simplistic of models defining binary states of ON or OFF to represent gene activation or inhibition, can effectively recapitulate gene expression *in silico,* allowing for larger scale modelling. Logical networks have been applied successfully to model various biological phenomena (Shmulevich and Kauffman, 2004; Schaltter et al.2009 and Tian et al.2013).

Even though Boolean PKT206 has demonstrated overall system attributes, the p53 network is extensive. In fact, over 1000 p53 responsive genes have been previously described (Riley et al.2008), and previous attempts to superimpose microarray data to PKT206 were problematic due to network size (unpublished data, Tian et al.2013). In addition, for greater representation of cancer dynamics, predictive models must incorporate and depict the heterogeneity of diseased states and the processes that

govern them. For example, defined as hallmarks of cancer, angiogenesis and apoptosis are pivotal properties to the tumour environment (Hanahan and Weinberg, 2011). Further, it is well established that perturbed apoptotic pathways are a major cause of chemo-resistance (Fulda, 2009). Therefore, consideration of such processes are crucial to correctly represent tumour dynamics (Wang, 2010), in particular for discovery of potential anti-cancer strategies

With this in mind, we have expanded PKT206 to generate a larger, more robust model for elucidation of p53 – cancer dynamics. We have incorporated three additional outputs (angiogenesis, cell cycle arrest and DNA repair) allowing for processes involved in p53 governed tumorigenesis to be modelled and analysed systematically, and ascertain if the expanded Boolean model can correctly predict overall system attributes in response to network perturbations by comparison to transcriptome data.

7.2.1 Results

7.2.1.1 Generation of the PMH260 model

The generation of PKT206 is described in detail elsewhere (Tian et al. 2013), also discussed here (section 4).

The PMH260 model was generated by expansion of PKT206 which originally comprised 206 nodes with 738 interactions. Given the fact that STRING was identified as the best source for p53 information from over 30 databases (Tian, K, PhD thesis, University of Manchester, 2013) for construction of the PMH260 network, we followed the same principle for consistency in accordance with PKT206 generation (Tian et al.2013). Additional interactions direct to p53 were extracted from the STRING database (v9.1) (Szklocyk, 2011). Interactions were only considered if their confidence score was high, set at 0.7 by a STRING schema. This resulted in a possible 81,000 STRING interactions described for p53.

Interactions were filtered according to the nature of their interaction (post translational modification, binding, expression, activation and inhibition) and any duplicated information removed arising from the value of direction. This resulted in a total of 12,545 possible interactions from 81,000. Additional filtering was undertaken to separate the first and second layer of the network, referring to proteins that directly interact with p53 and proteins which interact with each other respectively. For example, both ATM and CHK1 activate p53, these are direct and considered as the first layer, whilst, ATM activates CHK1, this defines interactions which are independent of p53 and refers to the second layer of the model. This resulted in a total of 967 possible interactions direct to p53 for manual curation.

As we initially aimed to expand the model slightly to test if the model could successfully simulate and predict overall system attributes, we created a preliminary model and considered 54 additional internal nodes. This resulted in an extra 242 interactions between existing (PKT206 nodes) and new nodes (n = 54). Manual curation for validation of these interactions were also undertaken for model accuracy and additionally confirmed with the kind help of supervisor, Prof. M. Demonacas. At least one documented scientific publication was used for an interaction, some described by more.

Three additional outputs were also included into PMH260 (cell cycle arrest, DNA repair and angiogenesis) and all internal nodes (n = 254) were linked to the biological processes that they regulate or are regulated by (DNA damage) via their edge function of inhibition, activation or ambivalent factor. These links were initially selected based upon their GO annotations via the Gene Ontology (GO) database, and additionally manually curated by scientific literature for confirmation of interactions. As the PKT206 model did not consider the three additional outputs, all internal nodes (n = 203) of the PKT206 network were linked to these outputs (cell cycle arrest, DNA repair and angiogenesis).

7.2.1.2 PMH260 network topology

The PMH260 model comprises a network considering 260 nodes (including 1 input and 5 outputs) with 980 interactions of activation or inhibition. A total of 42 nodes were regulated by the single input to the model (DNA damage) which serves as environmental stress. Of these, 37 were activated by DNA damage, 5 inhibited. Amongst the five outputs; 118 nodes regulated apoptosis, 42 regulated angiogenesis, 68 regulated cellular senescence, 28 regulated DNA repair, and 62 regulated the cell cycle arrest output.

Of the internal nodes linked to p53, 117 nodes were located upstream of p53, with 164 downstream, 27 nodes were considered as ambivalent factors (activating and inhibiting). 34 feedback loops were identified in the model, of these p53 participated in over 50 % (n = 18). Tables 7.2.1 – 7.2.6 summarise all nodes and their links to the single input or five outputs. Image 7.2 depicts the different layers of the PMH260 model, generated in Cytoscape (v.28).

Table 7.2 Total interaction list of all nodes in the PMH260 model.
Table includes interactions of activation or inhibition (excludes GO annotations). Some interactions are described by more than one literature source. PMID AND PMC IDs are supplied. For some sources, PMID/PMCs were not available, thus links or DOIs are provided. Interactions derived from Tian et al. (2013) are also included.

Source	Interaction	Target	PMID/PMC
AATF	Activates	p53	20708154
AATF	Activates	CDK5	18388733
APP	Inhibits	p53	10377452
AR	Inhibits	MMP1	8798622
ASPP1	Activates	p53	11684014
ASPP1	Activates	p53	22552744
ASPP2	Activates	p53	22552744
ATF3	Inhibits	MMP2	11792711
ATF3	Activates	CCND1	11375399
ATF3	Inhibits	IL6	16688168
ATM	Activates	p53	10608806
ATM	Activates	CHEK2	16936775
ATM	Activates	ATR	17088261
ATM	Activates	AATF	17157788
ATM	Inhibits	BCL6	18346918
ATM	Activates	BRCA1	12082091
ATM	Activates	DYRK2	19965871

ATM	Inhibits	MDM2	16943424
ATM	Inhibits	MDM4	16943424
ATR	Activates	p53	16557269
ATR	Activates	CHEK1	16557269
ATR	Activates	AATF	17157788
ATR	Activates	BRCA1	12082091
ATR	Inhibits	MDM2	16943424
AURKA	Inhibits	p53	14702041
AXIN1	Activates	p53	19513548
AXIN1	Inhibits	CCND1	11739413
AXIN1	Inhibits	TCF7L2	17768662
BAIAP2L1	Inhibits	p53	21887275
BAIP2L1	Inhibits	p53	PMC3160901
BCCIP	Activates	p53	15539944
BCL2	Activates	MMP2	19258038
BCL2	Activates	CCND1	11313702
BCL2	Activates	FOS	15326476
BCL2	Activates	VEGFA	12205045
BCL2	Activates	SLC2A1	15120582
BCL2	Activates	RAS	15326476
BCL3	Activates	EGFR	17881446
BCL6	Activates	p53	18524763
BCL6	Inhibits	p53	15577913
BCL6	Inhibits	CDKN1B	10981963
BRCA1	Activates	p53	11371136
BRCA1	Activates	CCND1	17278098
BTG2	Activates	p53	11814693
BTG2	Inhibits	CCND1	15378000
CCAR1	Activates	p53	PMC2562329
CCNA	Inhibits	CKM	8995365
CCNA	Activates	CDC25A	10926775
CCNA	Inhibits	FEN1	12853968
CCNA	Inhibits	E2F1	7838523
CCNA	Activates	AXIN1	15063782
CCND1	Inhibits	THBS1	17020778
CCND1	Activates	HSPA4	9121772
CCND1	Activates	E2F1	10504464
CD44	Inhibits	CCND1	17296798
CDC25A	Inhibits	EGFR	11912208
CDK2	Activates	p53	11078726
CDK2	Activates	CDC25A	10926775
CDK2	Inhibits	CDKN1B	8622855
CDK2	Activates	E2F1	7969176
CDK2	Activates	AXIN1	15063782

CDK2	Activates	CCNA	10652300
CDK2	Inhibits	MDM2	21278451
CDK4	Activates	CCND1	9099745
CDK4	Activates	BRCA1	10660629
CDK4	Inhibits	BRCA1	17334399
CDK5	Activates	p53	17591690
CDK5	Activates	MYC	18408012
CDK5	Activates	ERBB2	16203963
CDK5	Activates	CDKN1B	16341208
CDK9	Activates	p53	16741955
CDKN1A	Inhibits	CDK2	8756624
CDKN1B	Inhibits	BCL2	14676836
CDKN1B	Inhibits	CCNA	8547220
CDKN1B	Inhibits	CDK2	18354415
CDKN2A	Inhibits	CCND1	15205322
CDKN2A	Inhibits	MDM2	20523835
CDKN2A	Activates	MDM4	15907800
CDKN2A	Inhibits	MDM4	16492744
CHEK1	Activates	p53	10673501
CHEK1	Inhibits	CDC25A	12759351
CHEK1	Inhibits	MDM4	16511572
CHEK2	Activates	p53	10673500
CHEK2	Activates	MYC	19812253
CHEK2	Inhibits	CDC25A	12759351
CHEK2	Activates	BRCA1	14701743
CHEK2	Activates	E2F1	12717439
CHEK2	Activates	AATF	17157788
CHEK2	Inhibits	MDM4	16943424
CIAPIN1	Inhibits	p53	16410721
CIAPIN1	Inhibits	BAX	16410721
CIAPIN1	Inhibits	BCL2	18059532
CSNK2	Activates	FOS	1915270
CSNK2	Activates	p53	9244359
CSNK2	Activates	MDM2	16335531
CSNK2	Inhibits	MDM2	21769452
CSNK2	Activates	TCF7L2	11711551
CSNK2	Activates	PTEN	11035045
CSNK2	Activates	MYC	2663470
CSNK2	Activates	MYCN	1425701
CSNK2	Activates	NCL	3190709
CSNK2	Activates	HDAC1	11602581
CUL7	Inhibits	p53	17586686
CUL7	Inhibits	p53	17229476
CUL7	Inhibits	p53	16547496

CXCR4	Activates	VEGFA	17559806
CXCR4	Activates	TNFRSF10B	15990565
DAP	Activates	p53	11146619
DAXX	Activates	p53	12482984
DAXX	Inhibits	p53	15364927
DAXX	Inhibits	p53	15339933
DAXX	Activates	p53	17210684
DDX20	Inhibits	p53	22335944
DDX5	Activates	p53	15660129
DKK1	Activates	TGFB1	20019166
DNMT3A	Inhibits	p53	16131836
DUSP5	Inhibits	MAPK1	8221888
DYRK2	Activates	p53	17349958
DYRK2	Activates	p53AIP1	17349958
E2F1	Activates	p53	12625370
E2F1	Inhibits	MDM2	20837136
E2F1	Activates	HIC1	19491197
E2F1	Activates	SIVA1	15105421
E2F1	Activates	APAF1	18056406
E2F1	Inhibits	MCL1	11857079
E2F1	Inhibits	AR	17178887
E2F1	Activates	PCNA	12468739
E2F1	Activates	MYCN	14645238
E2F1	Activates	CHEK2	15024084
E2F1	Activates	SIAH1	20187294
E2F1	Activates	EZH2	19893569
EGFR	Activates	CCND1	19935697
EGFR	Activates	PTGS2	15781636
EGFR	Inhibits	NOTCH1	18604200
EGFR	Activates	VEGFA	21074412
EGFR	Activates	ESR1	19470835
EIF2AK2	Activates	p53	19210572
ELAVL1	Activates	p53	12821781
ELAVL1	Inhibits	CDKN1B	18354415
ELAVL1	Activates	PTGS2	14633672
ELAVL1	Inhibits	MYC	19574298
ERBB2	Inhibits	p53	8700512
ERBB2	Activates	CCND1	17483350
ERBB2	Activates	CXCR4	15542424
ERBB2	Inhibits	CDKN1B	16951165
ERBB2	Activates	PTGS2	11901151
ESR1	Activates	LTF	15525592
ESR1	Activates	CCND1	15544931
ESR1	Inhibits	IL6	16043358

ESR1	Inhibits	EGFR	9269899
ESR1	Activates	CKB	11746525
ESR1	Activates	MYC	19661132
EZH2	Inhibits	RAD51	16331887
FAS	Activates	p53	9358752
FGF2	Activates	MMP2	19107653
FGF2	Activates	CDK4	11889462
FGF2	Activates	THBS1	15927970
FGF2	Activates	ABCB1	17620438
FGF2	Activates	FOS	8783257
FGF2	Activates	MMP1	19107653
FGF2	Activates	BCL2	11380405
FGF2	Activates	PTGS2	9920767
FGF2	Activates	VEGFA	15485645
FGF2	Activates	PCNA	17003443
FHL2	Inhibits	MAPK1	14729955
FOS	Activates	CCND1	9710644
FOS	Activates	MMP1	21344389
FOS	Activates	BCL2	19079363
FOXM1	Activates	MMP2	17804744
FOXM1	Activates	VEGFA	17804744
FOXM1	Activates	CCNB1	11682060
GAPDH	Activates	SIAH1	15951807
H2AFZ	Inhibits	p53	17671089
HDAC1	Inhibits	p53	12426395
HF1A	Activates	CDKN1B	19342889
HIF1A	Activates	CXCR4	19212630
HIF1A	Activates	IL6	20600219
HIF1A	Activates	MMP1	17335808
HIF1A	Activates	VEGFA	17919812
HIF1A	Activates	SLC2A1	17387384
HIF1A	Activates	PLAUR	17335808
HIPK2	Inhibits	MDM2	16212962
HIPK2	Inhibits	HIF1A	19046997
HIPK2	Inhibits	POU4F1	15492043
HIPK2	Activates	p53	16601678
HIPK4	Activates	p53	18022393
HOXA10	Activates	p53	15044858
HOXA11	Inhibits	p53	19372592
HOXA5	Activates	p53	12490103
HOXA5	Inhibits	p53	12490102
HSP90AB1	Inhibits	MMP13	18593760
HSPA4	Activates	p53	17278883
HSPA4	Activates	p53	17278883

HSPA4	Inhibits	FOS	11189444
HTATIP2	Activates	p53	18519672
HTATIP2	Inhibits	MMP2	19349353
HTATIP2	Inhibits	VEGFA	19349353
HTATIP2	Inhibits	MYC	15073177
iASPP	Inhibits	p53	22552744
iASPP	Inhibits	p53	12524540
ICAM1	Activates	FOS	12097408
ID3	Inhibits	p53	19618124
IFNA1	Activates	p53	15254403
IFNA1	Activates	MDM2	15580300
IFNA1	Activates	CXCR4	18202009
IFNA1	Activates	IL6	12434062
IFNA1	Inhibits	FGF2	9485039
IFNA1	Activates	ICAM1	11593644
IFNA1	Inhibits	ABCB1	17331344
IFNA1	Activates	EGFR	1718587
IFNA1	Activates	TLR3	16087162
IFNA1	Activates	FOS	15970516
IFNA1	Inhibits	BCL2	12881711
IFNA1	Activates	PTGS2	16685393
IFNA1	Activates	FAS	14616354
IFNA1	Inhibits	MYC	11798827
IFNA1	Activates	MYC	10068671
IFNA1	Activates	TNFRSF10B	12642868
IFNA1	Inhibits	E2F1	10208422
IFNA1	Activates	EIF2AK2	15254208
IFNA1	Activates	PRKCA	17988665
IGF1R	Activates	p53	8710868
IGF1R	Activates	MDM2	17846171
IGF1R	Activates	RAS	19174523
IGFBP7	Inhibits	PTGS2	19374835
IGFBP7	Inhibits	VEGFA	19374835
IL6	Activates	MMP2	16934628
IL6	Activates	CXCR4	9933168
IL6	Activates	EGFR	9459124
IL6	Inhibits	BAX	12101271
IL6	Activates	TGFA	11892999
IL6	Activates	FOS	11713282
IL6	Activates	MMP1	16934628
IL6	Activates	MMP13	15601621
IL6	Activates	PTGS2	16837651
IL6	Activates	MYC	20974848
ING4	Activates	p53	12750254

ING4	Activates	p53	3742747
ING5	Activates	p53	12750254
JUN	Inhibits	p53	10072388
KLF4	Activates	p53	19696146
KLF4	Inhibits	p53	16244670
KLF4	Inhibits	CCNB1	14627709
LATS2	Activates	p53	17015431
LTF	Inhibits	CCND1	18697201
MAPK1	Activates	CCND1	9618377
MAPK1	Activates	p53	11409876
MAPK1	Activates	NR2C1	18682553
MAPK1	Activates	YBX1	16198352
MAPK1	Activates	RAF1	1730637
MAPK14	Activates	MMP2	15677464
MAPK14	Activates	SGK	12488318
MAPK14	Activates	p53	18265945
MAPK8	Activates	TGFB1	12760970
MAPK8	Activates	MMP2	16672691
MAPK8	Activates	CCND1	21135252
MAPK8	Activates	ICAM1	15389584
MAPK8	Activates	FOS	17085440
MAPK8	Activates	ATF3	18377912
MAPK8	Activates	PTGS2	15546960
MAPK8	Activates	p53	11057897
MAPK8	Activates	BAX	16709574
MAPK8	Activates	BCL2	11323415
MAPK8	Inhibits	E2F1	10075927
MAPK9	Activates	PTGS2	9786861
MAPK9	Activates	p53	17525747
MCTS1	Inhibits	p53	17416211
MCTS1	Activates	CCND1	11709712
MDM2	Inhibits	p53	21423613
MDM2	Activates	ABCB1	8883415
MDM2	Activates	HIF1A	15024078
MDM2	Inhibits	VEGFA	18199551
MDM2	Inhibits	MDM4	16557269
MDM2	Inhibits	DYRK2	19965871
MDM4	Activates	MDM2	16557269
MDM4	Inhibits	p53	16557269
MMP2	Activates	BAX	16857167
MTA2	Inhibits	p53	17914590
MTA2	Inhibits	p53	12920132
MUC1	Inhibits	p53	15710329
MUC1	Activates	CCND1	14688481

MUC1	Activates	EGFR	16082192
MYC	Activates	p53	9839551
MYC	Activates	MMP2	19258038
MYC	Activates	CCND1	7526316
MYC	Activates	MSH2	15814658
MYC	Activates	HSPA4	1459202
MYC	Activates	CDC25A	10205150
MYC	Inhibits	BCL2	11438662
MYC	Activates	BRCA1	21668996
MYC	Inhibits	GADD45A	15021909
MYC	Activates	VEGFA	15580293
MYC	Inhibits	CDKN1A	12408820
MYC	Activates	NME1	11960382
MYC	Activates	TNFRSF10A	17881904
MYC	Activates	E2F1	17784791
MYC	Activates	CDK2	8157956
MYCN	Activates	p53	20145147
MYCN	Activates	ABCC1	14737110
MYCN	Activates	ABCB1	12819037
MYCN	Inhibits	CD44	11035936
MYCN	Inhibits	MYC	7529553
MYCN	Inhibits	CDKN1B	18198336
MYST4	Activates	p53	19001415
NCL	Inhibits	p53	16213212
NCL	Inhibits	MDM2	16751805
NCL	Activates	BCL2	21048921
NME1	Activates	PTGS2	16415009
NME1	Activates	MYC	19170058
NOTCH1	Activates	ESR1	19838210
NOTCH1	Activates	EGFR	18359760
NOTCH1	Activates	PTGS2	19290049
NOTCH1	Inhibits	CCNA	14678992
NOV	Activates	MMP1	15611078
NTN1	Inhibits	p53	18922894
p53	Inhibits	CA9	480909
p53	Inhibits	CA9	18815219
p53	Inhibits	OP18	11072234
p53	Inhibits	OP18	10557083
p53	Inhibits	APP	19049493
p53	Inhibits	APP	23942195
p53	Activates	S100B	9632811
p53	Activates	S100B	10490652
p53	Activates	PML	1151544
p53	Inhibits	EXPORTIN 1	21683812

p53	Activates	UNC5A	20372800
p53	Activates	TFAP2A	16636674
p53	Activates	TFAP2C	16636674
p53	Activates	ABCC1	12647018
p53	Inhibits	BCL3	12808109
p53	Activates	GSTP1	18505928
p53	Inhibits	PDRG1	20453924
p53	Activates	ESR1	15012604
p53	Inhibits	BDKRB1	11400161
p53	Activates	MMP2	9343394
p53	Activates	CKM	7488858
p53	Activates	CD82	11212267
p53	Inhibits	CCND1	12808109
p53	Activates	GAPDH	18552833
p53	Inhibits	ECT2	16778203
p53	Activates	MSH2	10984493
p53	Activates	CD58	11812190
p53	Activates	DUSP4	16778175
p53	Inhibits	CXCR4	17130833
p53	Activates	RRM2B	19010910
p53	Activates	EDA2R	20434500
p53	Inhibits	SLC6A6	16734743
p53	Inhibits	XAF1	20198350
p53	Activates	DDB2	12509284
p53	Inhibits	CDK4	7851794
p53	Activates	MDM2	11313969
p53	Inhibits	IL6	11830554
p53	Activates	NOV	18418052
p53	Activates	THBS1	12609716
p53	Inhibits	THBS1	9849855
p53	Inhibits	PDGFRB	18697203
p53	Activates	ARID3A	12136662
p53	Activates	KAT2B	15153330
p53	Inhibits	FGF2	11313915
p53	Activates	ICAM1	15247038
p53	Inhibits	WWP1	16924229
p53	Activates	ABCB1	17666793
p53	Inhibits	ABCB1	11920581
p53	Inhibits	IGF1R	10023442
p53	Inhibits	NR2C1	8663350
p53	Activates	EGFR	19597475
p53	Inhibits	EGFR	18391986
p53	Activates	IGFBP1	18056423
p53	Inhibits	CD44	18614011

p53	Activates	CDKN1A	17585201
p53	Inhibits	PRKCA	15563462
p53	Activates	DUSP2	16474395
p53	Activates	FDXR	12370809
p53	Activates	BAX	18949380
p53	Activates	KRT8	8615594
p53	Activates	TGFA	7651386
p53	Activates	IFI16	18974396
p53	Activates	TLR3	18779317
p53	Inhibits	CKB	7969181
p53	Activates	Tp53I13	14767535
p53	Inhibits	RECQL4	15674334
p53	Inhibits	MGMT	19846904
p53	Inhibits	SP7	16380437
p53	Inhibits	HSPA4	8418500
p53	Activates	HSPA4	20180806
p53	Inhibits	CDC25A	17001315
p53	Activates	FEN1	16103874
p53	Inhibits	FOS	1946467
p53	Activates	DDIT4	19210572
p53	Inhibits	CDC20	17873905
p53	Inhibits	IQCB1	16322217
p53	Activates	MAP4K4	15958553
p53	Activates	HIC1	7585125
p53	Activates	SEMA3B	11922394
p53	Activates	RPRM	11313928
p53	Inhibits	EZH2	15208672
p53	Inhibits	MMP1	11850838
p53	Inhibits	PSEN1	18374905
p53	Activates	PEG3	11679586
p53	Inhibits	PRSS50	17283160
p53	Inhibits	IFITM2	19544527
p53	Activates	SIVA1	19240372
p53	Inhibits	HSP90AB1	15284248
p53	Inhibits	BCL2	11313951
p53	Activates	PCBP4	11313928
p53	Inhibits	HIF1A	18815219
p53	Activates	DFNA5	16897187
p53	Inhibits	MMP13	11850838
p53	Activates	CD59	11812190
p53	Inhibits	FOXM1	19806025
p53	Inhibits	HNF4A	16895524
p53	Activates	Tp53INP1	12438758
p53	Activates	FHL2	17352216

p53	Activates	CCNG1	21447558
p53	Inhibits	TCF7L2	14990988
p53	Inhibits	BRCA1	12802282
p53	Inhibits	EPHB4	16205642
p53	Activates	CASP8	12376477
p53	Inhibits	HMMR	18971636
p53	Activates	CDKN1B	12376477
p53	Activates	COL18A1	15958553
p53	Activates	BBC3	18657356
p53	Activates	APAF1	11559530
p53	Inhibits	MAP4	10521394
p53	Activates	BAK1	15105295
p53	Activates	NLRC4	15580302
p53	Inhibits	PRC1	15531928
p53	Activates	GTSE1	11313928
p53	Activates	CALD1	19349302
p53	Inhibits	KRT19	7515894
p53	Activates	ATF3	17108111
p53	Activates	PTGS2	15608668
p53	Inhibits	PTGS2	15921850
p53	Activates	RGS16	16405749
p53	Activates	SGK	16619268
p53	Activates	S100A2	18388131
p53	Inhibits	S100A6	18714402
p53	Inhibits	MCL1	18208354
p53	Activates	DUSP5	12944906
p53	Activates	IER3	9781666
p53	Activates	GADD45A	18350249
p53	Activates	NOTCH1	17534448
p53	Activates	FAS	9841917
p53	Activates	PTEN	11729185
p53	Inhibits	VEGFA	11559575
p53	Inhibits	SLC2A1	21862591
p53	Activates	AIFM2	15273740
p53	Activates	CDKN1A	17585201
p53	Activates	DKK1	15668788
p53	Activates	PRKG1	19955367
p53	Inhibits	AR	18084622
p53	Inhibits	TFDP1	9556576
p53	Inhibits	CKS2	17336302
p53	Activates	NME1	12669312
p53	Inhibits	NME1	12669312
p53	Inhibits	MYC	8479742
p53	Activates	PCNA	11682006

p53	Inhibits	PCNA	8570655
p53	Activates	C13orf15	17146433
p53	Activates	ISG15	11462054
p53	Activates	BNIP3L	15607964
p53	Inhibits	SLC2A4	20729871
p53	Inhibits	CCNB1	11162602
p53	Activates	TNFRSF10A	15289308
p53	Activates	TNFRSF10B	10942251
p53	Activates	IGFBP7	19638426
p53	Activates	LATS2	19855428
p53	Inhibits	RAD51	19942681
p53	Activates	SERPINB5	15578720
p53	Activates	RAS	11574421
p53	Inhibits	CCNA	8270002
p53	Activates	C12orf5	16557269
p53	Activates	PERP	16557269
p53	Activates	SIAH1	16557269
p53	Activates	LRDD	16557269
p53	Activates	p53AIP1	16557269
p53	Activates	SESN2	16557269
p53	Activates	SFN	16557269
p53	Inhibits	CDKN2A	9774662
p53	Activates	ZMAT3	19805223
p53	Activates	KLF4	19826046
p53	Activates	PPM1D	18265945
p53	Inhibits	PPM1D	20093361
p53	Activates	COL1A2	9764819
p53	Activates	PPID	PMC3383624
PAD4	Inhibits	p53	2493360
PADI4	Inhibits	p53	18499678
PARK2	Inhibits	p53	19801972
PDGFRB	Activates	CCND1	10688905
PHF20	Activates	p53	22334668
PIAS2	Inhibits	p53	19901969
PITX1	Activates	p53	17762884
PLAUR	Inhibits	p53	17110957
PML	Activates	p53	12810724
PML	Activates	p53	14992722
POU4F1	Activates	p53	10329733
POU4F1	Activates	BCL2	9722627
POU4F1	Activates	BRCA1	11470235
PPARG	Activates	p53	16887883
PPM1A	Activates	p53	12514180
PPM1D	Inhibits	p53	15870257

PPM1D	Inhibits	CHEK1	15870257
PPM1D	Activates	MDM4	19808970
PPM1D	Inhibits	MAPK14	18265945
PRAK	Activates	p53	17254968
PREP1	Activates	p53	2887940
PREP1	Activates	p53	20587415
PRKCA	Inhibits	CCND1	20141613
PRKCA	Activates	IL6	9523575
PRKCA	Inhibits	ABCB1	9823967
PRKCA	Activates	HSPA4	17208995
PRKCA	Activates	MMP1	16368506
PRKCA	Activates	VEGFA	1511446
PRKCA	Inhibits	MYC	20141613
PRKCA	Activates	ERBB2	17545611
PRKCA	Activates	ABCB1	15563462
PRKCA	Activates	RAF1	8321321
PRKD1	Activates	PTGS2	19794144
PRKD1	Activates	p53	12628923
PRKDC	Activates	p53	11042698
PRKG1	Activates	CDKN1A	18593937
PRKG1	Activates	CDKN1B	18593937
PRKG1	Inhibits	MAPK14	16990590
PSMD10	Inhibits	p53	19287195
PTEN	Inhibits	CCND1	16849370
PTEN	Inhibits	HIF1A	18158893
PTEN	Inhibits	EPHB4	15930280
PTEN	Inhibits	VEGFA	16527906
PTEN	Inhibits	PCNA	17826033
PTGS2	Activates	CXCR4	20110411
PTGS2	Activates	ABCB1	17510421
PTGS2	Inhibits	EGFR	19671676
PTGS2	Activates	CD44	12393872
PTGS2	Activates	HSPA4	14717913
PTGS2	Activates	FOS	16685273
PTGS2	Activates	MCL1	16000874
PTGS2	Activates	VEGFA	18533784
PTGS2	Inhibits	CDKN1B	14587561
PTTG1	Activates	p53	15242522
PTTG1	Inhibits	p53	19477929
PTTG1	Activates	MMP2	19433493
PTTG1	Activates	FGF2	21858218
PTTG1	Activates	BAX	15242522
PTTG1	Activates	MYC	11115508
RAF1	Activates	p53	10732786

RAS	Activates	GSTP1	11606500
RAS	Activates	MAPK14	15677464
RAS	Inhibits	CKM	3600660
RAS	Activates	CCND1	10201372
RAS	Inhibits	CCND1	12081197
RAS	Activates	CD44	8453616
RAS	Activates	FOS	7917786
RAS	Activates	PTGS2	19903783
RAS	Inhibits	PTEN	19000654
RAS	Activates	VEGFA	11507052
RAS	Activates	CDKN1A	19440234
RAS	Activates	CCNA	15737994
RAS	Activates	CDKN1B	14504289
RAS	Activates	RAF1	9020159
RAS	Activates	MAPK1	9020159
RB1CC1	Inhibits	p53	21775823
RFC	Inhibits	p53	10910354
RREB1	Activates	p53	19558368
S100A2	Inhibits	PTGS2	16908593
S100B	Inhibits	p53	15572370
SERPINB5	Inhibits	VEGFA	19374835
SERPINF1	Activates	p53	17651710
SERPINF1	Inhibits	VEGFA	16901919
SET	Inhibits	p53	3245910
SFN	Activates	MMP1	19533306
SFN	Inhibits	CCNB1	17573669
SFN	Inhibits	CDK2	10767298
SFN	Activates	CDKN1B	20642839
SGK	Inhibits	p53	19756449
SIAH1	Activates	HIF1A	15210114
SLC2A1	Activates	MMP2	12122099
SOX4	Activates	p53	19234109
STAT3	Inhibits	p53	1190305
SUB1	Activates	p53	21586571
SUMO2	Activates	p53	21900752
SUMO2	Inhibits	p53	17012228
TCF7L2	Activates	MYC	9727977
TFAP2A	Inhibits	p53	16288208
TFDP1	Activates	EZH2	20565746
TGFA	Activates	CCND1	9407106
TGFA	Activates	FOS	8783257
TGFA	Activates	PTGS2	12930301
TGFA	Activates	MYC	10839631
TGFB1	Activates	p53	11741524

TGFB1	Activates	IL6	2265243
TGFB1	Inhibits	IL6	2265243
TGFB1	Activates	THBS1	11955611
TGFB1	Inhibits	ICAM1	14500551
TGFB1	Activates	PRKCA	14749204
TGFB1	Inhibits	MMP1	16911716
TGFB1	Inhibits	MMP13	9009143
TGFB1	Activates	CCNG1	9696022
TGFB1	Inhibits	KRT19	14732924
TGFB1	Activates	PTGS2	10935498
TGFB1	Inhibits	PTEN	19940030
TGFB1	Activates	VEGFA	12615726
TGFB1	Activates	CDKN1A	7696178
TGFB1	Inhibits	MYC	12628347
THBS1	Activates	TGFB1	11021838
TIAF1	Activates	p53	14965474
TLR3	Inhibits	CXCR4	19652552
Tp53BP1	Activates	p53	9748285
Tp53RK	Activates	p53	16600182
TPT1	Activates	p53	24067374
UBE2A	Activates	p53	22083959
UBE2A	Inhibits	p53	22083959
UCHL1	Activates	p53	20395212
UCHL1	Activates	p53	22279545
VEGFA	Inhibits	TGFB1	19180561
VEGFA	Activates	SERPINF1	12670505
VEGFA	Inhibits	SERPINF1	16901919
VEGFA	Activates	MMP2	16584583
VEGFA	Activates	CXCR4	19391039
VEGFA	Activates	CD44	9242547
VEGFA	Activates	FOS	14741347
VEGFA	Activates	BCL2	11895790
VEGFA	Activates	PTGS2	21273371
VEGFA	Activates	DUSP5	19741200
VEGFA	Activates	NOTCH1	12482957
VEGFA	Activates	ID3	15494533
VRK1	Activates	p53	15542844
YBX1	Inhibits	p53	12835324
YBX1	Activates	p53	11175333
YBX1	Activates	MMP2	9278454
YBX1	Activates	ABCB1	17038319
YBX1	Activates	EGFR	1967130
YBX1	Inhibits	MMP13	17822788
YY1	Inhibits	p53	15295102

YY1	Activates	p53	PMC231595
ZMAT3	Activates	p53	12196512
ZNF307	Inhibits	p53	17910948

Table 7.2.1 Nodes regulating apoptosis in the PMH260 model.
A total of 118 apoptotic nodes are considered. Of these; 73 are pro- apoptotic and 45 are anti-apoptotic. Some links to apoptosis were not obtained via their GO annotations and were additionally searched by literature evidence. PMIDs and PMCs are supplied. Reference links are also supplied if no PMID is available. Apoptotic nodes described in Tian et al. (2013) are also supplied.

Source	Interaction	Target	GO Term	GO ID	PMID/PMC
AIFM2	Activates	apoptosis	induction of apoptosis	GO:0006917	21943319
APAF1	Activates	apoptosis	apoptotic process	GO:0006915	10791976
APP	Activates	apoptosis	Neuron apoptotic process	GO:0051402	19225519
AR	Activates	apoptosis			16479009
AR	Inhibits	apoptosis	negative regulation of apoptotic process	GO:0043066	21815189
ASPP1	Activates	apoptosis	Negative regulation of cell cycle	GO:0045786	11684014
ASPP1	Activates	apoptosis			14729977
ASPP1	Activates	apoptosis			14729977
ASPP1	Activates	apoptosis	Intrinsic apoptotic signalling pathway by p53 class mediator	GO:0072332	11684014
ASPP2	Activates	apoptosis			14729977
ASSP2	Activates	apoptosis			14729977
ASSP2	Activates	apoptosis			11684014
ATF3	Activates	apoptosis			18755691
ATF3	Inhibits	apoptosis			12392999
BAK1	Activates	apoptosis	regulation of apoptotic process	GO:0042981	20460378
BAX	Activates	apoptosis	regulation of apoptotic process	GO:0042981	19672311
BBC3	Activates	apoptosis	activation of pro-apoptotic gene products	GO:0008633	11572983
BCL2	Inhibits	apoptosis	anti-apoptosis	GO:0006916	8617294
BCL2	Inhibits	apoptosis	negative regulation of apoptotic process	GO:0043066	8617294
BCL2	Inhibits	apoptosis	regulation of apoptotic process	GO:0042981	8617294
BCL3	Inhibits	apoptosis	negative regulation of apoptotic process	GO:0043066	20800578
BNIP3L	Activates	apoptosis	positive regulation of apoptotic process	GO:0043065	10381623
C12orf5	Inhibits	apoptosis			16839880

CASP8	Activates	apoptosis	regulation of apoptotic process	GO:0042981	15029256
CCNG1	Activates	apoptosis			10467405
CCNG1	Inhibits	apoptosis	negative regulation of apoptotic process	GO:0043066	18497347
CD44	Activates	apoptosis			6208414
CD44	Inhibits	apoptosis			17045821
CDC25A	Activates	apoptosis			20368335
CDC25A	Inhibits	apoptosis			11416155
CDKN1A	Inhibits	apoptosis	induction of apoptosis by intracellular signals	GO:0008629	21815189
CDKN1A	Inhibits	apoptosis	negative regulation of apoptotic process	GO:0043066	21815189
CDKN1B	Activates	apoptosis			10208428
CDKN1B	Inhibits	apoptosis			10050878
CDKN2A	Activates	apoptosis	induction of apoptosis	GO:0006917	9403064
CKS2	Inhibits	apoptosis			18498131
COL18A1	Activates	apoptosis			11158588
CUL7	Inhibits	apoptosis			17229476
CXCR4	Activates	apoptosis	apoptotic process	GO:0006915	15705741
DAP	Activates	apoptosis	Apoptotic process	GO:0006915	7828849
DAP	Activates	apoptosis	Positive regulation of apoptotic process	GO:0043605	9118961
DAP	Activates	apoptosis	Regulation of apoptotic process	GO:0042981	11709549
DAXX	Activates	apoptosis	Extrinsic apoptotic signalling pathway via death domain receptors	GO:0008625	9215629
DAXX	Activates	apoptosis	Positive regulation of apoptotic signalling pathway	GO:2001235	11193028
DAXX	Activates	apoptosis	Apoptotic signalling pathway	GO:0097190	11003656
DAXX	Activates	apoptosis			12407442
DAXX	Activates	apoptosis			11773067
DAXX	Activates	apoptosis			12407442
DAXX	Inhibits	apoptosis			19017466
DAXX	Inhibits	apoptosis			16088932
DDIT4	Activates	apoptosis	apoptotic process	GO:0006915	18796435
DDIT4	Inhibits	apoptosis	apoptotic process	GO:0006915	19221489
DDX20	Activates	apoptosis	Positive regulation of apoptotic process	GO:0043065	16153597
DFNA5	Activates	apoptosis			21522185

DKK1	Activates	apoptosis			20549706
DUSP2	Activates	apoptosis	regulation of apoptotic process	GO:0042981	9501207
DUSP2	Inhibits	apoptosis	regulation of apoptotic process	GO:0042981	9501207
DUSP2	Inhibits	apoptosis			12673251
DUSP4	Activates	apoptosis			20124482
DUSP4	Inhibits	apoptosis			20860659
ECT2	Activates	apoptosis			12787561
EGFR	Activates	apoptosis			11226409
EGFR	Inhibits	apoptosis	negative regulation of apoptotic process	GO:0043066	15277479
EPHB4	Inhibits	apoptosis			20133814
ESR1	Activates	apoptosis	regulation of apoptotic process	GO:0042981	17615152
ESR1	Inhibits	apoptosis	regulation of apoptotic process	GO:0042981	9118519
EZH2	Inhibits	apoptosis			19079346
EZH2	Inhibits	apoptosis			19893569
FAS	Activates	apoptosis	apoptotic process	GO:0006915	7536620
FDXR	Activates	apoptosis			12370809
FGF2	Activates	apoptosis	apoptotic process	GO:0006915	20081577
FGF2	Inhibits	apoptosis	apoptotic process	GO:0006915	15856005
FHL2	Inhibits	apoptosis			21377781
FOS	Activates	apoptosis			8524298
FOS	Inhibits	apoptosis			19255142
GADD 45A	Activates	apoptosis	apoptotic process	GO:0006915	17474084
GSTP1	Inhibits	apoptosis			21637416
HNF4A	Activates	apoptosis			19835622
HOXA 10	Activates	apoptosis			
IER3	Inhibits	apoptosis	anti-apoptosis	GO:0006916	14688131
IFI16	Activates	apoptosis	DNA damage response, signal transduction by p53 class mediator resulting in induction of apoptosis	GO:0042771	14990579
IFITM2	Activates	apoptosis			19544527
IGF1R	Inhibits	apoptosis	anti-apoptosis	GO:0006916	14726697
IGF1R	Inhibits	apoptosis	negative regulation of apoptotic process	GO:0043066	14726697
IGF1R	Inhibits	apoptosis	positive regulation of anti-apoptosis	GO:0045768	14726697
IGFBP 7	Activates	apoptosis			18267069

IL6	Activates	apoptosis	negative regulation of cysteine-type endopeptidase activity involved in apoptotic process	GO:0043154	12714376
IL6	Activates	apoptosis	neutrophil apoptosis	GO:0001781	12714376
IL6	Activates	apoptosis	regulation of apoptotic process	GO:0042981	12714376
IL6	Inhibits	apoptosis	negative regulation of cysteine-type endopeptidase activity involved in apoptotic process	GO:0043154	11751424
IL6	Inhibits	apoptosis	neutrophil apoptosis	GO:0001781	11751424
IL6	Inhibits	apoptosis	regulation of apoptotic process	GO:0042981	11751424
ING4	Activates	apoptosis	Negative regulation of growth	GO:0045926	16387653
ING5	Activates	apoptosis	Positive regulation of apoptotic signalling pathway	GO:2001235	
JUN	Activates	apoptosis			1169773
KAT2B	Activates	apoptosis			PMC3847488
LATS2	Activates	apoptosis			15265683
LRDD	Activates	apoptosis	negative regulation of apoptotic process	GO:0043066	9403064
MAP4K4	Activates	apoptosis			15958553
MAP4K4	Inhibits	apoptosis			21196414
MCL1	Inhibits	apoptosis	regulation of apoptotic process	GO:0042981	18550749
MSH2	Activates	apoptosis	negative regulation of neuron apoptosis	GO:0043524	10097137
NLRC4	Activates	apoptosis	positive regulation of apoptotic process	GO:0043065	11374873
NOTCH1	Activates	apoptosis	positive regulation of apoptotic process	GO:0043065	12815466
NOTCH1	Inhibits	apoptosis	negative regulation of cell death	GO:0060548	10227380
P53AIP1	Activates	apoptosis	apoptotic process	GO:0006915	9403064
PCBP4	Activates	apoptosis	DNA damage response, signal transduction resulting in induction of apoptosis	GO:0008630	20817677
PDGFRB	Inhibits	apoptosis			21954875
PEG3	Activates	apoptosis	apoptotic process	GO:0006915	10681424
PERP	Activates	apoptosis	apoptotic process	GO:0006915	10733530

PITX1	Activates	apoptosis			17762884
PITX1	Activates	apoptosis			20563669
PML	Activates	apoptosis			14663483
PML	Activates	apoptosis	Positive regulation of apoptotic process involved in mammary gland involution	G0:0060058	11080164
PREP1	Inhibits	apoptosis			PMC2643814
PRKCA	Activates	apoptosis	apoptotic process	GO:0006915	10825394
PRKCA	Inhibits	apoptosis	apoptotic process	GO:0006915	DOI:10.1007/978-1-59745-199-4_2
PRSS50	Activates	apoptosis			21086474
PSEN1	Inhibits	apoptosis	anti-apoptosis	GO:0006916	10805794
PSEN1	Inhibits	apoptosis	apoptotic process	GO:0006915	10805794
PSEN1	Inhibits	apoptosis	negative regulation of neuron apoptosis	GO:0043524	10805794
PTEN	Activates	apoptosis	induction of apoptosis	GO:0006917	11159942
PTGS2	Activates	apoptosis			16544098
PTGS2	Inhibits	apoptosis			11046152
RBC1CC1	Inhibits	apoptosis	Negative regulation of apoptotic process	GO:0006916	2064504
RBC1CC1	Inhibits	apoptosis	Negative regulation of extrinsic apoptotic signalling pathway	GO:2001237	PMC2064504
SEMA3B	Activates	apoptosis			15273288
SERPINB5	Activates	apoptosis			15713631
SFN	Inhibits	apoptosis	apoptotic process	GO:0006915	10654934
SFN	Inhibits	apoptosis	DNA damage response, signal transduction resulting in induction of apoptosis	GO:0008630	15857577
SGK	Inhibits	apoptosis			12488318
SIAH1	Activates	apoptosis	apoptotic process	GO:0006915	9403064
SIAH1	Activates	apoptosis	neuron apoptosis	GO:0051402	9403064
SIAH1	Activates	apoptosis	: positive regulation of apoptotic process	GO:00043065	9403064
SIVA1	Activates	apoptosis	apoptotic process	GO:0006915	20727854
STAT3	Inhibits	apoptosis	Negative regulation of cell death	GO:0060548	20562100
STAT3	Inhibits	apoptosis	Negative regulation of cell death	GO:0060548	16540667
STAT3	Inhibits	apoptosis	Cell proliferation	GO:0008283	11171987
TCF7L2	Inhibits	apoptosis			21965303

TCF7L2	Inhibits	apoptosis			21357677
TFAP2A alpha	Activates	apoptosis	Negative regulation of cell proliferation	GO:0008285	20607706
TFAP2A alpha	Activates	apoptosis			14551210
TFAP2A alpha	Activates	apoptosis			12654297
TFAP2C	Activates	apoptosis			14573793
TFAP2C	Activates	apoptosis			21779369
TGFA	Inhibits	apoptosis	anti-apoptosis	GO:0006916	16079309
TGFA	Inhibits	apoptosis	negative regulation of neuron apoptosis	GO:0043524	16079309
TLR3	Activates	apoptosis	positive regulation of apoptotic process	GO:0043065	16585585
TNFRSF10A	Activates	apoptosis	induction of apoptosis	GO:0006917	21785270
TNFRSF10A	Activates	apoptosis	induction of apoptosis via death domain receptor	GO:0008625	21785270
TNFRSF10B	Activates	apoptosis	activation of pro-apoptotic gene products	GO:0008633	22046379
TNFRSF10B	Activates	apoptosis	apoptotic process	GO:0006915	22046379
TNFRSF10B	Activates	apoptosis	induction of apoptosis via death domain receptor	GO:0008625	22046379
TNFRSF10B	Activates	apoptosis	regulation of apoptotic process	GO:0042981	22046379
TP53INP1	Activates	apoptosis	induction of apoptosis	GO:0006917	21219856
TP53RK	Inhibits	apoptosis			20647325
TPT1	Inhibits	apoptosis	Negative regulation of intrinsic apoptotic signalling pathway in response to DNA damage	GO:1902230	11598139
TPT1	Inhibits	apoptosis	Negative regulation of apoptotic process	GO:0043066	16130169
TPT1	Inhibits	apoptosis	Regulation of apoptotic process	G0:0049281	15162379
TPT1	Inhibits	apoptosis			12149273
TPT1	Inhibits	apoptosis			15262975
UCHL1	Activates	apoptosis			18949367
UCHL1	Activates	apoptosis			18949367
UCHL1	Activates	apoptosis			24155778
VEGFA	Inhibits	apoptosis	anti-apoptosis	GO:0006916	11891765

VEGFA	Inhibits	apoptosis	negative regulation of apoptotic process	GO:0043066	11891765
WWP1	Inhibits	apoptosis			18806757
XAF1	Activates	apoptosis	apoptotic process	GO:0006915	21788101

Table 7.2.2 Nodes regulating angiogenesis in the PMH260 model.
A total of 42 angiogenic nodes are considered. Of these; 27 are pro- angiogenic and 15 are anti-angiogenic. Some links to angiogenesis were not obtained via their GO annotations and were additionally searched by literature evidence. PMIDs and PMCs are supplied. Reference links are also supplied if no PMID is available.

Source	Interaction	Target	GO Term	GO ID	PMID/PMC
BBC3	Activates	Angiogenesis			23122957
BCL2	Activates	Angiogenesis			18490895
BCL2	Activates	Angiogenesis			11280784
BDKRB1	Activates	Angiogenesis			21835216
CALD1	Activates	Angiogenesis	Angiogenesis		18980955
CALD1	Activates	Angiogenesis	Vasculogenesis		15161654
CALD1	Activates	Angiogenesis	Blood vessel endothelial cell migration		15161654
CCND1	Activates	Angiogenesis			PMC1986788
CD44	Activates	Angiogenesis			1698758
CDK2	Activates	Angiogenesis			23042366
CDK4	Activates	Angiogenesis			20603602
CDK5	Activates	Angiogenesis			20826806
EGFR	Activates	Angiogenesis			23856030
ELAVL1	Activates	Angiogenesis			25422430
ELAVL1	Activates	Angiogenesis			23516604
ELAVL1	Activates	Angiogenesis			25422430
EPHB4	Activates	Angiogenesis	Cell migration involved in sprouting angiogenesis	GO:0002042	12734395
EPHB4	Activates	Angiogenesis	Angiogenesis	GO:0001525	10518221
EPHB4	Activates	Angiogenesis	Angioblast cell migration involved in selective angioblast sprouting	GO:0035475	19815777
EPHB4	Activates	Angiogenesis			15930280
FGF2	Activates	Angiogenesis	Positive regulation of angiogenesis	GO:0045766	14702107
FGF2	Activates	Angiogenesis	Cell migration involved in sprouting angiogenesis	GO:0002042	17187775

FGF2	Activates	Angiogenesis	Positive regulation of blood vessel endothelial cell migration	GO:0043536	23856030
HIF1A	Activates	Angiogenesis	Positive regulation of vascular endothelial growth factor receptor signaling pathway	GO:0030949	18658046
HIF1A	Activates	Angiogenesis	positive regulation of angiogenesis	GO:0045766	8756616
HIF1A	Activates	Angiogenesis	positive regulation vascular endothelial growth factor production		12958148
HIF1A	Activates	Angiogenesis	Angiogenesis	GO:0001525	18037992
HIF1A	Activates	Angiogenesis	Positive regulation of vasculogenesis	GO:2001214	17636018
HSPA4	Activates	Angiogenesis	Positive regulation of angiogenesis	GO:00045766	22098710
HSPA4	Activates	Angiogenesis			15994930
HSPA4	Activates	Angiogenesis			PMC3980608
JUN	Activates	Angiogenesis	Angiogenesis	GO:0001525	25083991
MMP1	Activates	Angiogenesis			7512058
MMP13	Activates	Angiogenesis			22992737
NTN1	Activates	Angiogenesis			23824572
NTN1	Activates	Angiogenesis			20080097
PDGFRB	Activates	Angiogenesis	Fibroblast growth factor receptor signaling pathway	GO:0008543	18827023
PDGFRB	Activates	Angiogenesis	positive regulation of cell proliferation by VEGF-activated platelet derived growth factor receptor signaling pathway	GO:0038091	17470632
PDGFRB	Activates	Angiogenesis	Cell migration involved in coronary angiogenesis	GO:0060981	18555217
PDGFRB	Activates	Angiogenesis	Cell migration involved in vasculogenesis	GO:0035441	14998491
PRKCA	Activates	Angiogenesis	Positive regulation of angiogenesis	GO:0045786	11909826
PRKCA	Activates	Angiogenesis	Angiogenesis	GO:0001525	11909826
PRKCA	Activates	Angiogenesis	Positive regulation of endothelial cell proliferation	GO:0001938	11909826
PTGS2	Activates	Angiogenesis	Positive regulation of cell migration involved in sprouting angiogenesis	GO:0090050	9630216
PTGS2	Activates	Angiogenesis	Positive regulation vascular endothelial	GO:0010575	9630216

			growth factor production		
PTGS2	Activates	Angiogenesis	Positive regulation of fibroblast growth factor production	GO:0090271	9630216
S100B	Activates	Angiogenesis			23719262
SGK	Activates	Angiogenesis			24265802
SGK	Activates	Angiogenesis			20568246
STMN 1	Activates	Angiogenesis			15031128
TGFA	Activates	Angiogenesis	Angiogenesis	GO:0001938	14998491
TGFA	Activates	Angiogenesis			19481589
VEGFA	Activates	Angiogenesis	Angiogenesis	GO:0001525	11427521
VEGFA	Activates	Angiogenesis	Positive regulation of endothelial cell proliferation	GO:0001938	2575835
VEGFA	Activates	Angiogenesis	Tube formation	GO:0035148	21245381
VEGFA	Activates	Angiogenesis	vascular endothelial growth factor receptor signalling pathway	GO:0048010	16109918
VEGFA	Activates	Angiogenesis	Positive regulation of vascular permeability	GO:0043117	20497126
VEGFA	Activates	Angiogenesis	Positive regulation of endothelial cell chemotaxis by VEGF-activated vascular endothelial growth factor receptor signalling pathway	G0:0038033	16489009
VEGFA	Activates	Angiogenesis	Cellular response to vascular endothelial growth factor stimulus	GO:0035924	12714610
VEGFA	Activates	Angiogenesis	Growth factor activity	GO:0008083	9202027
VEGFA	Activates	Angiogenesis	Positive regulation of cell migration involved in sprouting angiogenesis	GO:0090050	18577655
VEGFA	Activates	Angiogenesis	Positive regulation of angiogenesis	GO:0045766	18440775
VEGFA	Activates	Angiogenesis	Cell migration involved in sprouting angiogenesis	GO:0002042	20497126
VEGFA	Activates	Angiogenesis	Blood vessel remodelling	GO:0001974	20551324
VEGFA	Activates	Angiogenesis	Patterning of blood vessels	GO:0001569	7929439
VEGFA	Activates	Angiogenesis			17470632
VEGFA	Activates	Angiogenesis			18440775
VEGFA	Activates	Angiogenesis			20660291

VEGFA	Activates	Angiogenesis			19033661

Table 7.2.3 Nodes regulating DNA repair in the PMH260 model.
A total of 28 nodes that regulate DNA repair are described. Of these; 20 and 8 are positive and negative regulators of DNA repair respectively. Some links to DNA repair were not obtained via their GO annotations and were additionally searched by literature evidence. PMIDs and PMCs are supplied. Reference links are also supplied if no PMID is available.

Source	Interaction	Target	GO Term	GO ID	PMID/PMC
ATM	Activates	DNA repair	DNA repair	GO:0006281	doi:10.1038/ncomms4347
ATR	Activates	DNA repair			PMC4176976
BCCIP	Activates	DNA repair	DNA repair	GO:0006281	17947333
BRCA1	Activates	DNA repair			14636569
CD44	Activates	DNA repair			16263582
CDKN1A	Activates	DNA repair			22735704
DDB2	Activates	DNA repair	UV-damage excision repair	GO:0070914	22334663
FEN1	Activates	DNA repair	Double-strand break repair	GO:0006302	8131753
FGF2	Activates	DNA repair			22732006
FGF2	Activates	DNA repair			20681019
GADD45A	Activates	DNA repair	DNA repair	GO:0006281	7973727
HSPA4	Activates	DNA repair			14627201
IFI16	Activates	DNA repair			18472023
KLF4	Inhibits	DNA repair			PMC3750599
MCL1	Activates	DNA repair			20647761
MDM2	Inhibits	DNA repair			18541670
MDM4	Inhibits	DNA repair			24608433
MGMT	Activates	DNA repair	DNA dealkylation involved in DNA repair	GO:0006307	1554415
MSH2	Activates	DNA repair	DNA repair	GO:0006281	8942985
MSH2	Activates	DNA repair	Mismatch repair	GO:0006298	1334021
MSH2	Activates	DNA repair	Mismatch repair	GO:0006298	11555625
MSH2	Activates	DNA repair	Post replication repair	GO:0006301	17715146
MYC	Inhibits	DNA repair			23308051
NME1	Activates	DNA repair			25017017
PCNA	Activates	DNA repair	Positive regulation of DNA repair	GO:0006281	16227586
PPM1D	Inhibits	DNA repair			15327777

PRKDC	Activates	DNA repair	Double-strand break repair via homologous recombination	GO:0000724	11418067
PTTG1	Inhibits	DNA repair	GO:0006281	DNA repair	
RAD51	Activates	DNA repair		GO:0000150	PMC2430071
SERPINE 1	Inhibits	DNA repair			23111469
SIAH1	Inhibits	DNA repair			20682032
YY1	Activates	DNA repair	Double strand break repair via homologous recombination	GO:0000724	18026119

Table 7.2.4 Nodes regulating cellular senescence in the PMH260 model.
A total of 68 nodes that regulate cellular senescence are described. Of these; 32 and 36 are positive and negative regulators of senescence respectively. Some links were not obtained via their GO annotations and were additionally searched by literature evidence. PMIDs and PMCs are supplied. Reference links are also supplied if no PMID is available. Table includes links to cellular senescence as described in Tian et al. (2013).

Source	Interaction	Target	GO Term	GO ID	PMID/PMC
APAF1	Inhibits	Cellular senescence			17652622
APP	Activates	Cellular senescence			24232259
AR	Activates	Cellular senescence			22403609
ARID3A	Inhibits	Cellular senescence			22010578
BAK1	Activates	Cellular senescence			19747230
BAK1	Inhibits	Cellular senescence			11557285
BCL2	Activates	Cellular senescence			12670482
BCL2	Inhibits	Cellular senescence			19855432
BRCA1	Inhibits	Cellular senescence			12533509
C12orf5	Activates	Cellular senescence			19710698
CD59	Activates	Cellular senescence			22918646
CD59	Inhibits	Cellular senescence			17188915
CDK4	Inhibits	Cellular senescence			12435633
CDKN1A	Activates	Cellular senescence	Cellular senescence	GO:0090398	15149599
CDKN1B	Activates	Cellular senescence			21795702
CDKN2A	Activates	Cellular senescence	Cellular senescence	GO:0090398	14966292
CDKN2A	Activates	Cellular senescence	Positive regulation of cellular senescence	GO:2000774	14966292
CKB	Inhibits	Cellular senescence			21980054
CUL7	Inhibits	Cellular senescence			18498745

DAXX	Inhibits	Cellular Senescence			23542781
DDB2	Activates	Cellular senescence			23109835
DDIT4	Inhibits	Cellular senescence			22629318
DKK1	Activates	Cellular senescence			22927647
DKK1	Inhibits	Cellular senescence			21712954
EGFR	Inhibits	Cellular senescence			21852385
ELAVL1	Inhibits	Cellular senescence			23028944
EZH2	Inhibits	Cellular senescence			15208672
EZH2	Inhibits	Cellular senescence			21383005
FGF2	Inhibits	Cellular senescence			17532297
FGF2	Inhibits	Cellular senescence			21990129
FHL2	Inhibits	Cellular senescence			19018287
FOXM1	Inhibits	Cellular senescence			23262037
GADD45A	Activates	Cellular senescence			16951155
GADD45A	Inhibits	Cellular senescence			21986581
GAPDH	Activates	Cellular senescence			22847419
GAPDH	Inhibits	Cellular senescence			21749859
HIF1A	Inhibits	Cellular senescence			18645006
HNF4A	Inhibits	Cellular senescence			21385945
IFI16	Activates	Cellular senescence			15208661
IFITM2	Activates	Cellular senescence			19071156
IGF1R	Activates	Cellular senescence			18216278
IGFBP7	Activates	Cellular senescence			21997538
IL6	Activates	Cellular senescence			22374671
LATS2	Activates	Cellular senescence			21498571
MCL1	Inhibits	Cellular senescence			22451485
MSH2	Activates	Cellular senescence			18986375
MSH2	Inhibits	Cellular senescence			23213348
MYC	Activates	Cellular senescence			20027199
MYC	Inhibits	Cellular senescence			17664422
NME1	Inhibits	Cellular senescence			20713695
NOTCH1	Activates	Cellular senescence			23078884
PCBP4	Inhibits	Cellular senescence			20817677
PML	Activates	Cellular senescence	Negative regulation of telomere maintenance via telomerase	GO:0032211	10950866
PML	Activates	Cellular senescence	Negative regulation of telomere maintenance via telomerase	GO:0032211	10910364
PML	Activates	Cellular senescence			12093737

PPM1D	Inhibits	Cellular senescence			22201816
PRAK	Activates	Cellular senescence			17254968
PRKCA	Activates	Cellular senescence			18162471
PSEN1	Activates	Cellular senescence			19181896
PTEN	Activates	Cellular senescence			23314408
PTEN	Inhibits	Cellular senescence			21072054
PTGS2	Activates	Cellular senescence			23328527
RAS	Activates	Cellular senescence	Cellular senescence	GO:0090398	15489886
RRM2B	Inhibits	Cellular senescence			23139867
S100A6	Inhibits	Cellular senescence			23095053
SESN2	Inhibits	Cellular senescence			20606249
SFN	Activates	Cellular senescence			19642975
SGK	Inhibits	Cellular senescence			15068796
TFDP1	Inhibits	Cellular senescence			15716376
TGFA	Activates	Cellular senescence			12593448
VEGFA	Inhibits	Cellular senescence			21618508
WWP1	Inhibits	Cellular senescence			22051607
WWP1	Inhibits	Cellular senescence			21795702

Table 7.2.5 Nodes regulating cell cycle arrest in the PMH260 model.
A total of 62 nodes that regulate cell cycle arrest are described. Of these; 34 and 28 are positive and negative regulators of cell cycle arrest respectively. Some links were not obtained via their GO annotations and were additionally searched by literature evidence. PMIDs and PMCs are supplied. Reference or DOI links are also supplied if no PMID is available.

Source	Interaction	Target	GO Term	GO ID	PMID/PMC
APAF1	Inhibits	Cell cycle arrest			18309324
APAF1	Inhibits	Cell cycle arrest			18042457
AR	Inhibits	Cell cycle arrest			16877366
AR	Inhibits	Cell cycle arrest			6483690
AR	Inhibits	Cell cycle arrest			9685369
ATF3	Activates	Cell cycle arrest			12386811
ATF3	Inhibits	Cell cycle arrest	Positive regulation of cell proliferation	GO:0008284	15990869
ATM	Activates	Cell cycle arrest	cell cycle arrest	GO:0007050	11721054
ATR	Activates	Cell cycle arrest			11721054
AURKA	Inhibits	Cell cycle arrest			24841948
BRCA1	Activates	Cell cycle arrest	Positive regulation of cell cycle arrest	GO:0071158	21102443
BRCA1	Activates	Cell cycle arrest			10644742
BRCA1	Activates	Cell cycle arrest			10644742
BRCA1	Activates	Cell cycle arrest			7954448

BTG2	Activates	Cell cycle arrest	DNA repair	GO:0006281	10669755
CCNA	Inhibits	Cell cycle arrest			25615569
CCNB1	Inhibits	Cell cycle arrest			2570636
CCNB1	Inhibits	Cell cycle arrest			1717476
CCNB1	Inhibits	Cell cycle arrest			8797586
CDK2	Inhibits	Cell cycle arrest			19445729
CDK5	Activates	Cell cycle arrest	Regulation of cell cycle arrest	GO:0071156	21473899
CDKN1B	Activates	Cell cycle arrest	Cell cycle arrest	GO:0007050	12093740
CDKN1B	Activates	Cell cycle arrest	G1/S transition of mitotic cell cycle	GO:0000082	10208428
CDKN1B	Activates	Cell cycle arrest	Mitotic cell cycle	GO:0000278	19266349
CDKN1B	Activates	Cell cycle arrest	Negative regulation of cyclin-dependent protein serine/threonine kinase activity	GO:0045736	15374880
CDKN1B	Activates	Cell cycle arrest	DNA damage response, signal transduction by p53 class mediator resulting in cell cycle arrest	GO:006977	8033213
CDKN1B	Activates	Cell cycle arrest	Response to G1 DNA damage checkpoint signalling	GO:0072432	8033213
CDKN2A	Activates	Cell cycle arrest	Cell cycle arrest	GO:0007050	23238983
CDKN2A	Activates	Cell cycle arrest	positive regulation of cell cycle arrest	GO:0071158	9529249
CHEK1	Activates	Cell cycle arrest			21034966
CHEK2	Activates	Cell cycle arrest			PMC316357
CKS2	Inhibits	Cell cycle arrest			1862572
CUL7	Inhibits	Cell cycle arrest			18498745
DKK1	Activates	Cell cycle arrest			20549706
DKK1	Activates	Cell cycle arrest			12740383
DUSP5	Activates	Cell cycle arrest			12944906
E2F1	Activates	Cell cycle arrest			9766435
EPHB4	Inhibits	Cell cycle arrest			15930280
EXPORTIN1	Activates	Cell cycle arrest			23615632

EXPORTIN1	Activates	Cell cycle arrest			22832492
GADD45A	Activates	Cell cycle arrest	Regulation of cell cycle	GO:0051726	12124778
GADD45A	Activates	Cell cycle arrest	Cell cycle arrest	GO:0007050	10747892
GADD45A	Activates	Cell cycle arrest	G2/M transition of mitotic cell cycle	GO:0000086	11964479
HDAC1	Inhibits	Cell cycle arrest			20194438
HOXA10	Activates	Cell cycle arrest			2731304
HOXA5	Activates	Cell cycle arrest			25590986
ID3	Activates	Cell cycle arrest			21498546
IER3	Inhibits	Cell cycle arrest			11311240
IGFBP7	Activates	Cell cycle arrest			23388612
ING4	Activates	Cell cycle arrest	Cell cycle		15251430
ING5	Inhibits	Cell cycle arrest	Negative regulation of cell proliferation	GO:0008285	12750254
ISG15	Inhibits	Cell cycle arrest			PMC4226694
JUN	Inhibits	Cell cycle arrest	Positive regulation of fibroblast proliferation	GO:0048146	1171114
KAT2B	Activates	Cell cycle arrest	Negative regulation of cell proliferation	GO:000825	8684459
KAT2B	Activates	Cell cycle arrest		G0:0006915	20809119
KLF4	Activates	Cell cycle arrest			PMC3750599
MAPK1	Activates	Cell cycle arrest			11821415
MCL1	Inhibits	Cell cycle arrest			22378300
MUC1	Inhibits	Cell cycle arrest	DNA damage response, signal transduction by p53 class mediator resulting in cell cycle arrest	GO:0006977	15710329
MYC	Inhibits	Cell cycle arrest	Cell cycle arrest	GO:0007050	10962037
MYCN	Inhibits	Cell cycle arrest			17495526
MYST4	Activates	Cell cycle arrest			19001415
PAD4	Activates	Cell cycle arrest			16502257
PARK2	Activates	Cell cycle arrest			24793136
POU4F1	Activates	Cell cycle arrest			18421303
PPARG	Activates	Cell cycle arrest			15916743
PRAK	Inhibits	Cell cycle arrest			DOI: 10.1007/s11684-009-0073-y

PTGS2	Activates	Cell cycle arrest	Negative regulation of cell cycle	GO:0045786	10567385
PTGS2	Activates	Cell cycle arrest			11606477
RAD51	Inhibits	Cell cycle arrest			19140342
RAF1	Activates	Cell cycle arrest			10022606
RAS	Activates	Cell cycle arrest			3510745
RAS	Activates	Cell cycle arrest			3049071
RB1CC1	Activates	Cell cycle arrest	Cell cycle	GO:0007049	16061648
RGS16	Inhibits	Cell cycle arrest			16405749
S100A6	Inhibits	Cell cycle arrest	Positive regulation of fibroblast proliferation	GO:0048146	12577318
S100A6	Inhibits	Cell cycle arrest			20013795
S100A6	Inhibits	Cell cycle arrest			23095053
SIVA1	Inhibits	Cell cycle arrest			23462994
SLC2A1	Inhibits	Cell cycle arrest			
STMN1	Activates	Cell cycle arrest			15368352
STMN1	Activates	Cell cycle arrest			15031128
TFAP2C	Activates	Cell cycle arrest			16867219
UBE2A	Inhibits	Cell cycle arrest	Positive regulation of cell proliferation	GO:0008284	1748683
VRK1	Inhibits	Cell cycle arrest			18286197
YBX1	Inhibits	Cell cycle arrest			20398058

Table 7.2.6 Nodes that are regulated by DNA damage in the PMH260 model.
A total of 42 nodes are regulated by DNA damage. Of these; 37 are activated by DNA damage, 5 are inhibited. Some links were not obtained via their GO annotations and were additionally searched by literature evidence. PMIDs and PMCs are supplied. Reference or DOI links are also supplied if no PMID is available. Table includes DNA damage nodes described in Tian et al. (2013).

Source	Interaction	Target	GO Term	GO ID	PMID/PMC
DNA damage	Activates	APP			18421302
DNA damage	Activates	ATM	DNA damage response, signal transduction resulting in induction of apoptosis	GO:0008630:	15279774
DNA damage	Activates	ATM	response to ionizing radiation	GO: 0010212	15322239
DNA damage	Activates	ATR	cellular response to UV	GO:0034644	15322239
DNA damage	Activates	ATR	response to DNA damage stimulus	GO:0006974	15322239

DNA damage	Inhibits	AURKA			21099343
DNA damage	Activates	BTG2	response to DNA damage stimulus	GO:0006974	8944033
DNA damage	Activates	CCAR1			12816952
DNA damage	Activates	CDK5			19151707
DNA damage	Activates	CUL7			17586686
DNA damage	Activates	DAP			15608685
DNA damage	Activates	DAXX			23539629
DNA damage	Activates	ERBB2			19406993
DNA damage	Activates	FAS			9660938
DNA damage	Activates	HTATIP2			21376742
DNA damage	Activates	ICAM1	Response to ionizing radiation	G0:0010212	7963663
DNA damage	Activates	ING5			23576563
DNA damage	Activates	JUN			16733206
DNA damage	Activates	MAPK8	induction of apoptosis by extracellular signals	GO:0008624	15696159
DNA damage	Activates	MAPK8	induction of apoptosis by intracellular signals	GO:0008629	
DNA damage	Activates	MAPK8	response to UV	O:000941	
DNA damage	Activates	MAPK9			17306896
DNA damage	Activates	MCTS1	response to DNA damage stimulus	GO:0006974	17016429
DNA damage	Inhibits	MDM2	Positive regulation of cell cycle arrest by p53-mediated DNA damage response.	GO:0006977	11960904
DNA damage	Inhibits	MDM2			16227609
DNA damage	Activates	MYC	cellular response to UV	GO:0034644	2687769
DNA damage	Activates	MYC	response to DNA damage stimulus	GO:0006974	
DNA damage	Inhibits	MYC	cellular response to UV	GO:003464	12761495
DNA damage	Inhibits	MYC	response to DNA damage stimulus	GO:0006974	12761495

DNA damage	Activates	MYST4			19001415
DNA damage	Activates	NCL			12000845
DNA damage	Activates	PHF20			PMC3454513
DNA damage	Activates	PITX1			20563669
DNA damage	Activates	PML			PMC156140
DNA damage	Activates	PRKD1			16911582
DNA damage	Activates	PRKDC			16908529
DNA damage	Inhibits	PTTG1			18047793
DNA damage	Activates	RFC			11336696
DNA damage	Activates	RFC			18245774
DNA damage	Activates	RFC			PMC87010
DNA damage	Activates	SOX4	DNA damage response, detection of DNA damage	GO:0042769	19234109
DNA damage	Activates	STAT3			20456494
DNA damage	Inhibits	STMN1			16909102
DNA damage	Activates	SUB1			19047459
DNA damage	Activates	TFAP2A			8962096
DNA damage	Activates	TGFB1			15652459
DNA damage	Activates	TP53BP1			14695167
DNA damage	Activates	TP53BP1			PMC150747
DNA damage	Activates	TP53RK			20647325
DNA damage	Activates	UBE2A	Response to UV	GO:0009411	1717990
DNA damage	Activates	UBE2A			23525009
DNA damage	Activates	YBX1	regulation of transcription, DNA-dependent	GO:0006355	12080043
DNA damage	Activates	YY1	Cellular response to UV	GO:0034644	18026119

DNA damage	Activates	YY1	Cellular response to DNA damage stimulus	GO:0006974	18026119

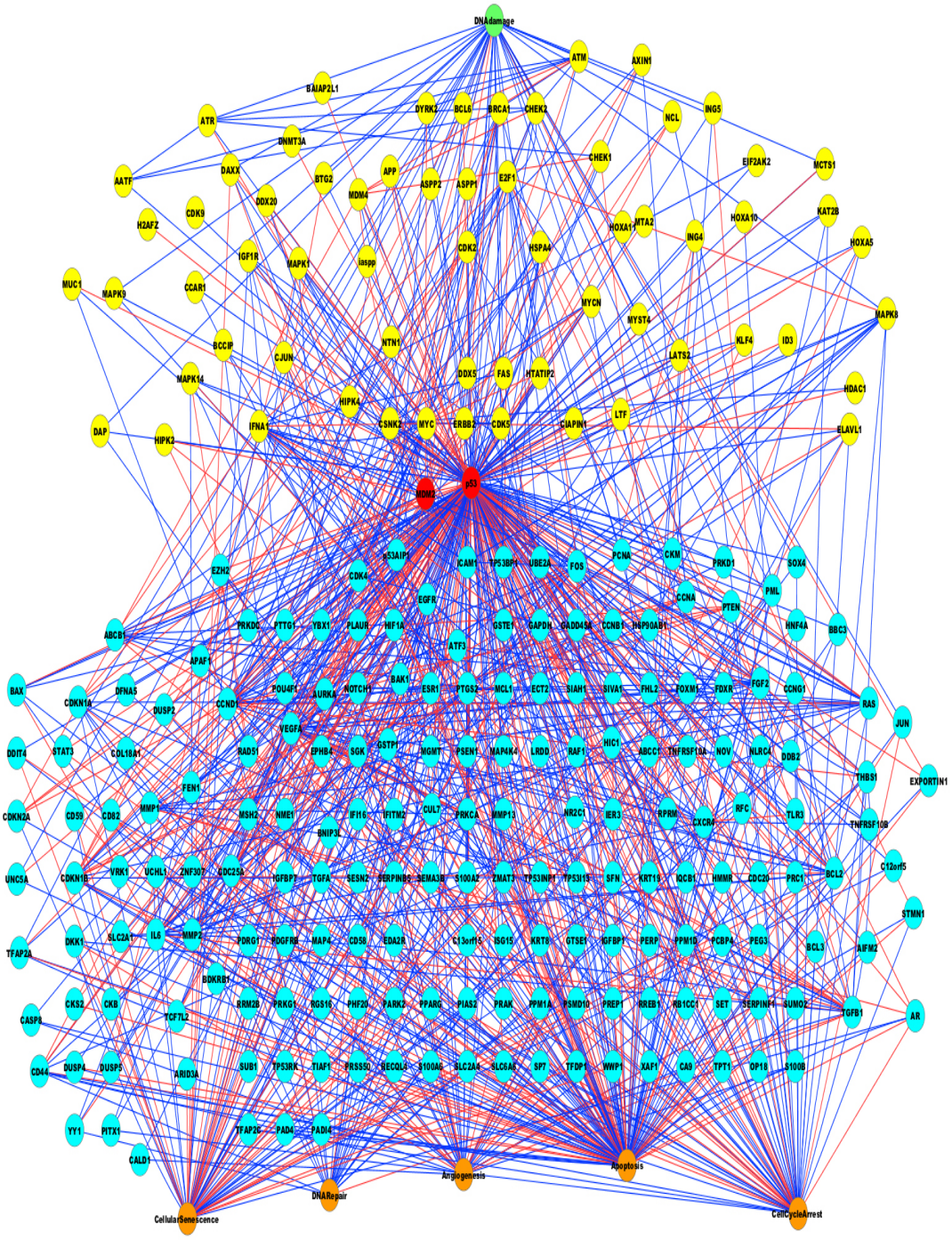

Image 7.2 The PMH260 p53-DNA damage model

Five layers are observed in accordance with node function; the input signal of DNA damage (green), upstream of p53 (yellow), the network hub, p53 (red) contained within the crucial

feedback loop with MDM2 (red), downstream of p53 (turquoise) and five downstream outputs (orange). Red lines signify inhibition, blue activation.

7.2.2 Analysis and validation of the PMH260 model

One of the main aims was to generate a larger model and ascertain if the extended model could correctly predict overall system attributes in response to network perturbations by comparison to experimental data. To investigate network perturbations of the PMH260 interactome in response to *in silico* manipulation of different node states and inputs, two methods were undertaken; Logical Steady State Analysis (LSSA) and dependency matrix calculations, both provided in CellNetAnalyzer (v.2015.1) (CNA). The PMH260 network was established in CNA in accordance with Klamt et al. (2006) discussed in detail in material and methods, section 6.2.1.2.

7.2.2.1 Logical steady state analysis of PMH260

The DNA damage input serves as environmental stress to the model. The *in silico* manipulation of this input can represent, for example, DNA damaging chemotherapeutic agents such as etoposide. To investigate network perturbations from loss of p53 and different DNA damage inputs (ON or OFF), we created four different *in silico* scenarios (section 6, table 6.2) and investigated the LSS of nodes in the PMH260 network as a result of these different conditions.

Under these conditions and globally, the majority of node states were determined in p53 wildtype backgrounds (78.5 % for p53 wild type with DNA damage OFF) (78.8 % for p53 wildtype with DNA damage ON) compared to node states in the p53 deleted backgrounds. In fact, over half of all nodes switched to an undetermined state when p53 was deleted from the network (57 % for DNA damage ON) (57.1 % for DNA damage OFF).

In the presence of p53, a greater number of upregulated nodes were observed compared to p53 KO backgrounds: 164 (63 %) when DNA damage was ON in the presence of p53, compared to 101 (39 %) when p53 was deleted with DNA damage ON (compare lanes 1 and 7, fig. 7.2). Nearly a 4-fold increase was observed in the number

of down-regulated nodes when DNA damage was switched ON in the presence of p53, 41 (15.7 %), when comparing to p53 KO, 11 (4 %), (compare lanes 2 and 8, fig. 7.2). A 2-fold increase in the number of down-regulated nodes was seen when DNA damage was OFF in the presence of p53, 56 (21.5 %), compared to when DNA damage was OFF in p53 KO background, 30 (11.6 %), (compare lanes 5 and 11, fig. 7.2). All output signals remained active across all scenarios. Table 7.2.7 provides a global list off all node state changes in response to the four *in silico* conditions.

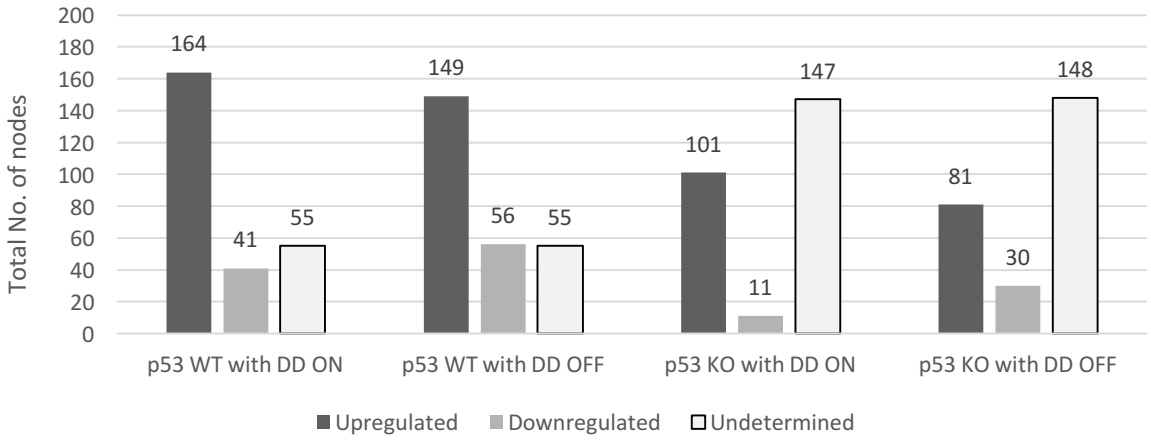

Figure 7.2 Global distribution of all PMH260 nodes under LSSA
Global distribution of node state changes in response to the four *in silico* scenarios generated of different DNA damage (DD) and p53 statuses: WT: Wild type. KO: Knockout.

Several nodes were exclusively *in silico* DNA damage responsive regardless of p53 status and some, unsurprisingly upregulated when the DNA damage input was switched ON, downregulated when OFF (ATM, ATR, JUN, DAXX, BTG2, CCAR1, DAP, HTATIP2, MAPK9, MYST4, PITX1, PRKD1, SOX4 and UBE2A). Other nodes were differentially regulated dependant on p53 *in silico* status. For example, GADD45A was downregulated in p53 deletion backgrounds, conversely upregulated when p53 was present. As highlighted in table 7.2.6 many nodes remained up or downregulated across all simulations, regardless of p53 status or DNA damage input.

Table 7.2.7 Global list of node state changes under LSSA in the PMH260 model in response to different DNA damage and p53 scenarios. Distribution of all nodes (n = 260) in PMH260 under LSSA in response to the four different simulations of different p53 (WT=wild type, KO=knockout), and DNA damage (DD) statuses (section 6, material and methods). In accordance with CNA, three states exist; 1 = upregulated, 0 = downregulated, NaN = undetermined.

Node ID	p53 WT with DD ON	p53 WT with DD OFF	p53 KO with DD ON	p53 KO with DD OFF
AATF	1	1	1	1
ABCB1	1	1	1	1
ABCC1	1	1	1	1
AIFM2	1	1	NaN	NaN
Angiogenesis	1	1	1	1
APAF1	1	1	1	1
Apoptosis	1	1	1	1
APP	NaN	NaN	NaN	NaN
AR	0	0	0	0
ARID3A	1	1	NaN	NaN
ASPP1	NaN	NaN	NaN	NaN
ASPP2	NaN	NaN	NaN	NaN
ATF3	1	1	1	1
ATM	1	0	1	0
ATR	1	0	1	0
AURKA	NaN	NaN	NaN	NaN
AXIN1	1	1	1	1
BAIA2PL1	NaN	NaN	NaN	NaN
BAIAP2L2	NaN	NaN	NaN	NaN
BAK1	1	1	NaN	NaN
BAX	1	1	1	1
BBC3	1	1	NaN	NaN
BCCIP	NaN	NaN	NaN	NaN
BCL2	1	1	1	1
BCL3	0	0	NaN	NaN
BCL6	0	1	0	1
BDKRB1	0	0	NaN	NaN
BNIP3L	1	1	NaN	NaN
BRCA1	1	1	1	1
BTG2	1	0	1	0
C12orf5	1	1	NaN	NaN
C13orf15	1	1	NaN	NaN
CA9	0	0	NaN	NaN
CALD1	1	1	NaN	NaN
CASP8	1	1	NaN	NaN
CCAR1	1	0	1	0
CCNA	1	1	1	1
CCNB1	0	0	NaN	NaN

CCND1	1	1	1	1
CCNG1	1	1	1	1
CD44	1	1	1	1
CD58	1	1	NaN	NaN
CD59	1	1	NaN	NaN
CD82	1	1	NaN	NaN
CDC20	0	0	NaN	NaN
CDC25A	1	1	1	1
CDK2	1	1	1	1
CDK4	NaN	1	NaN	1
CDK5	1	NaN	1	1
CDK9	NaN	1	NaN	NaN
CDKN1A	1	1	1	1
CDKN1B	1	1	1	1
CDKN2A	0	0	NaN	NaN
Cell Cycle Arrest	1	1	1	1
Cellular Senescence	1	1	1	1
CHEK1	1	0	1	NaN
CHEK2	1	1	1	1
CIAPIN1	NaN	NaN	NaN	NaN
CKB	1	1	1	1
CKM	1	1	0	0
CKS2	0	0	NaN	NaN
COL18A1	1	1	NaN	NaN
COL1A2	1	NaN	NaN	NaN
CSNK2	NaN	NaN	NaN	NaN
CUL7	1	0	1	1
CXCR4	1	1	1	1
DAP	1	0	1	0
DAXX	1	0	1	0
DDB2	1	1	NaN	NaN
DDIT4	1	1	NaN	NaN
DDX20	NaN	NaN	NaN	NaN
DDX5	NaN	NaN	NaN	NaN
DFNA5	1	1	NaN	NaN
DKK1	1	1	NaN	NaN
DNA damage	1	0	1	0
DNA repair	1	1	1	1
DNMT3A	NaN	NaN	1	NaN
DUSP2	1	1	NaN	NaN
DUSP4	1	1	NaN	1
DUSP5	1	1	1	0
DYRK2	1	0	1	1

E2F1	1	1	1	NaN
ECT2	0	0	NaN	NaN
EDA2R	1	1	NaN	1
EGFR	1	1	1	NaN
EIF2AK2	NaN	NaN	NaN	NaN
ELAVL1	1	1	1	0
EPHB4	0	0	1	NaN
ERBB2	1	1	1	1
ESR1	1	1	NaN	1
EXPORTIN1	0	1	0	1
EZH2	1	1	1	1
FAS	1	1	1	NaN
FDXR	1	1	NaN	NaN
FEN1	1	1	NaN	0
FGF2	NaN	1	0	1
FHL2	1	1	NaN	NaN
FOS	1	1	1	1
FOXM1	0	0	NaN	NaN
GADD45A	1	1	0	0
GAPDH	1	1	NaN	NaN
GSTP1	1	1	1	1
GTSE1	1	1	NaN	NaN
H2AFZ	NaN	NaN	NaN	NaN
HDAC1	NaN	NaN	NaN	NaN
HIC1	1	1	1	1
HIF1A	1	1	1	1
HIPK2	NaN	NaN	NaN	NaN
HIPK4	NaN	NaN	NaN	NaN
HMMR	0	0	NaN	NaN
HNF4A	0	0	NaN	NaN
HOXA10	NaN	NaN	NaN	NaN
HOXA11	NaN	NaN	NaN	NaN
HOXA5	NaN	NaN	NaN	NaN
HSP90AB1	0	0	NaN	NaN
HSPA4	1	1	1	1
HTATIP2	1	0	1	0
IASPP	NaN	NaN	NaN	NaN
ICAM1	1	1	1	1
ID3	1	1	1	1
IER3	1	1	NaN	NaN
IFI16	1	1	NaN	NaN
IFITM2	0	0	NaN	NaN
IFNA1	NaN	NaN	NaN	NaN
IGF1R	0	0	NaN	NaN

IGFBP1	1	1	NaN	NaN
IGFBP7	1	1	NaN	NaN
IL6	1	1	1	1
ING4	NaN	NaN	NaN	NaN
ING5	NaN	NaN	1	NaN
IQCB1	0	0	NaN	NaN
ISG15	1	1	NaN	NaN
JUN	1	0	1	0
KAT2B	1	1	NaN	NaN
KLF4	1	1	NaN	NaN
KRT19	0	0	0	NaN
KRT8	1	1	NaN	NaN
LATS2	1	1	NaN	NaN
LRDD	1	1	NaN	NaN
LTF	1	1	1	1
MAP4	0	0	NaN	NaN
MAP4K4	0	1	1	NaN
MAPK1	1	1	1	1
MAPK14	1	1	1	1
MAPK8	1	1	1	1
MAPK9	1	0	1	0
MCL1	1	1	1	1
MCTS1	1	0	1	0
MDM2	1	1	NaN	1
MDM4	1	1	NaN	1
MGMT	0	0	NaN	NaN
MMP1	0	1	1	1
MMP13	1	1	1	1
MMP2	1	1	1	1
MSH2	1	1	1	1
MTA2	NaN	NaN	NaN	NaN
MUC1	NaN	NaN	NaN	NaN
MYC	1	1	1	1
MYCN	1	1	1	1
MYST4	1	0	1	0
NCL	1	NaN	1	NaN
NLRC4	1	1	NaN	NaN
NME1	1	1	1	1
NOTCH1	1	1	1	1
NOV	1	1	NaN	NaN
NR2C1	1	1	1	1
NTN1	NaN	NaN	NaN	NaN
OP18	0	0	NaN	NaN
p53	1	1	0	0

p53AIP1	1	1	NaN	NaN
PAD4	NaN	NaN	NaN	NaN
PADI4	NaN	NaN	NaN	NaN
PARK2	1	0	NaN	0
PCBP4	1	1	NaN	NaN
PCNA	1	1	1	1
PDGFRB	0	0	1	0
PDRG1	0	0	NaN	NaN
PEG3	1	1	NaN	NaN
PERP	1	1	NaN	NaN
PHF20	NaN	NaN	NaN	NaN
PIAS2	NaN	NaN	NaN	NaN
PITX1	1	0	1	0
PLAUR	1	1	1	1
PML	1	1	1	0
POU4F1	NaN	NaN	NaN	NaN
PPARG	NaN	NaN	NaN	NaN
PPID	NaN	NaN	NaN	NaN
PPM1A	NaN	NaN	NaN	NaN
PPM1D	1	1	NaN	NaN
PRAK	0	1	0	1
PRC1	0	0	NaN	NaN
PREP1	NaN	NaN	NaN	NaN
PRKCA	1	1	NaN	NaN
PRKD1	1	0	1	0
PRKDC	1	0	1	0
PRKG1	1	1	NaN	NaN
PRSS50	0	0	NaN	NaN
PSEN1	1	1	1	1
PSMD10	NaN	NaN	NaN	NaN
PTEN	1	1	NaN	NaN
PTGS2	1	1	1	1
PTTG1	0	1	0	1
RAD51	0	0	0	0
RAF1	1	1	1	1
RAS	1	1	1	1
RB1CC1	NaN	NaN	NaN	NaN
RECQL4	0	0	NaN	NaN
RFC	NaN	NaN	NaN	NaN
RGS16	1	1	NaN	NaN
RPRM	1	1	NaN	NaN
RREB1	NaN	NaN	NaN	NaN
RRM2B	1	1	NaN	NaN
S100A2	1	1	NaN	NaN

S100A6	0	0	NaN	NaN
S100B	NaN	NaN	NaN	NaN
SEMA3B	1	1	NaN	NaN
SERPINB5	1	1	NaN	NaN
SERPINF1	1	1	1	1
SESN2	1	1	NaN	NaN
SET	NaN	NaN	NaN	NaN
SFN	1	1	NaN	NaN
SGK	1	1	1	1
SIAH1	1	1	1	1
SIVA1	1	1	1	1
SLC2A1	1	1	1	1
SLC2A4	0	0	NaN	NaN
SLC6A6	0	0	NaN	NaN
SOX4	1	0	1	0
SP7	0	0	NaN	NaN
STAT3	NaN	NaN	NaN	NaN
STMN1	0	1	0	1
SUB1	NaN	NaN	NaN	NaN
SUMO2	NaN	NaN	NaN	NaN
TCF7L2	NaN	NaN	NaN	NaN
TFAP2A	1	1	1	0
TFAP2C	1	1	NaN	NaN
TFDP1	0	0	NaN	NaN
TGFA	1	1	1	1
TGFB1	1	1	1	1
THBS1	1	1	1	1
TIAF1	NaN	NaN	NaN	NaN
TLR3	1	1	NaN	NaN
TNFRSF10A	1	1	1	1
TNFRSF10B	1	1	1	1
TP53BP1	1	0	NaN	NaN
TP53I13	1	1	NaN	NaN
TP53INP1	1	1	NaN	NaN
TP53RK	NaN	NaN	NaN	NaN
TPT1	1	1	NaN	NaN
UBE2A	1	0	1	0
UCHL1	NaN	NaN	NaN	NaN
UNC5A	1	1	1	0
VEGFA	1	1	1	1
VRK1	NaN	NaN	NaN	NaN
WWP1	0	0	NaN	NaN
XAF1	0	0	NaN	NaN
YBX1	1	1	NaN	1

YY1	NaN	NaN	NaN	NaN
ZMAT3	1	1	NaN	NaN
ZNF307	NaN	NaN	NaN	NaN

7.2.2.2 Genome wide analysis and validation of the PMH260 model

The Boolean PKT206- DNA damage model has generated good predictive ratios when compared to transcriptome data (Tian et al.2013). Thus, we investigated the predictive potential of the expanded logical model (PMH260) to predict differential gene changes when compared to the exact transcriptome data as applied in Tian et al. (2013) using node expression results generated from *in silico* LSSA of PMH260 (table 7.2.7).

Microarray profiles of untreated and etoposide (10 µM) treated human osteosarcoma cell lines; SaOS2 (p53 -/-) and U2OS (p53 +/+) available in (Tian et al.2013) and untreated HCT116 (p53 wild type and null) colon cancer cell lines from the Gene Expression Omnibus (GSE10795) were compared against the PMH260 interactome. The fold change and expression profiles of both transcriptomes *in vitro* and *in silico* LSS data were calculated in accordance with Christensen et al. (2009) and Tian et al. (2013). This formula is discussed in detail in material and methods, section 6.3.1.
A total of 202 genes were filtered from osteosarcoma and 172 from HCT116 colon cancer transcriptome profiles. Comparing osteosarcoma *in vitro* to *in silico* LSSA expression results, correct predictions were in the majority ranging between 55 to 71 % dependant on simulation, with an average of 61.2 % when considering all simulations. Large errors occupied the minority, resulting in less than 5 % for all predictions (average, 2.9 %). Small errors comprised 35 % when considering all simulations. Less correct predictions were derived for HCT116 simulation (55 % correct). Table 7.2.8 and figure 7.2.1 summarise the total number and percentage of all predictions respectively.

Table 7.2.8 Total number of all predictions from comparison of *in silico* data to *in vitro* microarray profiles. Correct predictions were in the majority across all simulations with large errors occupying a small percentage of results when comparing osteosarcoma transcriptome profiles to *in silico* data under LSSA. Table represents total numbers from osteosarcoma (n = 202) HCT116 (n= 172).

Experimental Source	Experimental Target	Model LSSA in silico simulation	Correct	Small error	Large error
			Total number		
U2OS cells with DNA damage	SaOS2 cells with DNA damage	p53 wild type DNA damage ON vs. p53 KO DNA damage ON	111	82	9
U2OS cells no DNA damage	SaOS2 cells no DNA damage	p53 wild type DNA damage OFF vs. p53 KO DNA damage OFF	117	75	10
U2OS cells no DNA damage	U2OS cells with DNA damage	p53 wild type DNA damage OFF vs. p53 wild type DNA damage ON	142	59	1
SaOS2 cells no DNA damage	SaOS2 cells with DNA damage	p53 KO DNA damage OFF vs. p53 KO DNA damage OFF	136	64	2
HCT116 p53 (+/+) no DNA damage	HCT116 p53 (+/+) no DNA damage	p53 WT DNA damage OFF vs. p53 KO DNA damage OFF	94.5	72.5	5

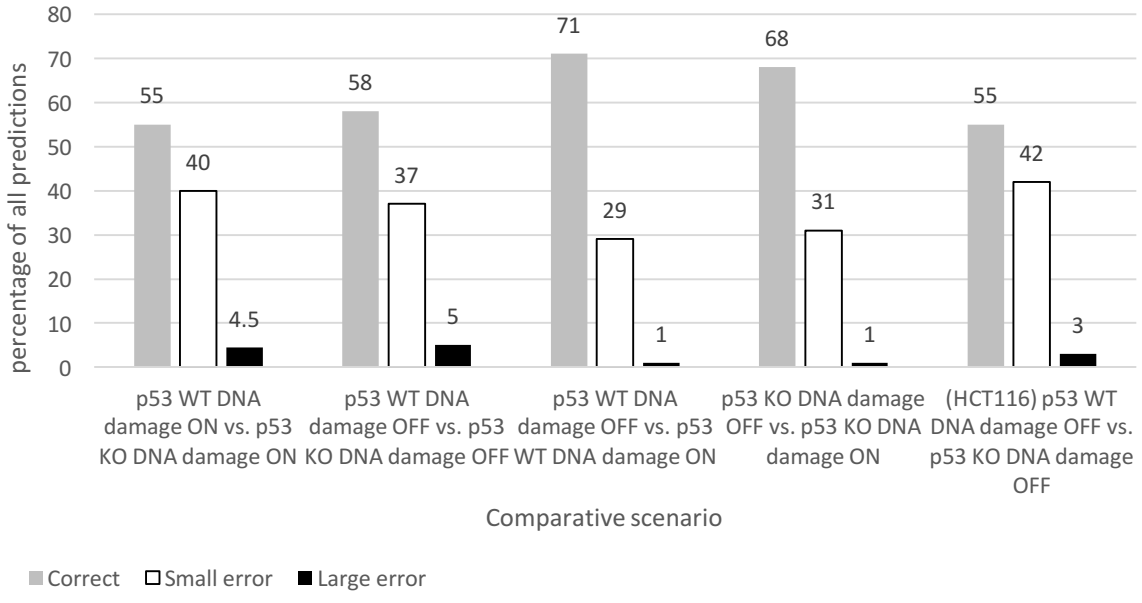

Figure 7.2.1 Percentage of all predictions from comparison of *in silico* data to *in vitro* osteosarcoma microarray profiles.

The differential gene expression changes in human osteosarcoma cells untreated and treated with 10 µM etoposide (24 h) were further explored. In general, the majority of genes remained unchanged across all three simulations. Of the 'no changes', the model predicted the majority as correct. Several genes that were correctly predicted were belonging to the growth factor family or growth factor regulated genes, such as FGF2 and EPHB4, and along with PTGS2, IGF1R and PDGFRB, and were differentially expressed dependant on cell type and p53 status. For example, FGF2 was downregulated in SaOS2 (p53 -/-) cells, conversely, anti-apoptotic genes, PDGFRB, IGF1R, EPHB4 and PTGS2 were all upregulated in SaOS2 cells. However, the input of differentially expressed genes into the DAVID functional annotation tool derived no significant over represented pathways of interest for each experimental condition. Table 7.2.9 summarises differential gene expression changes in osteosarcoma transcriptome profiles using the formula in accordance with Christensen et al. (2009).

Table 7.2.9 Global list of genes differentially expressed in untreated and etoposide treated human osteosarcoma cell lines. In accordance with Christensen et al. (2009), three different changes were possible; upregulated, downregulated or unchanged between *in vitro* to *in silico* data.

Experimental condition	Upregulated	Downregulated	Unchanged
U2OS cells with DNA damage vs. SaOS2 cells with DNA damage	**Total number**		
	19	**21**	**162**
	AR	ABCB1	AATF
	CDKN2A	BTG2	ABCC1
	CKM	C12orf5	AIFM2
	COL18A1	CCND1	APAF1
	DDIT4	CD44	ARID3A
	DKK1	CDKN1A	ATF3
	DYRK2	DDB2	ATM
	HIPK2	DFNA5	ATR
	ID3	DUSP2	AURKA
	IFITM2	FAS	AXIN1
	IGF1R	FDXR	BAK1
	IGFBP7	FGF2	BAX
	ISG15	FHL2	BBC3
	KLF4	MGMT	BCL2
	RPRM	PEG3	BCL3
	SEMA3B	RRM2B	BCL6
	SOX4	S100A2	BDKRB1

	SP7	SERPINF1	BNIP3L
	TNFRSF10A	SFN	BRCA1
		THBS1	C13orf15
		TNFRSF10B	CALD1
			CASP8
			CCNA
			CCNB1
			CCNG1
			CD58
			CD59
			CD82
			CDC20
			CDC25A
			CDK2
			CDK4
			CDK5
			CDK9
			CDKN1B
			CHEK1
			CHEK2
			CIAPIN1
			CKB
			CKS2
			CSNK2
			CXCR4
			DDX5
			DUSP4
			DUSP5
			E2F1
			ECT2
			EDA2R
			EGFR
			EIF2AK2
			ELAVL1
			EPHB4
			ERBB2
			ESR1
			EZH2
			FEN1
			FOS
			FOXM1
			GADD45A
			GAPDH
			GSTP1

			GTSE1
			H2AFZ
			HDAC1
			HIC1
			HIF1A
			HIPK4
			HMMR
			HNF4A
			HOXA11
			HSP90AB1
			HSPA4
			HTATIP2
			ICAM1
			IER3
			IFI16
			IFNA1
			IGFBP1
			IL6
			IQCB1
			KAT2B
			KRT19
			KRT8
			LATS2
			LRDD
			LTF
			MAP4
			MAP4K4
			MAPK1
			MAPK14
			MAPK8
			MAPK9
			MCL1
			MCTS1
			MDM2
			MDM4
			MMP1
			MMP13
			MMP2
			MSH2
			MUC1
			MYC
			MYCN
			NCL
			NLRC4

			NME1
			NOTCH1
			NOV
			NR2C1
			NTN1
			PADI4
			PARK2
			PCBP4
			PCNA
			PDGFRB
			PDRG1
			PERP
			PLAUR
			POU4F1
			PPM1A
			PPM1D
			PRC1
			PRKCA
			PRKD1
			PRKDC
			PRKG1
			PRSS50
			PSEN1
			PSMD10
			PTEN
			PTGS2
			PTTG1
			RAD51
			RAF1
			RAS
			RECQL4
			RGS16
			RREB1
			S100A6
			SERPINB5
			SESN2
			SGK1
			SIAH1
			SIVA1
			SLC2A1
			SLC2A4
			SLC6A6
			TCF7L2
			TFDP1

			TGFA
			TGFB1
			TIAF1
			TLR3
			TP53AIP1
			TP53I13
			TP53INP1
			VEGFA
			VRK1
			WWP1
			XAF1
			YBX1
			ZMAT3
U2OS cells untreated vs. SaOS2 cells untreated	**Upregulated**	**Downregulated**	**Unchanged**
	Total number		
	18	18	166
	CDK5	ABCB1	AATF
	CDKN2A	CCND1	ABCC1
	CKM	CD44	AIFM2
	COL18A1	CDC20	APAF1
	DKK1	CDKN1A	AR
	IFITM2	DDB2	ARID3A
	IGF1R	DFNA5	ATF3
	IGFBP7	DUSP2	ATM
	ISG15	FDXR	ATR
	KAT2B	FGF2	AURKA
	KLF4	MGMT	AXIN1
	MAP4	PEG3	BAK1
	RPRM	S100A2	BAX
	S100A6	SERPINF1	BBC3
	SEMA3B	SFN	BCL2
	SOX4	SLC2A1	BCL3
	SP7	THBS1	BCL6
	TNFRSF10A	TNFRSF10B	BDKRB1
			BNIP3L
			BRCA1
			BTG2
			C12orf5
			C13orf15
			CALD1
			CASP8
			CCNA
			CCNB1
			CCNG1

			CD58
			CD59
			CD82
			CDC25A
			CDK2
			CDK4
			CDK9
			CDKN1B
			CHEK1
			CHEK2
			CIAPIN1
			CKB
			CKS2
			CSNK2
			CXCR4
			DDIT4
			DDX5
			DUSP4
			DUSP5
			DYRK2
			E2F1
			ECT2
			EDA2R
			EGFR
			EIF2AK2
			ELAVL1
			EPHB4
			ERBB2
			ESR1
			EZH2
			FAS
			FEN1
			FHL2
			FOS
			FOXM1
			GADD45A
			GAPDH
			GSTP1
			GTSE1
			H2AFZ
			HDAC1
			HIC1
			HIF1A
			HIPK2

			HIPK4
			HMMR
			HNF4A
			HOXA11
			HSP90AB1
			HSPA4
			HTATIP2
			ICAM1
			ID3
			IER3
			IFI16
			IFNA1
			IGFBP1
			IL6
			IQCB1
			KRT19
			KRT8
			LATS2
			LRDD
			LTF
			MAP4K4
			MAPK1
			MAPK14
			MAPK8
			MAPK9
			MCL1
			MCTS1
			MDM2
			MDM4
			MMP1
			MMP13
			MMP2
			MSH2
			MUC1
			MYC
			MYCN
			NCL
			NLRC4
			NME1
			NOTCH1
			NOV
			NR2C1
			NTN1
			PADI4

			PARK2
			PCBP4
			PCNA
			PDGFRB
			PDRG1
			PERP
			PLAUR
			POU4F1
			PPM1A
			PPM1D
			PRC1
			PRKCA
			PRKD1
			PRKDC
			PRKG1
			PRSS50
			PSEN1
			PSMD10
			PTEN
			PTGS2
			PTTG1
			RAD51
			RAF1
			RAS
			RECQL4
			RGS16
			RREB1
			RRM2B
			SERPINB5
			SESN2
			SGK1
			SIAH1
			SIVA1
			SLC2A4
			SLC6A6
			TCF7L2
			TFDP1
			TGFA
			TGFB1
			TIAF1
			TLR3
			TP53AIP1
			TP53I13
			TP53INP1

			VEGFA
			VRK1
			WWP1
			XAF1
			YBX1
			ZMAT3
U2OS cells untreated vs. U2OS cells with DNA damage	**Upregulated**	**Downregulated**	**Undetermined**
	Total number		
	27	**22**	**154**
	ABCB1	AR	AATF
	BTG2	AURKA	ABCC1
	C12orf5	CCNA	AIFM2
	CD44	CCNB1	APAF1
	CD82	CDC20	ARID3A
	CDKN1A	CDKN1B	ATF3
	DDB2	CDKN2A	ATM
	DUSP2	CHEK1	ATR
	DUSP5	CHEK2	AXIN1
	FAS	DDIT4	BAK1
	FDXR	ECT2	BAX
	FHL2	GTSE1	BBC3
	FOS	HMMR	BCL2
	GADD45A	HSP90AB1	BCL3
	IER3	ID3	BCL6
	IL6	MAPK9	BDKRB1
	LRDD	PEG3	BNIP3L
	MAP4	PRC1	BRCA1
	MDM2	SERPINF1	C13orf15
	MMP1	SIAH1	CALD1
	PADI4	TCF7L2	CASP8
	PPM1D		CCND1
	RRM2B		CCNG1
	SFN		CD58
	SGK1		CD59
	TLR3		CDC25A
	ZMAT3		CDK2
			CDK4
			CDK5
			CDK9
			CIAPIN1
			CKB
			CKM
			CKS2
			COL18A1

			CSNK2
			CXCR4
			DDX5
			DFNA5
			DKK1
			DUSP4
			DYRK2
			E2F1
			EDA2R
			EGFR
			EIF2AK2
			ELAVL1
			EPHB4
			ERBB2
			ESR1
			EZH2
			FEN1
			FGF2
			FOXM1
			GAPDH
			GSTP1
			H2AFZ
			HDAC1
			HIC1
			HIF1A
			HIPK2
			HIPK4
			HNF4A
			HOXA11
			HSPA4
			HTATIP2
			ICAM1
			IFI16
			IFITM2
			IFNA1
			IGF1R
			IGFBP1
			IGFBP7
			IQCB1
			ISG15
			KAT2B
			KLF4
			KRT19
			KRT8

			LATS2
			LTF
			MAP4K4
			MAPK1
			MAPK14
			MAPK8
			MCL1
			MCTS1
			MDM4
			MGMT
			MMP13
			MMP2
			MSH2
			MUC1
			MYC
			MYCN
			NCL
			NLRC4
			NME1
			NOTCH1
			NOV
			NR2C1
			NTN1
			PARK2
			PCBP4
			PCNA
			PDGFRB
			PDRG1
			PERP
			PLAUR
			POU4F1
			PPM1A
			PRKCA
			PRKD1
			PRKDC
			PRKG1
			PRSS50
			PSEN1
			PSMD10
			PTEN
			PTGS2
			PTTG1
			RAD51
			RAF1

			RAS
			RECQL4
			RGS16
			RPRM
			RREB1
			S100A2
			S100A6
			SEMA3B
			SERPINB5
			SESN2
			SIVA1
			SLC2A1
			SLC2A4
			SLC6A6
			SOX4
			SP7
			TFDP1
			TGFA
			TGFB1
			THBS1
			TIAF1
			TNFRSF10A
			TNFRSF10B
			TP53AIP1
			TP53I13
			TP53INP1
			VEGFA
			VRK1
			WWP1
			XAF1
			YBX1
SaOS2 cells untreated vs SaOS2 cells with DNA damage	**Upregulated**	**Downregulated**	**Undetermined**
	Total number		
	30	**25**	**147**
	ATF3	AURKA	AATF
	BAX	CCNB1	ABCB1
	BBC3	CCND1	ABCC1
	BCL2	CDC20	AIFM2
	BRCA1	CXCR4	APAF1
	CDC25A	ECT2	AR
	CDK9	FGF2	ARID3A
	CDKN1A	GADD45A	ATM
	CHEK2	HMMR	ATR
	COL18A1	IFNA1	AXIN1

	DDB2	IL6	BAK1
	DDIT4	IQCB1	BCL3
	DKK1	KRT19	BCL6
	EPHB4	LTF	BDKRB1
	HIPK2	MAPK8	BNIP3L
	IGF1R	MAPK9	BTG2
	IGFBP7	MMP2	C12orf5
	KLF4	PARK2	C13orf15
	MUC1	PLAUR	CALD1
	NOTCH1	PRKCA	CASP8
	PDGFRB	PTTG1	CCNA
	PRKDC	S100A2	CCNG1
	PTGS2	SERPINF1	CD44
	RAD51	TGFA	CD58
	SIVA1	TP53INP1	CD59
	TCF7L2		CD82
	TLR3		CDK2
	VRK1		CDK4
	WWP1		CDK5
	ZMAT3		CDKN1B
			CDKN2A
			CHEK1
			CIAPIN1
			CKB
			CKM
			CKS2
			CSNK2
			DDX5
			DFNA5
			DUSP2
			DUSP4
			DUSP5
			DYRK2
			E2F1
			EDA2R
			EGFR
			EIF2AK2
			ELAVL1
			ERBB2
			ESR1
			EZH2
			FAS
			FDXR
			FEN1

			FHL2
			FOS
			FOXM1
			GAPDH
			GSTP1
			GTSE1
			H2AFZ
			HDAC1
			HIC1
			HIF1A
			HIPK4
			HNF4A
			HOXA11
			HSP90AB1
			HSPA4
			HTATIP2
			ICAM1
			ID3
			IER3
			IFI16
			IFITM2
			IGFBP1
			ISG15
			KAT2B
			KRT8
			LATS2
			LRDD
			MAP4
			MAP4K4
			MAPK1
			MAPK14
			MCL1
			MCTS1
			MDM2
			MDM4
			MGMT
			MMP1
			MMP13
			MSH2
			MYC
			MYCN
			NCL
			NLRC4
			NME1

			NOV
			NR2C1
			NTN1
			PADI4
			PCBP4
			PCNA
			PDRG1
			PEG3
			PERP
			POU4F1
			PPM1A
			PPM1D
			PRC1
			PRKD1
			PRKG1
			PRSS50
			PSEN1
			PSMD10
			PTEN
			RAF1
			RAS
			RECQL4
			RGS16
			RPRM
			RREB1
			RRM2B
			S100A6
			SEMA3B
			SERPINB5
			SESN2
			SFN
			SGK1
			SIAH1
			SLC2A1
			SLC2A4
			SLC6A6
			SOX4
			SP7
			TFDP1
			TGFB1
			THBS1
			TIAF1
			TNFRSF10A
			TNFRSF10B

			TP53AIP1
			TP53I13
			VEGFA
			XAF1
			YBX1

7.2.2.3 Dependency matrix changes from *in silico* knockout analysis

As good predictive ratios were achieved from superimposition of *in vitro* transcriptome data to the interactome, we further explored the effect of *in silico* node knockout on the PMH260 network. The *in silico* deletion of a particular node can mimic *in vivo* loss of functions and mutations, and as such represent a novel tool for identifying deregulated genes or pathways from their loss. To investigate network perturbations from absence of a particular node in PMH260, 3 *in silico* knockout tests of highly connected nodes (MDM2, p53 and FGF2) were undertaken. The effect of a node deletion on a given network can result in six dependency relationship changes, defined by six values (1- 6) described in detail in section 6, material and methods, summarised here in table 7.2.9.1.

Table 7.2.9.1 Alterations in the dependency matrix in response to 3 node deletions
3 nodes were deleted from the PMH260 network. The numbers of six types of effect elements in the dependency matrix were calculated as listed below which represent the 6 relationships described in effect row. The value "Null" in the selected gene column indicates the p53 wild type network. KO = knockout.

Effect	**No Effect**	**Ambivalent**	**Weak inhibitor**	**Weak activator**	**Strong inhibitor**	**Strong activator**	**Total**
Number effect	1	2	3	4	5	6	
***In silico* KO**							
Null	40653	20988	2761	3048	48	102	67600
p53	59864	6862	38	79	71	167	67081
MDM2	40607	20359	2847	3116	48	48	67081
FGF2	40462	20722	2725	3022	48	102	67081

The total number of dependencies (n = 67,600) (260 × 260) represents elements in the dependency matrix of the PMH260 p53 wild type model (null). Of these, 40653 correspond to interactions with no effect, 20988 are ambivalent factors, 2761 are weak

inhibitors, 3048 are weak activators, 48 comprising strong inhibitors and 102 strong activators. For each *in silico* knockout scenario the total number (n = 67,081) represents elements within the network after node deletion (259 x 259). We focused on changes to either strong activators or inhibitors as these have the greatest effect on the cell.

The majority of changes were derived as a result of p53 deletion. The removal of p53 resulted in a two-fold increase from the number of strong inhibitors (48 in p53 wild type to 71 in p53 knockout) (table 7.2.9.1). In comparison, p53s negative regulator, MDM2, which is contained within an intricate feedback loop with p53, induced only two changes when deleted. The majority of the dependency changes derived from *in silico* p53 knockout scenario were changes to strong activators (n = 65) and strong inhibitors (n = 23), from ambivalent factors in the wild type model. Interestingly, several nodes changed from having no influence on angiogenesis in the wild type scenario to having a strong inhibitory (COL181A, PPARG and PML), or activating (MAPK14, MMP2, MMP13, NTN1, S100B, SGK, PRAK and STMN1) angiogenic effect in the absence of p53. Similarly, TFDP1, GTSP1 and EZH2 had no influence on cell cycle arrest in the presence of p53, however the exclusion of p53 resulted in all three nodes changing to positive regulators of cell cycle arrest (table 7.2.9.2). For MDM2 KO, one dependency change to strong activator was observed (ATM to DYRK2). No changes were observed as a result of FGF2 deletion.

As a result, a total of 98 changes were derived from the 3 *in silico* knockout tests, of these, the majority arose from p53 deletion. To validate these potential predictions, scientific literature searches were undertaken. As a consequence, 13 from the total 98 were confirmed by literature or experimentally verified. The remaining were considered as potential novel predictions (PNPs). Table 7.2.9.2 lists all predictions with their status and reference if validated by literature.

Table 7.2.9.2 Summary of predictions derived from application of *in silico* knockout tests of 3 nodes (p53, FGF2 and MDM2) to dependency matrix elements. 98 predictions were obtained from 3 *in silico* deletions of highly connected nodes. The greatest change was seen in the absence of p53. Some predictions were verified from literature or laboratory experiments; others are potential novel predictions (PNP). Null = wildtype model

Deleted node	Source node	Target	Null	Knockout	Prediction
p53	LATS2	Apoptosis	Ambivalent factor	Strong activator	Ke et al. 2004
p53	CCAR1	Apoptosis	Ambivalent factor	Strong activator	PNP
p53	DAP	Apoptosis	Ambivalent factor	Strong activator	PNP
p53	DYRK2	Apoptosis	Ambivalent factor	Strong activator	PNP
p53	FAS	Apoptosis	Ambivalent factor	Strong activator	PNP
p53	ING4	Apoptosis	Ambivalent factor	Strong activator	PNP
p53	ING5	Apoptosis	Ambivalent factor	Strong activator	PNP
p53	KAT2B	Apoptosis	Ambivalent factor	Strong activator	PNP
p53	PAD4	Apoptosis	Ambivalent factor	Strong activator	PNP
p53	UCHL1	Apoptosis	Ambivalent factor	Strong activator	Jin et al. 2013
p53	PPARG	Apoptosis	Ambivalent factor	Strong activator	Fjas et al. 2003
p53	PML	Apoptosis	Ambivalent factor	Strong activator	Yang et al. 2002
p53	TFAP2A	Apoptosis	Ambivalent factor	Strong activator	Wajapeyee and Somasundrum 2003
p53	ASSP1	Apoptosis	Ambivalent factor	Strong activator	PNP
p53	ASSP2	Apoptosis	Ambivalent factor	Strong activator	PNP
p53	DAXX	Apoptosis	Ambivalent factor	Strong inhibitor	PNP
p53	RB1CC1	Apoptosis	Ambivalent factor	Strong inhibitor	PNP
p53	SGK	Apoptosis	Ambivalent factor	Strong inhibitor	PNP
p53	STAT3	Apoptosis	Ambivalent factor	Strong inhibitor	PNP
p53	PREP1	Apoptosis	Ambivalent factor	Strong inhibitor	PNP
p53	CUL7	Apoptosis	Ambivalent factor	Strong inhibitor	PNP
p53	PRAK	Apoptosis	Ambivalent factor	Strong inhibitor	PNP

p53	FOXM1	CCNB1	Ambivalent factor	Strong activator	PNP
p53	KLF4	CCNB1	Ambivalent factor	Strong inhibitor	Yoon et al. 2004
p53	SFN	CCNB1	Ambivalent factor	Strong inhibitor	PNP
p53	FGF2	CDK4	Ambivalent factor	Strong activator	PNP
p53	IFNA1	CDK4	Ambivalent factor	Strong inhibitor	PNP
p53	PTTG1	CDK4	Ambivalent factor	Strong activator	PNP
p53	ATM	CHK1	Ambivalent factor	Strong activator	Tian et al.2013
p53	ATR	CHK1	Ambivalent factor	Strong activator	Tian et al.2013
p53	PPM1D	CHK1	Weak inhibitor	Strong activator	PNP
p53	IFNA1	FAS	Ambivalent factor	Strong activator	PNP
p53	IFNA1	TLR3	Ambivalent factor	Strong activator	PNP
p53	IFNA1	FAS	Ambivalent factor	Strong inhibitor	PNP
p53	PTTG1	FGF2	Ambivalent factor	Strong activator	PNP
p53	MAPK14	BAX	Ambivalent factor	Strong activator	PNP
p53	MAPK14	MMP2	Ambivalent factor	Strong activator	PNP
p53	DYRK2	p53AIP1	Weak activator	Strong activator	PNP
p53	MAPK14	SGK	Weak activator	Strong activator	PNP
p53	RFC	DNA Repair	Ambivalent factor	Strong activator	PNP
p53	SOX4	DNA Repair	Ambivalent factor	Strong activator	PNP
p53	TP53BP1	DNA Repair	Ambivalent factor	Strong activator	PNP
p53	UBE2A	DNA Repair	Ambivalent factor	Strong activator	PNP
p53	YY1	DNA Repair	Ambivalent factor	Strong activator	PNP
p53	HOXA5	DNA Repair	Ambivalent factor	Strong activator	PNP
p53	PML	DNA Repair	Ambivalent factor	Strong activator	PNP
p53	COL181 A	Angiogenesis	No effect	Strong inhibitor	PNP

p53	ING4	Angiogenesis	Ambivalent factor	Strong inhibitor	PNP
p53	PPARG	Angiogenesis	No effect	Strong inhibitor	PNP
p53	PML	Angiogenesis	No effect	Strong inhibitor	PNP
p53	JUN	Angiogenesis	Ambivalent factor	Strong activator	PNP
p53	MAPK14	Angiogenesis	No effect	Strong activator	PNP
p53	MMP13	Angiogenesis	No effect	Strong activator	PNP
p53	NTN1	Angiogenesis	No effect	Strong activator	PNP
p53	S100B	Angiogenesis	Ambivalent factor	Strong activator	PNP
p53	MMP2	Angiogenesis	No effect	Strong activator	PNP
p53	SGK	Angiogenesis	No effect	Strong activator	PNP
p53	PRAK	Angiogenesis	No effect	Strong activator	PNP
p53	STMN1	Angiogenesis	No effect	Strong activator	PNP
p53	JUN	Cell cycle arrest	Ambivalent factor	Strong inhibitor	PNP
p53	ING5	Cell cycle arrest	Ambivalent factor	Strong inhibitor	PNP
p53	IER3	Cell cycle arrest	Ambivalent factor	Strong inhibitor	PNP
p53	BCCIP	Cell cycle arrest	Ambivalent factor	Strong inhibitor	PNP
p53	DDX5	Cell cycle arrest	Ambivalent factor	Strong activator	PNP
p53	PITX1	Cell cycle arrest	Ambivalent factor	Strong activator	PNP
p53	RFC	Cell cycle arrest	Ambivalent factor	Strong activator	PNP
p53	SOX4	Cell cycle arrest	Ambivalent factor	Strong activator	PNP
p53	UBE2A	Cell cycle arrest	Ambivalent factor	Strong activator	PNP
p53	MYST4	Cell cycle arrest	Ambivalent factor	Strong activator	PNP
p53	ING4	Cell cycle arrest	Ambivalent factor	Strong activator	PNP
p53	KAT2B	Cell cycle arrest	Ambivalent factor	Strong activator	PNP
p53	PPARG	Cell cycle arrest	Ambivalent factor	Strong activator	PNP

p53	TFAP2A	Cell cycle arrest	Ambivalent factor	Strong activator	Scibetta et al. 2010
p53	TFAP2C	Cell cycle arrest	Ambivalent factor	Strong activator	PNP
p53	EZH2	Cell cycle arrest	No effect	Strong activator	PNP
p53	GSTP1	Cell cycle arrest	No effect	Strong activator	PNP
p53	RB1CC1	Cell cycle arrest	Ambivalent factor	Strong activator	PNP
p53	TFDP1	Cell cycle arrest	No effect	Strong activator	PNP
p53	CUL7	Cell cycle arrest	Ambivalent factor	Strong activator	PNP
p53	MAPK14	Cellular senescence	Ambivalent factor	Strong inhibitor	PNP
p53	PPMID	Cellular senescence	Ambivalent factor	Strong inhibitor	PNP
p53	DAXX	Cellular senescence	Ambivalent factor	Strong inhibitor	PNP
p53	SGK	Cellular senescence	Ambivalent factor	Strong inhibitor	PNP
p53	LATS2	Cellular senescence	Ambivalent factor	Strong activator	Tschop et al. 2011
p53	UCHL1	Cellular senescence	Ambivalent factor	Strong activator	PNP
p53	PPARG	Cellular senescence	Ambivalent factor	Strong activator	PNP
p53	PML	Cellular senescence	Ambivalent factor	Strong activator	Scaglioni et al. 2012
p53	CUL7	Cellular senescence	Ambivalent factor	Strong activator	PNP
p53	PRAK	Cellular senescence	Ambivalent factor	Strong activator	PNP
p53	BCCIP	DNA repair	Ambivalent factor	Strong activator	PNP
p53	DNA damage	CHK1	Ambivalent factor	Strong activator	Reindhart et al. 2007
p53	DNA damage	FAS	Ambivalent factor	Strong activator	Manna et al. 2011
p53	DNA damage	FGF2	Ambivalent factor	Strong inhibitor	PNP
p53	DNA damage	PML	Ambivalent factor	Strong activator	PNP
p53	DNA damage	TFAP2A	Strong activator	AF	PNP
p53	DNA damage	PRAK	No effect	Strong inhibitor	PNP
MDM2	ATM	DYRK2	Ambivalent factor	Strong activator	PNP

7.2.3 Conclusion

The tumour suppressor p53 has a well-defined role for maintaining genomic integrity (Zilfou, 2009) and its mutation is the most frequently observed in over half of all human cancers. p53 is pivotal to anti-proliferative processes, critical to tumour suppression and typically confers sensitivity to chemo-therapeutic intervention (Lu and El-Diery, 2009). Thus, p53 is an attractive target for anti - cancer drug discovery and targeted strategies. Nevertheless, the complexity and vast literature base of p53 and its regulatory pathways makes it challenging to fully elucidate p53 – cancer dynamics. Thus there is a need to integrate this information at the molecular level into a coherent framework.

Systems biology teamed with traditional reductionist approaches are novel, yet promising tools to dissect and describe the complexity of disease systems such as cancer (Wang, 2010). Boolean networks are a promising predictive framework and have been applied successfully to model various biological phenomena. In particular, the Boolean model - PKT206 has demonstrated good predictive capability when compared to transcriptome data for p53 – DNA damage pathways (Tian et al.2013). Even so, the p53 network is extensive, with a plethora of p53 responsive genes described (Riley et al.2008). To capture these, a larger model is necessitated. Extensive models allow for a global system overview and thus better representation of biological phenomena.

With this in mind, we expanded the PKT206 model to generate the preliminary model - PMH260 which considers 980 interactions of activation or inhibition amongst 254 internal nodes. In addition, we included an additional 3 outputs of DNA repair, angiogenesis and cell cycle arrest to consider the heterogeneity of cancer dynamics and the processes that govern them. We undertook *in silico* knock out tests of highly connected nodes, and tested the predictive efficiency of PMH260 on a genome wide level against LSSA data, superimposing exact transcriptome data as used by Tian et al. (2013) to determine if the larger Boolean model can effectively identify p53 system attributes. This section confirms that PMH260 can effectively identify overall system attributes.

Under LSSA, several characteristic nodes were differentially expressed strengthening the models capability to correctly identify system attributes. For example, in response to DNA damage and p53 presence, ATM and ATR both well-established DNA damage responsive genes were upregulated when the *in silico* DNA damage input was switched ON. Similarly, for the p53 target, p21 was upregulated. With regard to well characterised p53 regulated apoptotic genes, both FAS and PUMA were upregulated in p53 wildtype backgrounds (table 7.2.9).

To mimic *in vivo* mutations and elucidate the role of deleted nodes on the PMH260 network, we imposed three *in silico* knockout tests of highly connected nodes using CNA. The greatest effect was observed with p53 exclusion, resulting in 98 changes. Conversely, only one change was as a result of MDM2 removal, and no strong dependency changes occurred with the deletion of FGF2. This was also observed in the PKT206 model using the same *in silico* knockout approach (Tian et al.2013). This is not surprising considering that p53 is the most highly connected 'hub' node in the network, and participates in the majority of feedback loops (>50 %) and interactions.
The effect of p53 on network stability was further highlighted by the fact that several nodes altered from having no angiogenic effect to a positive influence on angiogenesis in the absence of p53 (MAPK14, MMP2, MMP13, NTN1, S100B, SGK, PRAK and STMN1) (table 7.2.9.1). These are interesting findings and offer potential for further investigation in p53 null tumours. Similarly, two nodes changed from having no influence on the cell cycle in the wild type model to positive cell cycle regulators when p53 was deleted from the network. All these genes were classified as PNPs, however are worthy of further investigation, in particular for p53 mutated tumours.
We performed an extensive literature search for potential validations of the 98 predictions obtained from *in silico* tests. Of these, 13 were confirmed by literature or experimentally verified (table 7.2.9.1 provides all validated references). Of the 24 dependency changes described in PKT206 for p53 *in silico* knockout, 22 (83 %) in PMH260 were in agreement. This highlights the accuracy and reproducibility of the p53 interactome when enlarged. Indeed, majority of the prediction differences from dependency simulations arose from new nodes introduced into PMH260. This is unsurprising, as additional nodes are introduced, dependencies will change.

As PMH260 revealed both important established and novel predictions that could be of therapeutic interest, we further evaluated its predictive potential. We superimposed the exact transcriptome data as used in (Tian et al.2013), and compared etoposide treated and untreated human osteosarcoma and HCT116 expression profiles to the PMH260 interactome. Good prediction ratios were derived with 55-71 % of correct predictions across all simulations. This number significantly exceeds an expected probability of 33 % for a random model which has three possible prediction outcomes with equal probability (Christensen et al.2009). Predictive ratios here are similar to those obtained from the PKT206 interactome. This is promising, as the model increases so does network complexity, which is often difficult to simulate and analyse.

Comparing differential expression profiles of apoptotic and angiogenic factors *in silico* to 'omics' p53 wild type and null profiles has derived several important predictions of therapeutic relevance. For example, and in parallel with Tian et al. (2013), growth factors were also uncovered as contributing factors to osteosarcoma. For example, the pro-angiogenic and apoptotic ambivalent factor FGF2 was down-regulated in SaOS2 cells, whilst anti-apoptotic PDFGRB and IGF1R, along with growth factor regulated genes EPHB4 and PTGS2, were up-regulated in SaOS2 and HCT116 cells, suggestive of cell specific regulation. Indeed, growth factors and their receptors are strongly implicated in osteosarcoma. For example; PDGFRB (McGary et al.2002) and EPHB4 (Matsuo and Otaki, 2012). Whilst, Kujjier et al. (2013) has shown that inhibition of IGF1R signalling is linked to reduced proliferation in 75 % of osteosarcoma cell lines, highlighting that inhibition of IGF1R signalling may be a potential anti-cancer strategy in high grade osteosarcoma patients. Proceeding our model simulation here and implication of PTGS2 overexpression in osteosarcoma cell lines, a recent study by Liu et al. (2015), revealed that overexpression of PTGS2 is linked with osteosarcoma metastasis. These results strengthen the predictive potential of the expanded model to correctly simulate *in vitro* data, and along with previous reports our results highlight the importance of growth factors in p53 null osteosarcoma tumours. Furthermore, several novel predictions were obtained which may be of relevance contributing to the p53 null tumour phenotype. For example, 8 genes (described above) altered to pro-

angiogenic factors when p53 was removed, *in silico*, highlighting their potential for further investigation for putative anti-cancer targeted strategies in osteosarcoma p53 null tumours.

In summary, PMH260 has provided increased coverage of potential expression changes in cancer, and validation of its predictive potential through comparison to *in vitro* microarray profiles have derived good results. This highlights the predictive performance of large-scale Boolean models for the investigation of p53-DNA damage inducible pathways and offers potential to further expand this model for further increased coverage and elucidation of p53 – cancer dynamics using logical models.

7.3 Generation and analyses of the PMH302 model

The Boolean p53 DNA damage inducible models; PMH260 (section 7.2) and the earlier p53 model generated by Tian et al. (2013), have both demonstrated to successfully predict overall p53 system attributes. For example, the PMH260 Boolean model, comprising 206 nodes with 980 interactions (Hussain et al.2015), has previously demonstrated predictive potential of p53 network dynamics, deriving 71 % correct predictions when compared to various *in vitro* microarray profiles of etoposide treated human osteosarcoma (p53 +/+), (p53 -/-) and untreated human colon cancer (p53 +/+) and (p53 -/-) cell lines. Nevertheless, as previously discussed, the p53 network is extensive. For example, 1501 p53 responsive genes have been described from 33615 human genes on cDNA microarrays by Wang et al. (2001) also in (Riley et al.2008). Information about p53 interactions at the molecular level must be integrated with the cell environment that is crucial to development of optimal individualized targeted therapies. To capture these and depict a more accurate representation of the molecular pathways that govern p53 dynamics a larger model is essential to dissect the p53 – cancer network; capture mutation drivers, identify perturbed pathways and create sub networks of cell/tissue specific models. However, larger models can be difficult to simulate due to network complexity and size (Klamt et al.2006).

In addition, whilst the PMH260 network considers five biological processes that contribute to the malignant phenotype, only one input signal of DNA damage was included. For greater clinical representation, models must incorporate and depict tumour heterogeneity, and the processes that regulate and govern the malignant phenotype. Hypoxia for example is a pathophysiological feature common to the majority of solid tumours. Genomic instability owing to hypoxic conditions allows for the activation of proliferative signalling pathways involved in, for example, the regulation of angiogenesis and cell death contributing to tumour progression and survival. Indeed, tumour hypoxia has been associated with chemo-resistance and poor patient survival (Wilson and Hay, 2013).

In consideration of the above, and given the fact that the Boolean PMH260 model has successfully identified overall system attributes, we have further expanded the p53 model (PMH260) to generate a larger model designated PMH302 (p53 Michelle Hussain 302 nodes). In addition, to capture molecular deviations that govern tumour progression, we have further integrated an additional input of hypoxia into PMH302. Thus PMH302 may be more representative of p53-cancer dynamics than previous models.

Given the fact that the earlier p53 logical interactomes have all derived good prediction percentages when compared to transcriptome data, we used the same mathematical principles as previously applied to these models. We aimed to evaluate if a larger model can again be successfully simulated using a Boolean framework and, importantly, if greater predictive ratios can be achieved. In addition, as the earlier Boolean p53 models derived good predictive potential when comparing *in vitro* expression profiles, we aimed to extend this analyses to *in vivo* data to explore the clinical relevance of the PMH302 model.

7.3.1 Results

7.3.1.1 Generation of the PMH302 model

For consistency, we followed the same methodology previously used for generation of all earlier p53 models to construct the PMH302 network. All potential interactions direct to p53 and indirect (interactions amongst genes/proteins surrounding p53) were extracted from the STRING database (v9.1) using ULTRAEDIT, filtered in accordance with the STRING confidence schema of a 0.7 threshold. For accuracy, all potential interactions were also manually curated by extensive scientific literature search. Validation of all interactions were additionally confirmed by supervisor (Prof. M. Krstic–Demonacos), and also with the kind help of Dr Costas Demonacos.

Five outputs of cell cycle arrest, cellular senescence, DNA repair, angiogenesis and apoptosis are considered in the PMH302 model. In addition to the DNA damage input already included, a second input of hypoxia was also integrated. Dependant on the biological processes they regulate, or are regulated by, all internal nodes (n = 295) were linked to their relevant inputs (n = 2) and outputs (n = 5). These were initially determined by their GO annotations using the Gene Ontology database, and further confirmed by literature evidence. Table 7.3 summarises all interactions between nodes in the PMH302 model. Figure 7.3 illustrates the PMH302 network visualised in Cytoscape (v.28).

7.3.1.2 Network topology of PMH302

Including all GO annotations, a total number of 1398 interactions of activation or inhibition amongst 295 internal nodes (excluding inputs and outputs, n = 7) comprise the PMH302 model. Of these, 898 comprised activations, the remaining (n = 500) are inhibitory interactions. 295 nodes were linked direct to p53. Of these, p53 participated in a total of 325 direct interactions; 102 and 79 constituted upstream interactions of p53 activating or inhibiting target nodes respectively. The remaining were downstream of p53; activating (n = 92) or inhibiting (n = 52) p53. 30 of these direct interactions with p53 were ambivalent, these were located both up and downstream of p53 in the model. Table 7.3 summarises all interactions between nodes in the PMH302 model.

Figure 7.3 illustrates the PMH302 network visualised in Cytoscape (v.28). Tables 7.3.1 to 7.3.1.6 provides GO annotations for all nodes in the PMH302 network

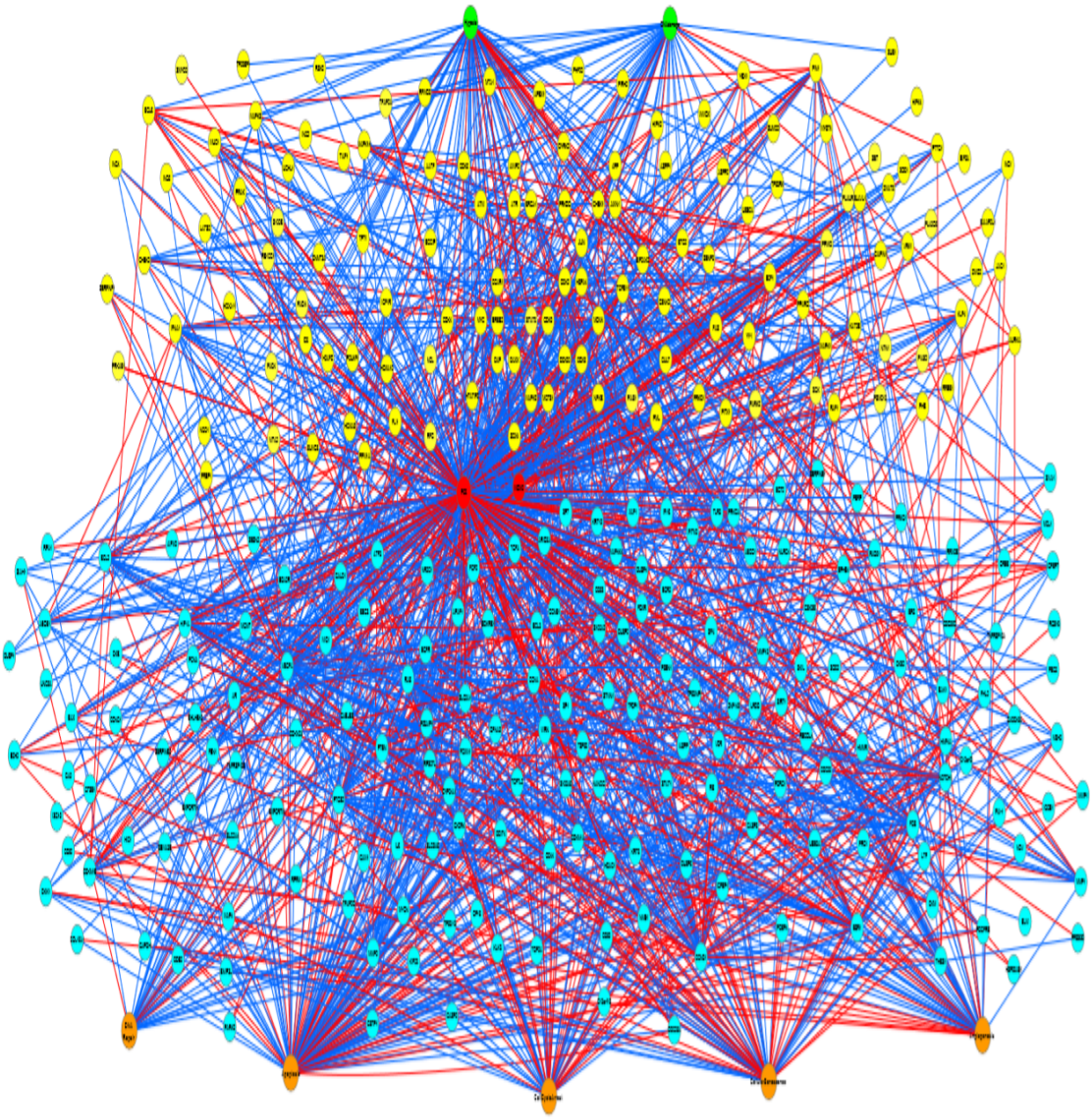

Image 7.3 The PMH302 model
The PMH302 p53–DNA damage and hypoxia inducible model. Five layers are observed in accordance with node function; the input signals of DNA damage and hypoxia (green), upstream of p53 (yellow), the network hub, p53 contained within the crucial feedback loop with MDM2 (red), downstream of p53 (turquoise) and five downstream outputs (orange). Red lines signify inhibition, blue activation. Constructed and visualised in Cytoscape (v.28).

Table 7.3 Total interaction list of nodes and interactions considered in PMH302.
A total of 1398 interactions between 295 nodes are considered in the PMH302 model. Of these 557 are activations (excluding GO annotations). PubMed IDs are supplied. Some PMID/PMCIDs were not available, for these their DOI are provided. This table does not consider GO annotations. These are described in separate tables**.**

Source	Interaction	Target	PMID/PMC
AATF	Activates	p53	20708154
AATF	Activates	CDK5	18388733
AIMP2	Activates	p53	18695251
APEX1	Activates	FEN1	12200445
APEX1	Activates	HIF1A	11018583
APEX1	Activates	HIF1A	PMC2587278
APP	Inhibits	p53	10377452
AR	Inhibits	MMP1	8798622
ASPP1	Activates	p53	11684014
ASPP1	Activates	p53	22552744
ASPP2	Activates	p53	22552744
ATF3	Activates	GDF15	20110283
ATF3	Activates	CCND1	11375399
ATF3	Inhibits	MMP2	11792711
ATF3	Inhibits	IL6	16688168
ATM	Activates	PRKDC	23761041
ATM	Activates	PCNA	22362778
ATM	Activates	p53	10608806
ATM	Activates	CHEK2	16936775
ATM	Activates	ATR	17088261
ATM	Activates	AATF	17157788
ATM	Activates	BRCA1	12082091
ATM	Activates	DYRK2	19965871
ATM	Inhibits	CCND1	25486524
ATM	Inhibits	CCND2	19071090
ATM	Inhibits	BCL6	18346918
ATM	Inhibits	MDM2	16943424
ATM	Inhibits	MDM4	16943424
ATR	Activates	p53	16557269
ATR	Activates	CHEK1	16557269
ATR	Activates	AATF	17157788
ATR	Activates	BRCA1	12082091
ATR	Inhibits	MDM2	16943424
AURKA	Inhibits	p53	14702041
AXIN1	Activates	HIPK2	PMC533058
AXIN1	Activates	p53	19513548
AXIN1	Inhibits	MYC	PMC2657573
AXIN1	Inhibits	CCND1	11739413
AXIN1	Inhibits	TCF7L2	17768662

BAIAP2L1	Inhibits	p53	21887275
BAIAP2L1	Inhibits	p53	PMC3160901
BAIAP2L2	Inhibits	p53	21887275
BCCIP	Activates	p53	15539944
BCL2	Activates	MMP2	19258038
BCL2	Activates	CCND1	11313702
BCL2	Activates	FOS	15326476
BCL2	Activates	VEGFA	12205045
BCL2	Activates	SLC2A1	15120582
BCL2	Activates	RAS	15326476
BCL3	Activates	JUN	10497212
BCL3	Activates	EGFR	17881446
BCL6	Activates	p53	18524763
BCL6	Inhibits	STAT3	17951530
BCL6	Inhibits	JUN	12165517
BCL6	Inhibits	p53	15577913
BCL6	Inhibits	CDKN1B	10981963
BDKRB1	Activates	FGF2	11387266
BHLHE40	Inhibits	STAT3	15223310
BHLHE40	Inhibits	STAT3	21761458
BRCA1	Activates	p53	11371136
BRCA1	Activates	CCND1	17278098
BRCA1	Inhibits	ESR1	PMC4030134
BRCA1	Inhibits	ESR1	PMC4030134
BTG2	Activates	p53	11814693
BTG2	Inhibits	PIN1	20569234
BTG2	Inhibits	CCND1	15378000
CABLES	Activates	CDK5	10896159
CABLES	Activates	CDK5	10896159
CABLES	Activates	CDK5	22898083
CABLES	Inhibits	CDK2	11585773
CCAR1	Activates	p53	18722177
CCNA	Activates	CDC25A	10926775
CCNA	Activates	AXIN1	15063782
CCNA	Inhibits	CCNB1	11018009
CCNA	Inhibits	CKM	8995365
CCNA	Inhibits	FEN1	12853968
CCNA	Inhibits	E2F1	7838523
CCNB1	Activates	CDK2	15818617
CCNB1	Activates	CDK2	15818617
CCND1	Activates	ESR1	9271411
CCND1	Activates	HDAC1	15713663
CCND1	Activates	CDK2	15355984
CCND1	Activates	HSPA4	9121772

CCND1	Activates	E2F1	10504464
CCND1	Activates	VEGFA	16899623
CCND1	Inhibits	CDK2	9925749
CCND1	Inhibits	MAPK1	18722177
CCND1	Inhibits	BCL6	19307668
CCND1	Inhibits	STAT3	11279133
CCND1	Inhibits	PPARG	12917338
CCND1	Inhibits	PPARG	15713663
CCND1	Inhibits	HNF4A	PMC3409010
CCND1	Inhibits	RB	24305655
CCND1	Inhibits	THBS1	17020778
CCNG1	Activates	CCNB1	16322753
CD44	Inhibits	CCND1	17296798
CD82	Inhibits	VEGFA	20569234
CD82	Inhibits	VEGFA	16461284
CD82	Inhibits	VEGFA	15616196
CD82	Inhibits	VEGFA	17562791
CD82	Inhibits	VEGFA	22390300
CDC25A	Inhibits	EGFR	11912208
CDK2	Activates	BRCA1	19445729
CDK2	Activates	FOXM1	15654331
CDK2	Activates	PTGS2	16452236
CDK2	Activates	CABLES	11585773
CDK2	Activates	p53	11078726
CDK2	Activates	CDC25A	10926775
CDK2	Activates	E2F1	7969176
CDK2	Activates	AXIN1	15063782
CDK2	Activates	CCNA	10652300
CDK2	Inhibits	BRCA1	PMC84283
CDK2	Inhibits	TFDP1	10329431
CDK2	Inhibits	RB	24305655
CDK2	Inhibits	CDKN1B	8622855
CDK2	Inhibits	MDM2	21278451
CDK4	Activates	RAD51	PMC3436568
CDK4	Activates	RAD51	10918579
CDK4	Activates	CCND1	9099745
CDK4	Activates	BRCA1	10660629
CDK4	Inhibits	BRCA1	17334399
CDK5	Activates	STAT3	17145757
CDK5	Activates	ATM	19151707
CDK5	Activates	p53	17591690
CDK5	Activates	MYC	18408012
CDK5	Activates	ERBB2	16203963
CDK5	Activates	CDKN1B	16341208

CDK5	Inhibits	PPARG	PMC2987584
CDK5	Inhibits	PPARG	20651683
CDK5	Inhibits	PPARG	23622515
CDK9	Activates	p53	16741955
CDKN1A	Activates	ESR1	15743834
CDKN1A	Inhibits	CDK4	15735718
CDKN1A	Inhibits	CCNB1	PMC2722839
CDKN1A	Inhibits	STAT3	20569234
CDKN1A	Inhibits	E2F1	10498892
CDKN1A	Inhibits	MYC	20569234
CDKN1A	Inhibits	PCNA	7885482
CDKN1A	Inhibits	CDK2	8756624
CDKN1B	Inhibits	CDK2	doi:10.1038/nrc2347
CDKN1B	Inhibits	BCL2	14676836
CDKN1B	Inhibits	CCNA	8547220
CDKN1B	Inhibits	CDK2	18354415
CDKN2A	Activates	MDM4	15907800
CDKN2A	Inhibits	CDK4	21170085+
CDKN2A	Inhibits	CCND1	15205322
CDKN2A	Inhibits	MDM2	20523835
CDKN2A	Inhibits	MDM4	20177397
CHEK1	Activates	p53	10673501
CHEK1	Inhibits	CDC25A	12759351
CHEK1	Inhibits	MDM4	16511572
CHEK2	Activates	p53	10673500
CHEK2	Activates	MYC	19812253
CHEK2	Activates	BRCA1	14701743
CHEK2	Activates	E2F1	12717439
CHEK2	Activates	AATF	17157788
CHEK2	Inhibits	CDC25A	12759351
CHEK2	Inhibits	MDM4	16943424
CHK1	Activates	RAD51	15665856
CHK1	Activates	PRKDC	24500207
CHK1	Inhibits	CDK2	12181445
CIAPIN1	Inhibits	p53	16410721
CIAPIN1	Inhibits	BAX	16410721
CIAPIN1	Inhibits	BCL2	18059532
CSNK2	Activates	FOS	1915270
CSNK2	Activates	p53	9244359
CSNK2	Activates	MDM2	16335531
CSNK2	Activates	TCF7L2	11711551
CSNK2	Activates	PTEN	11035045
CSNK2	Activates	MYC	2663470
CSNK2	Activates	MYCN	1425701

CSNK2	Activates	NCL	3190709
CSNK2	Activates	HDAC1	11602581
CSNK2	Inhibits	MDM2	21769452
CUL7	Inhibits	p53	17586686
CUL7	Inhibits	p53	17229476
CUL7	Inhibits	p53	16547496
CXCR4	Activates	VEGFA	17559806
CXCR4	Activates	TNFRSF10B	15990565
DAP	Activates	p53	11146619
DAP	Inhibits	PIN1	21504826
DAP	Inhibits	PIN1	21497122
DAXX	Activates	CCND1	26205068
DAXX	Activates	CCND1	PMC373322
DAXX	Activates	p53	12482984
DAXX	Activates	p53	17210684
DAXX	Inhibits	p53	15364927
DAXX	Inhibits	p53	15339933
DDX20	Inhibits	p53	22335944
DDX5	Activates	ESR1	12738788
DDX5	Activates	p53	15660129
DKK1	Activates	TGFB1	20019166
DNMT3A	Inhibits	p53	16131836
DUSP4	Inhibits	IL6	PMC4090144
DUSP4	Inhibits	MAPK1	17473844
DUSP5	Inhibits	MAPK1	8221888
DYRK2	Activates	p53	17349958
DYRK2	Activates	p53AIP1	17349958
E2F1	Activates	VRK1	16547155
E2F1	Activates	VRK1	12629169
E2F1	Activates	VRK1	doi:10.1016/0006-291X(91)91760-A
E2F1	Activates	p53	12625370
E2F1	Activates	HIC1	19491197
E2F1	Activates	SIVA1	15105421
E2F1	Activates	APAF1	18056406
E2F1	Activates	PCNA	12468739
E2F1	Activates	MYCN	14645238
E2F1	Activates	CHEK2	15024084
E2F1	Activates	SIAH1	20187294
E2F1	Activates	EZH2	19893569
E2F1	Inhibits	MDM2	20837136
E2F1	Inhibits	MCL1	11857079
E2F1	Inhibits	AR	17178887
EGFR	Activates	CCND1	19935697
EGFR	Activates	PTGS2	15781636

EGFR	Activates	VEGFA	21074412
EGFR	Activates	ESR1	19470835
EGFR	Inhibits	NOTCH1	18604200
EIF2AK2	Activates	p53	19210572
EIF5A	Activates	p53	15371445
ELAVL1	Activates	CCNB1	384372
ELAVL1	Activates	THBS1	3041167
ELAVL1	Activates	VEGFA	9497373
ELAVL1	Activates	GDF15	1369825
ELAVL1	Activates	p53	12821781
ELAVL1	Activates	PTGS2	14633672
ELAVL1	Inhibits	VEGFA	PMC3041167
ELAVL1	Inhibits	CDKN1B	18354415
ELAVL1	Inhibits	MYC	19574298
ERBB2	Activates	STAT3	14586404
ERBB2	Activates	MCL1	16467098
ERBB2	Activates	VEGFA	15582599
ERBB2	Activates	CCND1	17483350
ERBB2	Activates	CXCR4	15542424
ERBB2	Activates	PTGS2	11901151
ERBB2	Inhibits	MUC1	11410163
ERBB2	Inhibits	p53	8700512
ERBB2	Inhibits	CDKN1B	16951165
ESR1	Activates	VEGFA	2849827
ESR1	Activates	BRCA1	16229810
ESR1	Activates	PCNA	24283290
ESR1	Activates	LTF	15525592
ESR1	Activates	CCND1	15544931
ESR1	Activates	CKB	11746525
ESR1	Activates	MYC	19661132
ESR1	Inhibits	CDKN1A	16267837
ESR1	Inhibits	IL6	PMC146754
ESR1	Inhibits	IL6	16043358
ESR1	Inhibits	EGFR	9269899
EXPORTIN1	Inhibits	CCND1	DOI: 10.1186/s12885-015-1936-z
EZH2	Inhibits	RAD51	16331887
FAS	Activates	p53	9358752
FGF2	Activates	YY1	11487577
FGF2	Activates	YY1	19235591
FGF2	Activates	STAT3	PMC3307977
FGF2	Activates	IL6	PMC1220238
FGF2	Activates	MMP13	15564063
FGF2	Activates	IGF1R	1649391
FGF2	Activates	MMP2	19107653

FGF2	Activates	CDK4	11889462
FGF2	Activates	THBS1	15927970
FGF2	Activates	ABCB1	17620438
FGF2	Activates	FOS	8783257
FGF2	Activates	MMP1	19107653
FGF2	Activates	BCL2	11380405
FGF2	Activates	PTGS2	9920767
FGF2	Activates	VEGFA	15485645
FGF2	Activates	PCNA	17003443
FGF2	Inhibits	PRSS50	20506264
FGF2	Inhibits	CDKN1B	12657588
FGF2	Inhibits	CDKN1	11726615
FHL2	Activates	CCND1	18378678
FHL2	Activates	CCND1	12124778
FHL2	Inhibits	MAPK1	I14729955
FLI1	Inhibits	p53	22266186
FOS	Activates	PPARG	10678274
FOS	Activates	PPARG	PMC4023468
FOS	Activates	CCND1	9710644
FOS	Activates	MMP1	21344389
FOS	Activates	BCL2	19079363
FOS	Inhibits	ESR1	14684847
FOXM1	Activates	MMP2	17804744
FOXM1	Activates	VEGFA	17804744
FOXM1	Activates	CCNB1	11682060
GADD45A	Inhibits	AURKA	16772293
GAPDH	Activates	AR	17553795
GAPDH	Activates	SIAH1	15951807
GSK3B	Activates	BAX	15525785
GSK3B	Inhibits	CCND1	9832503
GSK3B	Inhibits	MYC	1312697
GSK3B	Inhibits	MYC	9727977
GSK3B	Inhibits	MYC	14563837
GSK3B	Inhibits	MYC	11980918
GSK3B	Inhibits	MYC	PMC3719674
H2AFZ	Inhibits	p53	17671089
HDAC1	Inhibits	ESR1	14506733
HDAC1	Inhibits	CDKN1A	17412634
HDAC1	Inhibits	PHB	21152868
HDAC1	Inhibits	TOP2A	11062478 11136718
HDAC1	Inhibits	p53	12426395
HF1A	Activates	CDKN1B	19342889
HIF1A	Activates	NOTCH1	19293180
HIF1A	Activates	SLC2A1	16136514

HIF1A	Activates	BNIP3L	19273585
HIF1A	Activates	CD44	22937154
HIF1A	Activates	FLI1	PMC2884367
HIF1A	Activates	FOXM1	19097132
HIF1A	Activates	NANOG	21712410
HIF1A	Activates	CXCR4	19212630
HIF1A	Activates	IL6	20600219
HIF1A	Activates	MMP1	17335808
HIF1A	Activates	VEGFA	17919812
HIF1A	Activates	SLC2A1	17387384
HIF1A	Activates	PLAUR	17335808
HIF1A	Inhibits	AURKA	23925655
HIF1A	Inhibits	DUSP2	21984126
HIPK2	Activates	p53	16601678
HIPK2	Inhibits	DAXX	doi: 10.1128/MCB.23.3.950-960.2003
HIPK2	Inhibits	MDM2	16212962
HIPK2	Inhibits	HIF1A	19046997
HIPK2	Inhibits	POU4F1	15492043
HIPK4	Activates	p53	18022393
HNF4A	Inhibits	ESR1	9794469
HNF4A	Inhibits	CCND1	22241473
HOXA10	Activates	CDKN1A	11040212
HOXA10	Activates	p53	15044858
HOXA11	Inhibits	p53	19372592
HOXA5	Activates	p53	12490103
HOXA5	Inhibits	p53	12490102
HSP90AB1	Inhibits	MMP13	18593760
HSPA4	Activates	NQO1	11821413
HSPA4	Activates	p53	17278883
HSPA4	Activates	p53	17278883
HSPA4	Inhibits	FOS	11189444
HTATIP2	Activates	p53	18519672
HTATIP2	Inhibits	MMP2	19349353
HTATIP2	Inhibits	VEGFA	19349353
HTATIP2	Inhibits	MYC	15073177
iASPP	Inhibits	p53	22552744
iASPP	Inhibits	p53	12524540
ICAM1	Activates	FOS	12097408
ID3	Inhibits	p53	19618124
IFNA1	Activates	p53	15254403
IFNA1	Activates	MDM2	15580300
IFNA1	Activates	CXCR4	18202009
IFNA1	Activates	IL6	12434062
IFNA1	Activates	ICAM1	11593644

IFNA1	Activates	EGFR	1718587
IFNA1	Activates	TLR3	16087162
IFNA1	Activates	FOS	15970516
IFNA1	Activates	PTGS2	16685393
IFNA1	Activates	FAS	14616354
IFNA1	Activates	MYC	10068671
IFNA1	Activates	TNFRSF10B	12642868
IFNA1	Activates	EIF2AK2	15254208
IFNA1	Activates	PRKCA	17988665
IFNA1	Inhibits	FGF2	9485039
IFNA1	Inhibits	ABCB1	17331344
IFNA1	Inhibits	BCL2	12881711
IFNA1	Inhibits	MYC	11798827
IFNA1	Inhibits	E2F1	10208422
IGF1R	Activates	PTGS2	11114729
IGF1R	Activates	p53	8710868
IGF1R	Activates	MDM2	17846171
IGF1R	Activates	RAS	19174523
IGF1R	Activates	VEGFA	21264842
IGFBP7	Inhibits	PTGS2	19374835
IGFBP7	Inhibits	VEGFA	19374835
IL6	Activates	MMP2	16934628
IL6	Activates	CXCR4	9933168
IL6	Activates	EGFR	9459124
IL6	Activates	TGFA	11892999
IL6	Activates	FOS	11713282
IL6	Activates	MMP1	16934628
IL6	Activates	MMP13	15601621
IL6	Activates	PTGS2	16837651
IL6	Activates	MYC	20974848
IL6	Activates	VEGFA	8557680
IL6	Inhibits	BAX	12101271
ING1	Activates	p53	21731648
ING2	Activates	p53	PMC1190357
ING4	Activates	p53	12750254
ING4	Activates	p53	3742747
ING5	Activates	p53	12750254
JAG1	Activates	p53	24098521
JUN	Activates	THBS1	11216860
JUN	Activates	CCND1	12668975
JUN	Inhibits	ESR1	1906001
JUN	Inhibits	p53	10072388
KAT2B	Activates	CCND1	10318892
KAT2B	Activates	E2F1	20530585

KAT2B	Activates	E2F1	doi: 10.1074/jbc.M402403200
KAT2B	Activates	MYC	15572685
KAT2B	Activates	p53	15153330
KAT2B	Inhibits	PTEN	doi:10.1074/jbc.M605391200
KLF4	Activates	CDKN1A	16372018
KLF4	Activates	CDKN1A	12087069
KLF4	Activates	CDKN1	PMC2668950
KLF4	Activates	NOTCH1	19717984
KLF4	Activates	MUC1	17908689
KLF4	Activates	KRT19	10859317
KLF4	Activates	p53	19696146
KLF4	Activates	VEGFA	PMC4467843
KLF4	Inhibits	p53	16244670
KLF4	Inhibits	CCNB1	14627709
KLF4	Inhibits	NOTCH1	20551324
LATS2	Activates	p53	17015431
LTF	Inhibits	CCND1	18697201
MAPK1	Activates	PRAK	9628874
MAPK1	Activates	PRAK	9628874
MAPK1	Activates	STAT3	15979846
MAPK1	Activates	FOS	16123044
MAPK1	Activates	FOS	DOI 10.1074/jbc.M204296200
MAPK1	Activates	PTGS2	20883667
MAPK1	Activates	JUN	22379036
MAPK1	Activates	CCND1	9618377
MAPK1	Activates	p53	11409876
MAPK1	Activates	NR2C1	18682553
MAPK1	Activates	YBX1	16198352
MAPK1	Activates	RAF1	1730637
MAPK1	Inhibits	CCND1	10952989
MAPK1	Inhibits	CALD1	PMC3084981
MAPK14	Activates	MMP1	18620911
MAPK14	Activates	PTGS2	doi.org/10.1016/j.cbi.2007.07.008
MAPK14	Activates	ELAVL1	PMC2725730
MAPK14	Activates	MMP2	15677464
MAPK14	Activates	SGK	12488318
MAPK14	Activates	p53	18265945
MAPK14	Inhibits	JUN	17468757
MAPK8	Activates	TGFB1	12760970
MAPK8	Activates	MMP2	16672691
MAPK8	Activates	CCND1	21135252
MAPK8	Activates	ICAM1	15389584
MAPK8	Activates	FOS	17085440
MAPK8	Activates	ATF3	18377912

MAPK8	Activates	PTGS2	15546960
MAPK8	Activates	p53	11057897
MAPK8	Activates	BAX	16709574
MAPK8	Activates	BCL2	11323415
MAPK8	Inhibits	E2F1	10075927
MAPK9	Activates	PTGS2	9786861
MAPK9	Activates	p53	17525747
MCTS1	Activates	CCND1	11709712
MCTS1	Inhibits	p53	17416211
MDM2	Activates	ESR1	11178989
MDM2	Activates	ABCB1	8883415
MDM2	Activates	HIF1A	15024078
MDM2	Activates	VEGFA	21986500
MDM2	Inhibits	CDKN1A	14761977
MDM2	Inhibits	KAT2B	14769800
MDM2	Inhibits	p53	21423613
MDM2	Inhibits	VEGFA	18199551
MDM2	Inhibits	MDM4	16557269
MDM2	Inhibits	DYRK2	19965871
MDM4	Activates	MDM2	16557269
MDM4	Inhibits	CDKN1A	doi: 10.1128/MCB.01198-07
MDM4	Inhibits	CDKN1A	18086887
MDM4	Inhibits	p53	16557269
MGMT	Inhibits	ESR1	11564893
MGMT	Inhibits	VEGFA	20179017
MMP2	Activates	BAX	16857167
MSH2	Activates	ESR1	15886699
MTA1	Activates	p53	19837670
MTA2	Inhibits	p53	17914590
MTA2	Inhibits	p53	12920132
MUC1	Activates	CCND1	PMC2864713
MUC1	Activates	CCND1	14688481
MUC1	Activates	EGFR	16082192
MUC1	Activates	VEGFA	23108411
MUC1	Activates	PDGFRB	23108411
MUC1	Inhibits	p53	15710329
MYC	Activates	CDK4	10688915
MYC	Activates	CCNB1	11983916
MYC	Activates	BRCA1	11983916
MYC	Activates	p53	9839551
MYC	Activates	MMP2	19258038
MYC	Activates	CCND1	7526316
MYC	Activates	MSH2	15814658
MYC	Activates	HSPA4	1459202

MYC	Activates	CDC25A	10205150
MYC	Activates	BRCA1	21668996
MYC	Activates	VEGFA	15580293
MYC	Activates	NME1	11960382
MYC	Activates	TNFRSF10A	17881904
MYC	Activates	E2F1	17784791
MYC	Activates	CDK2	8157956
MYC	Inhibits	CDKN1A	10319992
MYC	Inhibits	BCL2	11438662
MYC	Inhibits	GADD45A	15021909
MYC	Inhibits	CDKN1A	12408820
MYCN	Activates	p53	20145147
MYCN	Activates	ABCC1	14737110
MYCN	Activates	ABCB1	12819037
MYCN	Inhibits	CD44	11035936
MYCN	Inhibits	MYC	7529553
MYCN	Inhibits	CDKN1B	18198336
MYST4	Activates	p53	19001415
NANOG	Activates	PTK2	22493428
NCL	Activates	BCL2	21048921
NCL	Inhibits	p53	16213212
NCL	Inhibits	MDM2	16751805
NFKB	Activates	p53	8051093
NME1	Activates	PTGS2	16415009
NME1	Activates	MYC	19170058
NOTCH1	Activates	STAT3	19808903
NOTCH1	Activates	NFKB2	16546962
NOTCH1	Activates	CCND1	16546962
NOTCH1	Activates	CCND1	19915977
NOTCH1	Activates	CCND1	20887720
NOTCH1	Activates	CDKN1A	11432830
NOTCH1	Activates	PIN1	19151708
NOTCH1	Activates	ESR1	19838210
NOTCH1	Activates	EGFR	18359760
NOTCH1	Activates	PTGS2	19290049
NOTCH1	Inhibits	PTEN	21993533
NOTCH1	Inhibits	CCNA	14678992
NOV	Activates	MMP1	15611078
NQO1	Activates	FOS	20498278
NQO1	Activates	FOS	20498278
NQO1	Activates	p53	11867746
NQO1	Activates	p53	11867746
NR2C1	Inhibits	ESR1	12093804
NTN1	Inhibits	p53	18922894

p53	Activates	GDF15	22723347
p53	Activates	CASP2	18418048
p53	Activates	SERPINE1	16862142
p53	Activates	DUSP1	18403641
p53	Activates	BHLHE40	18025081
p53	Activates	S100B	9632811
p53	Activates	S100B	10490652
p53	Activates	PML	1151544
p53	Activates	UNC5A	20372800
p53	Activates	TFAP2A	16636674
p53	Activates	TFAP2C	16636674
p53	Activates	ABCC1	12647018
p53	Activates	GSTP1	18505928
p53	Activates	ESR1	15012604
p53	Activates	MMP2	9343394
p53	Activates	CKM	7488858
p53	Activates	CD82	11212267
p53	Activates	GAPDH	18552833
p53	Activates	MSH2	10984493
p53	Activates	CD58	11812190
p53	Activates	DUSP4	16778175
p53	Activates	RRM2B	19010910
p53	Activates	EDA2R	20434500
p53	Activates	DDB2	12509284
p53	Activates	MDM2	11313969
p53	Activates	NOV	18418052
p53	Activates	THBS1	12609716
p53	Activates	ARID3A	12136662
p53	Activates	KAT2B	15153330
p53	Activates	ICAM1	15247038
p53	Activates	ABCB1	17666793
p53	Activates	EGFR	19597475
p53	Activates	IGFBP1	18056423
p53	Activates	CDKN1A	17585201
p53	Activates	DUSP2	16474395
p53	Activates	FDXR	12370809
p53	Activates	BAX	18949380
p53	Activates	KRT8	8615594
p53	Activates	TGFA	7651386
p53	Activates	IFI16	18974396
p53	Activates	TLR3	18779317
p53	Activates	Tp53I13	14767535
p53	Activates	HSPA4	20180806
p53	Activates	FEN1	16103874

p53	Activates	DDIT4	19210572
p53	Activates	MAP4K4	15958553
p53	Activates	HIC1	7585125
p53	Activates	SEMA3B	11922394
p53	Activates	RPRM	11313928
p53	Activates	PEG3	11679586
p53	Activates	SIVA1	19240372
p53	Activates	PCBP4	11313928
p53	Activates	DFNA5	16897187
p53	Activates	CD59	11812190
p53	Activates	Tp53INP1	12438758
p53	Activates	FHL2	17352216
p53	Activates	CCNG1	21447558
p53	Activates	CASP8	12376477
p53	Activates	CDKN1B	12376477
p53	Activates	COL18A1	15958553
p53	Activates	BBC3	18657356
p53	Activates	APAF1	11559530
p53	Activates	BAK1	15105295
p53	Activates	NLRC4	15580302
p53	Activates	GTSE1	11313928
p53	Activates	CALD1	19349302
p53	Activates	ATF3	17108111
p53	Activates	PTGS2	15608668
p53	Activates	RGS16	16405749
p53	Activates	SGK	16619268
p53	Activates	S100A2	18388131
p53	Activates	DUSP5	12944906
p53	Activates	IER3	9781666
p53	Activates	GADD45A	18350249
p53	Activates	NOTCH1	17534448
p53	Activates	FAS	9841917
p53	Activates	PTEN	11729185
p53	Activates	AIFM2	15273740
p53	Activates	CDKN1A	17585201
p53	Activates	DKK1	15668788
p53	Activates	PRKG1	19955367
p53	Activates	NME1	12669312
p53	Activates	PCNA	11682006
p53	Activates	C13orf15	17146433
p53	Activates	ISG15	11462054
p53	Activates	BNIP3L	15607964
p53	Activates	TNFRSF10A	15289308
p53	Activates	TNFRSF10B	10942251

p53	Activates	IGFBP7	19638426
p53	Activates	LATS2	19855428
p53	Activates	SERPINB5	15578720
p53	Activates	RAS	11574421
p53	Activates	C12orf5	16557269
p53	Activates	PERP	16557269
p53	Activates	SIAH1	16557269
p53	Activates	LRDD	16557269
p53	Activates	p53AIP1	16557269
p53	Activates	SESN2	16557269
p53	Activates	SFN	16557269
p53	Activates	ZMAT3	19805223
p53	Activates	KLF4	19826046
p53	Activates	PPM1D	18265945
p53	Activates	TPT1	24067374
p53	Activates	EGR2	21042708
p53	Inhibits	APEX1	11018583
p53	Inhibits	CYP24A1	25519225
p53	Inhibits	NANOG	15619621
p53	Inhibits	RPA1	8361542
p53	Inhibits	WRN	11427532
p53	Inhibits	KLK3	11791186
p53	Inhibits	RPS27L	21170087
p53	Inhibits	SOD2	15867370
p53	Inhibits	TOP2A	8972219
p53	Inhibits	CA9	480909
p53	Inhibits	CA9	18815219
p53	Inhibits	STMN1	11072234
p53	Inhibits	STMN1	10557083
p53	Inhibits	APP	19049493
p53	Inhibits	APP	23942195
p53	Inhibits	EXPORTIN 1	21683812
p53	Inhibits	BCL3	12808109
p53	Inhibits	PDRG1	20453924
p53	Inhibits	BDKRB1	11400161
p53	Inhibits	CCND1	12808109
p53	Inhibits	ECT2	16778203
p53	Inhibits	CXCR4	17130833
p53	Inhibits	SLC6A6	16734743
p53	Inhibits	XAF1	20198350
p53	Inhibits	CDK4	7851794
p53	Inhibits	IL6	11830554
p53	Inhibits	THBS1	9849855
p53	Inhibits	PDGFRB	18697203

p53	Inhibits	FGF2	11313915
p53	Inhibits	WWP1	16924229
p53	Inhibits	ABCB1	11920581
p53	Inhibits	IGF1R	10023442
p53	Inhibits	NR2C1	8663350
p53	Inhibits	EGFR	18391986
p53	Inhibits	CD44	18614011
p53	Inhibits	PRKCA	15563462
p53	Inhibits	CKB	7969181
p53	Inhibits	RECQL4	15674334
p53	Inhibits	MGMT	19846904
p53	Inhibits	SP7	16380437
p53	Inhibits	HSPA4	8418500
p53	Inhibits	CDC25A	17001315
p53	Inhibits	FOS	1946467
p53	Inhibits	CDC20	17873905
p53	Inhibits	IQCB1	16322217
p53	Inhibits	EZH2	15208672
p53	Inhibits	MMP1	11850838
p53	Inhibits	PSEN1	18374905
p53	Inhibits	PRSS50	17283160
p53	Inhibits	IFITM2	19544527
p53	Inhibits	HSP90AB1	15284248
p53	Inhibits	BCL2	11313951
p53	Inhibits	HIF1A	18815219
p53	Inhibits	MMP13	11850838
p53	Inhibits	FOXM1	19806025
p53	Inhibits	HNF4A	16895524
p53	Inhibits	TCF7L2	14990988
p53	Inhibits	BRCA1	12802282
p53	Inhibits	EPHB4	16205642
p53	Inhibits	HMMR	18971636
p53	Inhibits	MAP4	10521394
p53	Inhibits	PRC1	15531928
p53	Inhibits	KRT19	7515894
p53	Inhibits	PTGS2	15921850
p53	Inhibits	S100A6	18714402
p53	Inhibits	MCL1	18208354
p53	Inhibits	VEGFA	11559575
p53	Inhibits	SLC2A1	21862591
p53	Inhibits	AR	18084622
p53	Inhibits	TFDP1	9556576
p53	Inhibits	CKS2	17336302
p53	Inhibits	NME1	12669312

p53	Inhibits	MYC	8479742
p53	Inhibits	PCNA	8570655
p53	Inhibits	SLC2A4	20729871
p53	Inhibits	CCNB1	11162602
p53	Inhibits	RAD51	19942681
p53	Inhibits	CCNA	8270002
p53	Inhibits	CDKN2A	9774662
p53	Inhibits	PPM1D	20093361
p53	Inhibits	PRSS50	17283160
p53	Inhibits	KIF23	PMC3641139
p53	Activates	COL1A2	9764819
p53	Activates	PPID	PMC3383624
PAD4	Inhibits	p53	2493360
PAD4	Inhibits	p53	18499678
PARK2	Inhibits	AIMP2	12783850
PARK2	Inhibits	p53	19801972
PCNA	Activates	ESR1	17636311
PDGFRB	Activates	STAT3	PMC84192
PDGFRB	Activates	CCND1	10688905
PEG3	Activates	VEGFA	PMC24782
PHB	Activates	p53	14500729
PHB	Inhibits	E2F1	10376528
PHF20	Activates	p53	22334668
PIAS1	Activates	SUMO2	23871671
PIAS1	Inhibits	STAT1	9724754
PIAS1	Inhibits	p53	PMC122440
PIAS2	Inhibits	p53	19901969
PIN1	Activates	CDKN1B	19584057
PIN1	Activates	CCND1	12540053
PIN1	Activates	CCND1	11805292
PIN1	Activates	CCND1	16865248
PIN1	Activates	ERBB2	19077306
PIN1	Activates	NOTCH1	19151708
PIN1	Activates	FOS	doi: 10.1074/jbc.C500353200
PIN1	Activates	MCL1	18676833
PIN1	Activates	MYC	PMC3719674
PIN1	Activates	JUN	11432833
PIN1	Activates	VEGFA	18294451
PIN1	Activates	VEGFA	doi: 10.1158/1535-7163.MCT-08-1061
PIN1	Activates	p53	12397362
PIN1	Inhibits	FOS	16123044
PIN1	Inhibits	BCL6	17828269
PIN1	Inhibits	DAXX	17938171
PIN1	Inhibits	CDC25C	9499405

PIN1	Inhibits	GSK3B	22184106
PIN1	Inhibits	MYC	26655473
PIN1	Inhibits	CREB	23380442
PIN1	Inhibits	CREB	PMC2963389
PIN1	Inhibits	AATF	17468107
PIRH2	Activates	p53	doi:10.1016/S0092-8674(03)00193-4
PIRH2	Inhibits	CDKN1B	18006823
PITX1	Activates	p53	17762884
PLA2G6	Inhibits	p53	16492706
PLAUR	Inhibits	p53	17110957
PML	Activates	p53	12810724
PML	Activates	p53	14992722
PML	Inhibits	MDM2	22869143
POU4F1	Activates	p53	10329733
POU4F1	Activates	BCL2	9722627
POU4F1	Activates	BRCA1	11470235
PPARG	Activates	CDKN1A	15041706
PPARG	Activates	p53	16887883
PPM1A	Activates	p53	12514180
PPM1A	Inhibits	PRKAB1	23088624
PPM1D	Activates	MDM4	19808970
PPM1D	Inhibits	p53	15870257
PPM1D	Inhibits	CHEK1	15870257
PPM1D	Inhibits	MAPK14	18265945
PRAK	Activates	p53	17254968
PREP1	Activates	p53	2887940
PREP1	Activates	p53	20587415
PRKAB1	Inhibits	p53	15866171
PRKCA	Activates	IL6	9523575
PRKCA	Activates	HSPA4	17208995
PRKCA	Activates	MMP1	16368506
PRKCA	Activates	VEGFA	1511446
PRKCA	Activates	ERBB2	17545611
PRKCA	Activates	ABCB1	15563462
PRKCA	Activates	RAF1	8321321
PRKCA	Inhibits	CCND1	20141613
PRKCA	Inhibits	ABCB1	9823967
PRKCA	Inhibits	MYC	20141613
PRKD1	Activates	PTGS2	19794144
PRKD1	Activates	p53	12628923
PRKDC	Activates	ESR1	20219974
PRKDC	Activates	ATM	15753361
PRKDC	Activates	p53	11042698
PRKDC	Inhibits	APEX1	24466051

PRKDC	Inhibits	WRN	11477099
PRKG1	Activates	CDKN1A	18593937
PRKG1	Activates	CDKN1B	18593937
PRKG1	Inhibits	MAPK14	16990590
PSMD10	Inhibits	p53	19287195
PTEN	Activates	THBS1	doi: 10.1073/pnas.081063798
PTEN	Activates	THBS1	PMC2669036
PTEN	Inhibits	CCND1	16849370
PTEN	Inhibits	HIF1A	18158893
PTEN	Inhibits	EPHB4	15930280
PTEN	Inhibits	VEGFA	16527906
PTEN	Inhibits	PCNA	17826033
PTGS2	Activates	CXCR4	20110411
PTGS2	Activates	ABCB1	17510421
PTGS2	Activates	CD44	12393872
PTGS2	Activates	HSPA4	14717913
PTGS2	Activates	FOS	16685273
PTGS2	Activates	MCL1	16000874
PTGS2	Activates	VEGFA	18533784
PTGS2	Inhibits	EGFR	19671676
PTGS2	Inhibits	CDKN1B	14587561
PTTG1	Activates	p53	15242522
PTTG1	Activates	MMP2	19433493
PTTG1	Activates	FGF2	21858218
PTTG1	Activates	BAX	15242522
PTTG1	Activates	MYC	11115508
PTTG1	Inhibits	AURKA	18663361
PTTG1	Inhibits	THBS1	PMC2988648
PTTG1	Inhibits	p53	19477929
RAF1	Activates	p53	10732786
RAS	Activates	GSTP1	11606500
RAS	Activates	MAPK14	15677464
RAS	Activates	CCND1	10201372
RAS	Activates	CD44	8453616
RAS	Activates	FOS	7917786
RAS	Activates	PTGS2	19903783
RAS	Activates	VEGFA	11507052
RAS	Activates	CDKN1A	19440234
RAS	Activates	CCNA	15737994
RAS	Activates	CDKN1B	14504289
RAS	Activates	RAF1	9020159
RAS	Activates	MAPK1	9020159
RAS	Inhibits	CKM	3600660
RAS	Inhibits	CCND1	12081197

RAS	Inhibits	PTEN	19000654
RB	Inhibits	E2F1	24305655
RB	Inhibits	CCNA	11018009
RB1CC1	Inhibits	p53	21775823
RCHY1	Inhibits	p53	12654245
RFC	Inhibits	p53	10910354
RFC1	Activates	FEN1	19208620
RFWD3	Activates	p53	PMC2842028
RPA1	Activates	BLM	10825162
RREB1	Activates	p53	19558368
RRM2B	Activates	VEGFA	19250552
RRM2B	Inhibits	THBS1	19250552
RSK2	Activates	p53	15867353
S100A2	Inhibits	PTGS2	16908593
S100B	Inhibits	p53	15572370
SENP3	Activates	p53	doi.org/10.1016/j.bbrc.2011.02.034
SERPINB5	Inhibits	VEGFA	19374835
SERPINF1	Activates	p53	17651710
SERPINF1	Inhibits	VEGFA	16901919
SET	Inhibits	p53	3245910
SFN	Activates	MMP1	19533306
SFN	Activates	CDKN1B	20642839
SFN	Inhibits	CCNB1	17573669
SFN	Inhibits	CDK2	10767298
SGK	Inhibits	p53	19756449
SGK1	Inhibits	NOTCH1	21147854
SIAH1	Activates	HIF1A	15210114
SIRT1	Activates	WRN	PMC2859066
SIRT1	Inhibits	WRN	17996922
SIRT1	Inhibits	WRN	PMC2859066
SIRT1	Inhibits	WRN	15317818
SLC2A1	Activates	MMP2	12122099
SMYD2	Inhibits	p53	17108971
SOD1	Activates	p53	20097285
SOD2	Activates	MMP2	11929863
SOX4	Activates	p53	19234109
STAT3	Activates	CCND1	10458605
STAT3	Activates	FOS	12600988
STAT3	Activates	HIF1A	18644974
STAT3	Activates	HIF1A	15919761
STAT3	Activates	MUC1	11084045
STAT3	Activates	PTGS2	20145033
STAT3	Activates	JUN	17951530
STAT3	Activates	VEGFA	11960372

STAT3	Activates	MYC	DOI: http://dx.doi.org/10.1182/blood-2007-04-087734
STAT3	Activates	BCL6	23716595
STAT3	Activates	BCL3	23149915
STAT3	Inhibits	BAX	10374878
STAT3	Inhibits	p53	16107692
SUB1	Activates	p53	21586571
SUMO2	Activates	p53	21900752
SUMO2	Inhibits	p53	17012228
SUMO3	Activates	p53	17012228
TCF7L2	Activates	MYC	9727977
TFAP2A	Activates	ESR1	7846046
TFAP2A	Inhibits	CDKN1A	PMC4096794
TFAP2A	Inhibits	p53	16288208
TFDP1	Activates	EZH2	20565746
TGFA	Activates	CCND1	9407106
TGFA	Activates	FOS	8783257
TGFA	Activates	PTGS2	12930301
TGFA	Activates	MYC	10839631
TGFB1	Activates	p53	11741524
TGFB1	Activates	IL6	2265243
TGFB1	Activates	THBS1	11955611
TGFB1	Activates	PRKCA	14749204
TGFB1	Activates	CCNG1	9696022
TGFB1	Activates	PTGS2	10935498
TGFB1	Activates	VEGFA	12615726
TGFB1	Activates	CDKN1A	7696178
TGFB1	Activates	IGFBP7	18711401
TGFB1	Inhibits	IL6	2265243
TGFB1	Inhibits	ICAM1	14500551
TGFB1	Inhibits	MMP1	16911716
TGFB1	Inhibits	MMP13	9009143
TGFB1	Inhibits	KRT19	14732924
TGFB1	Inhibits	PTEN	19940030
TGFB1	Inhibits	MYC	12628347
THBS1	Activates	TGFB1	11021838
THBS1	Inhibits	FGF2	17996481
TIAF1	Activates	p53	14965474
TLR3	Activates	HIF1A	PMC2907580
TLR3	Inhibits	CXCR4	19652552
Tp53BP1	Activates	p53	9748285
Tp53RK	Activates	p53	16600182
UBE2A	Activates	p53	22083959
UBE2A	Inhibits	p53	22083959
UBE3A	Inhibits	p53	15567145

UCHL1	Activates	p53	20395212
UCHL1	Activates	p53	22279545
VDR	Activates	CYP24A1	15601867
VEGFA	Activates	SERPINF1	12670505
VEGFA	Activates	MMP2	16584583
VEGFA	Activates	CXCR4	19391039
VEGFA	Activates	CD44	9242547
VEGFA	Activates	FOS	14741347
VEGFA	Activates	BCL2	11895790
VEGFA	Activates	PTGS2	21273371
VEGFA	Activates	DUSP5	19741200
VEGFA	Activates	NOTCH1	12482957
VEGFA	Activates	ID3	15494533
VEGFA	Activates	MMP1	1447317
VEGFA	Inhibits	TGFB1	19180561
VEGFA	Inhibits	SERPINF1	16901919
VRK1	Activates	CCND1	18713830
VRK1	Activates	CCND1	18286197
VRK1	Activates	JUN	15378002
VRK1	Activates	CREB	doi: 10.1242/jcs.026757
VRK1	Activates	p53	15542844
WRN	Activates	ATM	18596239
WWOX	Activates	p53	16219768
XAF1	Inhibits	VEGFA	24980821
YBX1	Activates	CCND1	24774443
YBX1	Activates	CCND1	12695516
YBX1	Activates	p53	11175333
YBX1	Activates	MMP2	9278454
YBX1	Activates	ABCB1	17038319
YBX1	Activates	EGFR	1967130
YBX1	Inhibits	p53	12835324
YBX1	Inhibits	MMP13	17822788
YY1	Activates	ERBB2	18218085
YY1	Activates	PTGS2	17220375
YY1	Activates	p53	PMC231595
YY1	Inhibits	NOTCH1	12913000
YY1	Inhibits	CDKN1A	17556661
YY1	Inhibits	p53	15295102
ZMAT3	Activates	p53	12196512
ZMIZ2	Activates	p53	PMC1935018
ZNF148	Activates	p53	PMC87140
ZNF307	Inhibits	p53	17910948

Amongst the five outputs, a total of 52 nodes were linked to angiogenesis; 35 of these were pro-angiogenic, 17 were anti-angiogenic, (table 7.3.1). 131 nodes regulated apoptosis, 50 were anti-apoptotic, the remaining 81 pro-apoptotic, (table 7.3.1.1.). Of the total 37 nodes regulating DNA repair; 8 were considered as negative regulators and 29 as positive regulators of DNA repair, (table 7.3.1.2). A total of 66 nodes regulated cell cycle arrest, 31 of these were inhibitors, the remaining 35 positive regulators of cell cycle arrest, (table 7.3.1.3). 74 nodes regulated cellular senescence, 38 were negative regulators, 36 positive senescence regulators (table 7.3.1.4)

Amongst the inputs (hypoxia and DNA damage), a total of 62 nodes are influenced by DNA damage. Of these, the majority are activated (n = 57) the remaining 5 inhibited (table 7.3.1.5). The network was highly connected to the hypoxia input with a total of 90 nodes regulated by hypoxia. Of these, 72 were activated, 18 inhibited (table 7.3.1.6).

Table 7.3.1 Nodes that regulate angiogenesis in the PMH302 model.
A total of 52 angiogenic nodes are considered. Of these; 35 are pro angiogenic, 17 anti-angiogenic nodes. GO IDs and terms are described for each interaction. Other interactions were confirmed by literature search. Some PMID/PMCIDs were not available. For these DOI or links are provided.

Source	Interaction	Target	GO ID	GO TERM	PMID/PMC
BBC3	Activates	Angiogenesis			23122957
BCL2	Activates	Angiogenesis			18490895
BCL2	Activates	Angiogenesis			11280784
BDKRB1	Activates	Angiogenesis			11387266
CALD1	Activates	Angiogenesis	GO:0001525	Angiogenesis	18980955
CALD1	Activates	Angiogenesis	GO:0001570	Vasculogenesis	15161654
CCND1	Activates	Angiogenesis			PMC1986788
CD44	Activates	Angiogenesis			1698758
CDK2	Activates	Angiogenesis			23042366
CDK4	Activates	Angiogenesis			20603602
CDK5	Activates	Angiogenesis			20826806
JUN	Activates	Angiogenesis	GO:0001525	Angiogenesis	25083991
EGFR	Activates	Angiogenesis			23856030
ELAVL1	Activates	Angiogenesis			25422430
ELAVL1	Activates	Angiogenesis			23516604
ELAVL1	Activates	Angiogenesis			25422430
EPHB4	Activates	Angiogenesis	GO:0002042	Cell migration involved in	12734395

				sprouting angiogenesis	
EPHB4	Activates	Angiogenesis	GO:0001525	Angiogenesis	10518221
EPHB4	Activates	Angiogenesis	GO:0035475	Angioblast cell migration involved in selective angioblast sprouting	19815777
EPHB4	Activates	Angiogenesis			14702107
FGF2	Activates	Angiogenesis	GO:0045766	Positive regulation of angiogenesis	17187775
FGF2	Activates	Angiogenesis	GO:0002042	Cell migration involved in sprouting angiogenesis	23856030
FGF2	Activates	Angiogenesis	GO:0043536	Positive regulation of blood vessel endothelial cell migration	18658046
HIF1A	Activates	Angiogenesis	GO:0030949	Positive regulation of vascular endothelial growth factor receptor signaling pathway	8756616
HIF1A	Activates	Angiogenesis	GO:0045766	positive regulation of angiogenesis	12958148
HIF1A	Activates	Angiogenesis		positive regulation vascular endothelial growth factor production	18037992
HIF1A	Activates	Angiogenesis	GO:0001525	Angiogenesis	17636018
HIF1A	Activates	Angiogenesis	GO:2001214	Positive regulation of vasculogenesis	22098710
HSPA4	Activates	Angiogenesis	GO:0004576 6	Positive regulation of angiogenesis	15994930
HSPA4	Activates	Angiogenesis			15994930
HSPA4	Activates	Angiogenesis			PMC3980608
MMP1	Activates	Angiogenesis			7512058
MMP13	Activates	Angiogenesis			22992737

NTN1	Activates	Angiogenesis			23824572
NTN1	Activates	Angiogenesis			20080097
PDGFRB	Activates	Angiogenesis	GO:0008543	Fibroblast growth factor receptor signalling pathway	18827023
PDGFRB	Activates	Angiogenesis	GO:0038091	positive regulation of cell proliferation by VEGF-activated platelet derived growth factor receptor signalling pathway	17470632
PDGFRB	Activates	Angiogenesis	GO:0060981	Cell migration involved in coronary angiogenesis	18555217
PDGFRB	Activates	Angiogenesis	GO:0035441	Cell migration involved in vasculogenesis	14998491
PRKCA	Activates	Angiogenesis	GO:0045786	Positive regulation of angiogenesis	11909826
PRKCA	Activates	Angiogenesis	GO:0001525	Angiogenesis	11909826
PRKCA	Activates	Angiogenesis	GO:0001938	Positive regulation of endothelial cell proliferation	11909826
PTGS2	Activates	Angiogenesis	GO:0090050	Positive regulation of cell migration involved in sprouting angiogenesis	9630216
PTGS2	Activates	Angiogenesis	GO:0010575	Positive regulation vascular endothelial growth factor production	9630216
PTGS2	Activates	Angiogenesis	GO:0090271	Positive regulation of fibroblast growth factor production	9630216

S100B	Activates	Angiogenesis			23719262
SGK	Activates	Angiogenesis			24265802
SGK	Activates	Angiogenesis			20568246
STMN1	Activates	Angiogenesis			15031128
TGFA	Activates	Angiogenesis	GO:0001938	Angiogenesis	14998491
TGFA	Activates	Angiogenesis			19481589
VEGFA	Activates	Angiogenesis	GO:0001525	Angiogenesis	11427521
VEGFA	Activates	Angiogenesis	GO:0001938	Positive regulation of endothelial cell proliferation	2575835
VEGFA	Activates	Angiogenesis	GO:0035148	Tube formation	21245381
VEGFA	Activates	Angiogenesis	GO:0048010	vascular endothelial growth factor receptor signaling pathway	16109918
VEGFA	Activates	Angiogenesis	GO:0043117	Positive regulation of vascular permeability	20497126
VEGFA	Activates	Angiogenesis	G0:0038033	Positive regulation of endothelial cell chemotaxis by VEGF-activated vascular endothelial growth factor receptor signalling pathway	16489009
VEGFA	Activates	Angiogenesis	GO:0035924	Cellular response to vascular endothelial growth factor stimulus	12714610
VEGFA	Activates	Angiogenesis	GO:0008083	Growth factor activity	9202027
VEGFA	Activates	Angiogenesis	GO:0090050	Positive regulation of cell migration involved in sprouting angiogenesis	18577655

VEGFA	Activates	Angiogenesis	GO:0045766	Positive regulation of angiogenesis	18440775
VEGFA	Activates	Angiogenesis	GO:0002042	Cell migration involved in sprouting angiogenesis	20497126
VEGFA	Activates	Angiogenesis	GO:0001974	Blood vessel remodelling	20551324
VEGFA	Activates	Angiogenesis	GO:0001569	Patterning of blood vessels	7929439
VEGFA	Activates	Angiogenesis			17470632
VEGFA	Activates	Angiogenesis			18440775
VEGFA	Activates	Angiogenesis			20660291
VEGFA	Activates	Angiogenesis			19033661
CD82	Inhibits	Angiogenesis			25149363
CD82	Inhibits	Angiogenesis			PMC3313899
IFI16	Inhibits	Angiogenesis			21488755
IFI16	Inhibits	Angiogenesis			14729471
CD59	Inhibits	Angiogenesis	GO:0016525	Negative regulation of angiogenesis	17237428
COL18A1	Inhibits	Angiogenesis	GO:0001525	Angiogenesis	15857886
COL18A1	Inhibits	Angiogenesis			10942434
NOTCH1	Inhibits	Angiogenesis	GO:0060979	Vasculogenesis involved in coronary vascular morphogenesis	20616313
NOTCH1	Inhibits	Angiogenesis	GO:002040	Sprouting angiogenesis	20616313
NOTCH1	Inhibits	Angiogenesis	GO:008285	Negative regulation of cell proliferation	20616313
NOTCH1	Inhibits	Angiogenesis	GO:0090051	Negative regulation of cell migration involved in sprouting angiogenesis	20616313
NOTCH1	Inhibits	Angiogenesis	GO:0035924	Cellular response to vascular endothelial growth factor stimulus	20616313
DKK1	Inhibits	Angiogenesis			24091497

ING4	Inhibits	Angiogenesis			15029197
ING4	Inhibits	Angiogenesis			19409049
HOXA5	Inhibits	Angiogenesis	GO:0016525	Negative regulation of angiogenesis	17957028
PPARG	Inhibits	Angiogenesis			15041792
PPARG	Inhibits	Angiogenesis			16082179
NQO1	Inhibits	Angiogenesis			DOI: 10.1158/0008-5472
PML	Inhibits	Angiogenesis			22589541
PML			GO:0030308	Negative regulation of cell growth	PMC359216
SERPINF1	Inhibits	Angiogenesis	GO:0016525	Negative regulation of angiogenesis	11562499
SERPINF1	Inhibits	Angiogenesis			24318110
ELAVL1	Inhibits	Angiogenesis			20724828
TGFB1	Inhibits	Angiogenesis			16373850
BNIP3L	Inhibits	Angiogenesis			17717605
PTEN	Inhibits	Angiogenesis			19437103
NANOG	Activates	Angiogenesis			21119109
PHB	Activates	Angiogenesis			PMC2213620
SERPINE1	Activates	Angiogenesis			11454712
SENP3	Activates	Angiogenesis			19680224
JAG1	Activates	Angiogenesis			25767274
MTA1	Activates	Angiogenesis			16630134
RSK2	Activates	Angiogenesis			25014166
MIC1	Activates	Angiogenesis			22484283
ING1	Inhibits	Angiogenesis			20066899

Table 7.3.1.1 Nodes that regulate apoptosis in the PMH302 model.
A total of 131 apoptotic nodes are considered. Of these; 81 are pro- apoptotic, 50 anti-apoptotic. GO IDs and terms are described; other interactions were confirmed by literature search. All interactions are supplied with their PMID or PMC ID, some described by more than one literature source. Some PMID/PMCIDs were not available. For these DOI or links are supplied.

Source	Interaction	Target	GO ID	GO Term	PMID/PMC
APEX1	Inhibits	Apoptosis			15694346
NANOG	Inhibits	Apoptosis			21706347
NANOG	Inhibits	Apoptosis			19906868
MIC1	Activates	Apoptosis			25180886
MIC1	Activates	Apoptosis			19540205

TOP2A	Activates	Apoptosis	GO:0030263	Apoptotic chromosome condensation	doi:10.1038/cddis.2013.287
CASP2	Activates	Apoptosis	GO:0097194	Execution phase of apoptosis	11832478
MTA1	Inhibits	Apoptosis			25502548
FLI1	Inhibits	Apoptosis			9178886
ZNF148	Activates	Apoptosis			17019648
NFKB	Activates	Apoptosis			10849002
NFKB	Inhibits	Apoptosis			11160126
WWOX	Activates	Apoptosis			PMC3380332
SERPINE1	Activates	Apoptosis			18483310
CYP24A1	Activates	Apoptosis			PMC3485377
ESR1	Activates	Apoptosis	GO:0042981:	regulation of apoptotic process	17615152
ECT2	Activates	Apoptosis			12787561
MSH2	Activates	Apoptosis	GO:0043524:	negative regulation of neuron apoptosis	20124482
DUSP4	Activates	Apoptosis			20860659
CXCR4	Activates	Apoptosis	GO:0006915:	apoptotic process	15705741
XAF1	Activates	Apoptosis	GO:0006915:	apoptotic process	21788101
IL6	Activates	Apoptosis	GO:0043154:	negative regulation of cysteine-type endopeptidase activity involved in apoptotic process	11751424
IL7	Activates	Apoptosis	GO:0001781:	neutrophil apoptosis	12714376
IL6	Activates	Apoptosis	GO:0042981:	regulation of apoptotic process	21954875
FGF2	Activates	Apoptosis	GO:0006915:	apoptotic process	15856005
EGFR	Activates	Apoptosis			20081577
CD44	Activates	Apoptosis			16208414
PRKCA	Activates	Apoptosis	GO:0006915:	apoptotic process	10825394

PRKCA	Activates	Apoptosis			DOI:10.1007/978-1-59745-199-4_2
DUSP2	Activates	Apoptosis	GO:0042981:	regulation of apoptotic process	12673251
DUSP2	Activates	Apoptosis			9501207
FDXR	Activates	Apoptosis			12370809
BAX	Activates	Apoptosis	GO:0042981:	regulation of apoptotic process	19672311
IFI16	Activates	Apoptosis	GO:0042771:	DNA damage response, signal transduction by p53 class mediator resulting in induction of apoptosis	14990579
TLR3	Activates	Apoptosis	GO:0043065:	positive regulation of apoptotic process	16585585
CDC25A	Activates	Apoptosis			15822194 ;
CDC25A	Activates	Apoptosis			20368335
FOS	Activates	Apoptosis			8524298
DDIT4	Activates	Apoptosis	GO:0006915:	apoptotic process	18796435
MAP4K4	Activates	Apoptosis			15958553
SEMA3B	Activates	Apoptosis			15273288
PEG3	Activates	Apoptosis	GO:0006915:	apoptotic process	11050235
PEG3	Activates	Apoptosis			10681424
PRSS50	Activates	Apoptosis			21086474
IFITM2	Activates	Apoptosis			19544527
SIVA1	Activates	Apoptosis	GO:0006915:	apoptotic process	20727854
SIVA1	Activates	Apoptosis	GO:0006917:	induction of apoptosis	20817677
PCBP4	Activates	Apoptosis	GO:0008630:	DNA damage response, signal transduction resulting in induction of apoptosis	21522185
DFNA5	Activates	Apoptosis			19835622
HNF4A	Activates	Apoptosis			21219856

TP53INP1	Activates	Apoptosis	GO:0006917:	induction of apoptosis	24608790
CCNG1	Activates	Apoptosis			10467405
CASP8	Activates	Apoptosis	GO:0042981:	regulation of apoptotic process	15029256
CDKN1B	Activates	Apoptosis			10208428
COL18A1	Activates	Apoptosis			11158588
BBC3	Activates	Apoptosis	GO:0008633:	activation of pro-apoptotic gene products	11572983
BBC3	Activates	Apoptosis	GO:0006915:	apoptotic process	11572983
BBC3	Activates	Apoptosis	GO:0006917:	induction of apoptosis	11572983
APAF1	Activates	Apoptosis	GO:0006915:	apoptotic process	10791976
APAF1	Activates	Apoptosis	GO:0042981:	regulation of apoptotic process	10791976
BAK1	Activates	Apoptosis	GO:0042981:	regulation of apoptotic process	20460378
NLRC4	Activates	Apoptosis	GO:0043065:	positive regulation of apoptotic process	11374873
ATF3	Activates	Apoptosis			18755691
PTGS2	Activates	Apoptosis			16544098
GADD45A	Activates	Apoptosis	GO:0006915:	apoptotic process	17474084
NOTCH1	Activates	Apoptosis	GO:0043065:	positive regulation of apoptotic process	10227380
FAS	Activates	Apoptosis	GO:0006915:	apoptotic process	7536620
FAS	Activates	Apoptosis			
PTEN	Activates	Apoptosis	GO:0006917:	induction of apoptosis	11159942
AIFM2	Activates	Apoptosis	GO:0006917:	induction of apoptosis	21943319
DKK1	Activates	Apoptosis			17026960;
AR	Activates	Apoptosis			16479009
BNIP3L	Activates	Apoptosis	GO:0043065:	positive regulation of apoptotic process	10381623

TNFRSF10A	Activates	Apoptosis	GO:0006917:	induction of apoptosis	21785270
TNFRSF10A	Activates	Apoptosis	GO:0008625:	induction of apoptosis via death domain receptor	21785270
TNFRSF10B	Activates	Apoptosis	GO:0008633:	activation of pro-apoptotic gene products	22046379
IGFBP7	Activates	Apoptosis			18267069
LATS2	Activates	Apoptosis			15265683
SERPINB5	Activates	Apoptosis			15713631
PERP	Activates	Apoptosis	GO:0006915:	apoptotic process	10733530
SIAH1	Activates	Apoptosis	GO:0006915:	apoptotic process	9403064
SIAH1	Activates	Apoptosis	GO:0051402:	neuron apoptosis	9403064
SIAH1	Activates	Apoptosis	GO:00043065	: positive regulation of apoptotic process	9403064
LRDD	Activates	Apoptosis	GO:0043066:	negative regulation of apoptotic process	16183742
P53AIP1	Activates	Apoptosis	GO:0006915:	apoptotic process	16467208
CDKN2A	Activates	Apoptosis	GO:0006917:	induction of apoptosis	12660818
KAT2B	Activates	Apoptosis			PMC3847488
PITX1	Activates	Apoptosis			17762884
PITX1	Activates	Apoptosis			20563669
DAXX	Activates	Apoptosis	GO:0008625	Extrinsic apoptotic signalling pathway via death domain receptors	9215629
DAXX	Activates	Apoptosis	GO:2001235	Positive regulation of apoptotic signalling pathway	11193028

DAXX	Activates	Apoptosis	GO:0097190	Apoptotic signalling pathway	11003656
DAXX	Activates	Apoptosis			12407442
DAXX	Activates	Apoptosis			11773067
DAXX	Activates	Apoptosis			12407442
DDX20	Activates	Apoptosis	GO:0043065	Positive regulation of apoptotic process	16153597
JUN	Activates	Apoptosis			1169773
ING5	Activates	Apoptosis	GO:2001235	Positive regulation of apoptotic signalling pathway	12750254
DAP	Activates	Apoptosis	GO:0006915	Apoptotic process	7828849
DAP	Activates	Apoptosis	GO:0043605	Positive regulation of apoptotic process	9118961
DAP	Activates	Apoptosis	GO:0042981	Regulation of apoptotic process	11709549
HOXA10	Activates	Apoptosis			
UCHL1	Activates	Apoptosis			18949367
UCHL1	Activates	Apoptosis			18949367
UCHL1	Activates	Apoptosis			24155778
APP	Activates	Apoptosis	GO:0051402	Neuron apoptotic process	19225519
PML	Activates	Apoptosis			14663483
PML	Activates	Apoptosis	G0:0060058	Positive regulation of apoptotic process involved in mammary gland involution	11080164
TFAP2C	Activates	Apoptosis			14573793
TFAP2C	Activates	Apoptosis			21779369
TFAP2A	Activates	Apoptosis	GO:0008285	Negative regulation of cell proliferation	20607706
TFAP2A	Activates	Apoptosis			14551210
TFAP2A	Activates	Apoptosis			12654297

ASPP1	Activates	Apoptosis	GO:0045786	Negative regulation of cell cycle	11684014
ASPP1	Activates	Apoptosis			14729977
ASPP1	Activates	Apoptosis			14729977
ASPP1	Activates	Apoptosis	GO:0072332	Intrinsic apoptotic signalling pathway by p53 class mediator	11684014
ASSP2	Activates	Apoptosis			14729977
ASSP2	Activates	Apoptosis			11684014
ASPP2	Activates	Apoptosis			14729977
ING4	Activates	Apoptosis	GO:0045926	Negative regulation of growth	16387653
BCL3	Inhibits	Apoptosis	GO:0043066		20800578
GSTP1	Inhibits	Apoptosis			21637416
ESR1	Inhibits	Apoptosis	GO:0042981		9118519
DUSP4	Inhibits	Apoptosis			20860659
IL6	Inhibits	Apoptosis	GO:0043154		11751424
IL6	Inhibits	Apoptosis	GO:0001781		11751424
IL6	Inhibits	Apoptosis	GO:0042981		11751424
PDGFRB	Inhibits	Apoptosis			21954875
FGF2	Inhibits	Apoptosis	GO:0006915		15856005
WWP1	Inhibits	Apoptosis			18806757
IGF1R	Inhibits	Apoptosis	GO:0006916		14726697
IGF1R	Inhibits	Apoptosis	GO:0043066		14726697
IGF1R	Inhibits	Apoptosis	GO:0045768		14726697
EGFR	Inhibits	Apoptosis	GO:0043066		15277479
CD44	Inhibits	Apoptosis			17045821
PRKCA	Inhibits	Apoptosis	GO:0006915:		DOI:10.1007/978-1-59745-199-4_2
DUSP2	Inhibits	Apoptosis	GO:0042981:		12673251
DUSP2	Inhibits	Apoptosis			9501207
TGFA	Inhibits	Apoptosis	GO:0006916:		16079309

CDC25A	Inhibits	Apoptosis			11416155
FOS	Inhibits	Apoptosis			19255142
DDIT4	Inhibits	Apoptosis	GO:0006915:		19221489
MAP4K4	Inhibits	Apoptosis			21196414
EZH2	Inhibits	Apoptosis			19893569;
EZH2	Inhibits	Apoptosis			19079346
PSEN1	Inhibits	Apoptosis	GO:0006916:		10805794
BCL2	Inhibits	Apoptosis	GO:0006916:		8617294
FHL2	Inhibits	Apoptosis			21377781
CCNG1	Inhibits	Apoptosis	GO:0043066:		18497347
TCF7L2	Inhibits	Apoptosis			21965303
EPHB4	Inhibits	Apoptosis			20133814
CDKN1B	Inhibits	Apoptosis			10050878
ATF3	Inhibits	Apoptosis			doi:10.1006/jmcc.2002.2091
PTGS2	Inhibits	Apoptosis			20027603
SGK	Inhibits	Apoptosis			12488318
MCL1	Inhibits	Apoptosis	GO:0042981:		18550749
IER3	Inhibits	Apoptosis	GO:0006916:		14688131
NOTCH1	Inhibits	Apoptosis	GO:0060548:		10227380
VEGFA	Inhibits	Apoptosis	GO:0006916:		11891765
CDKN1A	Inhibits	Apoptosis	GO:0008629:		21815189
AR	Inhibits	Apoptosis	GO:0043066:		16479009
CKS2	Inhibits	Apoptosis			18498131
C12orf5	Inhibits	Apoptosis			16839880
SFN	Inhibits	Apoptosis	GO:0006915:		15857577
SFN	Inhibits	Apoptosis	GO:0008630:		10654934
RB1CC1	Inhibits	Apoptosis	GO:0006916		2064504
RB1CC1	Inhibits	Apoptosis	GO:2001237		PMC2064504
STAT3	Inhibits	Apoptosis	GO:0060548		20562100
STAT3	Inhibits	Apoptosis	GO:0060548		16540667
STAT3	Inhibits	Apoptosis	GO:0008283		11171987

DAXX	Inhibits	Apoptosis			19017466
DAXX	Inhibits	Apoptosis			16088932
TP53RK	Inhibits	Apoptosis			20647325
TPT1	Inhibits	Apoptosis	GO:1902230		11598139
TPT1	Inhibits	Apoptosis	GO:0043066		16130169
TPT1	Inhibits	Apoptosis	G0:0049281		15162379
TPT1	Inhibits	Apoptosis			12149273
TPT1	Inhibits	Apoptosis			15262975
PREP1	Inhibits	Apoptosis			PMC2643814
CUL7	Inhibits	Apoptosis			17229476

Table 7.3.1.2 Nodes that regulate DNA repair in the PMH302 model.
A total of 37 nodes that regulate DNA repair are considered. Of these; 29 are positive regulators, 8 negative regulators of DNA repair. GO IDs and terms are described; other interactions were confirmed by literature search. All interactions are supplied with their PMID or PMCID. Some interactions are described by more than one literature source.

Source	Interaction	Target	GO ID	GO Term	PMID/PMC
ATM	Activates	DNA repair	GO:0006281	DNA repair	18066086
CD44	Activates	DNA repair			16263582
CDKN1A	Activates	DNA repair			22735704
DDB2	Activates	DNA repair	GO:0070914	UV-damage excision repair	22334663
FEN1	Activates	DNA repair	GO:0006302	Double-strand break repair	8131753
FGF2	Activates	DNA repair			20681019
HSPA4	Activates	DNA repair			PMC4041939
IFI16	Activates	DNA repair			18472023
MCL1	Activates	DNA repair			20647761
MGMT	Activates	DNA repair	GO:0006307	DNA dealkylation involved in DNA repair	1554415
MSH2	Activates	DNA repair	GO:0006281	DNA repair	8942985
MSH2	Activates	DNA repair	GO:0006298	Mismatch repair	1334021

MSH2	Activates	DNA repair	GO:0006298	Mismatch repair	11555625
MSH2	Activates	DNA repair	GO:0006301	Post replication repair	17715146
NME1	Activates	DNA repair			25017017
PCNA	Activates	DNA repair	GO:0006281	Positive regulation of DNA repair	16227586
PRKDC	Activates	DNA repair	GO:0000724	Double-strand break repair via homologous recombination	11418067
RAD51	Activates	DNA repair	GO:0000150		PMC2430071
ATM	Activates	DNA repair			doi:10.1038/ncomms4347
ATR	Activates	DNA repair			PMC4176976
BCCIP	Activates	DNA repair	GO:0006281	DNA repair	17947333
BRCA1	Activates	DNA repair			14636569
GADD45A	Activates	DNA repair	GO:0006281	DNA repair	7973727
YY1	Activates	DNA repair	GO:0000724	Double strand break repair via homologous recombination	18026119
KLF4	Inhibits	DNA repair			PMC3750599
MDM4	Inhibits	DNA repair			24608433
MYC	Inhibits	DNA repair			23308051
PTTG1	Inhibits	DNA repair	GO:0006281	DNA repair	18663361
SIAH1	Inhibits	DNA repair			20682032
PPMID	Inhibits	DNA repair			15327777
MDM2	Inhibits	DNA repair			18541670
APEX1	Activates	DNA Repair	GO:0006284	Base Excision Repair	25108836
APEX1	Activates	DNA Repair	GO:0000724	Double-strand break repair via	19052983

				homologous recombination	
APEX1	Activates	DNA Repair	GO:0006281	DNA Repair	9560228
APEX1	Activates	DNA Repair	GO:0045739	Positive regulation of DNA repair	9207062
PIN1	Activates	DNA Repair			23623683
PIAS1	Activates	DNA Repair			20016603
RPA1	Activates	DNA Repair	GO:0006281	DNA Repair	18469000
			GO:0000724	Double-strand break repair via homologous recombination	17765923
			GO:0006284	Base excision repair	9765279
			GO:0006298	Mismatch repair	9430682
ING1	Activates	DNA repair			23459830
SUMO3	Activates	DNA repair			20016603
RPS27L	Activates	DNA repair	GO:0006281	DNA repair	18056458
MTA1	Activates	DNA repair	GO:0006302	Double strand break repair	19805145
RFWD3	Activates	DNA repair	GO:0006281	DNA repair	21558276
SERPINE1	Inhibits	DNA repair			23111469

Table 7.3.1.3 Nodes that regulate cell cycle arrest in the PMH302 model.
A total of 58 nodes that regulate the cell cycle are considered. Of these; 28 are positive regulators, 30 are negative regulators of cell cycle arrest. GO IDs and terms are described; other interactions were confirmed by literature search. All interactions are supplied with their PMID or PMCID. Some interactions are described by more than one literature source.

Source	Interaction	Target	GO ID	GO Term	PMID/PMC
BRCA1	Activates	Cell cycle arrest	GO:0071158	Positive regulation of cell cycle arrest	21102443
BRCA1	Activates	Cell cycle arrest			10644742

BRCA1	Activates	Cell cycle arrest			10644742
BRCA1	Activates	Cell cycle arrest			7954448
CDKN1B	Activates	Cell cycle arrest	GO:0007050	Cell cycle arrest	12093740
CDKN1B	Activates	Cell cycle arrest	GO:0000082	G1/S transition of mitotic cell cycle	10208428
CDKN1B	Activates	Cell cycle arrest	GO:0000278	Mitotic cell cycle	19266349
CDKN1B	Activates	Cell cycle arrest	GO:0045736	Negative regulation of cyclin-dependent protein serine/threonine kinase activity	15374880
CDKN1B	Activates	Cell cycle arrest	GO:006977	DNA damage response, signal transduction by p53 class mediator resulting in cell cycle arrest	8033213
ATF3	Activates	Cell cycle arrest			12386811
PTGS2	Activates	Cell cycle arrest	GO:0045786	Negative regulation of cell cycle	10567385
PTGS2	Activates	Cell cycle arrest			11606477
GADD45A	Activates	Cell cycle arrest	GO:0051726	Regulation of cell cycle	12124778
GADD45A	Activates	Cell cycle arrest	GO:0007050	Cell cycle arrest	10747892
GADD45A	Activates	Cell cycle arrest	GO:0000086	G2/M transition of mitotic cell cycle	11964479
DKK1	Activates	Cell cycle arrest			20549706

DKK1	Activates	Cell cycle arrest			12740383
IGFBP7	Activates	Cell cycle arrest			23388612
RAS	Activates	Cell cycle arrest			3510745
RAS	Activates	Cell cycle arrest			3049071
KLF4	Activates	Cell cycle arrest			PMC3750599
E2F1	Activates	Cell cycle arrest			9766435
PAD4	Activates	Cell cycle arrest			16502257
CDK5	Activates	Cell cycle arrest	GO:0071156	Regulation of cell cycle arrest	21473899
CDKN2A	Activates	Cell cycle arrest	GO:0007050	Cell cycle arrest	23238983
CDKN2A	Activates	Cell cycle arrest	GO:0071158	positive regulation of cell cycle arrest	9529249
MAPK1	Activates	Cell cycle arrest			11821415
RAF1	Activates	Cell cycle arrest			10022606
RBC1CC1	Activates	Cell cycle arrest	GO:0007049	Cell cycle	16061648
KAT2B	Activates	Cell cycle arrest	GO:000825	Negative regulation of cell proliferation	8684459
KAT2B	Activates	Cell cycle arrest	G0:0006915		20809119
ING4	Activates	Cell cycle arrest		Cell cycle	15251430
STMN1	Activates	Cell cycle arrest			15368352

STMN1	Activates	Cell cycle arrest			15031128
HOXA10	Activates	Cell cycle arrest			2731304
HOXA5	Activates	Cell cycle arrest			25590986
MYST4	Activates	Cell cycle arrest			19001415
PPARG	Activates	Cell cycle arrest			15916743
EXPORTIN1	Activates	Cell cycle arrest			23615632
EXPORTIN1	Activates	Cell cycle arrest			22832492
TFAP2C	Activates	Cell cycle arrest			16867219
ID3	Activates	Cell cycle arrest			21498546
CHEK2	Activates	Cell cycle arrest			PMC316357
BTG2	Activates	Cell cycle arrest	GO:0006281	DNA repair	10669755
POU4F1	Activates	Cell cycle arrest			18421303
CHEK1	Activates	Cell cycle arrest			21034966
ATM	Activates	Cell cycle arrest	GO:0007050	cell cycle arrest	11721054
ATR	Activates	Cell cycle arrest			11721054
DUSP5	Activates	Cell cycle arrest			12944906
PARK2	Activates	Cell cycle arrest			24793136

EPHB4	Inhibits	Cell cycle arrest			15930280
APAF1	Inhibits	Cell cycle arrest			18309324
APAF1	Inhibits	Cell cycle arrest			18042457
ATF3	Inhibits	Cell cycle arrest	GO:0008284	Positive regulation of cell proliferation	15990869
RGS16	Inhibits	Cell cycle arrest			16405749
S100A6	Inhibits	Cell cycle arrest	GO:0048146	Positive regulation of fibroblast proliferation	12577318
S100A6	Inhibits	Cell cycle arrest			20013795
S100A6	Inhibits	Cell cycle arrest			23095053
IER3	Inhibits	Cell cycle arrest			11311240
SLC2A1	Inhibits	Cell cycle arrest			22689530
AR	Inhibits	Cell cycle arrest			16877366
AR	Inhibits	Cell cycle arrest			6483690
AR	Inhibits	Cell cycle arrest			9685369
MYCN	Inhibits	Cell cycle arrest			17495526
CCNB1	Inhibits	Cell cycle arrest			2570636
CCNB1	Inhibits	Cell cycle arrest			1717476

CCNB1	Inhibits	Cell cycle arrest			8797586
MYC	Inhibits	Cell cycle arrest	GO:0007050	Cell cycle arrest	10962037
MUC1	Inhibits	Cell cycle arrest	GO:0006977	DNA damage response, signal transduction by p53 class mediator resulting in cell cycle arrest	15710329
YBX1	Inhibits	Cell cycle arrest			20398058
HDAC1	Inhibits	Cell cycle arrest			20194438
CDK2	Inhibits	Cell cycle arrest			19445729
VRK1	Inhibits	Cell cycle arrest			18286197
AURKA	Inhibits	Cell cycle arrest			24841948
JUN	Inhibits	Cell cycle arrest	GO:0048146	Positive regulation of fibroblast proliferation	1171114
UBE2A	Inhibits	Cell cycle arrest	GO:0008284	Positive regulation of cell proliferation	1748683
ING5	Inhibits	Cell cycle arrest	GO:0008285	Negative regulation of cell proliferation	12750254
CUL7	Inhibits	Cell cycle arrest			18498745
PRAK	Inhibits	Cell cycle arrest			DOI: 10.1007/s11684-009-0073-y
SIVA1	Inhibits	Cell cycle arrest			23462994
MCL1	Inhibits	Cell cycle arrest			22378300

CKS2	Inhibits	Cell cycle arrest			1862572
ISG15	Inhibits	Cell cycle arrest			PMC4226694
RAD51	Inhibits	Cell cycle arrest			19140342
CCNA	Inhibits	Cell cycle arrest			25615569
PRKAB1	Activates	Cell cycle arrest	GO:0007050	Cell cycle arrest	11554766
PRKAB1	Activates	Cell cycle arrest			15866171
CASP2	Activates	Cell cycle arrest	GO:0006977	DNA damage response, signal transduction by p53 class mediator resulting in cell cycle arrest	21726810
CASP2	Activates	Cell cycle arrest			19528949
MTA1	Inhibits	Cell cycle arrest			PMC3751420
JAG1	Inhibits	Cell cycle arrest			doi:10.1038/cddis.2014.137
E2F1	Inhibits	Cell cycle arrest			11459832

Table 7.3.1.4 Nodes that regulate cellular senescence in the PMH302 model.
A total of 73 nodes that regulate cellular senescence are considered. Of these; 36 are positive regulators, 37 are negative regulators of senescence. GO IDs and terms are described; other interactions were confirmed by literature search. All interactions are supplied with their PMID or PMC ID. Some interactions are described by more than one literature source.

Source	Interaction	Target	GO ID	GO TERM	PMID/PMC
GAPDH	Activates	Cellular senescence			22847419
MSH2	Activates	Cellular senescence			18986375
DDB2	Activates	Cellular senescence			23109835
IL6	Activates	Cellular senescence			22374671
IGF1R	Activates	Cellular senescence			18216278
CDKN1A	Activates	Cellular senescence	GO:0090398	Cellular senescence	15149599
PRKCA	Activates	Cellular senescence			18162471
TGFA	Activates	Cellular senescence			12593448
IFI16	Activates	Cellular senescence			15208661
PSEN1	Activates	Cellular senescence			19181896
IFITM2	Activates	Cellular senescence			19071156
BCL2	Activates	Cellular senescence			12670482
CD59	Activates	Cellular senescence			22918646
CDKN1B	Activates	Cellular senescence			21795702
BAK1	Activates	Cellular senescence			19747230
PTGS2	Activates	Cellular senescence			23328527
GADD45A	Activates	Cellular senescence			16951155
NOTCH1	Activates	Cellular senescence			23078884
PTEN	Activates	Cellular senescence			23314408
DKK1	Activates	Cellular senescence			22927647
AR	Activates	Cellular senescence			22403609

MYC	Activates	Cellular senescence			20027199
IGFBP7	Activates	Cellular senescence			21997538
LATS2	Activates	Cellular senescence			21498571
RAS	Activates	Cellular senescence	GO:0090398	Cellular senescence	15489886
C12orf5	Activates	Cellular senescence			19710698
SFN	Activates	Cellular senescence			19642975
CDKN2A	Activates	Cellular senescence	GO:0090398	Cellular senescence	14966292
CDKN2A	Activates	Cellular senescence	GO:2000774	Positive regulation of cellular senescence	14966292
APP	Activates	Cellular senescence			24232259
PML	Activates	Cellular senescence	GO:0032211	Negative regulation of telomere maintenance via telomerase	10950866
PML	Activates	Cellular senescence	GO:0032211	Negative regulation of telomere maintenance via telomerase	10910364
PML	Activates	Cellular senescence			12093737
PRAK	Activates	Cellular senescence			17254968
GAPDH	Inhibits	Cellular senescence			21749859
MSH2	Inhibits	Cellular senescence			23213348
RRM2B	Inhibits	Cellular senescence			23139867

CDK4	Inhibits	Cellular senescence			12435633
ARID3A	Inhibits	Cellular senescence			22010578
FGF2	Inhibits	Cellular senescence			17532297
FGF2	Inhibits	Cellular senescence			21990129
WWP1	Inhibits	Cellular senescence			22051607
WWP1	Inhibits	Cellular senescence			21795702
EGFR	Inhibits	Cellular senescence			21852385
CKB	Inhibits	Cellular senescence			21980054
DDIT4	Inhibits	Cellular senescence			22629318
EZH2	Inhibits	Cellular senescence			15208672
EZH2	Inhibits	Cellular senescence			21383005
BCL2	Inhibits	Cellular senescence			19855432
PCBP4	Inhibits	Cellular senescence			20817677
HIF1A	Inhibits	Cellular senescence			18645006
CD59	Inhibits	Cellular senescence			17188915
FOXM1	Inhibits	Cellular senescence			23262037
HNF4A	Inhibits	Cellular senescence			21385945
FHL2	Inhibits	Cellular senescence			19018287
BRCA1	Inhibits	Cellular senescence			12533509
APAF1	Inhibits	Cellular senescence			17652622
BAK1	Inhibits	Cellular senescence			11557285
SGK	Inhibits	Cellular senescence			15068796
S100A6	Inhibits	Cellular senescence			23095053
MCL1	Inhibits	Cellular senescence			22451485
GADD45A	Inhibits	Cellular senescence			21986581

PTEN	Inhibits	Cellular senescence			21072054
VEGFA	Inhibits	Cellular senescence			21618508
DKK1	Inhibits	Cellular senescence			21712954
TFDP1	Inhibits	Cellular senescence			15716376
NME1	Inhibits	Cellular senescence			20713695
MYC	Inhibits	Cellular senescence			17664422
SESN2	Inhibits	Cellular senescence			20606249
PPM1D	Inhibits	Cellular senescence			22201816
DAXX	Inhibits	Cellular Senescence			23542781
CUL7	Inhibits	Cellular senescence			18498745
ELAVL1	Inhibits	Cellular senescence			23028944
PIN1	Activates	Cellular senescence			24375406
MIC1	Activates	Cellular senescence			PMC117570
BHLHE40	Activates	Cellular senescence			18025081
ING1	Activates	Cellular senescence			19121449
ING1	Activates	Cellular senescence			19442113
SOD2	Inhibits	Cellular senescence			22278880
PAI1	Activates	Cellular senescence			16862142
JAG1	Inhibits	Cellular senescence			doi.org/10.1371/journal.pone.0100359

Table 7.3.1.5 Nodes that are regulated by DNA damage in the PMH302 model.
A total of 57 nodes are regulated by the DNA damage input in the 302 model. Of these; 52 are activated, 5 are inhibited by DNA damage. GO IDs and terms are described; other interactions were confirmed by literature search. All interactions are supplied with their PMID or PMC ID. Some interactions are described by more than one literature source**.** For some interactions PMID/PMC ID was not available, thus links are provided.

Source	Interaction	Target	GO ID	GO Term	PMID/PMC
DNA damage	Inhibits	STMN1			16909102
DNA damage	Inhibits	MDM2	GO:0006977:	Positive regulation of cell cycle arrest by p53-mediated DNA damage response.	11960904
DNA damage	Inhibits	MDM2			16227609
DNA damage	Inhibits	PTTG1			18047793
DNA damage	Inhibits	MYC	GO:0034644:	cellular response to UV	12761495
DNA damage	Inhibits	AURKA			21099343
DNA damage	Activates	YY1	GO:0034644	Cellular response to UV	18026119
DNA damage	Activates	YY1	GO:0006974	Cellular response to DNA damage stimulus	18026119
DNA damage	Activates	STAT3			20456494
DNA damage	Activates	ICAM1	G0:0010212	Response to ionizing radiation	7963663
DNA damage	Activates	SUB1			19047459
DNA damage	Activates	PITX1			20563669
DNA damage	Activates	CCAR1			12816952
DNA damage	Activates	DAXX			23539629
DNA damage	Activates	JUN			16733206
DNA damage	Activates	UBE2A	GO:0009411	Response to UV	1717990
DNA damage	Activates	UBE2A			23525009
DNA damage	Activates	TP53RK			20647325
DNA damage	Activates	RFC			11336696
DNA damage	Activates	RFC			18245774

DNA damage	Activates	RFC			PMC87010
DNA damage	Activates	PHF20			PMC3454513
DNA damage	Activates	ING5			23576563
DNA damage	Activates	DAP			15608685
DNA damage	Activates	MYST4			19001415
DNA damage	Activates	PML			PMC156140
DNA damage	Activates	TFAP2A			8962096
DNA damage	Activates	TGFB1		GO:0001666: response to hypoxia	15652459
DNA damage	Activates	SOX4		GO:0042769: DNA damage response, detection of DNA damage	19234109
DNA damage	Activates	ERBB2			19406993
DNA damage	Activates	NCL			12000845
DNA damage	Activates	HTATIP2			21376742
DNA damage	Activates	BTG2	GO:0006974	response to DNA damage stimulus	8944033
DNA damage	Activates	MCTS1	GO:0006974	response to DNA damage stimulus	17016429
DNA damage	Activates	FAS			9660938
DNA damage	Activates	YBX1	GO:0006355	regulation of transcription, DNA-dependent	12080043
DNA damage	Activates	MYC	GO:0034644	cellular response to UV	2687769
DNA damage	Activates	CDK5			19151707
DNA damage	Activates	PRKD1			16911582
DNA damage	Activates	MAPK9			17306896
DNA damage	Activates	MAPK8	GO:0008624	induction of apoptosis by extracellular signals	15696159
DNA damage	Activates	MAPK8	GO:0008624	induction of apoptosis by intracellular signals	15696159
DNA damage	Activates	MAPK8	GO:0009411	response to UV	15696159

DNA damage	Activates	ATM	GO:0008630	DNA damage response, signal transduction resulting in induction of apoptosis	15279774
DNA damage	Activates	ATM	GO: 0010212	response to ionizing radiation	15322239
DNA damage	Activates	ATR	GO:0034644	cellular response to UV	15322239
DNA damage	Activates	PRKDC			16908529
DNA damage	Activates	TP53BP1			14695167
DNA damage	Activates	TP53BP1			PMC150747
DNA damage	Activates	CUL7			17586686
DNA damage	Activates	APP			18421302
DNA damage	Activates	PIAS1			22976298
DNA damage	Activates	RPA1	GO:0042769	DNA damage response, detection of DNA damage	7876222
DNA damage	Activates	RPA2			10653628
DNA damage	Activates	WRN	GO:0006974	Cellular response to DNA damage stimulus	18203716
DNA damage	Activates	ING2	GO:2001020	Regulation of response to DNA damage stimulus	23823870
DNA damage	Activates	ING4			PMC3705588
DNA damage	Activates	TOP2A	GO:0006974	Cellular response to DNA damage stimulus	16611985
DNA damage	Activates	PIRH2			12654245
DNA damage	Activates	PIRH3	GO:0006974	Cellular response to DNA damage stimulus	18056458

Table 7.3.1.6 Nodes that are regulated by hypoxia in the PMH302 model.
A total of 90 nodes are regulated by the hypoxia input in the 302 model. Of these; 72 are activated and 18 are inhibited by hypoxia. GO IDs and terms are described; other interactions were confirmed by literature search. All interactions are supplied with their PMID or PMC ID. Some interactions are described by more than one literature source. For some interactions PMID/PMC ID was not available, thus links are provided.

Source	Interaction	Target	GO ID	GO Term	PMID/PMC
Hypoxia	Activates	APP			21640074
Hypoxia	Activates	AR			16707435
Hypoxia	Activates	ICAM1	GO:0071456	Cellular response to hypoxia	20631551
Hypoxia	Activates	ICAM1			24626595
Hypoxia	Activates	ABCB1			22946104
Hypoxia	Inhibits	AIMP2			24626595
Hypoxia	Activates	AIMP2	GO:0001666	Response to hypoxia	12507893
Hypoxia	Activates	APAF1	GO:0001666	Response to hypoxia	PMC3973202
Hypoxia	Inhibits	APEX1			doi: 10.1161/hh1201.093162
Hypoxia	Activates	ATF3			18377912
Hypoxia	Activates	ATF4			doi:10.1038/sj.onc.1209781
Hypoxia	Activates	ATM			PMC2612523
Hypoxia	Activates	ATR			PMC2612523
Hypoxia	Inhibits	BAK1			18366759
Hypoxia	Activates	BCL2	GO:0071456	Cellular response to hypoxia	20307495
Hypoxia	Activates	BCL3			12173346
Hypoxia	Activates	BCL6		`	PMC3834117
Hypoxia	Activates	BHLHE40			25963661
Hypoxia	Activates	BHLHE40			15221940
Hypoxia	Activates	BTG2			doi:10.1152/ajpcell.00180.2011
Hypoxia	Activates	CA9	GO:0061418	Regulation of transcription from RNA polymerase II promoter in response to hypoxia	19564335
Hypoxia	Activates	CASP8			12396104
Hypoxia	Inhibits	CCNB1			22264882
Hypoxia	Activates	CCNG1			11112789

Hypoxia	Activates	CD59			PMC1779384
Hypoxia	Inhibits	CDC25A			19738433
Hypoxia	Inhibits	CDC25A			17671423
Hypoxia	Activates	CDK5			20977891
Hypoxia	Inhibits	CDKN2A			doi: 10.1158/1538-7445.AM2012-178
Hypoxia	Activates	CHEK1			DOI: 10.4161/cc.9.13.12059
Hypoxia	Inhibits	CUL7			22524683
Hypoxia	Activates	CXCR4	GO:0001666	Response to hypoxia	15174142
Hypoxia	Activates	DDIT4	GO:0001666	Response to hypoxia	20166753
Hypoxia	Inhibits	DDX5			24517586
Hypoxia	Activates	DKK1			24770633
Hypoxia	Activates	DUSP1			24267255
Hypoxia	Activates	EGFR			17670948
Hypoxia	Activates	EGFR			23185433
Hypoxia	Activates	EPHB4			16081502
Hypoxia	Inhibits	ERBB2			22792252
Hypoxia	Inhibits	ESR1			21458421
Hypoxia	Activates	EZH2			25189741
Hypoxia	Activates	UNC5A			PMC3793633
Hypoxia	Activates	FGF2			12088755
hypoxia	Activates	FOS	GO:0034614	Cellular response to reactive oxygen species	19241444
Hypoxia	Activates	GAPDH			doi:10.1006/bbrc.1999.1798
hypoxia	Activates	GLUT1			10572068
Hypoxia	Activates	GLUT4	GO:0034614	Cellular response to hypoxia	20868366
Hypoxia	Activates	GLUT4			15631691
Hypoxia	Activates	GLUT4		Response to Hypoxia	12482987
Hypoxia	Activates	GLUT4		Cellular response to hypoxia	16081502
Hypoxia	Inhibits	HNF4A			11553861
Hypoxia	Activates	HSPA4			24660549
Hypoxia	Inhibits	ID3			doi:10.1136/heartjnl-2012-302920y.9
Hypoxia	Activates	IER3			24758227
Hypoxia	Activates	IGFBP1			23748030
Hypoxia	Activates	IGFBP1			15644436

Hypoxia	Activates	JUN	GO:0001666	Response to hypoxia	11909946
Hypoxia	Activates	JUL	GO:0034614	Cellular response to hypoxia	
Hypoxia	Activates	JUN			19241444
Hypoxia	Activates	MAP4			PMC4540186
Hypoxia	Activates	MAPK1			24555431
Hypoxia	Activates	MAPK8			11062137
Hypoxia	Activates	MAPK9			10428063
Hypoxia	Activates	MCTS1			19876643
Hypoxia	Activates	MDM2	GO:0034614	Cellular response to hypoxia	15205329
Hypoxia	Activates	MDM2			20810912
Hypoxia	Activates	MDM4	GO:0034614	Cellular response to hypoxia	22556425
Hypoxia	Activates	MDM4			20810912
Hypoxia	Activates	MMP1			26343184
Hypoxia	Inhibits	MMP1			12817301
Hypoxia	Activates	MMP13	GO:0001666	Response to hypoxia	19241444
Hypoxia	Activates	MMP13			16965566
Hypoxia	Activates	MMP2			16210427
Hypoxia	Activates	MMP2			16980344
Hypoxia	Inhibits	MSH2			17275176
Hypoxia	Activates	MUC1	GO:0001666	Response to hypoxia	23108411
Hypoxia	Inhibits	MYC	GO:0034614	Cellular response to hypoxia	PMC3753854
Hypoxia	Activates	NFKB			20696840
Hypoxia	Activates	NME1			21912348
Hypoxia	Activates	NOTCH1	GO:0061419	Positive regulation of transcription from RNA polymerase II promoter in response to hypoxia	DOI: 10.1186/1756-8722-6-3
Hypoxia	Activates	NTN1			PMC3793633
Hypoxia	Activates	PLAUR	GO:0001666	Response to hypoxia	25509186
Hypoxia	Activates	PRKDC			15272235

Hypoxia	Activates	PTGS2	GO:0034614	Cellular response to hypoxia	16818642
Hypoxia	Inhibits	RAD51			15367671
Hypoxia	Activates	RAF1			8603510
Hypoxia	Activates	SERPINE1	GO:0034614	Cellular response to hypoxia	247582271
Hypoxia	Activates	SERPINE1			10590062
Hypoxia	Activates	SGK			19910698
Hypoxia	Inhibits	SLC6A6			23381576
Hypoxia	Activates	SOX4	GO:0001666	Response to hypoxia	doi.org/10.1155/2012/416927
Hypoxia	Activates	SP7			23805815
Hypoxia	Activates	STAT3			24525913
Hypoxia	Activates	TCF7L2			19644051
Hypoxia	Activates	TGFA			22863020
Hypoxia	Activates	TGFB	GO:0001666	Response to hypoxia	24626595
Hypoxia	Activates	TGFB			17213961
Hypoxia	Activates	THBS1	GO:0001666	Response to hypoxia	24195060
Hypoxia	Activates	THBS1			9304800
Hypoxia	Activates	TPT1			12817301
Hypoxia	Activates	VEGFA	GO:0061418	Regulation of transcription from RNA polymerase II promoter in response to hypoxia	7641334
Hypoxia	Activates	VEGFA	GO:0061419	Positive regulation of transcription from RNA polymerase II promoter in response to hypoxia	16081502
Hypoxia	Activates	VRK1			PMC3493170
Hypoxia	Activates	XAF1			18485100
Hypoxia	Activates	YY1			23580145
Hypoxia	Activates	CCND1			16155412
Hypoxia	Activates	ID3			20881097
Hypoxia	Activates	RAS			20532039

Hypoxia	Inhibits	WWP1			22227207

7.3.2 Analysis and validation of the PMH302 model

The PMH260 model was expanded to provide a greater overview of p53 – cancer dynamics, generating the model designated as PMH302. For a more accurate representation of tumour characteristics, an additional input of hypoxia was also integrated, and its effect on the network explored. This established a network of 1389 interactions between 295 internal nodes (excluding 2 inputs and 5 outputs). To investigate network perturbations of the p53-PMH302 interactome in response to *in silico* manipulation of different node states and inputs (hypoxia and DNA damage) two methods were undertaken; Logical Steady State Analysis (LSSA) and *in silico* knockout analysis using dependency matrix calculations. Both applications are provided in CellNetAnalyzer (v.2015.1) (CNA). *In silico* methods and analyses of the Boolean PMH302 network using CNA (v.2015.1) were undertaken in accordance with Klamt et al. (2007). Full methodology is provided in section 6, sub section 6.2.

7.3.2.1 Application of logical steady state analysis

For investigation of potential network perturbation arising from the *in silico* effect of node state changes under LSSA in response to loss of p53 and different input stresses, four *in silico* comparisons were generated (section 6, tables 6 – 6.3) comprising different statuses of DNA damage or hypoxia (ON or OFF) and p53 (knockout or wild type). All nodes in the PMH302 network were subsequently filtered dependant on the biological processes that they regulate (cell cycle arrest, DNA repair, apoptosis, cellular senescence, and angiogenesis) and their effect on the network explored. Of the different *in silico* conditions, we created four comparative scenarios and explored the effects of all node state changes regulating their outputs to ascertain if the PMH302 interactome can identify overall system attributes. Global list of node state changes under LSSA are provided in tables 7.3.1.7 and 7.3.1.8 for p53 - DNA damage and hypoxia simulations respectively.

7.3.2.2 DNA damage and p53 simulations

All nodes that regulate the five outputs in the PMH302 model (cell cycle arrest, DNA repair, apoptosis, cellular senescence, and angiogenesis) were filtered, and their effect on the network explored. Of these different *in silico* conditions, we further created four comparative scenarios and explored the effects of all node state changes regulating their outputs to ascertain if the PMH302 interactome can identify potential perturbations and overall system attributes. Global list of node state changes is provided in table 7.3.1.7

Table 7.3.1.7 Global list of node state changes under LSSA in PMH302 in response to different DNA damage and p53 status simulations. Distribution of all nodes (n = 302 in PMH302 under LSSA in response to the four different simulations of different p53 (WT=wild type, KO=knockout), and DNA damage statuses (section 2, material and methods). In accordance with CNA, three states exist; 1 = upregulated, 0 = downregulated, NaN = undetermined.

Node ID	p53 WT with DD ON	p53 WT with DD OFF	p53 KO with DD ON	p53 KO with DD OFF
AATF	1	1	1	1
ABCB1	1	1	1	1
ABCC1	1	1	1	1
AIFM2	1	1	0	NaN
AIMP2	1	1	NaN	1
Angiogenesis	1	1	1	1
APAF1	1	1	1	1
APEX1	1	1	NaN	1
Apoptosis	1	1	1	1
APP	1	0	1	0
AR	0	0	1	0
ARID3A	1	1	0	NaN
ASPP1	NaN	NaN	NaN	NaN
ASPP2	NaN	NaN	NaN	NaN
ATF3	1	1	1	1
ATM	1	0	1	0
ATR	1	0	1	0
AURKA	NaN	NaN	NaN	NaN
AXIN1	1	1	1	1
BAIAP2L1	NaN	NaN	NaN	NaN
BAIAP2L2	0	0	NaN	NaN
BAK1	1	1	NaN	1
BAX	1	1	1	1
BBC3	1	1	0	NaN

BCCIP	NaN	NaN	NaN	NaN
BCL2	1	1	1	1
BCL3	0	0	1	NaN
BCL6	0	1	NaN	1
BDKRB1	0	0	1	NaN
BHLHE40	0	0	NaN	0
BNIP3L	1	1	0	NaN
BRCA1	1	1	1	1
BTG2	1	0	1	0
C12orf5	1	1	0	NaN
C13orf15	1	1	0	NaN
CA9	0	0	1	0
CALD1	1	1	0	NaN
CASP2	NaN	NaN	NaN	NaN
CASP8	1	1	NaN	0
CCAR1	1	0	1	0
CCNA	1	1	1	1
CCNB1	1	1	1	1
CCND1	1	1	1	1
CCNG1	1	1	1	1
CD44	1	1	1	1
CD58	1	1	0	NaN
CD59	1	1	NaN	0
CD82	1	1	0	NaN
CDC20	0	0	1	NaN
CDC25A	1	1	1	1
CDK2	1	1	1	1
CDK4	NaN	1	1	1
CDK5	1	1	1	1
CDK9	NaN	NaN	NaN	NaN
CDKN1A	1	1	1	1
CDKN1B	1	1	1	1
CDKN2A	1	1	1	1
Cell Cycle Arrest	1	1	1	1
Cellular Senescence	1	1	1	1
CHEK1	1	0	1	NaN
CHEK2	1	1	1	1
CIAPIN1	NaN	NaN	NaN	NaN
CKB	1	1	1	1
CKM	1	1	0	0

CKS2	0	0	1	NaN
COL18A1	1	1	0	NaN
COL1A2	NaN	NaN	NaN	NaN
CSNK2	NaN	NaN	NaN	NaN
CUL7	1	1	1	1
CXCR4	1	1	1	1
CYP24A1	NaN	NaN	NaN	NaN
DAP	1	0	1	0
DAXX	1	0	1	0
DDB2	1	1	0	NaN
DDIT4	1	1	NaN	0
DDX20	NaN	NaN	NaN	NaN
DDX5	1	1	NaN	1
DFNA5	1	1	0	NaN
DKK1	1	1	NaN	0
DNA damage	1	0	1	0
DNA Repair	1	1	1	1
DNMT3A	NaN	NaN	NaN	NaN
DUSP1	1	0	1	0
DUSP2	1	1	0	NaN
DUSP4	1	1	0	NaN
DUSP5	1	1	1	1
DYRK2	1	0	1	0
E2F1	1	1	1	1
ECT2	0	0	1	NaN
EDA2R	1	1	0	NaN
EGFR	1	1	1	1
EGR2	1	1	0	NaN
EIF2AK2	NaN	NaN	NaN	NaN
EIF5A	NaN	NaN	NaN	NaN
ELAVL1	NaN	NaN	NaN	NaN
EPHB4	0	0	1	NaN
ERBB2	1	1	1	1
ESR1	1	1	1	1
EXPORTIN1	0	0	1	NaN
EZH2	1	1	1	1
FAS	1	1	1	NaN
FDXR	1	1	0	NaN
FEN1	1	1	0	0
FGF2	NaN	1	1	1
FHL2	1	1	0	NaN
FLI1	1	0	1	0

FOS	1	1	1	1
FOXM1	0	0	1	NaN
GADD45A	1	1	0	0
GAPDH	1	1	NaN	0
GSTP1	1	1	1	1
GTSE1	1	1	0	NaN
H2AFZ	NaN	NaN	NaN	NaN
HDAC1	NaN	NaN	NaN	NaN
HIC1	1	1	1	1
HIF1A	1	1	1	1
HIPK2	NaN	NaN	NaN	NaN
HIPK4	NaN	NaN	NaN	NaN
HMMR	0	0	1	NaN
HNF4A	1	1	1	1
HOXA10	NaN	NaN	NaN	NaN
HOXA11	NaN	NaN	NaN	NaN
HOXA5	NaN	NaN	NaN	NaN
HSP90AB1	0	0	1	NaN
HSPA4	1	1	1	1
HTATIP2	1	0	1	0
Hypoxia	0	0	0	0
ICAM1	1	1	1	1
ID3	1	1	1	1
IER3	1	1	NaN	0
IFI16	1	1	0	NaN
IFITM2	0	0	1	NaN
IFNA1	NaN	NaN	NaN	NaN
IGF1R	0	0	1	NaN
IGFBP1	1	1	NaN	0
IGFBP7	1	1	0	NaN
IL6	1	1	1	1
ING1	NaN	NaN	NaN	NaN
ING2	1	0	1	0
ING4	NaN	NaN	NaN	NaN
ING5	1	0	1	0
IQCB1	0	0	1	NaN
ISG15	1	1	0	NaN
JAG1	NaN	NaN	NaN	NaN
JUN	1	1	1	1
KAT2B	1	1	0	NaN
KIF23	0	0	1	NaN
KLF4	1	1	NaN	0

KLK3	NaN	NaN	NaN	NaN
KRT19	0	0	1	0
KRT8	1	1	0	NaN
LATS2	1	1	0	NaN
LRDD	1	1	0	NaN
LTF	1	1	1	1
MAP4	0	0	1	0
MAP4K4	1	1	0	NaN
MAPK1	1	1	1	1
MAPK14	1	1	1	1
MAPK8	1	1	1	1
MAPK9	1	0	1	0
MCL1	1	1	1	1
MCTS1	1	0	1	0
MDM2	1	1	1	1
MDM4	1	1	1	1
MGMT	0	0	1	NaN
MIC1	NaN	NaN	NaN	NaN
MMP1	1	1	1	1
MMP13	1	1	1	1
MMP2	1	1	1	1
MSH2	1	1	1	1
MTA1	1	0	1	0
MTA2	NaN	NaN	NaN	NaN
MUC1	0	0	NaN	0
MYC	1	1	1	1
MYCN	1	1	1	1
MYST4	1	0	1	0
NANOG	NaN	NaN	NaN	NaN
NCL	1	NaN	1	NaN
NFKB2	1	0	1	0
NLRC4	1	1	0	NaN
NME1	1	1	1	1
NOTCH1	1	1	1	1
NOV	1	1	0	NaN
NQO1	NaN	NaN	NaN	NaN
NR2C1	1	1	1	1
NTN1	0	0	NaN	0
P53	1	1	0	0
P53AIP1	1	1	1	0
PAD4	NaN	NaN	NaN	NaN
PARK2	NaN	NaN	NaN	NaN

PCBP4	1	1	0	NaN
PCNA	1	1	1	1
PDGFRB	0	0	1	NaN
PDRG1	0	0	1	NaN
PEG3	1	1	0	NaN
PERP	1	1	0	NaN
PHB	NaN	NaN	NaN	NaN
PHF20	NaN	NaN	NaN	NaN
PIAS1	1	0	1	0
PIAS2	NaN	NaN	NaN	NaN
PIN1	NaN	NaN	NaN	NaN
PIRH2	1	0	1	0
PITX1	1	0	1	0
PLA2G6	NaN	NaN	NaN	NaN
PLAUR	1	1	1	1
PML	1	1	1	0
POU4F1	NaN	NaN	NaN	NaN
PPARG	NaN	NaN	NaN	NaN
PPID	NaN	NaN	NaN	NaN
PPM1A	NaN	NaN	NaN	NaN
PPM1D	1	1	1	NaN
PRAK	NaN	NaN	NaN	NaN
PRC1	0	0	1	NaN
PREP1	NaN	NaN	NaN	NaN
PRKAB1	NaN	NaN	NaN	NaN
PRKCA	1	1	1	1
PRKD1	1	0	1	0
PRKDC	1	0	1	0
PRKG1	1	1	0	NaN
PRSS50	0	0	1	NaN
PSEN1	0	0	1	NaN
PSMD10	NaN	NaN	NaN	NaN
PTEN	1	1	NaN	NaN
PTGS2	1	1	1	1
PTTG1	0	1	0	1
RAD51	1	1	1	1
RAF1	1	1	1	1
RAS	1	1	1	1
RB	NaN	NaN	NaN	NaN
RB1CC1	NaN	NaN	NaN	NaN
RECQL4	0	0	1	NaN
RFC	NaN	NaN	NaN	NaN

RFWD3	1	0	1	0
RGS16	1	1	0	NaN
RPA1	1	0	1	0
RPRM	1	1	0	NaN
RPS27L	1	0	1	0
RREB1	NaN	NaN	NaN	NaN
RRM2B	1	1	0	NaN
RSK2	1	0	1	0
S100A2	1	1	0	NaN
S100A6	0	0	1	NaN
S100B	NaN	NaN	NaN	NaN
SEMA3B	1	1	0	NaN
SENP3	NaN	NaN	NaN	NaN
SERPINB5	1	1	0	NaN
SERPINE1	0	0	NaN	0
SERPINF1	1	1	1	1
SESN2	1	1	0	NaN
SET	NaN	NaN	NaN	NaN
SFN	1	1	0	NaN
SGK	1	1	1	1
SIAH1	1	1	1	1
SIVA1	1	1	1	1
SKIL	NaN	NaN	NaN	NaN
SLC2A1	1	1	1	1
SLC2A4	0	0	1	0
SLC6A6	1	1	1	1
SMYD2	NaN	NaN	NaN	NaN
SOD1	NaN	NaN	NaN	NaN
SOD2	NaN	NaN	NaN	NaN
SOX4	1	0	1	0
SP1	1	0	NaN	0
SP7	0	0	1	0
STAT3	1	1	1	1
STMN1	0	1	0	1
SUB1	1	0	1	0
SUMO2	NaN	NaN	NaN	NaN
SUMO3	NaN	NaN	NaN	NaN
TCF7L2	NaN	NaN	1	NaN
TFAP2A	1	1	1	0
TFAP2C	1	1	0	NaN
TFDP1	0	0	1	NaN
TGFA	1	1	1	1

TGFB1	1	1	1	1
THBS1	1	1	1	1
TIAF1	NaN	NaN	NaN	NaN
TLR3	1	1	NaN	NaN
TNFRSF10A	1	1	1	1
TNFRSF10B	1	1	1	1
TOP2A	1	0	1	0
TP53BP1	1	0	1	0
TP53I13	1	1	0	0
TP53INP1	1	1	0	0
TP53RK	NaN	NaN	NaN	NaN
TPT1	1	1	NaN	0
UBE2A	1	0	1	0
UBE3A	NaN	NaN	NaN	NaN
UCHL1	NaN	NaN	NaN	NaN
UNC5A	1	1	NaN	0
VEGFA	1	1	1	1
VRK1	0	0	NaN	0
WRN	1	0	1	0
WWOX	1	0	1	0
WWP1	1	1	1	1
XAF1	0	0	1	0
YBX1	1	1	1	1
YY1	0	0	NaN	0
ZMAT3	1	1	0	NaN
ZMIZ2	NaN	NaN	NaN	NaN
ZNF148	NaN	NaN	NaN	NaN
ZNF307	NaN	NaN	NaN	NaN

7.3.2.2.1 Nodes regulating apoptosis under LSSA

We filtered all nodes that regulate apoptosis from the PMH302 network. Of the total 131 nodes regulating apoptosis in the PMH302 model, globally, a greater number of pro-apoptotic nodes were upregulated in the p53 wild type backgrounds compared to p53 knockouts backgrounds, with a slight increase in the total number when DNA damage was switched ON. Comparable, a greater number of anti-apoptotic nodes were downregulated in the p53 wild type backgrounds globally, compared to p53 knockout backgrounds (table 7.3.1.8, figure 7.3).

Table. 7.3.1.8 Distribution of anti-apoptotic nodes under LSSA in the PMH302 model. Total number of anti-apoptotic node with three possible state changes; upregulated, downregulated or undetermined. A total of 50 anti-apoptotic nodes are considered in the PMH302 network.

***In silico* simulation**	**Upregulated**	**Downregulated**	**Undetermined**
	Total number of nodes		
p53 wild type with DNA damage ON	**37**	**7**	**6**
	NFKB2	AR	FGF2
	APEX1	BCL3	NANOG
	FLI1	CKS2	PREP1
	MTA1	EPHB4	TCF7L2
	ATF3	IGF1R	TP53RK
	BCL2	PDGFRB	RB1CC1
	C12orf5	PSEN1	
	CCNG1		
	CD44		
	CDC25A		
	CDKN1A		
	CDKN1B		
	CUL7		
	DAXX		
	DDIT4		
	DUSP2		
	DUSP4		
	EGFR		
	ESR1		
	EZH2		
	FHL2		
	FOS		
	GSTP1		
	IER3		
	IL6		
	MAP4K4		
	MCL1		
	NOTCH1		
	PRKCA		
	PTGS2		
	SFN		
	SGK		
	STAT3		
	TGFA		
	TPT1		

	VEGFA		
	WWP1		
p53 wild type with DNA damage OFF	**Upregulated**	**Downregulated**	**Undetermined**
	Total number		
	34	**11**	**5**
	APEX1	AR	NANOG
	ATF3	BCL3	PREP1
	BCL2	CKS2	TCF7L2
	C12orf5	DAXX	TP53RK
	CCNG1	EPHB4	RB1CC1
	CD44	FLI1	
	CDC25A	IGF1R	
	CDKN1A	MTA1	
	CDKN1B	PDGFRB	
	CUL7	PSEN1	
	DDIT4	NFKB2	
	DUSP2		
	DUSP4		
	EGFR		
	ESR1		
	EZH2		
	FGF2		
	FHL2		
	FOS		
	GSTP1		
	IER3		
	IL6		
	MAP4K4		
	MCL1		
	NOTCH1		
	PRKCA		
	PTGS2		
	SFN		
	SGK		
	STAT3		
	TGFA		
	TPT1		
	VEGFA		
	WWP1		
p53 knockout with DNA damage ON	**Upregulated**	**Downregulated**	**Undetermined**
	Total number		
	36	**6**	**8**

	NFKB2	C12ORF5	NANOG
	AR	DUSP2	PREP1
	FLI1	DUSP4	TP53RK
	MTA1	FHL2	RB1CC1
	ATF3	MAP4K4	APEX1
	BCL2	SFN	DDIT4
	CCNG1		IER3
	CD44		TPT1
	CDC25A		
	CDKN1A		
	CDKN1B		
	CUL7		
	DAXX		
	EGFR		
	ESR1		
	EZH2		
	FOS		
	GSTP1		
	IL6		
	MCL1		
	NOTCH1		
	PRKCA		
	PTGS2		
	SGK		
	STAT3		
	TGFA		
	VEGFA		
	WWP1		
	BCL3		
	CKS2		
	EPHB4		
	FGF2		
	IGF1R		
	PDGFRB		
	PSEN1		
	TCF7L2		
p53 knockout with DNA damage OFF	**Upregulated**	**Downregulated**	**Undetermined**
		Total number	
	25	**8**	**17**
	APEX1	FLI1	BCL3
	ATF3	MTA1	C12orf5
	BCL2	AR	CKS2

	CCNG1	DAXX	DUSP2
	CD44	DDIT4	DUSP4
	CDC25A	IER3	EPHB4
	CDKN1A	TPT1	FHL2
	CDKN1B	NFKB2	IGF1R
	CUL7		MAP4K4
	EGFR		NANOG
	ESR1		PDGFRB
	EZH2		PREP1
	FGF2		PSEN1
	FOS		SFN
	GSTP1		TCF7L2
	IL6		TP53RK
	MCL1		RB1CC1
	NOTCH1		
	PRKCA		
	PTGS2		
	SGK		
	STAT3		
	TGFA		
	VEGFA		
	WWP1		

Table 7.3.1.9 Distribution of pro - apoptotic nodes under LSSA in PMH302.
Total number of pro-apoptotic node with three possible state changes of upregulated, downregulated or undetermined. A total of 81 pro apoptotic nodes were described in the PMH302 network.

***In silico* simulation**	**Upregulated**	**Downregulated**	**Undetermined**
	Total number of nodes		
p53 wild type with DNA damage ON	**64**	**6**	**11**
	TOP2A	SERPINE1	ASPP1
	WWOX	AR	ASPP2
	AIFM2	ECT2	CASP2
	APAF1	IFITM2	DDX20
	APP	PRSS50	FGF2
	ATF3	XAF1	HOXA10
	BAK1		ING4
	BAX		MIC1
	BBC3		UCHL1
	BNIP3L		ZNF148

	CASP8		CYP24A1
	CCNG1		
	CD44		
	CDC25A		
	CDKN1B		
	CDKN2A		
	COL18A1		
	CXCR4		
	DAP		
	DAXX		
	DDIT4		
	DFNA5		
	DKK1		
	DUSP2		
	DUSP4		
	EGFR		
	ESR1		
	FAS		
	FDXR		
	FOS		
	GADD45A		
	HNF4A		
	IFI16		
	IGFBP7		
	IL6		
	ING5		
	JUN		
	KAT2B		
	LATS2		
	LRDD		
	MAP4K4		
	MSH2		
	NLRC4		
	NOTCH1		
	P53AIP1		
	PCBP4		
	PEG3		
	PERP		
	PITX1		
	PML		

	PRKCA		
	PTEN		
	PTGS2		
	SEMA3B		
	SERPINB5		
	SIAH1		
	SIVA1		
	TFAP2C		
	TLR3		
	TNFRSF10A		
	TNFRSF10B		
	TP53INP1		
	NFKB2		
	TFAP2A		
p53 wild type with DNA damage OFF	**Upregulated**	**Downregulated**	**Undetermined**
	Total number		
	57	**14**	**10**
	AIFM2	APP	ASPP1
	APAF1	AR	ASPP2
	ATF3	DAP	CASP2
	BAK1	DAXX	DDX20
	BAX	ECT2	HOXA10
	BBC3	IFITM2	ING4
	BNIP3L	ING5	MIC1
	CASP8	PITX1	UCHL1
	CCNG1	PRSS50	CYP24A1
	CD44	SERPINE1	ZNF148
	CDC25A	TOP2A	
	CDKN1B	WWOX	
	CDKN2A	XAF1	
	COL18A1	NFKB2	
	CXCR4		
	DDIT4		
	DFNA5		
	DKK1		
	DUSP2		
	DUSP4		
	EGFR		
	ESR1		
	FAS		
	FDXR		
	FGF2		

	FOS		
	GADD45A		
	HNF4A		
	IFI16		
	IGFBP7		
	IL6		
	JUN		
	KAT2B		
	LATS2		
	LRDD		
	MAP4K4		
	MSH2		
	NLRC4		
	NOTCH1		
	P53AIP1		
	PCBP4		
	PEG3		
	PERP		
	PML		
	PRKCA		
	PTEN		
	PTGS2		
	SEMA3B		
	SERPINB5		
	SIAH1		
	SIVA1		
	TFAP2C		
	TLR3		
	TNFRSF10A		
	TNFRSF10B		
	TP53INP1		
	TFAP2A		
p53 knockout with DNA damage ON	**Upregulated**	**Downregulated**	**Undetermined**
	Total number		
	42	**23**	**16**
	TOP2A	SERPINE1	ASPP1
	WWOX	AIFM2	ASPP2
	APAF1	BBC3	CASP2
	APP	BNIP3L	DDX20
	ATF3	COL18A1	HOXA10
	AR	GADD45A	ING4
	BAX	DFNA5	MIC1

	CCNG1	TP53NP1	PTEN
	CD44	DUSP2	TLR3
	CDC25A	DUSP4	UCHL1
	CDKN1B	FDXR	CYP24A1
	CDKN2A	IFI16	ZNF148
	CXCR4	IGFBP7	BAK1
	DAP	KAT2B	CASP8
	DAXX	LATS2	DDIT4
	EGFR	LRDD	DKK1
	ESR1	MAP4K4	
	FAS	NLRC4	
	FOS	PCBP4	
	HNF4A	PEG3	
	IL6	TFAP2C	
	ING5	SERPINB5	
	JUN	SEMA3B	
	MSH2		
	NOTCH1		
	P53AIP1		
	PITX1		
	PML		
	PRKCA		
	PTGS2		
	SIAH1		
	SIVA1		
	TNFRSF10A		
	TNFRSF10B		
	XAF1		
	NFKB2		
	TFAP2A		
	ECT2		
	FGF2		
	IFITM2		
	PERP		
	PRSS50		
p53 knockout with DNA damage OFF	**Upregulated**	**Downregulated**	**Undetermined**
	Total number		
	25	**19**	**37**
	APAF1	SERPINE1	AIFM2
	ATF3	TOP2A	ASPP1
	BAK1	WWOX	ASPP2
	BAX	APP	BBC3

	CCNG1	AR	BNIP3L
	CD44	CASP8	CASP2
	CDC25A	DAP	CYP24A1
	CDKN1B	DAXX	COL18A1
	CDKN2A	DDIT4	DDX20
	CXCR4	DKK1	DFNA5
	EGFR	GADD45A	DUSP2
	ESR1	ING5	DUSP4
	FGF2	P53AIP1	ECT2
	FOS	PITX1	FAS
	HNF4A	PML	FDXR
	IL6	TP53INP1	HOXA10
	JUN	XAF1	IFI16
	MSH2	NFKB2	IFITM2
	NOTCH1	TFAP2A	IGFBP7
	PRKCA		ING4
	PTGS2		KAT2B
	SIAH1		LATS2
	SIVA1		LRDD
	TNFRSF10A		MAP4K4
	TNFRSF10B		MIC1
			NLRC4
			PCBP4
			PEG3
			PERP
			PRSS50
			PTEN
			SEMA3B
			SERPINB5
			TFAP2C
			TLR3
			UCHL1
			ZNF148

Nearly a twofold upregulation was observed in pro- apoptotic nodes (n=64) in the presence of p53 under DNA damage, compared to pro- apoptotic nodes in the absence of p53 with no DNA damage (n=42) (compare lanes 1 and 3 fig. 7.3). These node IDs are given in table 7.3.1.2.

Surprisingly, the number of anti-apoptotic nodes upregulated was greater in the presence of p53 than when p53 was deleted from the network when *in silico* DNA damage was ON (compare lanes 13 and 15 in fig.7.3). However, the majority of those upregulated also have anti-proliferative roles in apoptosis and cellular senescence and include, SFN, MAP4K4, DUSP2/4, DDIT4 and C12Orf5 (table 7.3.1.8).

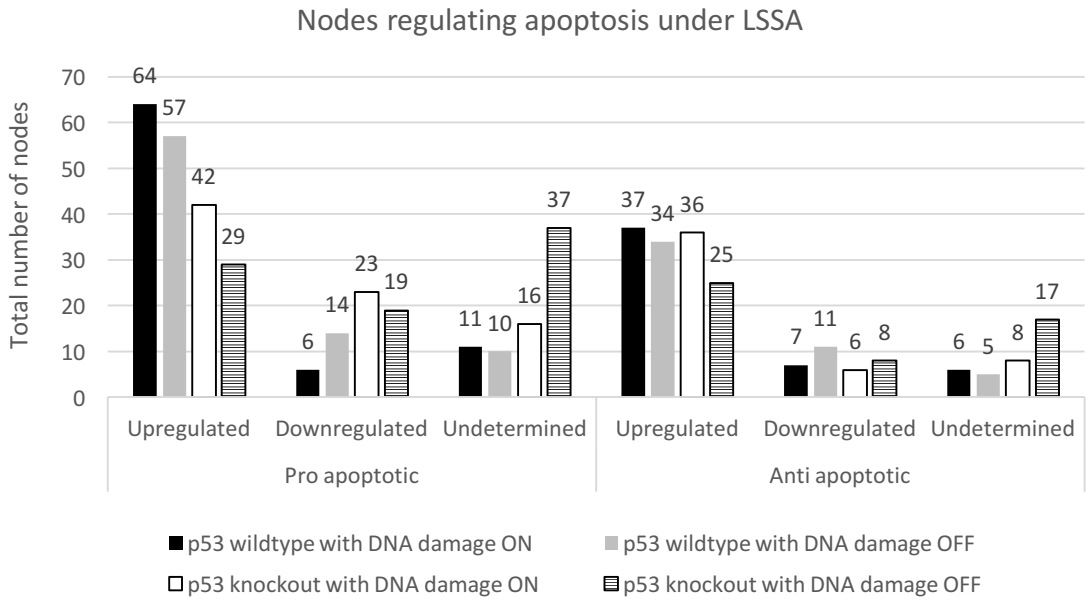

Figure 7.3 Total number and distribution of nodes regulating apoptosis under LSSA in PMH302. A total of 131 nodes that regulated apoptosis are considered in PMH302. A greater shift towards pro-apoptotic nodes upregulated compared to anti-apoptotic nodes upregulated in p53 wild type backgrounds were observed (see lanes 1 and 2 to lanes 13 and 14)

7.3.2.2.2 Nodes regulating angiogenesis under LSSA.

Globally, of the total 52 angiogenic nodes described in PMH302, a greater number of pro- angiogenic nodes (41) were upregulated than anti- angiogenic (22) nodes in the p53 wild type backgrounds. A similar number of total pro-angiogenic nodes were upregulated when comparing p53 backgrounds; 41 and 42 for p53 wild type aand p53 deletion backgrounds respectively. A descriptive list of angiogenic nodes and their state changes under LSSA are summarised in tables 7.3.2 and 7.3.2.1 for anti and pro angiogenic respectively, and graphically in figure 7.3.1.

Comparing the p53 wildtype backgrounds with DNA damage OFF and ON, a similar number of upregulated pro-angiogenic nodes were observed, regardless of the DNA

damage effect (compare lanes 1 and 2, figure 7.3.1). Of the 20 upregulated when DNA damage was ON, to 21 upregulated when DNA damage was OFF (compare lanes 1 and 2 in fig. 7.3.1), BBC3 and CALD1, along with MTA1, RSK2, and CCND1 were differentially *in silico* expressed when the in silico DNA damage input was ON (table 7.3.2.1). The number of anti-angiogenic nodes upregulated were identical, 11 for both DNA damage conditions in p53 wild type backgrounds (compare lanes 13 and 14). No anti-angiogenic nodes were downregulated (see lanes 17 and 18).

A comparable number of pro-angiogenic nodes was also noted in DNA damage ON backgrounds; 20 upregulated in the presence of p53 compared to 23 upregulated in the absence of p53 (compare lanes 1 and 3, figure 7.3.1). Of these, all nodes were identical (table 7.3.2.1) apart from the upregulation of BBC3 and CALD1 in the presence of p53. Conversely, a greater number of anti-angiogenic nodes were upregulated (nearly three-fold) in the p53 wild type background (n=11), compared to when p53 was deleted (n=4) both under DNA damage (compare lanes 13 and 15) BNIP3L, CD59, COL18A1, DKK1, IFI16, and PTEN were considered as *in silico* p53 responsive nodes regardless of the DNA damage effect (table 7.3.2).

Table 7.3.2 Distribution of anti angiogenic nodes under LSSA in PMH302. A total of 17 anti-angiogenic nodes were considered in the PMH302 model. Three node state changes are possible; upregulated, downregulated or undetermined.

***In silico* simulation**	**Upregulated**	**Downregulated**	**Undetermined**
	Total number of nodes		
p53 wild type with DNA damage ON	**11**	**0**	**6**
	BNIP3L		ELAVL1
	CD59		HOXA5
	CD82		ING1
	COL18A1		ING4
	DKK1		NQO1
	IFI16		PPARG
	NOTCH1		
	PML		
	PTEN		
	SERPINF1		
	TGFB1		
p53 wild type with DNA damage OFF	**Upregulated**	**Downregulated**	**Undetermined**

	Total number		
	11	**0**	**6**
	BNIP3L		ELAVL1
	CD59		HOXA5
	CD82		ING1
	COL18A1		ING4
	DKK1		NQO1
	IFI16		PPARG
	NOTCH1		
	PML		
	PTEN		
	SERPINF1		
	TGFB1		
p53 knockout with DNA damage ON	**Upregulated**	**Downregulated**	**Undetermined**
	Total number		
	4	**4**	**9**
	NOTCH1	BNIP3L	CD59
	PML	CD82	DKK1
	SERPINF1	COL18A1	ELAVL1
	TGFB1	IFI16	HOXA5
			ING1
			ING4
			NQO1
			PPARG
			PTEN
p53 knockout with DNA damage OFF	**Upregulated**	**Downregulated**	**No change**
	Total number		
	3	**3**	**11**
	NOTCH1	CD59	BNIP3L
	SERPINF1	DKK1	CD82
	TGFB1	PML	COL18A1
			ELAVL1
			HOXA5
			IFI16
			ING1
			ING4
			NQO1
			PPARG
			PTEN

Table 7.3.2.1 Distribution of pro - angiogenic nodes under LSSA in PMH302.

A total of 35 pro angiogenic nodes are considered in the PMH302 model

***In silico* simulation**	**Upregulated**	**Downregulated**	**Undetermined**
p53 wild type with DNA damage ON	**Total number of nodes**		
	20	**6**	**9**
	MTA1	STMN1	CDK4
	RSK2	NTN1	FGF2
	BBC3	PDGFRB	JAG1
	BCL2	EPHB4	MIC1
	CALD1	EPHB4	NANOG
	CCND1	SERPINE1	PHB
	CD44		S100B
	CDK2		SENP3
	CDK5		ELAVL1
	EGFR		
	HIF1A		
	HSPA4		
	JUN		
	MMP1		
	MMP13		
	PRKCA		
	PTGS2		
	SGK		
	TGFA		
	VEGFA		
p53 wild type with DNA damage OFF	**Upregulated**	**Downregulated**	**Undetermined**
	Total number		
	21	**7**	**7**
	BBC3	BDKRB1	ELAVL1
	BCL2	EPHB4	JAG1
	CALD1	MTA1	MIC1
	CCND1	NTN1	NANOG
	CD44	PDGFRB	PHB
	CDK2	RSK2	S100B
	CDK4	SERPINE1	SENP3
	CDK5		
	EGFR		
	FGF2		
	HIF1A		
	HSPA4		
	JUN		
	MMP1		

	MMP13		
	PRKCA		
	PTGS2		
	SGK		
	STMN1		
	TGFA		
	VEGFA		
p53 knockout with DNA damage ON	**Upregulated**	**Downregulated**	**Undetermined**
	Total number		
	23	**3**	**9**
	MTA1	BBC3	SERPIN1
	RSK2	CALD1	NTN1
	BCL2	STMN1	ELAVL1
	CCND1		JAG1
	CD44		MIC1
	CDK2		NANOG
	CDK5		PHB
	EGFR		S100B
	HIF1A		SENP3
	HSPA4		
	JUN		
	MMP1		
	MMP13		
	PRKCA		
	PTGS2		
	SGK		
	TGFA		
	VEGFA		
	BDKRB1		
	CDK4		
	EPHB4		
	FGF2		
	PDGFRB		
p53 knockout with DNA damage OFF	**Upregulated**	**Downregulated**	**Undetermined**
	Total number		
	19	**4**	**12**
	BCL2	MTA1	BBC3
	CCND1	RSK2	BDKRB1
	CD44	SERPINE1	CALD1
	CDK2	NTN1	ELAVL1
	CDK4		EPHB4
	CDK5		JAG1

	EGFR		MIC1
	FGF2		NANOG
	HIF1A		PDGFRB
	HSPA4		PHB
	JUN		S100B
	MMP1		SENP3
	MMP13		
	PRKCA		
	PTGS2		
	SGK		
	STMN1		
	TGFA		
	VEGFA		

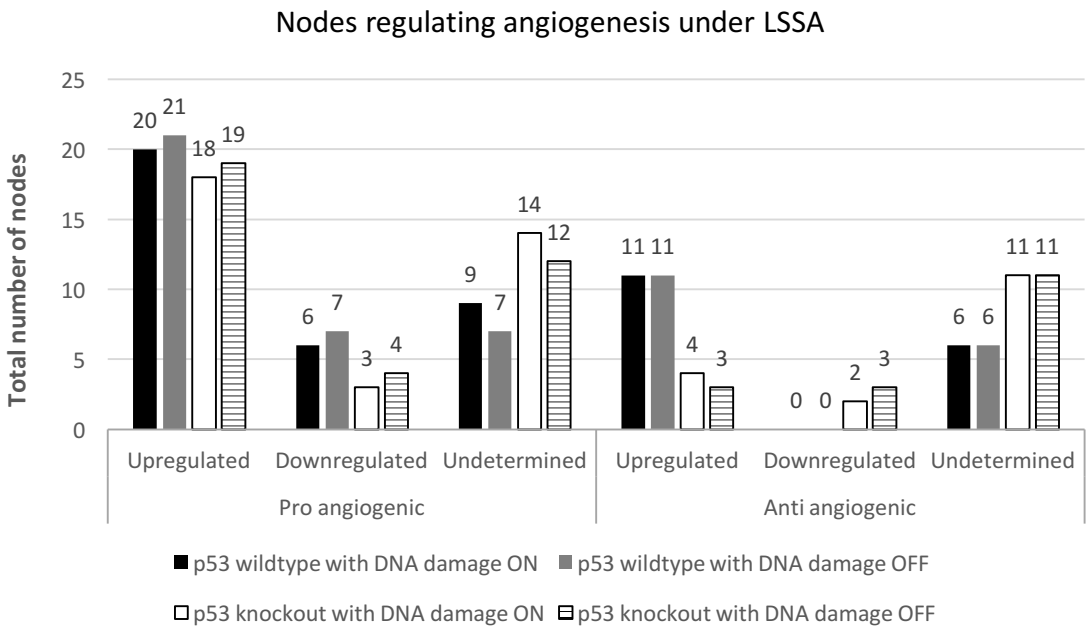

Figure 7.3.1 Total number and distribution of nodes regulating angiogenesis under LSSA in PMH302. Globally, an increased upregulation of pro-angiogenic nodes is observed compared to anti-angiogenic nodes in both p53 wild type and p53 knockout backgrounds

7.3.2.2.3 Nodes regulating DNA repair under LSSA

A total of 37 nodes that regulate DNA repair are described in PMH302. Of these, only a small minority (n = 8) were negative regulators, with the remaining positively regulating DNA repair (n = 29).

Investigating the effect of p53 in the presence of DNA damage; an increase in the upregulation of positive regulators of DNA repair was observed in the presence of p53 (n=22) compared to when p53 was deleted (n=19) (compare lanes 1 and 3 of fig. 7.3.1.1). No major change in node states was observed of those downregulated in response to DNA damage; 2 and 4 for p53 wild type and p53 knockout backgrounds respectively (compare lanes 2 and 7, figure 7.3.1.1).

Comparing node state changes between negative regulators of DNA repair in response to different DNA damage inputs; a twofold increase in nodes upregulated was observed from 6 to 3 in the presence and absence of p53 respectively (compare lanes 13 and 15, figure 7.3.1.1). However, when DNA damage was ON, and in the presence of p53, unsurprisingly, increased pro-DNA repair nodes were upregulated compared to all other conditions (see lane 1, figure 7.3.1.1). Identical numbers and nodes that negatively regulate DNA repair was noted when DNA damage was ON and OFF in p53 wild type backgrounds (n = 6) (lanes 13 and 14, figure 7.3.1.1). In comparison, 5 anti-DNA repair nodes were upregulated in p53 deletion backgrounds compared to the 6 as described for p53 wild type backgrounds, this was regardless of DNA damage effect (compare lanes 13 and 14 to lanes 15 and 16, figure 7.3.1.1).

Table 7.3.2.2 Distribution of nodes that negatively regulate DNA repair under LSSA in PMH302. A total of 8 anti - DNA repair nodes are considered in the PMH302 model.

***In silico* condition**	**Upregulated**	**Downregulated**	**Undetermined**
	Total number of nodes		
p53 wild type with DNA damage ON	**6**	**2**	**0**
	KLF4	SERPINE1	
	MDM2	PTTG1	
	MDM4		
	MYC		
	SIAH1		
	PPMID		
p53 wild type with DNA damage OFF	**Upregulated**	**Downregulated**	**Undetermined**
	Total number		
	6	**1**	**1**
	KLF4	SERPINE1	PTTG1
	MDM2		
	MDM4		

	MYC		
	SIAH1		
	PPMID		
p53 knockout with DNA damage ON	**Upregulated**	**Downregulated**	**Undetermined**
	Total number		
	5	**1**	**2**
	MDM2	PTTG1	KLF4
	MYC		SERPINE1
	SIAH1		
	MDM4		
	PPMID		
p53 knockout with DNA damage OFF	**Upregulated**	**Downregulated**	**Undetermined**
	Total number		
	5	**2**	**1**
	MDM2	SERPINE1	PPM1D
	MDM4	KLF4	
	MYC		
	SIAH1		
	PTTG1		

Table 7.3.2.3 Distribution of nodes that positively regulate DNA repair under LSSA in PMH302. A total of 29 pro DNA repair nodes are considered in the PMH302 model.

***In silico* simulation**	**Upregulated**	**Downregulated**	**Undetermined**
	Total number of nodes		
p53 wild type with DNA damage ON	**22**	**2**	**5**
	APEX1	MGMT	BCCIP
	MTA1	YY1	FGF2
	PIAS1		ING1
	RFWD3		PIN1
	RPA1		SUMO3
	RPS27L		
	ATM		
	ATR		
	BRCA1		
	CD44		
	CDKN1A		
	DDB2		
	FEN1		
	GADD45A		
	HSPA4		
	IFI16		
	MCL1		

	MSH2		
	NME1		
	PCNA		
	PRKDC		
	RAD51		
p53 wild type with DNA damage OFF	**Upregulated**	**Downregulated**	**Undetermined**
	Total number		
	15	**10**	**4**
	APEX1	ATM	BCCIP
	BRCA1	ATR	ING1
	CD44	MGMT	PIN1
	CDKN1A	MTA1	SUMO3
	DDB2	PIAS1	
	FEN1	PRKDC	
	FGF2	RFWD3	
	GADD45A	RPA1	
	HSPA4	RPS27L	
	IFI16	YY1	
	MCL1		
	MSH2		
	NME1		
	PCNA		
	RAD51		
p53 knockout with DNA damage ON	**Upregulated**	**Downregulated**	**Undetermined**
	Total number		
	19	**4**	**6**
	FGF2	FEN1	BCCIP
	MTA1	GADD45A	APEX1
	PIAS1	DDB2	YY1
	RFWD3	IFI16	ING1
	RPA1		PIN1
	RPS27L		SUMO3
	ATM		
	ATR		
	BRCA1		
	CD44		
	CDKN1A		
	HSPA4		
	MCL1		
	MSH2		
	NME1		
	PCNA		

	PRKDC		
	RAD51		
	MGMT		
p53 knockout with DNA damage OFF	**Upregulated**	**Downregulated**	**Undetermined**
	Total number		
	11	**11**	**7**
	APEX1	MTA1	BCCIP
	BRCA1	PIAS1	DDB2
	CD44	RFWD3	IFI16
	CDKN1A	RPA1	ING1
	FGF2	RPS27L	MGMT
	HSPA4	ATM	PIN1
	MCL1	ATR	SUMO3
	MSH2	FEN1	
	NME1	GADD45A	
	PCNA	PRKDC	
	RAD51	YY1	

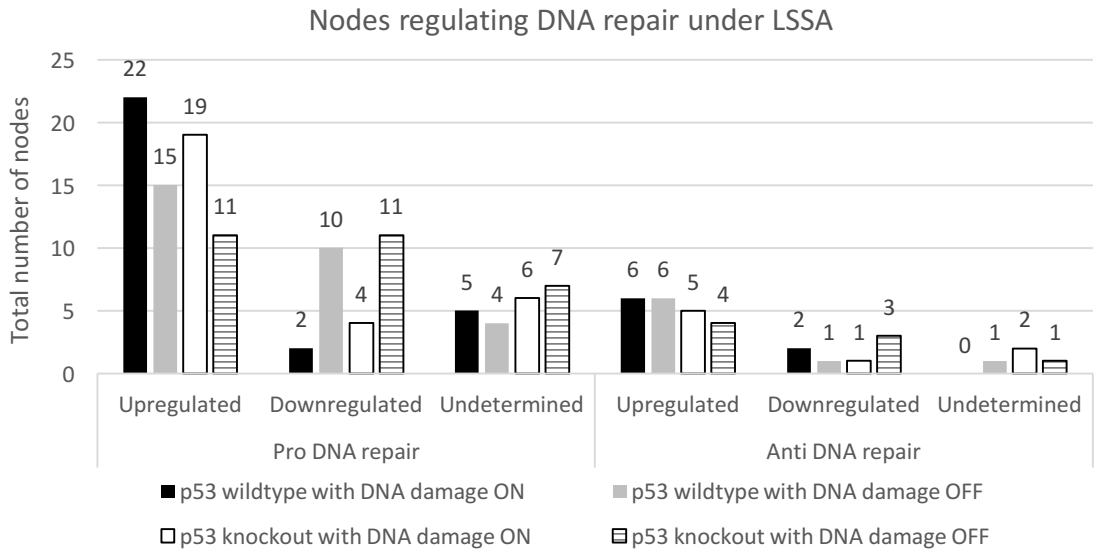

Figure 7.3.1.1 Total number and distribution of nodes regulating DNA repair under LSSA in PMH302 A greater number of pro-DNA repair nodes were upregulated in the presence of p53 (lanes 1 and 2). However, only a minority of anti-repair nodes are considered (n = 8)

7.3.2.2.4 Nodes regulating cell cycle arrest under LSSA

Globally, increased upregulation of nodes that activate cell cycle arrest was observed in p53 wild type backgrounds compared to p53 deletion backgrounds. However identical numbers of upregulated pro-cell cycle arrest nodes were noted when compared to

those that negatively regulate cell cycle arrest. In the absence of p53, the majority of nodes shifted to an undetermined state (compare lanes 9 and 10 to 11 and 12, and lanes 21 and 22 to lanes 23 and 24, fig. 7.3.1.2). Descriptive summary of node state changes and their IDs are given in tables 7.3.2.4 and 7.3.2.5.

Under DNA damage and in the presence of p53 increased numbers of positive regulators of cell cycle arrest was observed (n=24) compared to when p53 was absent with DNA damage ON (n=19) (compare lanes 1 and 3 in fig. 7.3.1.2). DKK1, GADD45A, IGFBP7, KAT2B and TFAP2C were differentially *in silico* expressed, downregulated or undetermined in the absence of p53. Of the positive regulators of cell cycle arrest, only 2 were downregulated in the presence of p53, compared to 5 when p53 was removed *in silico* with DNA damage ON respectively (compare lanes 5 and 7).

Of the nodes which inhibit cell cycle arrest, there was a slight increase in nodes upregulated in the absence of p53 when DNA damage was ON (n=22) than in p53 absence (n=21) (compare lanes 13 and 15, fig. 7.3.1.2). Of these, the majority were identical apart from ISG15, IER3 and RGS16 upregulated in the presence of p53 (table 7.3.2.5).

22 anti-cell cycle arrest nodes were upregulated in when DNA damage was ON, compared to only 15 when DNA damage was OFF in p53 deletion backgrounds (compare lanes 15 and 16, fig. 7.3.1.2) with MTA1, ING5, UBE2A, AR, CKS2, EPHB4 and S100A6 the additional anti – cell cycle arrest nodes upregulated when DNA damage was ON (table 7.3.2.4).

Table 7.3.2.4 Distribution of nodes that negatively regulate cell cycle arrest under LSSA in PMH302. A total of 31 anti-cell cycle arrest nodes are considered in the PMH302 model

***In silico* simulation**	**Upregulated**	**Downregulated**	**Undetermined**
	Total number of nodes		
p53 wild type with DNA damage ON	**21**	**6**	**4**
	MTA1	AR	AURKA
	APAF1	CKS2	HDAC1
	ATF3	EPHB4	JAG1
	CCNA	MUC1	PRAK

	CCNB1	S100A6	
	CDK2	VRK1	
	CUL7		
	E2F1		
	IER3		
	ING5		
	ISG15		
	JUN		
	MCL1		
	MYC		
	RAD51		
	RGS16		
	SIVA1		
	SLC2A1		
	UBE2A		
	YBX1		
	MYCN		
p53 wild type with DNA damage OFF	**Upregulated**	**Downregulated**	**Undetermined**
	Total number		
	18	**9**	**4**
	APAF1	AR	AURKA
	ATF3	CKS2	HDAC1
	CCNA	EPHB4	JAG1
	CCNB1	ING5	PRAK
	CDK2	MTA1	
	CUL7	MUC1	
	E2F1	S100A6	
	IER3	UBE2A	
	ISG15	VRK1	
	JUN		
	MCL1		
	MYC		
	RAD51		
	RGS16		
	SIVA1		
	SLC2A1		
	YBX1		
	MYCN		
p53 knockout with DNA damage ON	**Upregulated**	**Downregulated**	**Undetermined**
	Total number		
	22	**2**	**7**
	MTA1	ISG15	AURKA

	APAF1	RSG16	HDAC1
	ATF3		JAG1
	CCNA		PRAK
	CCNB1		IER3
	CDK2		MUC1
	CUL7		VRK1
	E2F1		
	ING5		
	JUN		
	MCL1		
	MYC		
	RAD51		
	SIVA1		
	SLC2A1		
	UBE2A		
	YBX1		
	MYCN		
	AR		
	CKS2		
	EPHB4		
	S100A6		
p53 knockout with DNA damage OFF	**Upregulated**	**Downregulated**	**Undetermined**
	Total number		
	15	**7**	**9**
	APAF1	MTA1	AURKA
	ATF3	AR	CKS2
	CCNA	IER3	EPHB4
	CCNB1	ING5	HDAC1
	CDK2	MUC1	ISG15
	CUL7	UBE2A	JAG1
	E2F1	VRK1	PRAK
	JUN		RGS16
	MCL1		S100A6
	MYC		
	RAD51		
	SIVA1		
	SLC2A1		
	YBX1		
	MYCN		

Table 7.3.2.5 Distribution of nodes that positively regulate cell cycle arrest under LSSA in PMH302. A total of 35 pro-cell cycle arrest nodes are considered in the PMH302 model

***In silico* simulation**	**Upregulated**	**Downregulated**	**Undetermined**
	Total number of nodes		
p53 wild type with DNA damage ON	**24**	**2**	**9**
	ATF3	EXPORTIN1	HOXA10
	ATM	STMN1	HOXA5
	ATR		ING4
	BTG2		PPARG
	CDK5		PRKAB1
	CHEK1		CASP2
	CHEK2		PADI4
	DKK1		POU4F1
	DUSP5		PARK2
	E2F1		
	GADD45A		
	ID3		
	IGFBP7		
	KAT2B		
	KLF4		
	MAPK1		
	MYST4		
	PTGS2		
	RAF1		
	RAS		
	TFAP2C		
	BRCA1		
	CDKN1B		
	CDKN2A		
p53 wild type with DNA damage OFF	**Upregulated**	**Downregulated**	**Undetermined**
	Total number		
	20	**6**	**9**
	ATF3	ATM	HOXA10
	CDK5	ATR	HOXA5
	CHEK2	BTG2	ING4
	DKK1	CHEK1	PPARG
	DUSP5	EXPORTIN1	PRKAB1
	E2F1	MYST4	CASP2
	GADD45A		PADI4
	ID3		POU4F1
	IGFBP7		PARK2
	KAT2B		

	KLF4		
	MAPK1		
	PTGS2		
	RAF1		
	RAS		
	STMN1		
	TFAP2C		
	BRCA1		
	CDKN1B		
	CDKN2A		
p53 knockout with DNA damage ON	**Upregulated**	**Downregulated**	**Undetermined**
	Total number		
	19	**5**	**11**
	ATF3	IGFBP7	KLF4
	ATM	GADD45A	HOXA10
	ATR	STMN1	HOXA5
	BTG2	KAT2B	DKK1
	CDK5	TFAP2C	ING4
	CHEK1		PPARG
	CHEK2		PRKAB1
	DUSP5		CASP2
	E2F1		PADI4
	ID3		PARK2
	EXPORTIN1		POU4F1
	MAPK1		
	MYST4		
	PTGS2		
	RAF1		
	RAS		
	BRCA1		
	CDKN1B		
	CDKN2A		
p53 knockout with DNA damage OFF	**Upregulated**	**Downregulated**	**Undetermined**
	Total number		
	14	**7**	**14**
	ATF3	ATM	CHEK1
	CDK5	ATR	EXPORTIN1
	CHEK2	BTG2	HOXA10
	DUSP5	DKK1	HOXA5
	E2F1	GADD45A	IGFBP7
	ID3	KLF4	ING4
	MAPK1	MYST4	KAT2B

	PTGS2		PPARG
	RAF1		PRKAB1
	RAS		TFAP2C
	BRCA1		CASP2
	CDKN1B		PADI4
	CDKN2A		PARK2
			POU4FA

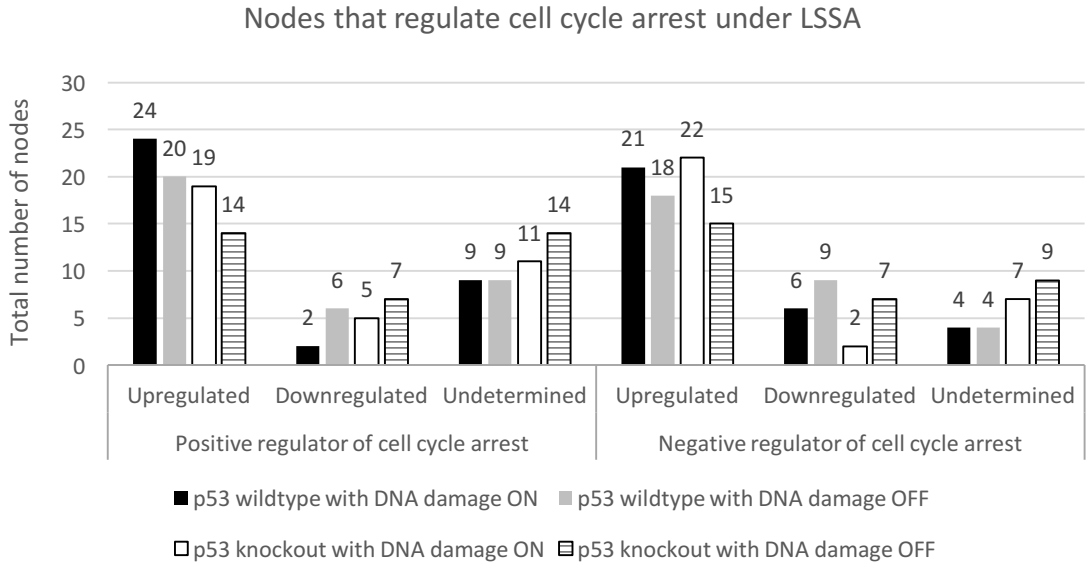

Figure 7.3.1.2 Total number and distribution of nodes regulating cell cycle arrest under LSSA in PMH302. Nodes that regulate cell cycle arrest under LSSA in response to the 4 different DNA damage and p53 simulations. The majority of pro-cell cycle arrest nodes were upregulated in p53 wild type (WT) backgrounds compared to knockout (KO).

7.3.2.2.5 Nodes regulating cellular senescence under LSSA

Of the total 73 nodes that regulate cellular senescence and globally, a greater shift towards nodes that activate cellular senescence was observed in p53 wild type backgrounds than in p53 deletion backgrounds. Conversely, a larger number of nodes that inhibit cellular senescence was also noted in p53 backgrounds compared to pro - senescence nodes in p53 presence. However, to note, the majority (> 90 %) of these anti-cell cycle arrest nodes also have other anti-proliferative roles. Tables 7.3.2.6 and 7.3.2.7 summarise node IDs and their state changes for anti and pro - cell cycle arrest nodes respectively, graphically represented in figure 7.3.1.3.

30 anti - senescence nodes were upregulated in the presence of p53 compared to 23 in the absence of p53 under DNA damage (compare lanes 13 and 15, fig. 7.3.1.3), however of these, only 5 nodes solely negatively regulated senescence, several others had additional anti-proliferative roles (DDIT4, DKK1, GADD45A, GAPDH, NME1, PCBP4, and PTEN).

Unsurprisingly, an increase in the number of pro-senescence nodes upregulated was observed in the p53 wild type background (n = 26) compared to when p53 was deleted from the network (n=18) under *in silico* DNA damage (compare lanes 1 and 3, fig. 7.3.1.3). This was similarly noted when DNA damage was OFF, the majority of nodes that inhibit cellular senescence was greater in the p53 wild type background (n=31) compared to the p53 deleted background (n=18) (compare lanes 14 and 16, fig 7.3.1.3).

Of the pro-senescence nodes downregulated, 8 for p53 deletion and 6 for p53 wild type backgrounds, CD59, DKK1, GADD45A, GAPDH and PML were downregulated in the absence of p53, whilst IFITM2, IGF1R and PSEN1 were downregulated in the presence of p53 with *in silico* DNA damage OFF (table 7.3.2.7).

Table 7.3.2.6 Nodes that negatively regulate cellular senescence in PMH302.
A total of 38 anti-cellular senescence nodes are described in PMH302.

In silico simulation	Upregulated	Downregulated	Undetermined
	Total number of nodes		
p53 wild type with DNA damage ON	**30**	**3**	**5**
	APAF1	FOXM1	CDK4
	ARID3A	S100A6	ELAVL1
	BAK1	TFDP1	FGF2
	BCL2		JAG1
	BRCA1		SOD2
	CD59		
	CKB		
	CUL7		
	DAXX		
	DDIT4		
	DKK1		
	EGFR		
	EZH2		

	FHL2		
	GADD45A		
	GAPDH		
	HIF1A		
	HNF4A		
	MCL1		
	MSH2		
	MYC		
	NME1		
	PCBP4		
	PPM1D		
	PTEN		
	RRM2B		
	SESN2		
	SGK		
	VEGFA		
	WWP1		
p53 wild type with DNA damage OFF	**Upregulated**	**Downregulated**	**Undetermined**
	Total number		
	31	**4**	**3**
	APAF1	DAXX	ELAVL1
	ARID3A	FOXM1	JAG1
	BAK1	S100A6	SOD2
	BCL2	TFDP1	
	BRCA1		
	CD59		
	CDK4		
	CKB		
	CUL7		
	DDIT4		
	DKK1		
	EGFR		
	EZH2		
	FGF2		
	FHL2		
	GADD45A		
	GAPDH		
	HIF1A		
	HNF4A		
	MCL1		
	MSH2		
	MYC		

	NME1		
	PCBP4		
	PPM1D		
	PTEN		
	RRM2B		
	SESN2		
	SGK		
	VEGFA		
	WWP1		
p53 knockout with DNA damage ON	**Upregulated**	**Downregulated**	**Undetermined**
	Total number		
	23	**6**	**9**
	APAF1	GADD45A	ELAVL1
	BCL2	ARID3A	JAG1
	BRCA1	FHL2	PTEN
	CKB	PCBP4	SOD2
	CUL7	RRM2B	BAK1
	DAXX	SESN2	CD59
	EGFR		DDIT4
	EZH2		DKK1
	HIF1A		GAPDH
	HNF4A		
	MCL1		
	MSH2		
	MYC		
	NME1		
	SGK		
	VEGFA		
	WWP1		
	CDK4		
	FGF2		
	FOXM1		
	PPM1D		
	S100A6		
	TFDP1		
p53 knockout with DNA damage OFF	**Upregulated**	**Downregulated**	**Undetermined**
	Total number		
	19	**6**	**13**
	APAF1	CD59	ARID3A
	BAK1	DAXX	ELAVL1
	BCL2	DDIT4	FHL2
	BRCA1	DKK1	FOXM1

	CDK4	GADD45A	JAG1
	CKB	GAPDH	PCBP4
	CUL7		PPM1D
	EGFR		PTEN
	EZH2		RRM2B
	FGF2		S100A6
	HIF1A		SESN2
	HNF4A		SOD2
	MCL1		TFDP1
	MSH2		
	MYC		
	NME1		
	SGK		
	VEGFA		
	WWP1		

Table 7.3.2.7 Nodes that positively regulate cellular senescence in PMH302.
A total of 35 pro -cellular senescence nodes are described in the PMH302 model.

***In silico* simulation**	**Upregulated**	**Downregulated**	**Undetermined**
	Total number of nodes		
p53 wild type with DNA damage ON	**26**	**5**	**4**
	APP	BHLHE40	ING1
	BAK1	AR	MIC1
	BCL2	IFITM2	PIN1
	C12orf5	IGF1R	PRAK
	CD59	PSEN1	
	CDKN1A		
	CDKN1B		
	CDKN2A		
	DDB2		
	DKK1		
	GADD45A		
	GAPDH		
	IFI16		
	IGFBP7		
	IL6		
	LATS2		
	MSH2		
	MYC		
	NOTCH1		

	PML		
	PRKCA		
	PTEN		
	PTGS2		
	RAS		
	SFN		
	TGFA		
p53 wild type with DNA damage OFF	**Upregulated**	**Downregulated**	**Undetermined**
	Total number		
	25	**6**	**4**
	BAK1	APP	ING1
	BCL2	AR	MIC1
	CD59	BHLHE40	PIN1
	DKK1	IFITM2	PRAK
	GADD45A	IGF1R	
	GAPDH	PSEN1	
	MSH2		
	MYC		
	PTEN		
	C12orf5		
	CDKN1A		
	CDKN1B		
	CDKN2A		
	DDB2		
	IFI16		
	IGFBP7		
	IL6		
	LATS2		
	NOTCH1		
	PML		
	PRKCA		
	PTGS2		
	RAS		
	SFN		
	TGFA		
p53 knockout with DNA damage ON	**Upregulated**	**Downregulated**	**Undetermined**
	Total number		
	18	**7**	**10**
	APP	GADD45A	ING1
	BCL2	C12ORF5	MIC1
	CDKN1A	DDB2	PIN1
	CDKN1B	IFI16	PRAK

	CDKN2A	IGFBP7	PTEN
	IL6	LATS2	BAK1
	MSH2	SFN	BHLHE40
	MYC		CD59
	NOTCH1		DKK1
	PML		GAPDH
	PRKCA		
	PTGS2		
	RAS		
	TGFA		
	AR		
	IFITM2		
	IGF1R		
	PSEN1		
p53 knockout with DNA damage OFF	**Upregulated**	**Downregulated**	**Undetermined**
	Total number		
	13	**8**	**14**
	BAK1	BHLHE40	C12orf5
	BCL2	APP	DDB2
	CDKN1A	AR	IFI16
	CDKN1B	CD59	IFITM2
	CDKN2A	DKK1	IGF1R
	IL6	GADD45A	IGFBP7
	MSH2	GAPDH	ING1
	MYC	PML	LATS2
	NOTCH1		MIC1
	PRKCA		PIN1
	PTGS2		PRAK
	RAS		PSEN1
	TGFA		PTEN
			SFN

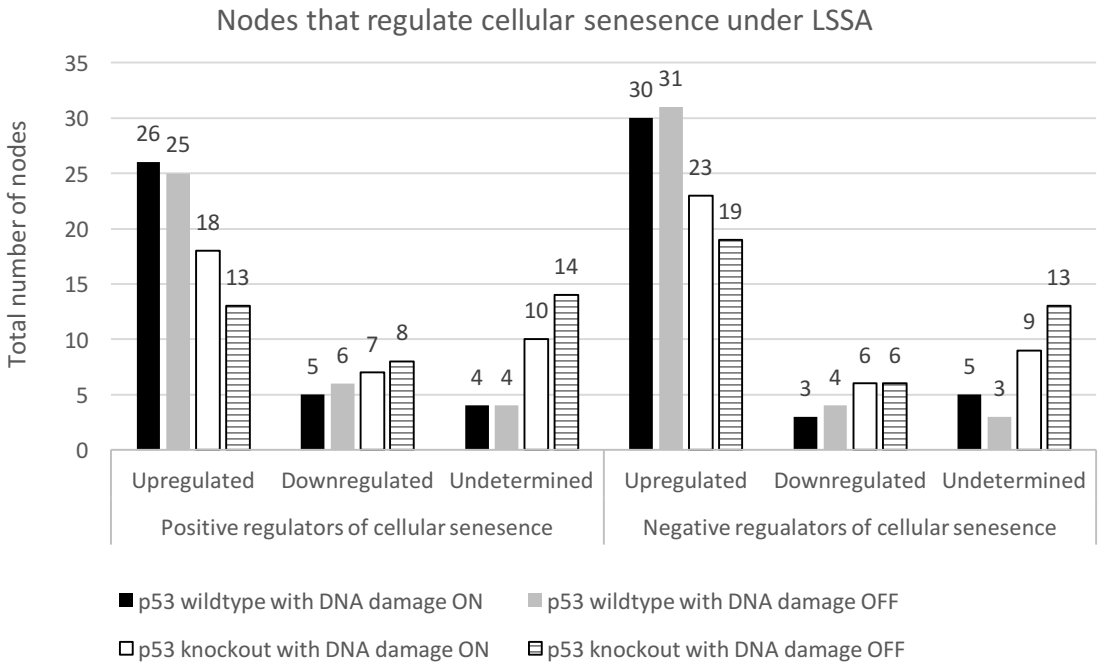

Figure 7.3.1.3 Total number and distribution of nodes regulating cellular senescence under LSSA

7.3.2.3 Hypoxia and p53 LSSA simulations

As hypoxia was included into the 302 model as another input, a further four *in silico* conditions were generated of different hypoxia inputs (ON/OFF), and p53 statuses (wild type / knockout). Their response to these conditions onto cellular fate were investigated under LSSA. The four comparative scenarios and conditions are summarised in section 6 of material and methods. A global list of all nodes under LSSA is given in table 7.3.2.8.

Table 7.3.2.8 Global list of node state changes under LSSA in PMH302 in response to different hypoxia and p53 status simulations. Distribution of all nodes (n = 302) in PMH302 under LSSA in response to the four different simulations of different p53 (WT=wild type, KO=knockout), and hypoxia statuses (section 2, material and methods). In accordance with CNA, three states exist; 1 = upregulated, 0 = downregulated, NaN = undetermined.

Node ID	p53 WT with Hypoxia ON	p53 WT with Hypoxia OFF	p53 KO with Hypoxia ON	p53 KO with Hypoxia OFF
AATF	1	1	1	1
ABCB1	1	1	1	1
ABCC1	1	1	1	1
AIFM2	1	1	NaN	NaN
AIMP2	1	1	1	1
Angiogenesis	1	1	1	1
APAF1	1	1	1	1

APEX1	0	1	0	1
Apoptosis	1	1	1	1
APP	1	0	1	0
AR	1	0	1	0
ARID3A	1	1	NaN	NaN
ASPP1	NaN	NaN	NaN	NaN
ASPP2	NaN	NaN	NaN	NaN
ATF3	1	1	1	1
ATM	1	0	1	0
ATR	1	0	1	0
AURKA	NaN	NaN	NaN	NaN
AXIN1	1	1	1	1
BAIAP2L1	NaN	NaN	NaN	NaN
BAIAP2L2	0	0	NaN	NaN
BAK1	1	1	0	1
BAX	1	1	1	1
BBC3	1	1	NaN	NaN
BCCIP	NaN	NaN	NaN	NaN
BCL2	1	1	1	1
BCL3	0	0	NaN	NaN
BCL6	1	1	1	1
BDKRB1	0	0	NaN	NaN
BHLHE40	1	0	1	0
BNIP3L	1	1	NaN	NaN
BRCA1	1	1	1	1
BTG2	1	0	1	0
C12orf5	1	1	NaN	NaN
C13orf15	1	1	NaN	NaN
CA9	1	0	1	0
CALD1	1	1	NaN	NaN
CASP2	NaN	NaN	NaN	NaN
CASP8	1	1	1	0
CCAR1	0	0	0	0
CCNA	1	1	1	1
CCNB1	0	1	1	1
CCND1	1	1	1	1
CCNG1	1	1	1	1
CD44	1	1	1	1
CD58	1	1	NaN	NaN
CD59	1	1	1	0
CD82	1	1	NaN	NaN
CDC20	0	0	NaN	NaN
CDC25A	1	1	1	1
CDK2	1	1	1	1

CDK4	1	1	1	1
CDK5	1	1	1	1
CDK9	NaN	NaN	NaN	NaN
CDKN1A	1	1	1	1
CDKN1B	1	1	1	1
CDKN2A	0	1	0	1
Cell Cycle Arrest	1	1	1	1
Cellular Senescence	1	1	1	1
CHEK1	1	0	1	NaN
CHEK2	1	1	1	1
CIAPIN1	NaN	NaN	NaN	NaN
CKB	1	1	1	1
CKM	1	1	0	0
CKS2	0	0	NaN	NaN
COL18A1	1	1	NaN	NaN
COL1A2	NaN	NaN	NaN	NaN
CSNK2	NaN	NaN	NaN	NaN
CUL7	0	1	0	1
CXCR4	1	1	1	1
CYP24A1	NaN	NaN	NaN	NaN
DAP	0	0	0	0
DAXX	0	0	0	0
DDB2	1	1	NaN	NaN
DDIT4	1	1	1	0
DDX20	NaN	NaN	NaN	NaN
DDX5	0	1	0	1
DFNA5	1	1	NaN	NaN
DKK1	1	1	1	0
DNA damage	0	0	0	0
DNA Repair	1	1	1	1
DNMT3A	NaN	NaN	NaN	NaN
DUSP1	1	0	1	0
DUSP2	1	1	NaN	NaN
DUSP4	1	1	NaN	NaN
DUSP5	1	1	1	1
DYRK2	1	0	1	0
E2F1	1	1	1	1
ECT2	0	0	NaN	NaN
EDA2R	1	1	NaN	NaN
EGFR	1	1	1	1
EGR2	1	1	NaN	NaN
EIF2AK2	NaN	NaN	NaN	NaN
EIF5A	NaN	NaN	NaN	NaN

ELAVL1	NaN	NaN	NaN	NaN
EPHB4	1	0	1	NaN
ERBB2	1	1	1	1
ESR1	1	1	1	1
EXPORTIN1	0	0	NaN	NaN
EZH2	1	1	1	1
FAS	1	1	NaN	NaN
FDXR	1	1	NaN	NaN
FEN1	1	1	0	0
FGF2	1	1	1	1
FHL2	1	1	NaN	NaN
FLI1	0	0	0	0
FOS	1	1	1	1
FOXM1	0	0	NaN	NaN
GADD45A	1	1	0	0
GAPDH	1	1	1	0
GSTP1	1	1	1	1
GTSE1	1	1	NaN	NaN
H2AFZ	NaN	NaN	NaN	NaN
HDAC1	NaN	NaN	NaN	NaN
HIC1	1	1	1	1
HIF1A	1	1	1	1
HIPK2	NaN	NaN	NaN	NaN
HIPK4	NaN	NaN	NaN	NaN
HMMR	0	0	NaN	NaN
HNF4A	0	1	0	1
HOXA10	NaN	NaN	NaN	NaN
HOXA11	NaN	NaN	NaN	NaN
HOXA5	NaN	NaN	NaN	NaN
HSP90AB1	0	0	NaN	NaN
HSPA4	1	1	1	1
HTATIP2	0	0	0	0
Hypoxia	1	0	1	0
ICAM1	1	1	1	1
ID3	1	1	1	1
IER3	1	1	1	0
IFI16	1	1	NaN	NaN
IFITM2	0	0	NaN	NaN
IFNA1	NaN	NaN	NaN	NaN
IGF1R	0	0	NaN	NaN
IGFBP1	1	1	1	0
IGFBP7	1	1	NaN	NaN
IL6	1	1	1	1
ING1	NaN	NaN	NaN	NaN

ING2	0	0	0	0
ING4	NaN	NaN	NaN	NaN
ING5	0	0	0	0
IQCB1	0	0	NaN	NaN
ISG15	1	1	NaN	NaN
JAG1	NaN	NaN	NaN	NaN
JUN	1	1	1	1
KAT2B	1	1	NaN	NaN
KIF23	0	0	NaN	NaN
KLF4	1	1	0	0
KLK3	NaN	NaN	NaN	NaN
KRT19	0	0	0	0
KRT8	1	1	NaN	NaN
LATS2	1	1	NaN	NaN
LRDD	1	1	NaN	NaN
LTF	1	1	1	1
MAP4	1	0	1	0
MAP4K4	1	1	NaN	NaN
MAPK1	1	1	1	1
MAPK14	1	1	1	1
MAPK8	1	1	1	1
MAPK9	1	0	1	0
MCL1	1	1	1	1
MCTS1	1	0	1	0
MDM2	1	1	1	1
MDM4	1	1	1	1
MGMT	0	0	NaN	NaN
MIC1	NaN	NaN	NaN	NaN
MMP1	1	1	1	1
MMP13	1	1	1	1
MMP2	1	1	1	1
MSH2	1	1	1	1
MTA1	0	0	0	0
MTA2	NaN	NaN	NaN	NaN
MUC1	1	0	1	0
MYC	1	1	1	1
MYCN	1	1	1	1
MYST4	0	0	0	0
NANOG	NaN	NaN	NaN	NaN
NCL	NaN	NaN	NaN	NaN
NFKB2	1	0	1	0
NLRC4	1	1	NaN	NaN
NME1	1	1	1	1
NOTCH1	1	1	1	1

NOV	1	1	NaN	NaN
NQO1	NaN	NaN	NaN	NaN
NR2C1	1	1	1	1
NTN1	1	0	1	0
P53	1	1	0	0
P53AIP1	1	1	1	0
PAD4	NaN	NaN	NaN	NaN
PARK2	NaN	NaN	NaN	NaN
PCBP4	1	1	NaN	NaN
PCNA	1	1	1	1
PDGFRB	0	0	NaN	NaN
PDRG1	0	0	NaN	NaN
PEG3	1	1	NaN	NaN
PERP	1	1	NaN	NaN
PHB	NaN	NaN	NaN	NaN
PHF20	NaN	NaN	NaN	NaN
PIAS1	0	0	0	0
PIAS2	NaN	NaN	NaN	NaN
PIN1	NaN	NaN	NaN	NaN
PIRH2	0	0	0	0
PITX1	0	0	0	0
PLA2G6	NaN	NaN	NaN	NaN
PLAUR	1	1	1	1
PML	1	1	0	0
POU4F1	NaN	NaN	NaN	NaN
PPARG	NaN	NaN	NaN	NaN
PPID	NaN	NaN	NaN	NaN
PPM1A	NaN	NaN	NaN	NaN
PPM1D	1	1	NaN	NaN
PRAK	NaN	NaN	NaN	NaN
PRC1	0	0	NaN	NaN
PREP1	NaN	NaN	NaN	NaN
PRKAB1	NaN	NaN	NaN	NaN
PRKCA	1	1	1	1
PRKD1	0	0	0	0
PRKDC	1	0	1	0
PRKG1	1	1	NaN	NaN
PRSS50	0	0	NaN	NaN
PSEN1	0	0	NaN	NaN
PSMD10	NaN	NaN	NaN	NaN
PTEN	1	1	NaN	NaN
PTGS2	1	1	1	1
PTTG1	1	1	1	1
RAD51	0	1	0	1

RAF1	1	1	1	1
RAS	1	1	1	1
RB	NaN	NaN	NaN	NaN
RB1CC1	NaN	NaN	NaN	NaN
RECQL4	0	0	NaN	NaN
RFC	NaN	NaN	NaN	NaN
RFWD3	0	0	0	0
RGS16	1	1	NaN	NaN
RPA1	0	0	0	0
RPRM	1	1	NaN	NaN
RPS27L	0	0	0	0
RREB1	NaN	NaN	NaN	NaN
RRM2B	1	1	NaN	NaN
RSK2	0	0	0	0
S100A2	1	1	NaN	NaN
S100A6	0	0	NaN	NaN
S100B	NaN	NaN	NaN	NaN
SEMA3B	1	1	NaN	NaN
SENP3	NaN	NaN	NaN	NaN
SERPINB5	1	1	NaN	NaN
SERPINE1	1	0	1	0
SERPINF1	1	1	1	1
SESN2	1	1	NaN	NaN
SET	NaN	NaN	NaN	NaN
SFN	1	1	NaN	NaN
SGK	1	1	1	1
SIAH1	1	1	1	1
SIVA1	1	1	1	1
SKIL	NaN	NaN	NaN	NaN
SLC2A1	1	1	1	1
SLC2A4	1	0	1	0
SLC6A6	0	1	0	1
SMYD2	NaN	NaN	NaN	NaN
SOD1	NaN	NaN	NaN	NaN
SOD2	NaN	NaN	NaN	NaN
SOX4	1	0	1	0
SP1	0	0	0	0
SP7	1	0	1	0
STAT3	1	1	1	1
STMN1	1	1	1	1
SUB1	0	0	0	0
SUMO2	NaN	NaN	NaN	NaN
SUMO3	NaN	NaN	NaN	NaN
TCF7L2	1	NaN	1	NaN

TFAP2A	1	1	0	0
TFAP2C	1	1	NaN	NaN
TFDP1	0	0	NaN	NaN
TGFA	1	1	1	1
TGFB1	1	1	1	1
THBS1	1	1	1	1
TIAF1	NaN	NaN	NaN	NaN
TLR3	1	1	NaN	NaN
TNFRSF10A	1	1	1	1
TNFRSF10B	1	1	1	1
TOP2A	0	0	0	0
TP53BP1	0	0	0	0
TP53I13	1	1	0	0
TP53INP1	1	1	0	0
TP53RK	NaN	NaN	NaN	NaN
TPT1	1	1	1	0
UBE2A	0	0	0	0
UBE3A	NaN	NaN	NaN	NaN
UCHL1	NaN	NaN	NaN	NaN
UNC5A	1	1	1	0
VEGFA	1	1	1	1
VRK1	1	0	1	0
WRN	0	0	0	0
WWOX	0	0	0	0
WWP1	0	1	0	1
XAF1	1	0	1	0
YBX1	1	1	1	1
YY1	1	0	1	0
ZMAT3	1	1	NaN	NaN
ZMIZ2	NaN	NaN	NaN	NaN
ZNF148	NaN	NaN	NaN	NaN
ZNF307	NaN	NaN	NaN	NaN

7.3.2.3.1 Nodes regulating angiogenesis under LSSA.

Under conditions of hypoxia ON and OFF, and globally, nearly a three-fold increase in anti - angiogenic nodes upregulated was seen in the p53 wild type backgrounds (n=22) compared to p53 wild type backgrounds (n=8). Conversely, a slight increase in pro-angiogenic nodes upregulated was seen in the p53 wild type backgrounds (n=45), compared to p53 deleted backgrounds (n=41). A descriptive summary of node IDs and

their LSS changes under these conditions are given in tables 7.3.2.9 and 7.3.3 for anti and pro – angiogenic nodes respectively.

No major differences were noted in upregulated pro-angiogenic node state changes between different p53 status under hypoxias; 24 in the presence of p53, 22 in the p53 deleted background (compare lanes 1 and 3 in fig. 7.3.1.4) all these nodes were identical (table 7.3.3) apart from BBC3 and CALD1 upregulated in the p53 wild type background. A two-fold upregulation of these anti-angiogenic nodes was observed when p53 was present (n=11), to when p53 was deleted (n=5) (compare lanes 13 and 15) the difference being BNIP3L, CD82, COL18A1, IFI16, PTEN, and PML, all shifted to an undetermined state when p53 was removed from the network, apart from PML which was downregulated. No anti-angiogenic nodes were downregulated in the presence of p53 under hypoxia, in fact, all (n = 11) were upregulated (table 7.3.2.9).

Comparing the *in silico* hypoxia effect in the presence of p53, nearly a two-fold increase of pro- angiogenic nodes downregulated was observed in the presence of p53 (n=7), compared to when p53 was deleted (n=4) (compare lanes 6 and 8). EPHB4, NTN1 and SERPINE1 were hypoxia responsive, upregulated when *in silico* hypoxia was ON, downregulated when OFF, this was regardless of p53 status (table 7.3.3)

Table 7.3.2.9 Anti - angiogenic nodes under LSSA in PMH302 hypoxia simulations.
A total of 15 anti-angiogenic nodes are described. Three node state changes are possible; upregulated, downregulated or undetermined (no change)

In silico simulation	Upregulated	Downregulated	Undetermined
	Total number of nodes		
p53 wild type with hypoxia ON	**11**	**0**	**6**
	BNIP3L		ELAVL1
	CD59		HOXA5
	CD82		ING1
	COL18A1		ING4
	DKK1		NQO1
	IFI16		PPARG
	NOTCH1		
	PML		
	PTEN		
	SERPINF1		

	TGFB1		
p53 wild type with DNA hypoxia OFF	**Upregulated**	**Downregulated**	**Undetermined**
	Total number		
	11	**0**	**6**
	BNIP3L		ELAVL1
	CD59		HOXA5
	CD82		ING1
	COL18A1		ING4
	DKK1		NQO1
	IFI16		PPARG
	NOTCH1		
	PML		
	PTEN		
	SERPINF1		
	TGFB1		
p53 knockout with hypoxia ON	**Upregulated**	**Downregulated**	**Undetermined**
	Total number		
	5	**1**	**11**
	CD59	PML	BNIP3L
	DKK1		CD82
	NOTCH1		COL18A1
	SERPINF1		ELAVL1
	TGFB1		HOXA5
			IFI16
			ING1
			ING4
			NQO1
			PPARG
			PTEN
p53 knockout with hypoxia OFF	**Upregulated**	**Downregulated**	**Undetermined**
	Total number		
	3	**3**	**11**
	NOTCH1	CD59	BNIP3L
	SERPINF1	DKK1	CD82
	TGFB1	PML	COL18A1
			ELAVL1
			HOXA5
			IFI16
			ING1
			ING4
			NQO1
			PPARG
			PTEN

Table 7.3.3 Pro- angiogenic nodes under LSSA in PMH302 hypoxia simulations
A total of 35 pro-angiogenic nodes are described in the PMH302 model

In silico simulation	Upregulated	Downregulated	Undetermined
	Total number of nodes		
p53 wild type with hypoxia ON	**24**	**4**	**7**
	BBC3	BDKRB1	ELAVL1
	BCL2	MTA1	JAG1
	CALD1	PDGFRB	MIC1
	CCND1	RSK2	NANOG
	CD44		PHB
	CDK2		S100B
	CDK4		SENP3
	CDK5		
	EGFR		
	EPHB4		
	FGF2		
	HIF1A		
	HSPA4		
	JUN		
	MMP1		
	MMP13		
	NTN1		
	PRKCA		
	PTGS2		
	SERPINE1		
	SGK		
	STMN1		
	TGFA		
	VEGFA		
p53 wild type with hypoxia OFF	**Upregulated**	**Downregulated**	**Undetermined**
	Total number		
	21	**7**	**7**
	BBC3	BDKRB1	ELAVL1
	BCL2	EPHB4	JAG1
	CALD1	MTA1	MIC1
	CCND1	NTN1	NANOG
	CD44	PDGFRB	PHB
	CDK2	RSK2	S100B
	CDK4	SERPINE1	SENP3
	CDK5		
	EGFR		
	FGF2		
	HIF1A		

	HSPA4		
	JUN		
	MMP1		
	MMP13		
	PRKCA		
	PTGS2		
	SGK		
	STMN1		
	TGFA		
	VEGFA		
p53 knockout with hypoxia ON	**Upregulated**	**Downregulated**	**Undetermined**
	Total number		
	22	**2**	**11**
	BCL2	MTA1	BBC3
	CCND1	RSK2	BDKRB1
	CD44		CALD1
	CDK2		ELAVL1
	CDK4		JAG1
	CDK5		MIC1
	EGFR		NANOG
	EPHB4		PDGFRB
	FGF2		PHB
	HIF1A		S100B
	HSPA4		SENP3
	JUN		
	MMP1		
	MMP13		
	NTN1		
	PRKCA		
	PTGS2		
	SERPINE1		
	SGK		
	STMN1		
	TGFA		
	VEGFA		
p53 knockout with hypoxia OFF	**Upregulated**	**Downregulated**	**Undetermined**
	Total number		
	19	**4**	**12**
	BCL2	MTA1	BBC3
	CCND1	NTN1	BDKRB1
	CD44	RSK2	CALD1
	CDK2	SERPINE1	ELAVL1
	CDK4		EPHB4
	CDK5		JAG1

	EGFR		MIC1
	FGF2		NANOG
	HIF1A		PDGFRB
	HSPA4		PHB
	JUN		S100B
	MMP1		SENP3
	MMP13		
	PRKCA		
	PTGS2		
	SGK		
	STMN1		
	TGFA		
	VEGFA		

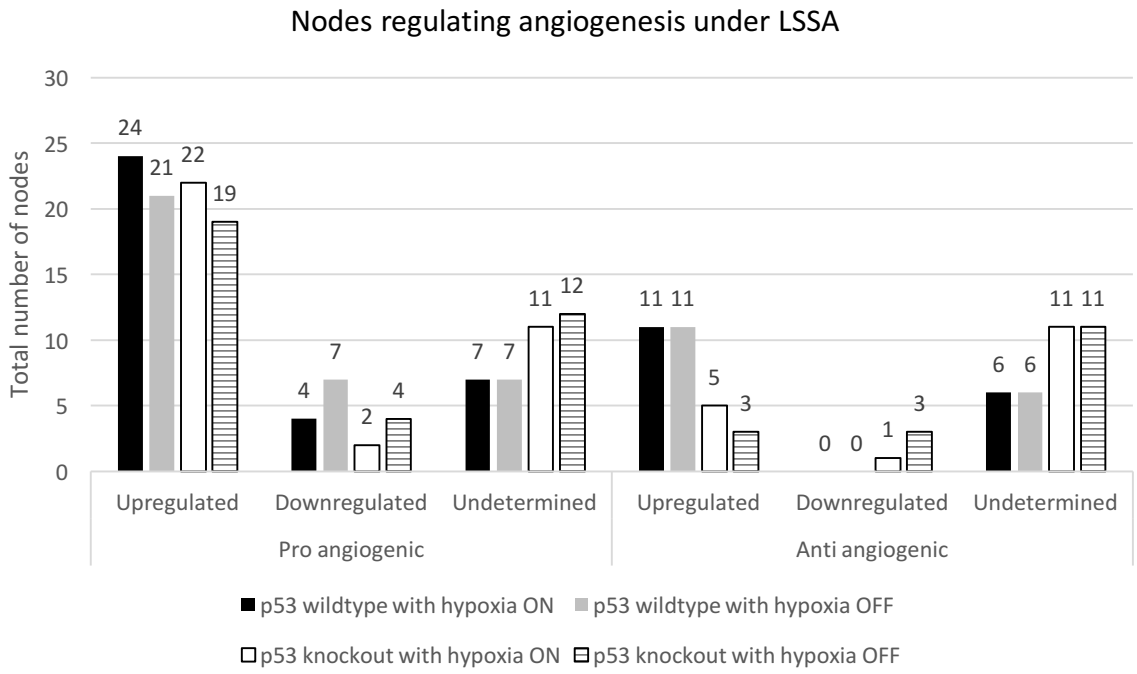

Figure 7.3.1.4 Total number and distribution of nodes regulating angiogenesis under LSSA in PMH302 hypoxia simulations

7.3.2.3.2 Nodes regulating apoptosis under LSSA

A total of 131 apoptotic nodes were described in the 302 model, of these 50 were considered as anti-apoptotic and 81 pro-apoptotic. Globally for these apoptotic nodes under differential *in silico* hypoxic conditions a greater number of pro-apoptotic nodes were upregulated in the presence of p53, compared to pro-apoptotic nodes upregulated in the absence of p53. However, an increase in anti-apoptotic nodes

upregulated in p53 wild type backgrounds compared to p53 deleted backgrounds under *in silico* hypoxia was also observed. A list of node IDs and their LSS changes in response to the four conditions are summarised in tables 7.3.3.1 and 7.3.3.2 for pro and anti-apoptotic nodes respectively. Figure 7.3.1.5 provides a graphical representation, globally.

Nearly a two – fold increase was observed in pro-apoptotic nodes upregulated in the presence of p53 (n=60) compared to 31 in the p53 deleted background under hypoxia (compare lanes 1 and 3 in fig. 7.3.1.5). Of the anti-apoptotic nodes, 35 were upregulated in the presence of p53 compared to only 29 in p53 absence under in silico hypoxia. Of these nodes, all were identical (table 7.3.3.2) apart from, C12orf5, DUSP2/4, MAP4K4, PTGS2 and SFN upregulated in the presence of p53 under *in silico* hypoxia. Another major change noted was the number of nodes that shifted to an undetermined state when p53 was deleted from the network; 10 for p53 wild type and 37 for p53 knockout.

No major difference in the number of anti-apoptotic nodes upregulated in p53 wild type backgrounds when hypoxia was OFF and ON; 35 and 34 for hypoxia ON and OFF respectively (compare lanes 13 and 14 fig. 7.3.1.5) however, of these, AR, EPHB4, NFKB2, TCF7L2 and WWP1 were all upregulated when hypoxia was ON (table 7.3.3.2).

29 and 25 anti-apoptotic nodes were upregulated when hypoxia was ON compared to when it was OFF respectively in p53 deletion backgrounds. Of these, AR, IER3, NFKB2, TCF7L2, TPT1 were all upregulated in response to *in silico* hypoxia ON (table 7.3.3.2). Whilst, WWP1, APEX1 and CUL7 were upregulated when OFF

Table 7.3.3.1 Pro apoptotic nodes under LSSA in PMH302 hypoxia simulations.
A total of 81 pro – apoptotic nodes are described in PMH302.

***In silico* simulation**	**Upregulated**	**Downregulated**	**Undetermined**
	Total number of nodes		
p53 wild type with hypoxia ON	**60**	**11**	**10**
	AIFM2	DAP	ASPP1
	APAF1	DAXX	ASPP2
	APP	ECT2	CASP2

	AR	IFITM2	CYP24A1
	ATF3	ING5	DDX20
	BAK1	PITX1	HOXA10
	BAX	PRSS50	ING4
	BBC3	SERPINE1	MIC1
	BNIP3L	TOP2A	UCHL1
	CASP8	WWOX	ZNF148
	CCNG1	XAF1	
	CD44		
	CDC25A		
	CDKN1B		
	COL18A1		
	CXCR4		
	DDIT4		
	DFNA5		
	DKK1		
	DUSP2		
	DUSP4		
	EGFR		
	ESR1		
	FAS		
	FDXR		
	FGF2		
	FOS		
	GADD45A		
	IFI16		
	IGFBP7		
	IL6		
	JUN		
	KAT2B		
	LATS2		
	LRDD		
	MAP4K4		
	MSH2		
	NLRC4		
	NOTCH1		
	P53AIP1		
	PCBP4		
	PEG3		
	PERP		
	PML		
	PRKCA		
	PTEN		
	PTGS2		
	SEMA3B		
	SERPINB5		
	SERPINE1		
	SIAH1		
	SIVA1		
	TFAP2C		

	TLR3		
	TNFRSF10A		
	TNFRSF10B		
	TP53INP1		
	XAF1		
	TFAP2A		
	NFKB2		
p53 wild type with hypoxia OFF	**Upregulated**	**Downregulated**	**Undetermined**
	Total number		
	57	**14**	**10**
	AIFM2	APP	ASPP1
	APAF1	AR	ASPP2
	ATF3	DAP	CASP2
	BAK1	DAXX	CYP24A1
	BAX	ECT2	DDX20
	BBC3	IFITM2	HOXA10
	BNIP3L	ING5	ING4
	CASP8	PITX1	MIC1
	CCNG1	PRSS50	UCHL1
	CD44	SERPINE1	ZNF148
	CDC25A	TOP2A	
	CDKN1B	WWOX	
	CDKN2A	XAF1	
	COL18A1	NFKB2	
	CXCR4		
	DDIT4		
	DFNA5		
	DKK1		
	DUSP2		
	DUSP4		
	EGFR		
	ESR1		
	FAS		
	FDXR		
	FGF2		
	FOS		
	GADD45A		
	HNF4A		
	IFI16		
	IGFBP7		
	IL6		
	JUN		
	KAT2B		
	LATS2		
	LRDD		
	MAP4K4		
	MSH2		
	NLRC4		
	NOTCH1		
	P53AIP1		

	PCBP4		
	PEG3		
	PERP		
	PML		
	PRKCA		
	PTEN		
	PTGS2		
	SEMA3B		
	SERPINB5		
	SIAH1		
	SIVA1		
	TFAP2C		
	TLR3		
	TNFRSF10A		
	TNFRSF10B		
	TP53INP1		
	TFAP2A		
p53 knockout with hypoxia ON	**Upregulated**	**Downregulated**	**Undetermined**
	Total number		
	31	**13**	**37**
	APAF1	BAK1	AIFM2
	APP	CDKN2A	ASPP1
	AR	DAP	ASPP2
	ATF3	DAXX	BBC3
	BAX	GADD45A	BNIP3L
	CASP8	HNF4A	CASP2
	CCNG1	ING5	COL18A1
	CD44	PITX1	CYP24A1
	CDC25A	PML	DDX20
	CDKN1B	TOP2A	DFNA5
	CXCR4	TP53INP1	DUSP2
	DDIT4	WWOX	DUSP4
	DKK1	TFAP2A	ECT2
	EGFR		FAS
	ESR1		FDXR
	FGF2		HOXA10
	FOS		IFI16
	IL6		IFITM2
	JUN		IGFBP7
	MSH2		ING4
	NOTCH1		KAT2B
	P53AIP1		LATS2
	PRKCA		LRDD
	PTGS2		MAP4K4
	SERPINE1		MIC1
	SIAH1		NLRC4
	SIVA1		PCBP4
	TNFRSF10A		PEG3
	TNFRSF10B		PERP
	XAF1		PRSS50

	NFKB2		PTEN
			SEMA3B
			SERPINB5
			TFAP2C
			TLR3
			UCHL1
			ZNF148
p53 knockout with hypoxia OFF	**Upregulated**	**Downregulated**	**Undetermined**
	Total number		
	25	**19**	**37**
	APAF1	APP	ASPP1
	ATF3	AR	ASPP2
	BAK1	CASP8	BBC3
	BAX	DAP	BNIP3L
	CCNG1	DAXX	CASP2
	CD44	DDIT4	COL18A1
	CDC25A	DKK1	CYP24A1
	CDKN1B	GADD45A	DDX20
	CDKN2A	ING5	DFNA5
	CXCR4	P53AIP1	DUSP2
	EGFR	PITX1	DUSP4
	ESR1	PML	ECT2
	FGF2	SERPINE1	FAS
	FOS	TOP2A	FDXR
	HNF4A	TP53INP1	HOXA10
	IL6	WWOX	IFI16
	JUN	XAF1	IFITM2
	MSH2	NFKB2	IGFBP7
	NOTCH1	TFAP2A	ING4
	PRKCA		KAT2B
	PTGS2		LATS2
	SIAH1		LRDD
	SIVA1		MAP4K4
	TNFRSF10A		MIC1
	TNFRSF10B		NLRC4
			PCBP4
			PEG3
			PERP
			PRSS50
			PTEN
			SEMA3B
			SERPINB5
			TFAP2C
			TLR3
			UCHL1
			ZNF148

Table 7.3.3.2 Anti -apoptotic nodes under LSSA in PMH302 hypoxia simulations.
A total of 50 anti – apoptotic nodes are described in PMH302.

In silico scenario	Upregulated	Downregulated	Undetermined
	Total number of nodes		
p53 wild type with hypoxia ON	**35**	**11**	**4**
	AR	APEX1	NANOG
	ATF3	BCL3	PREP1
	BCL2	CKS2	RB1CC1
	C12orf5	CUL7	TP53RK
	CCNG1	DAXX	
	CD44	FLI1	
	CDC25A	IGF1R	
	CDKN1A	MTA1	
	CDKN1B	PDGFRB	
	DDIT4	PSEN1	
	DUSP2	WWP1	
	DUSP4		
	EGFR		
	EPHB4		
	ESR1		
	EZH2		
	FGF2		
	FHL2		
	FOS		
	GSTP1		
	IER3		
	IL6		
	MAP4K4		
	MCL1		
	NFKB2		
	NOTCH1		
	PRKCA		
	PTGS2		
	SFN		
	SGK		
	STAT3		
	TCF7L2		
	TGFA		
	TPT1		
	VEGFA		
p53 wild type with hypoxia OFF	**Upregulated**	**Downregulated**	**Undetermined**
	Total number of nodes		
	34	**11**	**4**
	APEX1	AR	NANOG
	ATF3	BCL3	PREP1

	BCL2	CKS2	RB1CC1
	C12orf5	DAXX	TCF7L2
	CCNG1	EPHB4	TP53RK
	CD44	FLI1	
	CDC25A	IGF1R	
	CDKN1A	MTA1	
	CDKN1B	NFKB2	
	CUL7	PDGFRB	
	DDIT4	PSEN1	
	DUSP2		
	DUSP4		
	EGFR		
	ESR1		
	EZH2		
	FGF2		
	FHL2		
	FOS		
	GSTP1		
	IER3		
	IL6		
	MAP4K4		
	MCL1		
	NOTCH1		
	PRKCA		
	PTGS2		
	SFN		
	SGK		
	STAT3		
	TGFA		
	TPT1		
	VEGFA		
	WWP1		
p53 knockout with hypoxia ON	**Upregulated**	**Downregulated**	**Undetermined**
	Total number of nodes		
	29	**6**	**15**
	AR	APEX1	BCL3
	ATF3	CUL7	C12orf5
	BCL2	DAXX	CKS2
	CCNG1	FLI1	DUSP2
	CD44	MTA1	DUSP4
	CDC25A	WWP1	FHL2
	CDKN1A		IGF1R
	CDKN1B		MAP4K4
	DDIT4		NANOG

	EGFR		PDGFRB
	EPHB4		PREP1
	ESR1		PSEN1
	EZH2		RB1CC1
	FGF2		SFN
	FOS		TP53RK
	GSTP1		
	IER3		
	IL6		
	MCL1		
	NFKB2		
	NOTCH1		
	PRKCA		
	PTGS2		
	SGK		
	STAT3		
	TCF7L2		
	TGFA		
	TPT1		
	VEGFA		
p53 knockout with hypoxia OFF	**Upregulated**	**Downregulated**	**Undetermined**
	Total number of nodes		
	25	**8**	**17**
	APEX1	AR	BCL3
	ATF3	DAXX	C12orf5
	BCL2	DDIT4	CKS2
	CCNG1	FLI1	DUSP2
	CD44	IER3	DUSP4
	CDC25A	MTA1	EPHB4
	CDKN1A	NFKB2	FHL2
	CDKN1B	TPT1	IGF1R
	CUL7		MAP4K4
	EGFR		NANOG
	ESR1		PDGFRB
	EZH2		PREP1
	FGF2		PSEN1
	FOS		RB1CC1
	GSTP1		SFN
	IL6		TCF7L2
	MCL1		TP53RK
	NOTCH1		
	PRKCA		
	PTGS2		
	SGK		

	STAT3		
	TGFA		
	VEGFA		
	WWP1		

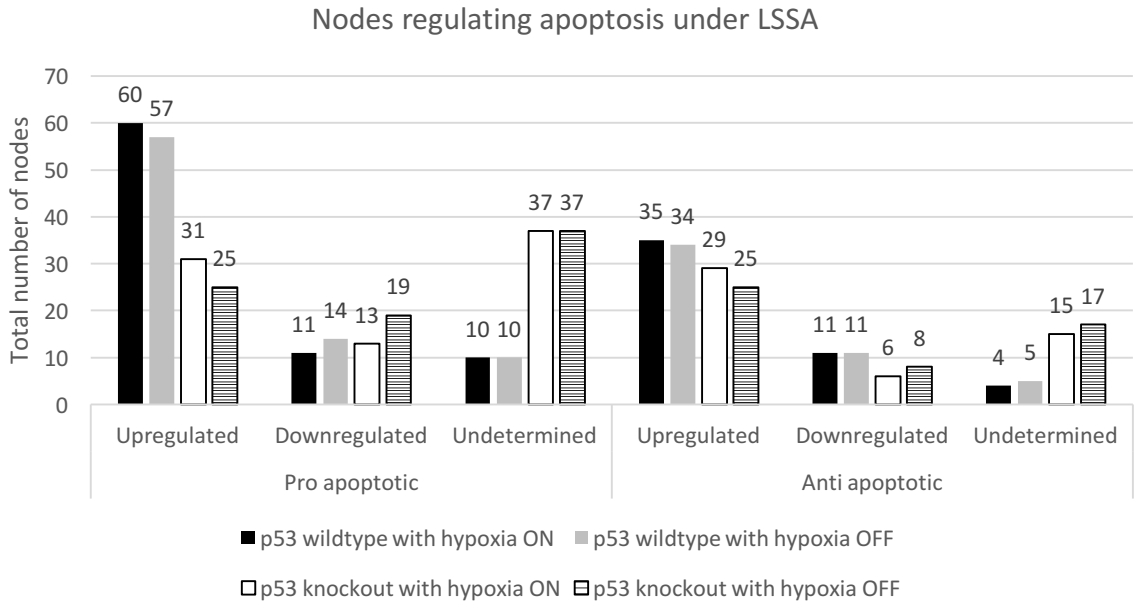

Figure 7.3.1.5 Total number and distribution of nodes regulating apoptosis in PMH302 hypoxia simulations under LSSA.

7.3.2.3.3 Nodes regulating cell cycle arrest under LSSA.

A total of 66 nodes regulating cell cycle arrest are described in PMH302. Globally, comparing pro and anti-cell cycle arrest nodes and under differential *in silico* hypoxic conditions a greater shift to nodes upregulated that activate cell cycle arrest was noted compared to nodes upregulated that inhibit cell cycle arrest in the p53 wild type backgrounds

Under *in silico* hypoxia, in the presence of p53 there was an increase of pro-cell cycle arrest upregulated (n=23) compared to the p53 deletion background (n=18) (compare lanes 1 and 3 in fig. 7.3.1.6). A similar number of anti-cell cycle arrest nodes were upregulated regardless of p53 status; 19 upregulated for p53 wild type and 18 upregulated for p53 knockout under hypoxia (compare lanes 13 and 15). Of these,

CCNB1 was exclusively upregulated in the absence of p53 under hypoxia, whilst ISG15 and RGS16 were upregulated in the presence of p53 (table 7.3.3.3). In fact, ISG15, RGS16 were exclusively p53 responsive. Tables 7.3.3.3 and 7.3.3.4 summarise node state changes for anti and pro- cell cycle arrest nodes respectively.

Table 7.3.3.3 Nodes that negatively regulate cell cycle arrest under LSSA in PMH302 hypoxia simulations. A total of 31 anti-cell cycle arrest nodes are described.

***In silico* simulation**	**Upregulated**	**Downregulated**	**Undetermined**
	Total number of nodes		
p53 wild type with hypoxia ON	**19**	**8**	**4**
	APAF1	CCNB1	AURKA
	AR	CKS2	HDAC1
	ATF3	CUL7	JAG1
	CCNA	ING5	PRAK
	CDK2	MTA1	
	E2F1	RAD51	
	EPHB4	S100A6	
	IER3	UBE2A	
	ISG15		
	JUN		
	MCL1		
	MUC1		
	MYC		
	RGS16		
	SIVA1		
	SLC2A1		
	VRK1		
	YBX1		
	MYC		
p53 wild type with hypoxia OFF	**Upregulated**	**Downregulated**	**Undetermined**
	Total number		
	18	**9**	**4**
	APAF1	AR	AURKA
	ATF3	CKS2	HDAC1
	CCNA	EPHB4	JAG1
	CCNB1	ING5	PRAK
	CDK2	MTA1	
	CUL7	MUC1	
	E2F1	S100A6	
	IER3	UBE2A	
	ISG15	VRK1	
	JUN		
	MCL1		

	MYC		
	RAD51		
	RGS16		
	SIVA1		
	SLC2A1		
	YBX1		
	MYCN		
p53 knockout with hypoxia ON	**Upregulated**	**Downregulated**	**Undetermined**
	Total number		
	18	**5**	**8**
	APAF1	CUL7	AURKA
	AR	ING5	CKS2
	ATF3	MTA1	HDAC1
	CCNA	RAD51	ISG15
	CCNB1	UBE2A	JAG1
	CDK2		PRAK
	E2F1		RGS16
	EPHB4		S100A6
	IER3		
	JUN		
	MCL1		
	MUC1		
	MYC		
	SIVA1		
	SLC2A1		
	VRK1		
	YBX1		
	MYCN		
p53 knockout with hypoxia OFF	**Upregulated**	**Downregulated**	**Undetermined**
	Total number		
	15	**7**	**9**
	APAF1	AR	AURKA
	ATF3	IER3	CKS2
	CCNA	ING5	EPHB4
	CCNB1	MTA1	HDAC1
	CDK2	MUC1	ISG15
	CUL7	UBE2A	JAG1
	E2F1	VRK1	PRAK
	JUN		RGS16
	MCL1		S100A6
	MYC		
	RAD51		
	SIVA1		
	SLC2A1		

	YBX1		
	MYCN		

Table 7.3.3.4 Nodes that positively regulate cell cycle arrest under LSSA in PMH302 hypoxia simulations. A total of 35 pro-cell cycle arrest nodes are described in PMH302.

***In silico* simulation**	**Upregulated**	**Downregulated**	**Undetermined**
	Total number of nodes		
p53 wild type with hypoxia ON	**23**	**3**	**9**
	ATF3	EXPORTIN1	HOXA10
	ATM	MYST4	HOXA5
	ATR	CDKN2A	ING4
	BTG2		PPARG
	CDK5		PRKAB1
	CHEK1		CASP2
	CHEK2		PADI4
	DKK1		PARK2
	DUSP5		POU4F1
	E2F1		
	GADD45A		
	ID3		
	IGFBP7		
	KAT2B		
	KLF4		
	MAPK1		
	PTGS2		
	RAF1		
	RAS		
	STMN1		
	TFAP2C		
	CDKN1B		
	BRCA1		
p53 wild type with hypoxia OFF	**Upregulated**	**Downregulated**	**Undetermined**
	Total number		
	20	**6**	**9**
	ATF3	ATM	HOXA10
	E2F1	ATR	HOXA5
	CDK5	BTG2	ING4
	CHEK2	CHEK1	PPARG
	DKK1	EXPORTIN1	PRKAB1
	DUSP5	MYST4	CASP2
	GADD45A		PADI4

	ID3		PARK2
	IGFBP7		POU4F1
	KAT2B		
	KLF4		
	MAPK1		
	PTGS2		
	RAF1		
	RAS		
	STMN1		
	TFAP2C		
	BRCA1		
	CDKN1B		
	CDKN2A		
p53 knockout with hypoxia ON	**Upregulated**	**Downregulated**	**Undetermined**
	Total number		
	18	**4**	**9**
	ATF3	GADD45A	EXPORTIN1
	ATM	KLF4	HOXA10
	ATR	MYST4	HOXA5
	BTG2	CDKN2A	IGFBP7
	CDK5		ING4
	CHEK1		KAT2B
	CHEK2		PPARG
	DKK1		PRKAB1
	DUSP5		TFAP2C
	E2F1		POU4F1
	ID3		PARK2
	MAPK1		PADI4
	PTGS2		CASP2
	RAF1		
	RAS		
	STMN1		
	BRCA1		
	CDKN1B		
p53 knockout with hypoxia OFF	**Upregulated**	**Downregulated**	**Undetermined**
	Total number		
	14	7	14
	ATF3	ATM	CHEK1
	CDK5	ATR	EXPORTIN1
	CHEK2	BTG2	HOXA10
	DUSP5	DKK1	HOXA5
	E2F1	GADD45A	IGFBP7
	ID3	KLF4	ING4
	MAPK1	MYST4	KAT2B

	PTGS2		PPARG
	RAF1		PRKAB1
	RAS		TFAP2C
	STMN1		POU4F1
	BRCA1		PARK2
	CDKN1B		PADI4
	CDKN2A		CASP2

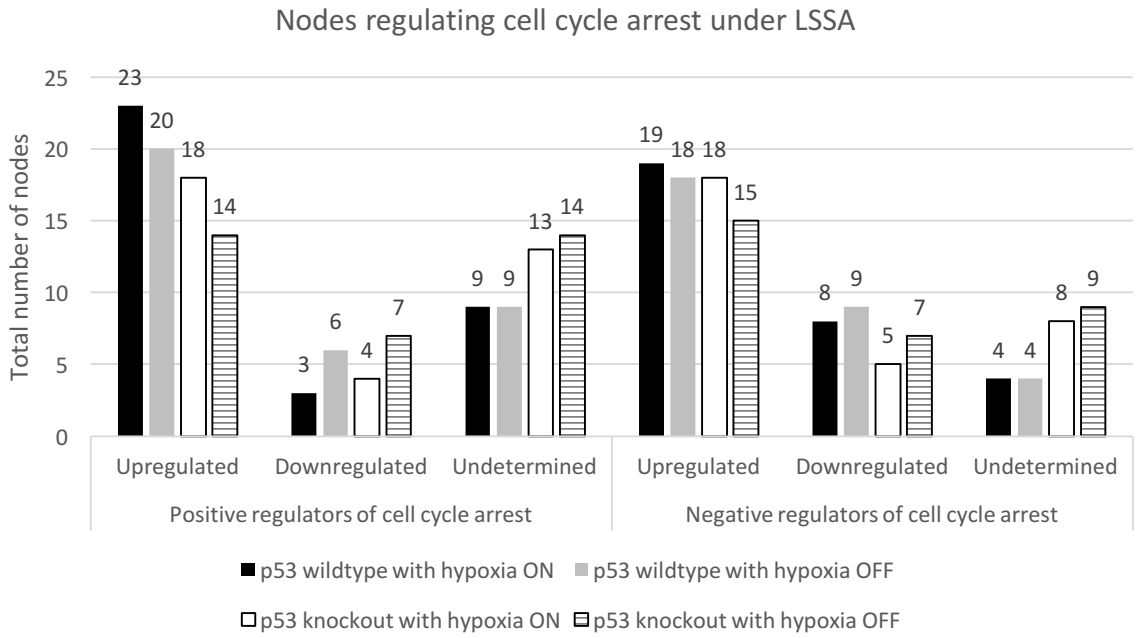

Figure 7.3.1.6 Total number and distribution of nodes regulating cell cycle arrest under LSSA in PMH302 hypoxia simulations. A total of 66 nodes that regulated cell cycle arrest were considered in PMH302. The majority of pro-cell cycle arrest nodes were upregulated in p53 wild type compared to knockout backgrounds.

7.3.2.3.4 Nodes regulating cellular senescence under LSSA

A total of 73 nodes that regulate cellular senescence are described in PMH302. Of these, 35 are positive regulators, 38 negative regulators of senescence. Globally across all conditions under differential *in silico* hypoxic conditions, a greater number of pro - cellular senescence nodes were upregulated in the presence of p53, than in p53s absence.

Investigating the effect of p53 status when the hypoxic input was switched OFF, nearly a two-fold increase in pro-senescence nodes upregulated was observed in the presence of p53 (n=25) than in its absence (n=13) (compare lanes 2 and 4 in fig. 7.3.1.7). Comparable to this, 31 anti –senescence nodes were upregulated in p53 wild type background compared to 19 in the p53 deleted background (compare lanes 14 and 16). Of the pro-senescence nodes downregulated, 8 in the absence of p53 compared to 6 in p53 presence, PML, GAPDH, GADD45A, DKK1 and CD59 were exclusively downregulated in the absence of p53, whilst IFITM2, IGF1R and PSEN1 were downregulated when p53 was present (table 7.3.3.6).

In the p53 wild type backgrounds, 31 anti-senescence nodes upregulated when hypoxia was OFF, compared to 28 upregulated when hypoxia was ON. Of these, CUL7, DKK1 and HNF4A were the differential nodes upregulated in the absence of hypoxia (table 7.3.3.5).

The number of anti-senescence nodes upregulated and downregulated were identical regardless of hypoxic input in p53 knockout backgrounds; 19 upregulated for both hypoxia ON and OFF (compare lanes 13 and 16 fig. 7.3.1.7). Even so, of these anti-senescence nodes, CD59, DDIT4 and DKK1 were upregulated in response to *in silico* hypoxia, whilst BAK1, CUL7 and HNF4A were upregulated when hypoxia was switched OFF (table 7.3.3.5). The number of pro-senescence nodes downregulated was identical (n=4) for both conditions, however BAK1, CDKN2A and PML were downregulated when hypoxia was ON, whilst CD59, DKK1 and GAPDH were downregulated when hypoxia was OFF in p53 deletion backgrounds. GADD45A was p53 responsive, downregulated in both conditions, regardless of hypoxia (table 7.3.3.6). As in all other p53 deleted conditions, majority of nodes shifted to an undetermined state when p53 was removed from the network. Tables 7.3.3.5 and 7.3.3.6 summarise their node state changes in response to the four conditions of different hypoxia input and p53 statuses under LSSA.

Table 7.3.3.5 Nodes that negatively regulate cellular senescence under LSSA in PMH302 hypoxia simulations. A total of 38 anti – senescence nodes are described in PMH302.

In silico simulation	Upregulated	Downregulated	Undetermined
	Total number of nodes		
p53 wild type with hypoxia ON	**28**	**7**	**3**
	APAF1	CUL7	ELAVL1
	ARID3A	DAXX	JAG1
	BAK1	FOXM1	SOD2
	BCL2	HNF4A	
	BRCA1	S100A6	
	CD59	TFDP1	
	CDK4	WWP1	
	CKB		
	DDIT4		
	DKK1		
	EGFR		
	EZH2		
	FGF2		
	FHL2		
	GADD45A		
	GAPDH		
	HIF1A		
	MCL1		
	MSH2		
	MYC		
	NME1		
	PCBP4		
	PPM1D		
	PTEN		
	RRM2B		
	SESN2		
	SGK		
	VEGFA		
p53 wild type with hypoxia OFF	**Upregulated**	**Downregulated**	**Undetermined**
	Total number		
	31	**4**	**3**
	APAF1	DAXX	ELAVL1
	ARID3A	FOXM1	JAG1
	BAK1	S100A6	SOD2
	BCL2	TFDP1	
	BRCA1		
	CD59		
	CDK4		
	CKB		
	CUL7		
	DDIT4		
	DKK1		
	EGFR		
	EZH2		

	FGF2		
	FHL2		
	GADD45A		
	GAPDH		
	HIF1A		
	HNF4A		
	MCL1		
	MSH2		
	MYC		
	NME1		
	PCBP4		
	PPM1D		
	PTEN		
	RRM2B		
	SESN2		
	SGK		
	VEGFA		
	WWP1		
p53 knockout with hypoxia ON	**Upregulated**	**Downregulated**	**Undetermined**
	Total number		
	19	**6**	**13**
	APAF1	BAK1	ARID3A
	BCL2	CUL7	ELAVL1
	BRCA1	DAXX	FHL2
	CD59	GADD45A	FOXM1
	CDK4	HNF4A	JAG1
	CKB	WWP1	PCBP4
	DDIT4		PPM1D
	DKK1		PTEN
	EGFR		RRM2B
	EZH2		S100A6
	FGF2		SESN2
	GAPDH		SOD2
	HIF1A		TFDP1
	MCL1		
	MSH2		
	MYC		
	NME1		
	SGK		
	VEGFA		
p53 knockout with hypoxia OFF	**Upregulated**	**Downregulated**	**Undetermined**
	Total number		
	19	6	13
	APAF1	CD59	ARID3A
	BAK1	DAXX	ELAVL1
	BCL2	DDIT4	FHL2
	BRCA1	DKK1	FOXM1
	CDK4	GADD45A	JAG1
	CKB	GAPDH	PCBP4
	CUL7		PPM1D

	EGFR		PTEN
	EZH2		RRM2B
	FGF2		S100A6
	HIF1A		SESN2
	HNF4A		SOD2
	MCL1		TFDP1
	MSH2		
	MYC		
	NME1		
	SGK		
	VEGFA		
	WWP1		

Table 7.3.3.6 Nodes that positively regulate cellular senescence under LSSA in PMH302 hypoxia simulations. A total of 35 pro – senescence nodes are described in PMH302.

***In silico* simulation**	**Upregulated**	**Downregulated**	**Undetermined**
	Total number of nodes		
p53 wild type with hypoxia ON	**27**	**4**	**4**
	APP	CDKN2A	ING1
	AR	IFITM2	MIC1
	BAK1	IGF1R	PIN1
	BCL2	PSEN1	PRAK
	BHLHE40		
	C12orf5		
	CD59		
	CDKN1A		
	CDKN1B		
	DDB2		
	DKK1		
	GADD45A		
	GAPDH		
	IFI16		
	IGFBP7		
	IL6		
	LATS2		
	MSH2		
	MYC		
	NOTCH1		
	PML		
	PRKCA		
	PTEN		
	PTGS2		
	RAS		
	SFN		

	TGFA		
p53 wild type with DNA hypoxia OFF	**Upregulated**	**Downregulated**	**Undetermined**
	Total number		
	25	**6**	**4**
	BAK1	APP	ING1
	BCL2	AR	MIC1
	C12orf5	BHLHE40	PIN1
	CD59	IFITM2	PRAK
	CDKN1A	IGF1R	
	CDKN1B	PSEN1	
	CDKN2A		
	DDB2		
	DKK1		
	GADD45A		
	GAPDH		
	IFI16		
	IGFBP7		
	IL6		
	LATS2		
	MSH2		
	MYC		
	NOTCH1		
	PML		
	PRKCA		
	PTEN		
	PTGS2		
	RAS		
	SFN		
	TGFA		
p53 knockout with hypoxia ON	**Upregulated**	**Downregulated**	**Undetermined**
		Total number	
	17	**4**	**14**
	APP	BAK1	C12orf5
	AR	CDKN2A	DDB2
	BCL2	GADD45A	IFI16
	BHLHE40	PML	IFITM2
	CD59		IGF1R
	CDKN1A		IGFBP7
	CDKN1B		ING1
	DKK1		LATS2
	GAPDH		MIC1
	IL6		PIN1
	MSH2		PRAK
	MYC		PSEN1

	NOTCH1		PTEN
	PRKCA		SFN
	PTGS2		
	RAS		
	TGFA		
p53 knockout with hypoxia OFF	**Upregulated**	**Downregulated**	**Undetermined**
		Total number	
	13	**8**	**14**
	BAK1	CD59	PTEN
	BCL2	DKK1	C12orf5
	MSH2	GADD45A	DDB2
	MYC	GAPDH	IFI16
	CDKN1A	APP	IFITM2
	CDKN1B	AR	IGF1R
	CDKN2A	BHLHE40	IGFBP7
	IL6	PML	ING1
	NOTCH1		LATS2
	PRKCA		MIC1
	PTGS2		PIN1
	RAS		PRAK
	TGFA		PSEN1
			SFN

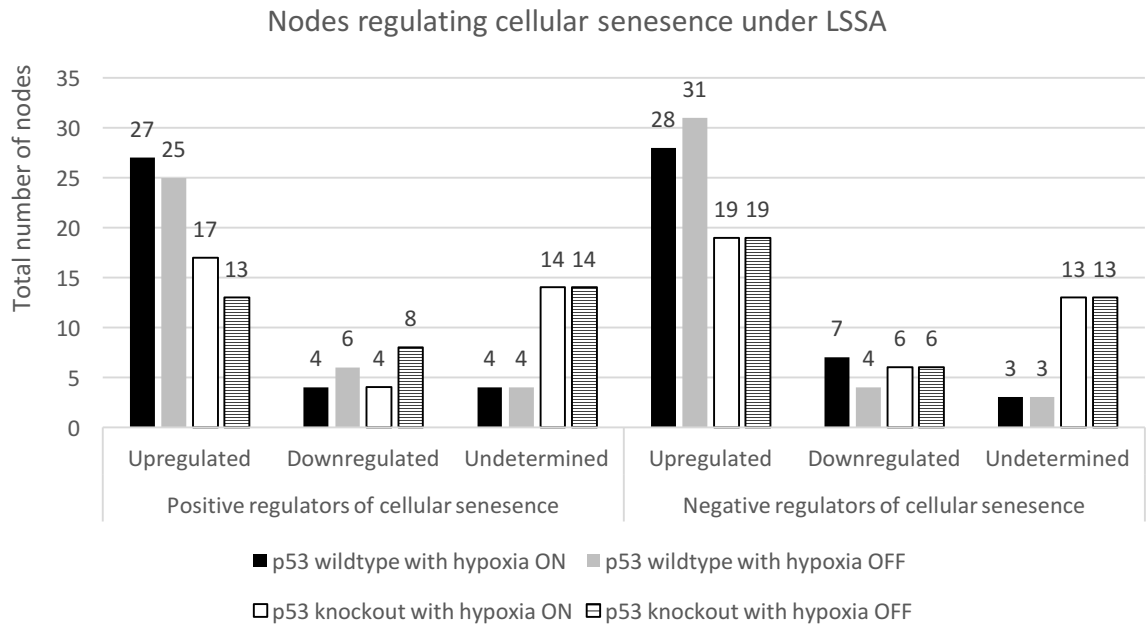

Figure 7.3.1.7 Total number and distribution of nodes regulating cellular senescence under LSSA in PMH302 hypoxia simulations.

7.3.2.3.5 Nodes regulating DNA repair under LSSA

investigating the effect of p53 under hypoxia, an increase in pro- DNA repair nodes upregulated in the presence of p53 (n=17) was noted, compared to the p53 deleted background (n=13) (compare lanes 1 and 3 in fig.7.3.1.8). The number of upregulated anti -DNA repair nodes were similar regardless of p53 status; 6 for p53 wild type and 5 for p53 knockout background (compare lanes 13 and 15) with PPM1D and KLF4 the difference, upregulated when p53 was present (table 7.3.3.7). Of the pro-DNA repair nodes downregulated, MGMT was exclusively downregulated in the presence of p53, whilst FEN1 and GADD45A were downregulated in the absence of p53 (table 7.3.3.8).

In p53 wild type backgrounds, nearly all anti - DNA repair nodes were upregulated regardless of hypoxia effect, 8 when hypoxia was switched ON, 7 when switched OFF (compare lanes 13 and 14) all nodes were identical, apart from SERPINE1 upregulated in response to hypoxia switched ON (table 7.3.3.7).

In p53 deletion backgrounds, 9 pro - DNA repair nodes were downregulated when hypoxia was ON compared to 11 pro-DNA repair nodes downregulated when hypoxia was OFF (compare lanes 7 and 8). Of these, ATM, ATR, PRKDC and YY1 were downregulated when hypoxia was OFF, whilst APEX1 and RAD51 were downregulated in response to hypoxia ON (table 7.3.3.8). The upregulation of SERPINE1 in response to in silico hypoxia was the only difference in p53 deletion backgrounds (table 7.3.3.7).

Table 7.3.3.7 Nodes that negatively regulate DNA repair under LSSA in PMH302 hypoxia simulations. Only a minority of nodes (n = 8) that negatively regulate DNA repair are described in the PMH302 model

***In silico* simulation**	**Upregulated**	**Downregulated**	**Undetermined**
	Total number of nodes		
p53 wild type with hypoxia ON	**8**	**0**	**0**
	KLF4		
	MDM2		
	MDM4		
	MYC		
	SERPINE1		
	SIAH1		

	PPM1D		
	PTTG1		
p53 wild type with hypoxia OFF	**Upregulated**	**Downregulated**	**Undetermined**
	Total number		
	7	**1**	**0**
	KLF4	SERPINE1	
	MDM2		
	MDM4		
	MYC		
	SIAH1		
	PPM1D		
	PTTG1		
p53 knockout with hypoxia ON	**Upregulated**	**Downregulated**	**Undetermined**
	Total number		
	6	**1**	**1**
	MDM2	KLF4	PPMID
	MDM4		
	MYC		
	SERPINE1		
	SIAH1		
	PTTG1		
p53 knockout with hypoxia OFF	**Upregulated**	**Downregulated**	**Undetermined**
	Total number		
	5	**2**	**1**
	MDM2	KLF4	PPMID
	MDM4	SERPINE1	
	MYC		
	SIAH1		
	PTTG1		

.

Table 7.3.3.8 Nodes that positively regulate DNA repair under LSSA in PMH302 hypoxia simulations. A total of 29 pro –DNA repair nodes are described in PMH302

***In silico* simulation**	**Upregulated**	**Downregulated**	**Undetermined**
	Total number of nodes		
p53 wild type with hypoxia ON	**17**	**8**	**4**
	ATM	APEX1	BCCIP
	ATR	MGMT	ING1
	BRCA1	MTA1	PIN1
	CD44	PIAS1	SUMO3
	CDKN1A	RAD51	
	DDB2	RFWD3	
	FEN1	RPA1	
	FGF2	RPS27L	

	GADD45A		
	HSPA4		
	IFI16		
	MCL1		
	MSH2		
	NME1		
	PCNA		
	PRKDC		
	YY1		
p53 wild type with DNA hypoxia OFF	**Upregulated**	**Downregulated**	**Undetermined**
	Total number		
	15	**10**	**4**
	APEX1	ATM	BCCIP
	BRCA1	ATR	ING1
	CD44	MGMT	PIN1
	CDKN1A	MTA1	SUMO3
	DDB2	PIAS1	
	FEN1	PRKDC	
	FGF2	RFWD3	
	GADD45A	RPA1	
	HSPA4	RPS27L	
	IFI16	YY1	
	MCL1		
	MSH2		
	NME1		
	PCNA		
	RAD51		
p53 knockout with hypoxia ON	**Upregulated**	**Downregulated**	**Undetermined**
	Total number		
	13	**9**	**7**
	ATM	APEX1	BCCIP
	ATR	FEN1	DDB2
	BRCA1	GADD45A	IFI16
	CD44	MTA1	ING1
	CDKN1A	PIAS1	MGMT
	FGF2	RAD51	PIN1
	HSPA4	RFWD3	SUMO3
	MCL1	RPA1	
	MSH2	RPS27L	
	NME1		
	PCNA		
	PRKDC		
	YY1		
p53 knockout with hypoxia OFF	**Upregulated**	**Downregulated**	**Undetermined**

	Total number		
	11	**11**	**7**
	APEX1	ATM	BCCIP
	BRCA1	ATR	DDB2
	CD44	FEN1	IFI16
	CDKN1A	GADD45A	ING1
	FGF2	MTA1	MGMT
	HSPA4	PIAS1	PIN1
	MCL1	PRKDC	SUMO3
	MSH2	RFWD3	
	NME1	RPA1	
	PCNA	RPS27L	
	RAD51	YY1	

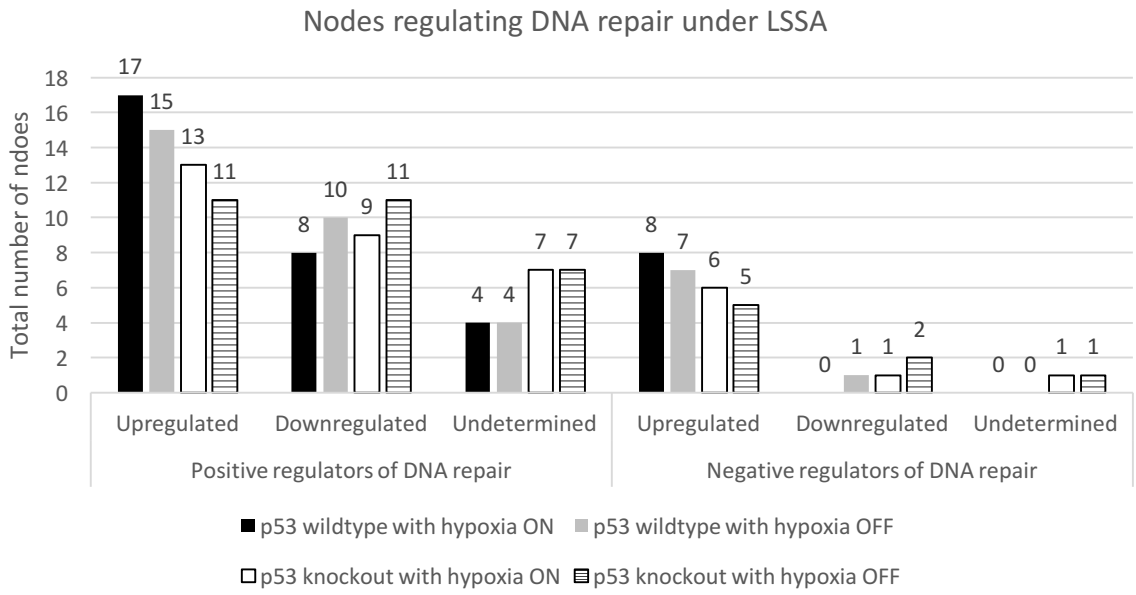

Figure 7.3.1.8 Total number and distribution of nodes regulating DNA repair under LSSA in PMH302 hypoxia simulations. Only a small number of anti-DNA repair nodes are considered in the PMH302 network (n=8).

7.3.3 In *silico* node knockout analysis using dependency matrix calculations

Logical dependencies between genes / proteins are represented by the dependency matrix, (Klamt *et al*.2006;2011). This denotes the effects between all binary nodes in the PMH302 model. In accordance with Klamt et al. (2006:2011) six types of relationships are defined by CellNetAnalyzer. This is based upon whether positive and negative paths exist between pairwise nodes. These six relationships are described in

detail in material and methods, section 6. 2.1 and table 7.3.3.9 where the numbers 1- 6 correspond to; no effect, ambivalent, weak inhibitor, weak activator, strong inhibitor and strong activator respectively.

To investigate node dependency relationships in response to various *in silico* knockouts (KOs), the connectivity degree of all nodes were determined in the PMH302 network. As expected, the hub of the network – p53 was connected to over 300 interactions, 65 nodes were connected to 10 – 100 interactions, the remaining were connected to 10 or less (figure 7.3.1.9). Of the highly connected, seven nodes connected to over 10 % of all other nodes (>30 nodes), were chosen for *in silico* deletion. Selected nodes and corresponding edges were deleted from the model to represent *in vivo* KO or mutation. Depending on the effect of a particular node KO, the relationships between remaining nodes within the network are defined by these six dependency relationships.

The total number of dependencies (n = 91204) (302×302) represents elements in the dependency matrix of the p53 wild-type model (null). Of these, 61336 correspond to interactions with no effect, 23590 are ambivalent factors, 2946 are weak inhibitors, 3147 are weak activators, 59 are strong inhibitors and 126 strong activators. For any knockout scenario the total number (n = 90601) represents the elements within the network after a particular node deletion (301x301). We focused on changes in strong activators or strong inhibitors as these typically have the greatest effect on the cell.

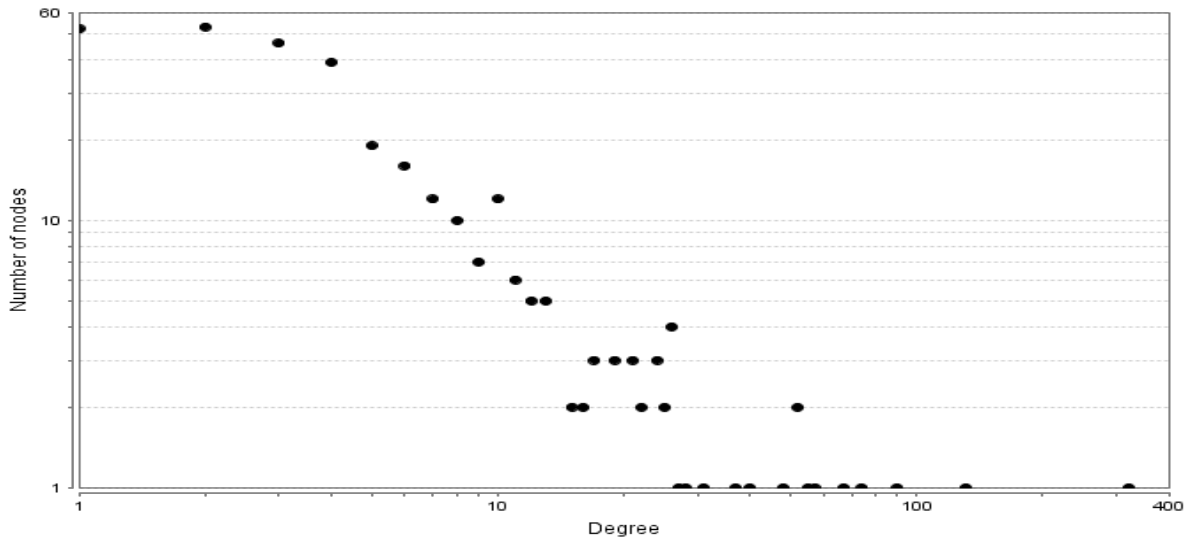

Figure 7.3.1.9 Connectivity degree distribution of all nodes in PMH302.
Axes are in logarithmic scale. As expected, the only node with over 300 interactions was p53 (far right of figure)

The greatest effect was seen when p53 was deleted from the network, with nearly a two-fold increase in strong activators and strong inhibitors from the null model (table 7.3.3.9). 514 potential novel predictions (PNPs) were obtained from dependency changes in response to *in silico* deletion of the seven highly connected nodes (table 7.3.4). Of these, the removal of p53 and E2F1 from the network resulted in the majority of changes, deriving 134 and 124 dependency changes (predictions) respectively. 66 and 70 changes were as a result of FGF2 and HIF1A removal respectively. VEGFA, MDM2 and MYC resulted in the least changes; 32, 48 and 41 respectively when deleted from the network. These predictions are summarised in table 7.3.4.

Table 7.3.3.9 Alterations in the dependency matrix upon node deletions
A single node was deleted from the PMH302 network. The numbers of six types of effect elements in the dependency matrix were calculated as listed below. The value "Null" in the selected node column indicates p53 wild type.

Effect	No Effect	Ambivalent	Weak inhibitor	Weak activator	Strong inhibitor	Strong activator	Total
Number effect	**1**	**2**	**3**	**4**	**5**	**6**	
***In silico* KO**							
Null	61336	23590	2946	3147	59	126	91204
p53	82300	7883	38	94	91	195	90601
E2F1	61233	22539	3193	3450	59	127	90601
FGF2	61263	23123	2911	3118	59	127	90601
MDM2	61078	23147	3007	3184	59	126	90601
MYC	61265	22867	3030	3253	60	126	90601
HIF1A	61601	22719	2949	3141	61	130	90601
VEGFA	62123	22134	2972	3177	63	132	90601

Table 7.3.4 Summary of predictions derived from application of *in silico* KOs of 7 nodes to dependency matrix elements. 514 predictions were obtained from various *in silico* deletions of highly connected nodes. The greatest change was in the absence of p53. Some predictions were verified from literature or laboratory experiments; others are novel predictions (PNP).

Deleted node	Source node	Target node	Wild type	Knockout	Prediction status	Reference
p53	ASPP1	Apoptosis	Ambivalent factor	Strong activator	PNP	
p53	ASPP2	Apoptosis	Ambivalent factor	Strong activator	PNP	
p53	BCCIP	DNA repair	Ambivalent factor	Strong activator	PNP	
p53	BDKRB1	CDK4	Ambivalent factor	Strong activator	PNP	
p53	BDKRB1	FGF2	Weak activator	Strong activator	PNP	
p53	BHLHE40	Apoptosis	Ambivalent factor	Strong activator	PNP	
p53	BHLHE40	STAT3	Weak inhibitor	Strong inhibitor	PNP	
p53	CUL7	Apoptosis	Ambivalent factor	Strong inhibitor	PNP	
p53	CUL7	Cellular senescence	Ambivalent factor	Strong inhibitor	PNP	
p53	DAP	Apoptosis	Ambivalent factor	Strong activator	PNP	
p53	DAXX	Apoptosis	Ambivalent factor	Strong inhibitor	PNP	

p53	DAXX	Cellular senescence	Ambivalent factor	Strong inhibitor	PNP	
p53	DDX20	Apoptosis	Ambivalent factor	Strong activator	PNP	
p53	DNA damage	PML	Ambivalent factor	Strong activator	PNP	
p53	DNA damage	TFAP2A	Ambivalent factor	Strong activator	PNP	
p53	DNA damage	APP	Ambivalent factor	Strong activator	PNP	
p53	DNA damage	CDK4	Ambivalent factor	Strong inhibitor	Laboratory verified here	Inconsistent with prediction
p53	DNA damage	FAS	Ambivalent factor	Strong activator	Literature verified	Manna et.al 2011
p53	DYRK2	Apoptosis	Ambivalent factor	Strong activator	PNP	
p53	DYRK2	P53AIP1	Weak activator	Strong activator	PNP	
p53	FAS	Apoptosis	Ambivalent factor	Strong activator	PNP	
p53	FGF2	CDK4	Ambivalent factor	Strong activator	Laboratory verified here	Confirmed
p53	FLI1	Apoptosis	Ambivalent factor	Strong inhibitor	PNP	
p53	HOXA5	Cell cycle arrest	Ambivalent factor	Strong activator	PNP	
p53	Hypoxia	BAK1	Ambivalent factor	Strong inhibitor	PNP	
p53	Hypoxia	CA9	Ambivalent factor	Strong activator	PNP	
p53	Hypoxia	CASP8	Ambivalent factor	Strong activator	PNP	
p53	Hypoxia	CD59	Ambivalent factor	Strong activator	PNP	
p53	Hypoxia	CDK4	Ambivalent factor	Strong activator	PNP	
p53	Hypoxia	CDKN2A	Ambivalent factor	Strong inhibitor	PNP	
p53	Hypoxia	DDIT4	Ambivalent factor	Strong activator	PNP	
p53	Hypoxia	DDX5	Ambivalent factor	Strong activator	PNP	
p53	Hypoxia	FGF2	Ambivalent factor	Strong activator	PNP	

p53	Hypoxia	GAPDH	Ambivalent factor	Strong activator	PNP	
p53	Hypoxia	HNF4A	Ambivalent factor	Strong activator	PNP	
p53	Hypoxia	IER3	Ambivalent factor	Strong activator	PNP	
p53	Hypoxia	IGFBP1	Ambivalent factor	Strong activator	PNP	
p53	Hypoxia	MAP4	Ambivalent factor	Strong activator	PNP	
p53	Hypoxia	SLC2A4	Ambivalent factor	Weak activator	PNP	
p53	Hypoxia	SLC6A6	Ambivalent factor	Strong inhibitor	PNP	
p53	Hypoxia	SP7	Ambivalent factor	Strong activator	PNP	
p53	Hypoxia	TPT1	Ambivalent factor	Strong activator	PNP	
p53	Hypoxia	UNC5A	Ambivalent factor	Strong activator	PNP	
p53	Hypoxia	WWP1	Ambivalent factor	Strong inhibitor	PNP	
p53	Hypoxia	XAF1	Ambivalent factor	Strong activator	PNP	
p53	ID3	Cell cycle arrest	Ambivalent factor	Strong activator	PNP	
p53	IFNA1	CDK4	Ambivalent factor	Strong inhibitor	PNP	
p53	IFNA1	FAS	Ambivalent factor	Strong activator	PNP	
p53	IFNA1	TLR3	Ambivalent factor	Strong activator	Opposite to prediction	Taura et al.2004
p53	IGFBP7	CDK4	Ambivalent factor	Strong inhibitor	PNP	
p53	ING4	Apoptosis	Ambivalent factor	Strong activator	PNP	
p53	ING4	Cell cycle arrest	Ambivalent factor	Strong activator	PNP	
p53	ING5	Apoptosis	Ambivalent factor	Strong activator	PNP	
p53	ING5	Cell cycle arrest	Ambivalent factor	Strong inhibitor	PNP	
p53	JUN	Angiogenesis	Ambivalent factor	Strong activator	PNP	
p53	JUN	Apoptosis	Ambivalent factor	Strong activator	PNP	
p53	JUN	Cell cycle arrest	Ambivalent factor	Strong inhibitor	PNP	
p53	KAT2B	Apoptosis	Ambivalent factor	Strong activator	PNP	

p53	KAT2B	Cell cycle arrest	Ambivalent factor	Strong activator	PNP	
p53	KLF4	Cell cycle arrest	Ambivalent factor	Strong activator	PNP	
p53	KLF4	CCNB1	Ambivalent factor	Strong inhibitor	Literature verified	Yoon and Yang, 2004
p53	KLF4	DNA repair	Ambivalent factor	Strong inhibitor	PNP	
p53	LATS2	Apoptosis	Ambivalent factor	Strong activator	Literature verified	Ke at al.2004
p53	LATS2	Cellular senescence	Ambivalent factor	Strong activator	Literature verified	Tschop et al. 2011
p53	MAPK 14	Angiogenesis	Ambivalent factor	Strong activator	PNP	
p53	MAPK 14	BAX	Ambivalent factor	Strong activator	Literature verified	Gomez et al.2008
p53	MAPK 14	MMP2	Ambivalent factor	Strong activator	PNP	
p53	MAPK 14	SGK	Weak activator	Strong activator	PNP	
p53	MAPK 14	Cellular senescence	Ambivalent factor	Strong inhibitor	PNP	
p53	MYST 4	Cell cycle arrest	Ambivalent factor	Strong activator	PNP	
p53	NTN1	Angiogenesis	Ambivalent factor	Strong activator	PNP	
p53	P53AIP1	Apoptosis	Ambivalent factor	Strong activator	PNP	
p53	PADI4	Cell cycle arrest	Ambivalent factor	Strong activator	PNP	
p53	PARK2	Cell cycle arrest	Ambivalent factor	Strong activator	PNP	
p53	PCBP4	Apoptosis	Ambivalent factor	Strong activator	PNP	
p53	PCBP4	Cellular senescence	Ambivalent factor	Strong inhibitor	PNP	
p53	PEG3	Apoptosis	No effect	Strong activator	PNP	
p53	PHB	Angiogenesis	No effect	Strong activator	PNP	
p53	PIAS1	DNA repair	Ambivalent factor	Strong activator	PNP	
p53	PITX1	Apoptosis	No effect	Strong activator	PNP	
p53	PML	Angiogenesis	Ambivalent factor	Strong inhibitor	PNP	
p53	PML	Apoptosis	Ambivalent factor	Strong activator	Literature verified	Yang et al.2002

p53	PML	Cellular senescence	Ambivalent factor	Strong activator	Literature verified	Scaglioni et al.2012
p53	PPARG	Angiogenesis	Ambivalent factor	Strong inhibitor	PNP	
p53	PPARG	Cell cycle arrest	Ambivalent factor	Strong activator	PNP	
p53	PRAK	Cellular senescence	Ambivalent factor	Strong activator	PNP	
p53	PREP1	Apoptosis	No effect	Strong inhibitor	PNP	
p53	PRKAB1	Cell cycle arrest	Ambivalent factor	Strong activator	PNP	
p53	PRSS50	Apoptosis	Ambivalent factor	Strong activator	PNP	
p53	PSEN1	Cellular senescence	No effect	Strong activator	PNP	
p53	PTTG1	CDK4	Ambivalent factor	Strong activator	PNP	
p53	PTTG1	FGF2	Ambivalent factor	Strong activator	PNP	
p53	RAD51	DNA repair	Ambivalent factor	Strong activator	PNP	
p53	RB1CC1	Apoptosis	No effect	Strong inhibitor	PNP	
p53	RB1CC1	Cell cycle arrest	No effect	Strong activator	PNP	
p53	RGS16	Cell cycle arrest	No effect	Strong inhibitor	PNP	
p53	RPA1	DNA repair	No effect	Strong activator	PNP	
p53	RPS27L	DNA repair	No effect	Strong activator	PNP	
p53	RSK2	Angiogenesis	Ambivalent factor	Strong activator	PNP	
p53	S100A6	Cell cycle arrest	Ambivalent factor	Strong inhibitor	PNP	
p53	S100A6	Cellular senescence	Ambivalent factor	Strong inhibitor	PNP	
p53	S100B	Angiogenesis	No effect	Strong activator	PNP	
p53	SEMA3B	Apoptosis	Ambivalent factor	Strong activator	PNP	
p53	SENP3	Angiogenesis	No effect	Strong activator	PNP	
p53	SERPINB5	Apoptosis	No effect	Strong activator	PNP	

p53	SERPINE1	Angiogenesis	No effect	Strong activator	PNP	
p53	SERPINE1	DNA repair	No effect	Strong inhibitor	PNP	
p53	SESN2	Cellular senescence	Ambivalent factor	Strong inhibitor	PNP	
p53	SGK	Angiogenesis	Ambivalent factor	Strong activator	PNP	
p53	SGK	Apoptosis	Ambivalent factor	Strong inhibitor	PNP	
p53	SGK	Cellular senescence	Ambivalent factor	Strong inhibitor	PNP	
p53	SIVA1	Apoptosis	Ambivalent factor	Strong activator	PNP	
p53	SLC2A1	Apoptosis	No effect	Strong activator	PNP	
p53	SLC2A1	BAX	No effect	Strong activator	PNP	
p53	SOD2	Cellular senescence	Ambivalent factor	Strong inhibitor	PNP	
p53	STAT3	Apoptosis	No effect	Strong inhibitor	PNP	
p53	STMN1	Angiogenesis	Ambivalent factor	Strong activator	PNP	
p53	STMN1	Cell cycle arrest	Ambivalent factor	Strong activator	PNP	
p53	SUMO3	DNA repair	Ambivalent factor	Strong activator	PNP	
p53	TFAP2A	Apoptosis	Ambivalent factor	Strong activator	Literature verified	Wajapeyee and Somasundara, 2002
p53	TFAP2C	Apoptosis	Ambivalent factor	Strong activator	PNP	
p53	TFAP2C	Cell cycle arrest	Ambivalent factor	Strong activator	PNP	
p53	TFDP1	Cellular senescence	No effect	Strong inhibitor	PNP	
p53	TFDP1	DNA repair	No effect	Strong inhibitor	PNP	
p53	TNFRSF10A	Apoptosis	Ambivalent factor	Strong activator	PNP	
p53	TP53INP1	Apoptosis	No effect	Strong activator	PNP	
p53	TPT1	Apoptosis	Ambivalent factor	Strong inhibitor	PNP	
p53	UBE2A	Cell cycle arrest	No effect	Strong inhibitor	PNP	

p53	UCHL1	Apoptosis	No effect	Strong activator	Literature verified	Jin et al.2013
p53	WWP1	Apoptosis	No effect	Strong inhibitor	PNP	
p53	WWP1	Cellular senescence	No effect	Strong inhibitor	PNP	
p53	YY1	DNA repair	Ambivalent factor	Strong activator	PNP	
E2F1	HSP90AB1	Angiogenesis	Ambivalent factor	Strong inhibitor	PNP	
E2F1	IFI16	Angiogenesis	No effect	Strong inhibitor	PNP	
E2F1	ING1	Angiogenesis	Ambivalent factor	Strong inhibitor	PNP	
E2F1	JAG1	Angiogenesis	No effect	Strong activator	PNP	
E2F1	MIC1	Angiogenesis	No effect	Strong activator	PNP	
E2F1	MMP13	Angiogenesis	No effect	Strong activator	PNP	
E2F1	MTA1	Angiogenesis	No effect	Strong activator	PNP	
E2F1	NANOG	Angiogenesis	Ambivalent factor	Strong activator	PNP	
E2F1	NQO1	Angiogenesis	No effect	Strong inhibitor	PNP	
E2F1	PHB	Angiogenesis	No effect	Strong activator	PNP	
E2F1	RSK2	Angiogenesis	Ambivalent factor	Strong activator	PNP	
E2F1	SENP3	Angiogenesis	No effect	Strong activator	PNP	
E2F1	SERPINE1	Angiogenesis	No effect	Strong activator	PNP	
E2F1	STMN1	Angiogenesis	Ambivalent factor	Strong activator	PNP	
E2F1	Hypoxia	APEX1	No effect	Strong inhibitor	PNP	
E2F1	AIFM2	Apoptosis	Strong activator	Strong activator	PNP	
E2F1	APAF1	Apoptosis	Strong activator	Strong activator	PNP	
E2F1	APEX1	Apoptosis	Strong inhibitor	Strong inhibitor	PNP	
E2F1	APP	Apoptosis	Strong activator	Strong activator	PNP	
E2F1	BAK1	Apoptosis	Strong activator	Strong activator	PNP	
E2F1	BAX	Apoptosis	Strong activator	Strong activator	PNP	

E2F1	BBC3	Apoptosis	Strong activator	Strong activator	PNP	
E2F1	BNIP3L	Apoptosis	Strong activator	Strong activator	PNP	
E2F1	C12orf5	Apoptosis	Strong inhibitor	Strong inhibitor	PNP	
E2F1	CASP8	Apoptosis	Strong activator	Strong activator	PNP	
E2F1	CKS2	Apoptosis	Strong inhibitor	Strong inhibitor	PNP	
E2F1	COL18A1	Apoptosis	Strong activator	Strong activator	PNP	
E2F1	DFNA5	Apoptosis	Strong activator	Strong activator	PNP	
E2F1	ECT2	Apoptosis	Ambivalent factor	Strong activator	PNP	
E2F1	EPHB4	Apoptosis	Ambivalent factor	Strong inhibitor	PNP	
E2F1	EZH2	Apoptosis	No effect	Strong inhibitor	PNP	
E2F1	FDXR	Apoptosis	Ambivalent factor	Strong activator	PNP	
E2F1	GADD45A	Apoptosis	Ambivalent factor	Strong activator	PNP	
E2F1	GSTP1	Apoptosis	Ambivalent factor	Strong inhibitor	PNP	
E2F1	HNF4A	Apoptosis	No effect	Strong activator	PNP	
E2F1	HOXA10	Apoptosis	Strong activator	Strong activator	PNP	
E2F1	IER3	Apoptosis	Ambivalent factor	Strong inhibitor	PNP	
E2F1	IFI16	Apoptosis	Strong inhibitor	Strong activator	PNP	
E2F1	IFITM2	Apoptosis	Strong activator	Strong activator	PNP	
E2F1	LRDD	Apoptosis	Ambivalent factor	Strong activator	PNP	
E2F1	MCL1	Apoptosis	Ambivalent factor	Strong inhibitor	PNP	
E2F1	MMP2	Apoptosis	No effect	Strong activator	PNP	
E2F1	MSH2	Apoptosis	Strong activator	Strong activator	PNP	
E2F1	MTA1	Apoptosis	Strong activator	Strong inhibitor	PNP	
E2F1	NANOG	Apoptosis	Ambivalent factor	Strong inhibitor	PNP	
E2F1	NFKB2	Apoptosis	Ambivalent factor	Strong inhibitor	PNP	

E2F1	NLRC4	Apoptosis	Strong inhibitor	Strong activator	PNP	
E2F1	P53AIP1	Apoptosis	Ambivalent factor	Strong activator	PNP	
E2F1	PCBP4	Apoptosis	Ambivalent factor	Strong activator	PNP	
E2F1	PEG3	Apoptosis	No effect	Strong activator	PNP	
E2F1	PERP	Apoptosis	Strong activator	Strong activator	PNP	
E2F1	PRSS50	Apoptosis	Ambivalent factor	Strong activator	PNP	
E2F1	PSEN1	Apoptosis	Strong activator	Strong inhibitor	PNP	
E2F1	SEMA3B	Apoptosis	Ambivalent factor	Strong activator	PNP	
E2F1	SERPINB5	Apoptosis	No effect	Strong activator	PNP	
E2F1	SIVA1	Apoptosis	Ambivalent factor	Strong activator	PNP	
E2F1	SLC2A1	Apoptosis	No effect	Strong activator	PNP	
E2F1	TFAP2C	Apoptosis	Ambivalent factor	Strong activator	PNP	
E2F1	TFDP1	Apoptosis	Strong activator	Strong inhibitor	PNP	
E2F1	TNFRSF10A	Apoptosis	Ambivalent factor	Strong activator	PNP	
E2F1	TNFRSF10B	Apoptosis	Strong activator	Strong activator	PNP	
E2F1	TP53INP1	Apoptosis	No effect	Strong activator	PNP	
E2F1	TPT1	Apoptosis	Ambivalent factor	Strong inhibitor	PNP	
E2F1	WWP1	Apoptosis	No effect	Strong inhibitor	PNP	
E2F1	XAF1	Apoptosis	Strong inhibitor	Strong activator	PNP	
E2F1	MMP2	BAX	No effect	Strong activator	PNP	
E2F1	SLC2A1	BAX	No effect	Strong activator	PNP	
E2F1	DNA damage	AATF	Ambivalent factor	Strong activator	PNP	
E2F1	DNA damage	CDK5	Ambivalent factor	Strong activator		Verified here
E2F1	EPHB4	Cell cycle arrest	Ambivalent factor	Strong inhibitor	PNP	

E2F1	EXPORTIN1	Cell cycle arrest	Ambivalent factor	Strong activator	PNP	
E2F1	IER3	Cell cycle arrest	Ambivalent factor	Strong inhibitor	PNP	
E2F1	JAG1	Cell cycle arrest	No effect	Strong inhibitor	PNP	
E2F1	MTA1	Cell cycle arrest	No effect	Strong inhibitor	PNP	
E2F1	PRKAB1	Cell cycle arrest	Ambivalent factor	Strong activator	PNP	
E2F1	RGS16	Cell cycle arrest	No effect	Strong inhibitor	PNP	
E2F1	S100A6	Cell cycle arrest	Ambivalent factor	Strong inhibitor	PNP	
E2F1	STMN1	Cell cycle arrest	Ambivalent factor	Strong activator	PNP	
E2F1	TFAP2C	Cell cycle arrest	Ambivalent factor	Strong activator	PNP	
E2F1	EZH2	Cellular senescence	No effect	Strong inhibitor	PNP	
E2F1	HNF4A	Cellular senescence	No effect	Strong inhibitor	PNP	
E2F1	IFI16	Cellular senescence	No effect	Strong activator	PNP	
E2F1	JAG1	Cellular senescence	No effect	Strong inhibitor	PNP	
E2F1	MCL1	Cellular senescence	Ambivalent factor	Strong inhibitor	PNP	
E2F1	MIC1	Cellular senescence	No effect	Strong activator	PNP	
E2F1	PCBP4	Cellular senescence	Ambivalent factor	Strong inhibitor	PNP	
E2F1	PSEN1	Cellular senescence	No effect	Strong activator	PNP	
E2F1	S100A6	Cellular senescence	Ambivalent factor	Strong inhibitor	PNP	
E2F1	SESN2	Cellular senescence	Ambivalent factor	Strong inhibitor	PNP	
E2F1	SOD2	Cellular senescence	Ambivalent factor	Strong inhibitor	PNP	

E2F1	TFDP1	Cellular senescence	No effect	Strong inhibitor	PNP	
E2F1	WWP1	Cellular senescence	No effect	Strong inhibitor	PNP	
E2F1	Hypoxia	CUL7	No effect	Strong inhibitor	PNP	
E2F1	EZH2	DNA repair	No effect	Strong inhibitor	PNP	
E2F1	FEN1	DNA repair	No effect	Strong activator	PNP	
E2F1	IFI16	DNA repair	No effect	Strong activator	PNP	
E2F1	ING1	DNA repair	Ambivalent factor	Strong activator	PNP	
E2F1	MGMT	DNA repair	Ambivalent factor	Strong activator	PNP	
E2F1	MSH2	DNA repair	No effect	Strong activator	PNP	
E2F1	RAD51	DNA repair	Ambivalent factor	Strong activator	PNP	
E2F1	RPA1	DNA repair	No effect	Strong activator	PNP	
E2F1	RPS27L	DNA repair	No effect	Strong activator	PNP	
E2F1	SERPINE1	DNA repair	No effect	Strong inhibitor	PNP	
E2F1	SUMO3	DNA repair	Ambivalent factor	Strong activator	PNP	
E2F1	TFDP1	DNA repair	No effect	Strong inhibitor	PNP	
E2F1	Hypoxia	DUSP1	No effect	Strong activator	PNP	
E2F1	IFNA1	EIF2AK2	No effect	Strong activator	PNP	
E2F1	TFDP1	EZH2	No effect	Strong activator	PNP	
E2F1	Hypoxia	MAPK9	No effect	Strong activator	PNP	
E2F1	Hypoxia	MCTS1	No effect	Strong activator	PNP	
E2F1	NOV	MMP1	Ambivalent factor	Strong activator	PNP	
E2F1	HSP90AB1	MMP13	Ambivalent factor	Strong inhibitor	PNP	
E2F1	SLC2A1	MMP2	No effect	Strong activator	PNP	
E2F1	Hypoxia	MUC1	No effect	Strong activator	PNP	

E2F1	CSNK2	MYCN	Ambivalent factor	Strong activator	PNP	
E2F1	Hypoxia	NFKB2	No effect	Strong activator	PNP	
E2F1	Hypoxia	NTN1	No effect	Strong activator	PNP	
E2F1	HIPK2	POU4F1	No effect	Strong inhibitor	PNP	
E2F1	Hypoxia	PRKDC	No effect	Strong activator	PNP	
E2F1	Hypoxia	SERPINE1	No effect	Strong activator	PNP	
E2F1	Hypoxia	SOX4	No effect	Strong activator	PNP	
E2F1	Hypoxia	VRK1	No effect	Strong activator	PNP	
E2F1	EZH2	RAD51	No effect	Strong inhibitor	PNP	
E2F1	TFDP1	RAD51	No effect	Strong inhibitor	PNP	
FGF2	BDKRB1	Angiogenesis	Ambivalent factor	Strong activator	PNP	
FGF2	HSP90AB1	Angiogenesis	Ambivalent factor	Strong inhibitor	PNP	
FGF2	IFI16	Angiogenesis	No effect	Strong inhibitor	PNP	
FGF2	ING1	Angiogenesis	Ambivalent factor	Strong inhibitor	PNP	
FGF2	JAG1	Angiogenesis	No effect	Strong activator	PNP	
FGF2	MIC1	Angiogenesis	No effect	Strong activator	PNP	
FGF2	MMP13	Angiogenesis	No effect	Strong activator	PNP	
FGF2	MTA1	Angiogenesis	No effect	Strong activator	PNP	
FGF2	NANOG	Angiogenesis	Ambivalent factor	Strong activator	PNP	
FGF2	NQO1	Angiogenesis	No effect	Strong inhibitor	PNP	
FGF2	PHB	Angiogenesis	No effect	Strong activator	PNP	
FGF2	RSK2	Angiogenesis	Ambivalent factor	Strong activator	PNP	
FGF2	SENP3	Angiogenesis	No effect	Strong activator	PNP	
FGF2	SERPINE1	Angiogenesis	No effect	Strong activator	PNP	
FGF2	STMN1	Angiogenesis	Ambivalent factor	Strong activator	PNP	

FGF2	GADD 45A	Apoptosis	Ambivalent factor	Strong activator	PNP	
FGF2	GSTP1	Apoptosis	Ambivalent factor	Strong inhibitor	PNP	
FGF2	HNF4 A	Apoptosis	No effect	Strong activator	PNP	
FGF2	IER3	Apoptosis	Ambivalent factor	Strong inhibitor	PNP	
FGF2	LRDD	Apoptosis	Ambivalent factor	Strong activator	PNP	
FGF2	MCL1	Apoptosis	Ambivalent factor	Strong inhibitor	PNP	
FGF2	MMP2	Apoptosis	No effect	Strong activator	PNP	
FGF2	NANO G	Apoptosis	Ambivalent factor	Strong inhibitor	PNP	
FGF2	NFKB2	Apoptosis	Ambivalent factor	Strong inhibitor	PNP	
FGF2	P53AI P1	Apoptosis	Ambivalent factor	Strong activator	PNP	
FGF2	PCBP4	Apoptosis	Ambivalent factor	Strong activator	PNP	
FGF2	PEG3	Apoptosis	No effect	Strong activator	PNP	
FGF2	PRSS5 0	Apoptosis	Ambivalent factor	Strong activator	PNP	
FGF2	SEMA 3B	Apoptosis	Ambivalent factor	Strong activator	PNP	
FGF2	SERPI NB5	Apoptosis	No effect	Strong activator	PNP	
FGF2	SIVA1	Apoptosis	Ambivalent factor	Strong activator	PNP	
FGF2	SLC2A 1	Apoptosis	No effect	Strong activator	PNP	
FGF2	TFAP2 C	Apoptosis	Ambivalent factor	Strong activator	PNP	
FGF2	TNFRS F10A	Apoptosis	Ambivalent factor	Strong activator	PNP	
FGF2	TP53I NP1	Apoptosis	No effect	Strong activator	PNP	
FGF2	TPT1	Apoptosis	Ambivalent factor	Strong inhibitor	PNP	
FGF2	WWP 1	Apoptosis	No effect	Strong inhibitor	PNP	
FGF2	IER3	Cell cycle arrest	Ambivalent factor	Strong inhibitor	PNP	
FGF2	JAG1	Cell cycle arrest	No effect	Strong inhibitor	PNP	
FGF2	MTA1	Cell cycle arrest	No effect	Strong inhibitor	PNP	

FGF2	PRKAB1	Cell cycle arrest	Ambivalent factor	Strong activator	PNP	
FGF2	RGS16	Cell cycle arrest	No effect	Strong inhibitor	PNP	
FGF2	S100A6	Cell cycle arrest	Ambivalent factor	Strong inhibitor	PNP	
FGF2	STMN1	Cell cycle arrest	Ambivalent factor	Strong activator	PNP	
FGF2	TFAP2C	Cell cycle arrest	Ambivalent factor	Strong activator	PNP	
FGF2	HNF4A	Cellular senescence	No effect	Strong inhibitor	PNP	
FGF2	IFI16	Cellular senescence	No effect	Strong activator	PNP	
FGF2	JAG1	Cellular senescence	No effect	Strong inhibitor	PNP	
FGF2	MCL1	Cellular senescence	Ambivalent factor	Strong inhibitor	PNP	
FGF2	MIC1	Cellular senescence	No effect	Strong activator	PNP	
FGF2	PCBP4	Cellular senescence	Ambivalent factor	Strong inhibitor	PNP	
FGF2	PSEN1	Cellular senescence	No effect	Strong activator	PNP	
FGF2	S100A6	Cellular senescence	Ambivalent factor	Strong inhibitor	PNP	
FGF2	SESN2	Cellular senescence	Ambivalent factor	Strong inhibitor	PNP	
FGF2	SOD2	Cellular senescence	Ambivalent factor	Strong inhibitor	PNP	
FGF2	TFDP1	Cellular senescence	No effect	Strong inhibitor	PNP	
FGF2	WWP1	Cellular senescence	No effect	Strong inhibitor	PNP	
FGF2	IFI16	DNA repair	No effect	Strong activator	PNP	
FGF2	ING1	DNA repair	Ambivalent factor	Strong activator	PNP	

FGF2	MGMT	DNA repair	Ambivalent factor	Strong activator	PNP	
FGF2	MSH2	DNA repair	No effect	Strong activator	PNP	
FGF2	RAD51	DNA repair	Ambivalent factor	Strong activator	PNP	
FGF2	RPA1	DNA repair	No effect	Strong activator	PNP	
FGF2	RPS27L	DNA repair	No effect	Strong activator	PNP	
FGF2	SERPINE1	DNA repair	No effect	Strong inhibitor	PNP	
FGF2	SUMO3	DNA repair	Ambivalent factor	Strong activator	PNP	
FGF2	TFDP1	DNA repair	No effect	Strong inhibitor	PNP	
VEGFA	CXCR4	Apoptosis	Ambivalent factor	Strong activator	PNP	
VEGFA	CXCR4	TOP2A	No effect	Strong activator	PNP	
VEGFA	DNA damage	PIAS2	No effect	Strong activator	PNP	
VEGFA	DNA damage	PLA2G6	No effect	Strong activator	PNP	
VEGFA	DNA damage	PRKG1	Ambivalent factor	Strong activator	PNP	
VEGFA	DNA damage	RAD51	Ambivalent factor	Strong inhibitor	PNP	
VEGFA	DNA damage	RGS16	Ambivalent factor	Strong activator	PNP	
VEGFA	DNA damage	RPRM	Ambivalent factor	Strong activator	PNP	
VEGFA	DNA damage	RREB1	No effect	Strong activator	PNP	
VEGFA	DNA damage	S100A2	Ambivalent factor	Strong activator	PNP	
VEGFA	DNA damage	SP7	Ambivalent factor	Strong activator	PNP	
VEGFA	DNA damage	SUB1	Strong activator	Strong inhibitor	PNP	

VEGFA	DNA damage	SUMO2	No effect	Strong activator	PNP	
VEGFA	DNA damage	TP53I13	Ambivalent factor	Strong activator	PNP	
VEGFA	DNA damage	UBE3A	No effect	Strong activator	PNP	
VEGFA	EZH2	RAF1	No effect	Strong inhibitor	PNP	
VEGFA	FOXM1	Apoptosis	Ambivalent factor	Strong activator	PNP	
VEGFA	FOXM1	BAX	Ambivalent factor	Strong activator	PNP	
VEGFA	FOXM1	CCNB1	Ambivalent factor	Strong activator	PNP	
VEGFA	FOXM1	Cell cycle arrest	Ambivalent factor	Strong inhibitor	PNP	
VEGFA	FOXM1	Cellular senescence	Ambivalent factor	Strong inhibitor	PNP	
VEGFA	FOXM1	MMP2	Ambivalent factor	Strong activator	PNP	
VEGFA	FOXM1	MMP2	No effect	Strong activator	PNP	
VEGFA	Hypoxia	PRKG1	Ambivalent factor	Strong activator	PNP	
VEGFA	Hypoxia	SERPINF1	Ambivalent factor	Strong activator	PNP	
VEGFA	Hypoxia	SP7	Ambivalent factor	Strong activator	PNP	
VEGFA	RSK2	Cellular senescence	Ambivalent factor	Strong inhibitor	PNP	
VEGFA	SESN2	Angiogenesis	Ambivalent factor	Strong inhibitor	PNP	
VEGFA	SLC2A4	BAX	No effect	Strong activator	PNP	
VEGFA	TGFA	EZH2	Ambivalent factor	Strong activator	PNP	
VEGFA	TGFA	RAF1	Ambivalent factor	Strong inhibitor	PNP	
VEGFA	WWP1	Apoptosis	No effect	Strong inhibitor	PNP	
MYC	NANOG	Angiogenesis	Ambivalent factor	Strong activator	PNP	
MYC	NQO1	Angiogenesis	No effect	Strong inhibitor	PNP	
MYC	PHB	Angiogenesis	No effect	Strong activator	PNP	

MYC	RSK2	Angiogenesis	Ambivalent factor	Strong activator	PNP	
MYC	SENP3	Angiogenesis	No effect	Strong activator	PNP	
MYC	SERPINE1	Angiogenesis	No effect	Strong activator	PNP	
MYC	STMN1	Angiogenesis	Ambivalent factor	Strong activator	PNP	
MYC	NANOG	Apoptosis	Ambivalent factor	Strong inhibitor	PNP	
MYC	NFKB2	Apoptosis	Ambivalent factor	Strong inhibitor	PNP	
MYC	P53AIP1	Apoptosis	Ambivalent factor	Strong activator	PNP	
MYC	PCBP4	Apoptosis	Ambivalent factor	Strong activator	PNP	
MYC	PEG3	Apoptosis	No effect	Strong activator	PNP	
MYC	PRSS50	Apoptosis	Ambivalent factor	Strong activator	PNP	
MYC	SEMA3B	Apoptosis	Ambivalent factor	Strong activator	PNP	
MYC	SERPINB5	Apoptosis	No effect	Strong activator	PNP	
MYC	SIVA1	Apoptosis	Ambivalent factor	Strong activator	PNP	
MYC	SLC2A1	Apoptosis	No effect	Strong activator	PNP	
MYC	TCF7L2	Apoptosis	No effect	Strong inhibitor	PNP	
MYC	TFAP2C	Apoptosis	Ambivalent factor	Strong activator	PNP	
MYC	TNFRSF10A	Apoptosis	Ambivalent factor	Strong activator	PNP	
MYC	TP53INP1	Apoptosis	No effect	Strong activator	PNP	
MYC	TPT1	Apoptosis	Ambivalent factor	Strong inhibitor	PNP	
MYC	WWP1	Apoptosis	No effect	Strong inhibitor	PNP	
MYC	PRKAB1	Cell cycle arrest	Ambivalent factor	Strong activator	PNP	
MYC	RGS16	Cell cycle arrest	No effect	Strong inhibitor	PNP	
MYC	S100A6	Cell cycle arrest	Ambivalent factor	Strong inhibitor	PNP	
MYC	STMN1	Cell cycle arrest	Ambivalent factor	Strong activator	PNP	
MYC	TFAP2C	Cell cycle arrest	Ambivalent factor	Strong activator	PNP	

MYC	PCBP4	Cellular senescence	Ambivalent factor	Strong inhibitor	PNP	
MYC	PSEN1	Cellular senescence	No effect	Strong activator	PNP	
MYC	S100A6	Cellular senescence	Ambivalent factor	Strong inhibitor	PNP	
MYC	SESN2	Cellular senescence	Ambivalent factor	Strong inhibitor	PNP	
MYC	SOD2	Cellular senescence	Ambivalent factor	Strong inhibitor	PNP	
MYC	TFDP1	Cellular senescence	No effect	Strong inhibitor	PNP	
MYC	WWP1	Cellular senescence	No effect	Strong inhibitor	PNP	
MYC	RAD51	DNA repair	Ambivalent factor	Strong activator	PNP	
MYC	RPA1	DNA repair	No effect	Strong activator	PNP	
MYC	RPS27L	DNA repair	No effect	Strong activator	PNP	
MYC	SERPINE1	DNA repair	No effect	Strong inhibitor	PNP	
MYC	SUMO3	DNA repair	Ambivalent factor	Strong activator	PNP	
MYC	TFDP1	DNA repair	No effect	Strong inhibitor	PNP	
MDM2	MIC1	Angiogenesis	No effect	Strong activator	PNP	
MDM2	MMP13	Angiogenesis	No effect	Strong activator	PNP	
MDM2	MTA1	Angiogenesis	No effect	Strong activator	PNP	
MDM2	NANOG	Angiogenesis	Ambivalent factor	Strong activator	PNP	
MDM2	NQO1	Angiogenesis	No effect	Strong inhibitor	PNP	
MDM2	PHB	Angiogenesis	No effect	Strong activator	PNP	
MDM2	RSK2	Angiogenesis	Ambivalent factor	Strong activator	PNP	
MDM2	SENP3	Angiogenesis	No effect	Strong activator	PNP	
MDM2	SERPINE1	Angiogenesis	No effect	Strong activator	PNP	

MDM2	STMN1	Angiogenesis	Ambivalent factor	Strong activator	PNP	
MDM2	MMP2	Apoptosis	No effect	Strong activator	PNP	
MDM2	NANOG	Apoptosis	Ambivalent factor	Strong inhibitor	PNP	
MDM2	NFKB2	Apoptosis	Ambivalent factor	Strong inhibitor	PNP	
MDM2	P53AIP1	Apoptosis	Ambivalent factor	Strong activator	PNP	
MDM2	PCBP4	Apoptosis	Ambivalent factor	Strong activator	PNP	
MDM2	PEG3	Apoptosis	No effect	Strong activator	PNP	
MDM2	PRSS50	Apoptosis	Ambivalent factor	Strong activator	PNP	
MDM2	SEMA3B	Apoptosis	Ambivalent factor	Strong activator	PNP	
MDM2	SERPINB5	Apoptosis	No effect	Strong activator	PNP	
MDM2	SIVA1	Apoptosis	Ambivalent factor	Strong activator	PNP	
MDM2	SLC2A1	Apoptosis	No effect	Strong activator	PNP	
MDM2	TFAP2C	Apoptosis	Ambivalent factor	Strong activator	PNP	
MDM2	TNFRSF10A	Apoptosis	Ambivalent factor	Strong activator	PNP	
MDM2	TP53INP1	Apoptosis	No effect	Strong activator	PNP	
MDM2	TPT1	Apoptosis	Ambivalent factor	Strong inhibitor	PNP	
MDM2	WWP1	Apoptosis	No effect	Strong inhibitor	PNP	
MDM2	MTA1	Cell cycle arrest	No effect	Strong inhibitor	PNP	
MDM2	PRKAB1	Cell cycle arrest	Ambivalent factor	Strong activator	PNP	
MDM2	RGS16	Cell cycle arrest	No effect	Strong inhibitor	PNP	
MDM2	S100A6	Cell cycle arrest	Ambivalent factor	Strong inhibitor	PNP	
MDM2	STMN1	Cell cycle arrest	Ambivalent factor	Strong activator	PNP	
MDM2	TFAP2C	Cell cycle arrest	Ambivalent factor	Strong activator	PNP	
MDM2	MIC1	Cellular senescence	No effect	Strong activator	PNP	

MDM2	PCBP4	Cellular senescence	Ambivalent factor	Strong inhibitor	PNP	
MDM2	PSEN1	Cellular senescence	No effect	Strong activator	PNP	
MDM2	S100A6	Cellular senescence	Ambivalent factor	Strong inhibitor	PNP	
MDM2	SESN2	Cellular senescence	Ambivalent factor	Strong inhibitor	PNP	
MDM2	SOD2	Cellular senescence	Ambivalent factor	Strong inhibitor	PNP	
MDM2	TFDP1	Cellular senescence	No effect	Strong inhibitor	PNP	
MDM2	WWP1	Cellular senescence	No effect	Strong inhibitor	PNP	
MDM2	MGMT	DNA repair	Ambivalent factor	Strong activator	PNP	
MDM2	MSH2	DNA repair	No effect	Strong activator	PNP	
MDM2	RAD51	DNA repair	Ambivalent factor	Strong activator	PNP	
MDM2	RPA1	DNA repair	No effect	Strong activator	PNP	
MDM2	RPS27L	DNA repair	No effect	Strong activator	PNP	
MDM2	SERPINE1	DNA repair	No effect	Strong inhibitor	PNP	
MDM2	SUMO3	DNA repair	Ambivalent factor	Strong activator	PNP	
MDM2	TFDP1	DNA repair	No effect	Strong inhibitor	PNP	
HIF1A	HSP90AB1	Angiogenesis	Ambivalent factor	Strong inhibitor	PNP	
HIF1A	IFI16	Angiogenesis	No effect	Strong inhibitor	PNP	
HIF1A	ING1	Angiogenesis	Ambivalent factor	Strong inhibitor	PNP	
HIF1A	JAG1	Angiogenesis	No effect	Strong activator	PNP	
HIF1A	MIC1	Angiogenesis	No effect	Strong activator	PNP	
HIF1A	MMP13	Angiogenesis	No effect	Strong activator	PNP	
HIF1A	MTA1	Angiogenesis	No effect	Strong activator	PNP	

HIF1A	NANOG	Angiogenesis	Ambivalent factor	Strong activator	PNP	
HIF1A	NQO1	Angiogenesis	No effect	Strong inhibitor	PNP	
HIF1A	PHB	Angiogenesis	No effect	Strong activator	PNP	
HIF1A	RSK2	Angiogenesis	Ambivalent factor	Strong activator	PNP	
HIF1A	SENP3	Angiogenesis	No effect	Strong activator	PNP	
HIF1A	SERPINE1	Angiogenesis	No effect	Strong activator	PNP	
HIF1A	STMN1	Angiogenesis	Ambivalent factor	Strong activator	PNP	
HIF1A	IER3	Cell cycle arrest	Ambivalent factor	Strong inhibitor	PNP	
HIF1A	JAG1	Cell cycle arrest	No effect	Strong inhibitor	PNP	
HIF1A	MTA1	Cell cycle arrest	No effect	Strong inhibitor	PNP	
HIF1A	PRKAB1	Cell cycle arrest	Ambivalent factor	Strong activator	PNP	
HIF1A	RGS16	Cell cycle arrest	No effect	Strong inhibitor	PNP	
HIF1A	S100A6	Cell cycle arrest	Ambivalent factor	Strong inhibitor	PNP	
HIF1A	STMN1	Cell cycle arrest	Ambivalent factor	Strong activator	PNP	
HIF1A	TFAP2C	Cell cycle arrest	Ambivalent factor	Strong activator	PNP	
HIF1A	HNF4A	Cellular senescence	No effect	Strong inhibitor	PNP	
HIF1A	IFI16	Cellular senescence	No effect	Strong activator	PNP	
HIF1A	JAG1	Cellular senescence	No effect	Strong inhibitor	PNP	
HIF1A	MCL1	Cellular senescence	Ambivalent factor	Strong inhibitor	PNP	
HIF1A	MIC1	Cellular senescence	No effect	Strong activator	PNP	
HIF1A	PCBP4	Cellular senescence	Ambivalent factor	Strong inhibitor	PNP	
HIF1A	PSEN1	Cellular senescence	No effect	Strong activator	PNP	

HIF1A	S100A6	Cellular senescence	Ambivalent factor	Strong inhibitor	PNP	
HIF1A	SESN2	Cellular senescence	Ambivalent factor	Strong inhibitor	PNP	
HIF1A	SOD2	Cellular senescence	Ambivalent factor	Strong inhibitor	PNP	
HIF1A	TFDP1	Cellular senescence	No effect	Strong inhibitor	PNP	
HIF1A	WWP1	Cellular senescence	No effect	Strong inhibitor	PNP	
HIF1A	GAPDH	DNA repair	Ambivalent factor	Strong inhibitor	PNP	
HIF1A	IFI16	DNA repair	No effect	Strong activator	PNP	
HIF1A	ING1	DNA repair	Ambivalent factor	Strong activator	PNP	
HIF1A	MGMT	DNA repair	Ambivalent factor	Strong activator	PNP	
HIF1A	MSH2	DNA repair	No effect	Strong activator	PNP	
HIF1A	RAD51	DNA repair	Ambivalent factor	Strong activator	PNP	
HIF1A	RPA1	DNA repair	No effect	Strong activator	PNP	
HIF1A	RPS27L	DNA repair	No effect	Strong activator	PNP	
HIF1A	SERPINE1	DNA repair	No effect	Strong inhibitor	PNP	
HIF1A	SIAH1	DNA repair	Ambivalent factor	Strong inhibitor	PNP	
HIF1A	SUMO3	DNA repair	Ambivalent factor	Strong activator	PNP	
HIF1A	TFDP1	DNA repair	No effect	Strong inhibitor	PNP	
HIF1A	Hypoxia	PLAUR	Ambivalent factor	Strong activator	PNP	
HIF1A	GAPDH	SIAH1	Weak activator	Strong activator	PNP	
HIF1A	GAPDH	Apoptosis	Ambivalent factor	Strong activator	PNP	
HIF1A	HNF4A	Apoptosis	No effect	Strong activator	PNP	
HIF1A	IER3	Apoptosis	Ambivalent factor	Strong inhibitor	PNP	
HIF1A	LRDD	Apoptosis	Ambivalent factor	Strong activator	PNP	

HIF1A	MCL1	Apoptosis	Ambivalent factor	Strong inhibitor	PNP	
HIF1A	MMP2	Apoptosis	No effect	Strong activator	PNP	
HIF1A	NANOG	Apoptosis	Ambivalent factor	Strong inhibitor	PNP	
HIF1A	NFKB2	Apoptosis	Ambivalent factor	Strong inhibitor	PNP	
HIF1A	P53AIP1	Apoptosis	Ambivalent factor	Strong activator	PNP	
HIF1A	PCBP4	Apoptosis	Ambivalent factor	Strong activator	PNP	
HIF1A	PEG3	Apoptosis	No effect	Strong activator	PNP	
HIF1A	PRSS50	Apoptosis	Ambivalent factor	Strong activator	PNP	
HIF1A	SEMA3B	Apoptosis	Ambivalent factor	Strong activator	PNP	
HIF1A	SERPINB5	Apoptosis	No effect	Strong activator	PNP	
HIF1A	SIAH1	Apoptosis	Ambivalent factor	Strong activator	PNP	
HIF1A	SIVA1	Apoptosis	Ambivalent factor	Strong activator	PNP	
HIF1A	SLC2A1	Apoptosis	No effect	Strong activator	PNP	
HIF1A	TFAP2C	Apoptosis	Ambivalent factor	Strong activator	PNP	
HIF1A	TNFRSF10A	Apoptosis	Ambivalent factor	Strong activator	PNP	
HIF1A	TP53INP1	Apoptosis	No effect	Strong activator	PNP	
HIF1A	TPT1	Apoptosis	Ambivalent factor	Strong inhibitor	PNP	
HIF1A	WWP1	Apoptosis	No effect	Strong inhibitor	PNP	

The majority of dependency changes from a given knockout scenario were altered from ambivalent factors to strong activators and strong inhibitors. A large majority of nodes (n = 199), changed from having no influence (no effect), on a target node to a strong activating (n =126), or strong inhibitory effect (n = 73).

To evaluate the models predictive capacity to detect perturbations from *in silico* node knockout, extensive literature search was undertaken for validation of changes derived

from the various knockout tests (n=7). Of the 514 predictions (table 7.3.4) 15 were confirmed as true by literature verification or laboratory verified. Four of these predictions were verified here in our laboratory. However, an important note to consider is that not all predictions were literature searched for validation due to time constraints.

7.3.4 Genome wide analysis and validation of the PMH302 model

In order to evaluate the capability of the Boolean PMH302 model to predict differential gene expression changes, we performed LSSA (tables 7.3.1.7 and 7.3.2.8) and compared the results on a genome wide level gene using transcriptome *in vitro* and *in vivo* data. For comparison of model to experimental data, we used the formula in accordance with Christensen et al. (2009) and Tian et al. (2013) also described in detail in section 6.3.

7.3.4.1 Superimposition of U2OS cell line (p53 +/+) gene expression profiles to PMH302.

Tian et al. (2013) and Hussain et al. (2015) (section 7.2) previously superimposed human osteosarcoma cell lines; SaoS2 (p53 -/-) and U2OS p53 +/+) to the earlier p53 models; PKT206 and PMH260 respectively. Good predictive ratios were obtained of over 70 % for both. As we have generated a larger model, we again superimposed U2OS cells treated with etoposide and untreated to PMH302 to explore and compare the predictive ratios of the larger model. 203 genes were filtered from U2OS expression profiles and compared to the 302 model using the same formula as described by Christensen et al. (2009). Correct predictions remained the same as previously obtained for PMH260 of 141 (70 %), similarly small errors were in the minority (1 %). Total number and percentage of predictions are summarised in table 7.3.4.1.

Table 7.3.4.1 Correct predictions for superimposition of U2OS (p53 +/+) gene expression profiles to in silico LSSA results of PMH302. Identical microarray profiles of human osteosarcoma cell lines compared against PKT206 and PMH260 were again superimposed to the larger model - PMH302. The same prediction ratios were obtained as those derived from PMH260. Total number and percentages are shown.

Experimental condition	*in silico* condition	Correct	Small error	Large error
U2OS cells treated with etoposide vs. U2OS cells untreated	p53 wild type with DNA damage ON vs. p53 wild type with DNA damage OFF	142 (70 %)	59 (29 %)	2 (1 %)

7.3.4.2 Superimposition of mesothelioma *in vitro* transcriptome data to the PMH302 model

For comparison to *in vitro* data, microarray profiles of human Mero-14 malignant mesothelioma cell lines treated under a hypoxic environment of 1 % oxygen (24 h) and DNA damage conditions with 10 μM etoposide (24 h) and a control of untreated (37 ^{o} C with 5% CO_2) were superimposed against PMH302. Using these *in vitro* conditions to compare *in silico* results derived from the LSSA, the *in silico* hypoxia and DNA damage input was switched 'ON' to mimic conditions of cells treated with hypoxia or etoposide, and 'OFF' to mimic cells untreated. No p53 knockout scenario was generated as no p53 null cell lines were used to create a p53 wild type vs. p53 knockout scenario.

Log fold changes of >1.5, <-1.5 and *P* values of < 0.05 were used to obtain significantly differentially expressed genes from mesothelioma gene expression profiles using Affymetrix expression platform. Simulations for experimental comparisons were undertaken in the Affymetrix expression platform and also Bioconductor, available in R with the kind help of Dr Tian for Bioconductor. From these profiles, 247 genes were described for hypoxia and 210 genes for etoposide in the 302 model.

The total number of correct predictions, small and large errors are summarised in table 7.3.4.2 and their percentages in figure 7.3.2. Correct predictions were in the majority globally (see lanes 1-3 figure 7.3.2) with an average of 75.5 % when considering all 3 scenarios. For the simulation of mesothelioma cells treated with 10 μM etoposide vs. cells untreated a total of 144 correct predictions, (68.5 %) were obtained with 64 small

errors (30.5 %). Large errors occupied the minority of all these predictions comprising a total number of 2 (1 %). The greatest number of correct predictions were obtained for hypoxia simulations, with a total of 175 predictions correctly predicted (83 %) from the total 210 genes analysed in mesothelioma cells treated with 10 μM etoposide vs. cells under 1 % O_2. No large errors were obtained for this simulation. 184 (75%) correct predictions were obtained from cells under hypoxic conditions vs. cells untreated from the total 247 genes analysed (table 7.3.4.2).

Concerning the experimental data, the differential gene expression of malignant mesothelioma cells untreated and treated with 1 % 0_2 and 10 μM etoposide for 24 h were further explored in accordance with the formula described by Christensen et al. (2009) (table 7.3.4.3). In general, the majority of genes across the three conditions remained unchanged in response these conditions.

Table. 7.3.4.2 Total number of correct, small and large error predictions from superimposition of mesothelioma 'omics' data to PMH302 interactome. Three outcomes are possible in accordance with Christensen et al. (2009) Correct, small error and large error.

Experimental to in silico comparison		**Predictions**		
		Correct	**Small error**	**Large error**
***In vitro* condition**	***in silico* simulation**	**Total number**		
Cells treated with etoposide vs cells untreated	DNA damage ON vs. DNA damage OFF	144	64	2
Cells treated with hypoxia vs. cells untreated	Hypoxia ON vs. hypoxia OFF	184	61	2
Cells treated with etoposide vs cells treated with hypoxia	DNA damage ON vs. hypoxia ON	175	35	0

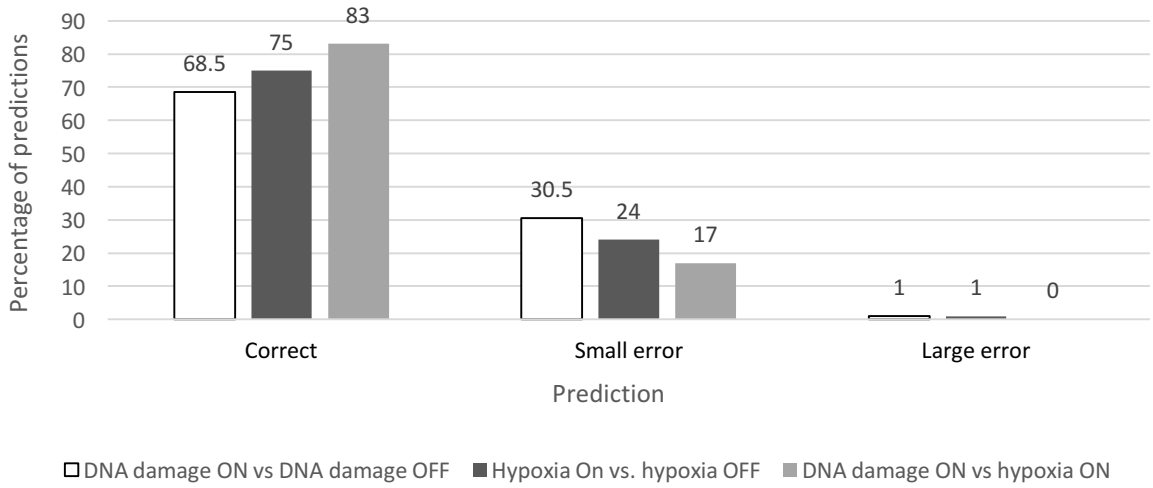

Figure 7.3.2 Percentage of correct, small and large error predictions between *in vitro* and *in silico* data in PMH302. Gene expression profiles of malignant mesothelioma cell lines untreated and treated with 1 % O_2 and 10 µM etoposide (24 h) were superimposed and compared to *in silico* LSSA results. Correct predictions were in the majority for all comparisons (see lanes 1-3). Percentage data labels are shown.

Table 7.3.4.3 Global list of genes differentially expressed in human mesothelioma cancer cell lines under the 3 comparative scenarios. In accordance with Christensen et al. (2009), three different changes were possible; 1 = upregulated, -1 = downregulated or 0 = unchanged comparing *in vitro* data to *in silico* data. Total number of genes, 247 for hypoxia and 210 for DNA damage simulations.

Experimental condition	Upregulated	Downregulated	No change
Mesothelioma cells treated with etoposide vs. cells untreated	Total number		
	19	23	168
	AURKA	ATF3	APEX1
	BNIP3L	BRCA1	APP
	CA9	CDKN1A	ARID3A
	CCNB1	DDX20	ATM
	CDC20	DKK1	ATR
	COL18A1	DUSP2	AXIN1
	EPHB4	EZH2	BAIAP2L1
	FOS	FAS	BAK1
	KRT19	FEN1	BAX
	MGMT	GADD45A	BBC3
	MMP2	JAG1	BCCIP
	MYCN	JUN	BCL2
	PDGFRB	KLF4	BCL6
	PTEN	MSH2	BDKRB1
	PTTG1	MUC1	BHLHE40
	TP53BP1	MYC	CALD1

	WWOX	PCNA	CASP2
	YY1	PDRG1	CASP8
	ZNF148	PTGS2	CCAR1
		RFWD3	CCND1
		SESN2	CCNG1
		TLR3	CD44
		TNFRSF10B	CD58
			CD59
			CD82
			CDC25A
			CDK2
			CDK4
			CDKN1B
			CDKN2A
			CHEK1
			CHEK2
			CIAPIN1
			CKM
			CKS2
			CUL7
			CXCR4
			CYP24A1
			DAP
			DAXX
			DDB2
			DFNA5
			DNMT3A
			DUSP1
			DUSP4
			E2F1
			ECT2
			EDA2R
			EGFR
			EIF2AK2
			ELAVL1
			ERBB2
			ESR1
			FDXR
			FHL2
			FOXM1
			GAPDH
			GSTP1
			GTSE1
			H2AFZ

			HDAC1
			HIC1
			HIF1A
			HIPK4
			HMMR
			HOXA10
			HOXA11
			HOXA5
			HSP90AB1
			HSPA4
			HTATIP2
			ICAM1
			ID3
			IER3
			IFITM2
			IFNA1
			IGF1R
			IGFBP7
			ING1
			ING2
			ING4
			ING5
			ISG15
			KAT2B
			KIF23
			LATS2
			LTF
			MAPK8
			MAPK9
			MCL1
			MDM4
			MMP1
			MMP13
			MTA1
			NCL
			NFKB2
			NLRC4
			NOTCH1
			NOV
			NQO1
			NR2C1
			NTN1
			P53
			PADI4

			PARK2
			PCBP4
			PERP
			PHB
			PHF20
			PIAS2
			PIN1
			PITX1
			PLA2G6
			PLAUR
			PML
			PPARG
			PPM1A
			PPM1D
			PRC1
			PRKAB1
			PRKCA
			PRKD1
			PRKG1
			PSEN1
			PSMD10
			RAF1
			RB1CC1
			RGS16
			RPA1
			RPRM
			RPS27L
			RREB1
			RRM2B
			S100A2
			S100A6
			S100B
			SERPINB5
			SERPINF1
			SFN
			SIAH1
			SIVA1
			SKIL
			SLC6A6
			SMYD2
			SOD1
			SOD2
			SOX4
			STAT3

			STMN1
			SUB1
			SUMO3
			TFAP2A
			TFAP2C
			TFDP1
			TGFA
			TGFB1
			THBS1
			TNFRSF10A
			TP53I13
			TP53INP1
			TP53RK
			UBE2A
			UBE3A
			UCHL1
			UNC5A
			WRN
			ZMAT3
			ZMIZ2
Mesothelioma cells treated with hypoxia vs. cells untreated	**Upregulated**	**Downregulated**	**No change**
	24	**28**	**195**
	ABCC1	ATF3	AIMP2
	AIFM2	BBC3	APAF1
	APEX1	CDK2	APP
	AURKA	CDKN1A	AR
	CCNB1	CXCR4	ARID3A
	CD82	DDX5	ATM
	COL18A1	DKK1	ATR
	HIF1A	DUSP2	AXIN1
	HIPK2	DUSP5	BAIAP2L1
	IFITM2	EZH2	BAK1
	KAT2B	FEN1	BAX
	KRT19	FHL2	BCCIP
	MGMT	GADD45A	BCL2
	MYCN	ID3	BCL3
	NME1	IER3	BCL6
	NQO1	ING2	BDKRB1
	NTN1	JUN	BNIP3L
	PDGFRB	KLF4	BRCA1
	PRKCA	MYC	CA9
	PRKD1	PPM1D	CALD1
	PRKDC	RECQL4	CASP2

	PTEN	SESN2	CASP8
	TLR3	TFAP2C	CCAR1
	WWOX	TGFB1	CCND1
		TP53INP1	CCNG1
		VEGFA	CD44
		BHLHE40	CD58
		GDF15	CD59
			CDC20
			CDC25A
			CDK4
			CDK5
			CDK9
			CDKN1B
			CDKN2A
			CHEK1
			CHEK2
			CIAPIN1
			CKM
			CKS2
			CUL7
			CYP24A1
			DAP
			DAXX
			DDB2
			DDIT4
			DDX20
			DNMT3A
			DUSP1
			DUSP4
			E2F1
			ECT2
			EDA2R
			EGFR
			EIF2AK2
			ELAVL1
			EPHB4
			ERBB2
			ESR1
			FAS
			FDXR
			FGF2
			FLI1
			FOS
			FOXM1

			GAPDH
			GSTP1
			GTSE1
			H2AFZ
			HDAC1
			HIC1
			HIPK4
			HMMR
			HOXA10
			HOXA11
			HOXA5
			HSP90AB1
			HSPA4
			HTATIP2
			ICAM1
			IFI16
			IFNA1
			IGF1R
			IGFBP1
			IGFBP7
			IL6
			ING1
			ING4
			ING5
			IQCB1
			ISG15
			JAG1
			KIF23
			KLK3
			KRT8
			LATS2
			LTF
			MAP4K4
			MAPK1
			MAPK14
			MAPK8
			MAPK9
			MCL1
			MDM2
			MDM4
			MMP1
			MMP13
			MMP2
			MSH2

			MTA1
			MTA2
			NCL
			NFKB2
			NLRC4
			NOTCH1
			NOV
			NR2C1
			PADI4
			PARK2
			PCBP4
			PCNA
			PDRG1
			PEG3
			PERP
			PHB
			PHF20
			PIAS1
			PIAS2
			PIN1
			PITX1
			PLA2G6
			PLAUR
			PML
			POU4F1
			PPARG
			PPM1A
			PRC1
			PRKAB1
			PRKG1
			PRSS50
			PSEN1
			PSMD10
			PTGS2
			PTTG1
			RAF1
			RB1CC1
			RFWD3
			RGS16
			RPA1
			RPRM
			RPS27L
			RREB1
			RRM2B

			S100A2
			S100A6
			S100B
			SEMA3B
			SENP3
			SERPINB5
			SERPINF1
			SFN
			SIAH1
			SIVA1
			SKIL
			SLC2A1
			SLC2A4
			SLC6A6
			SMYD2
			SOD1
			SOD2
			STAT3
			STMN1
			SUB1
			SUMO2
			SUMO3
			TFAP2A
			TFDP1
			TGFA
			THBS1
			TNFRSF10A
			TNFRSF10B
			TOP2A
			TP53
			TP53BP1
			TP53I13
			TP53RK
			UBE2A
			UBE3A
			UCHL1
			UNC5A
			WRN
			YY1
			ZMAT3
			ZMIZ2
			ZNF148

Mesothelioma cells treated with etoposide vs. cells treated with hypoxia	Upregulated	Downregulated	No change
	0	**2**	**208**
		BCL2	APEX1
		PPARG	APP
			ARID3A
			ATF3
			ATM
			ATR
			AURKA
			AXIN1
			BAIAP2L1
			BAK1
			BAX
			BBC3
			BCCIP
			BCL6
			BDKRB1
			BNIP3L
			BRCA1
			CA9
			CALD1
			CASP2
			CASP8
			CCAR1
			CCNB1
			CCND1
			CCNG1
			CD44
			CD58
			CD59
			CD82
			CDC20
			CDC25A
			CDK2
			CDK4
			CDKN1A
			CDKN1B
			CDKN2A
			CHEK1
			CHEK2
			CIAPIN1
			CKM
			CKS2
			COL18A1

			CUL7
			CXCR4
			CYP24A1
			DAP
			DAXX
			DDB2
			DDX20
			DFNA5
			DKK1
			DNMT3A
			DUSP1
			DUSP2
			DUSP4
			E2F1
			ECT2
			EDA2R
			EGFR
			EIF2AK2
			ELAVL1
			EPHB4
			ERBB2
			ESR1
			EZH2
			FAS
			FDXR
			FEN1
			FHL2
			FOS
			FOXM1
			GADD45A
			GAPDH
			GSTP1
			GTSE1
			H2AFZ
			HDAC1
			HIC1
			HIF1A
			HIPK4
			HMMR
			HOXA10
			HOXA11
			HOXA5
			HSP90AB1
			HSPA4

			HTATIP2
			ICAM1
			ID3
			IER3
			IFITM2
			IFNA1
			IGF1R
			IGFBP7
			ING1
			ING2
			ING4
			ING5
			ISG15
			JAG1
			JUN
			KAT2B
			KIF23
			KLF4
			KRT19
			LATS2
			LTF
			MAPK8
			MAPK9
			MCL1
			MDM4
			MGMT
			MMP1
			MMP13
			MMP2
			MSH2
			MTA1
			MYC
			MYCN
			NCL
			NFKB2
			NLRC4
			NOTCH1
			NOV
			NQO1
			NR2C1
			NTN1
			PADI4
			PARK2
			PCBP4

			PCNA
			PDGFRB
			PDRG1
			PERP
			PHB
			PHF20
			PIAS2
			PIN1
			PITX1
			PLA2G6
			PLAUR
			PML
			PPM1A
			PPM1D
			PRC1
			PRKAB1
			PRKCA
			PRKD1
			PRKG1
			PSEN1
			PSMD10
			PTEN
			PTGS2
			PTTG1
			RAF1
			RB1CC1
			RFWD3
			RGS16
			RPA1
			RPRM
			RPS27L
			RREB1
			RRM2B
			S100A2
			S100A6
			S100B
			SERPINB5
			SERPINF1
			SESN2
			SFN
			SIAH1
			SIVA1
			SKIL
			SLC6A6

			SMYD2
			SOD1
			SOD2
			STAT3
			STMN1
			SUB1
			SUMO3
			TFAP2A
			TFAP2C
			TFDP1
			TGFA
			TGFB1
			THBS1
			TLR3
			TNFRSF10A
			TNFRSF10B
			TP53BP1
			TP53I13
			TP53INP1
			TP53RK
			UBE2A
			UBE3A
			UCHL1
			UNC5A
			WRN
			WWOX
			YY1
			ZMAT3
			ZMIZ2
			ZNF148
			BHLHE40
			MUC1
			P53
			SOX4